Analysis of Design Methodologies of Free From Damage Moment Resisting Frames

Candidate name: Eliana Inca Cabrera
Supervisors: Prof. Ph.D. Raffaele Landolfo,
Assist. Prof. Ph.D. Mario D'Aniello
Co-Supervisor: Eng. Mariana Zimbru

Thesis submitted in partial fulfilment of the requirements for the Degree of Master of Science in Construction of Steel and Composite Structures European Erasmus Mundus Masters Course Sustainable Construction Under Natural Hazards and Catastrophic Events

University of Naples "Federico II"
Date: 14th February 2017

STATEMENT OF THESIS APPROVAL

This thesis prepared by **Eliana Inca Cabrera** entitled 'Analysis of Design Methodologies of Free From Damage Moment Resisting Frames' is approved in partial fulfillment of the requirements for the degree of Master of Science by the following faculty members served as the supervisory committee chair and members.

_____,Chair _____
Date Approved

_____,Member _____
Date Approved

_____,Member _____
Date Approved

Student's signature _____

Date of Submission _____

To my parents: Elisa and Victor
For their unconditional support and love.

Acknowledgments

This dissertation work would not been possible without the support of many people. I am deeply indebted to my supervisor, Assist. Professor Ph.D. Mario D'ANIELLO, for his guidance, encouragement and support throughout this research work. I also would like to give a special acknowledgment to Eng. Mariana ZIMBRU for her patience and guidance during the investigation process and for her support facing new challenges.

My sincere thanks to Professor František WALD, Professor Dan DUBINA, Professor Luís Simões da Silva, Professor Jean-Pierre JASPART, Professor Raffaele LANDOLFO and Professor Milan Veljkovic as coordinators of our SUSCOS_ M European Erasmus Mundus Master program (Sustainable Constructions under natural hazards and catastrophic events 520121-1-2011-1-CZ-ERA MUNDUS-EMMC), for organizing this excellent master degree program and for their assistance and guidance in Coimbra, Prague and Naples. Without their help, this program would not have been possible. I would like to express my gratitude especially to Professor Raffaele Landolfo and all the academic staff of the Department of Structures for Engineering and Architecture of the University of Naples "Federico II", for opening their doors and gave us a pleasant environment for finalize this work here in Naples.

I would like to thank my colleagues in SUSCOS_M program, for all the shared experiences along the masters course. I've found great colleges and friends, and gained a cultural and educational enrichment from all.

I would like to acknowledge the European Union, namely the Erasmus Mundus Scholarship Commission, as without this funding I would not have the opportunity to participate in this master degree course and meet the above mentioned excellent people.

Finally, my deepest gratitude to my parents Elisa Cabrera and Victor Inca, exceptional human beings from whom example and constant support contributed to my personal and academic growth , thank you for the confidence. All of this wouldn't be possible without gods guidance, all presented here is not my willing but his.

Abstract

The well-known destructive capacity of earthquakes around the world, justifies by itself every study made to improve the design methodologies that structural engineers use nowadays. Over the past years an important field of study was focused in develop low-damage buildings, either by a design conception where all members remain elastic or by introducing seismic isolation, damping devices or other techniques.

One of the most commonly used lateral force resisting systems are Moment Resisting Frames (MRFs), regarding seismic design, MRFs require to fulfill higher stiffness demands and often the designer is forced to use larger members in order to satisfy code drift limit criteria. Usually, MRF's traditional joint typologies have heavily over designed welds due to the full-strength beam-to-column joints criteria, the brittleness of the here mention welds, lead the use of more bolted connections and more recently, friction connections (FFD) which have been studied from both behavioral and economical point of view, particularly owed to the dissipative components of this type of connections, stable behavior and easily reparation.

The current work deals with a new approach for designing MRFs with dissipative joints i.e. friction joints, in particular, with the comparison of the traditional EN 1998-1 seismic design methodology with two proposed design methodologies following different assumptions: (i)Design Procedure A (DP-A) assuming the damper design forces from the seismic combination, (ii) Design Procedure B (DP-B) assuming the damper design forces as a function of the plastic resistance of the beam; aiming to define a straightforward design methodology consistent with the current design procedure for MRFs of EC8.

Overall twenty-four MRFs were designed with the three methodologies, arranged in sets of eight frames, where the number of bays, span length and seismic hazard are the variables for the different configurations. The MRFs seismic performance was studied by a parametric investigation based on both nonlinear static and dynamic analyses, both were performed using SeismoStruct v2016 software.

The non-linear static (pushover) analysis (NLSA) was performed for all the frames considering two cases for the lateral load distribution, as required by EN 1998-1 4.3.3.4.2.2, *Uniform* and *Triangular* load patterns. Capacity curves i.e. top displacement against base

shear were obtained for all the frames. Three performance levels were investigated: Damage Limitation (DL), Significant Damage (SD) and Near Collapse limit state (NC). The response parameters monitored by the performed pushover analyses were the over-strength factors, ductility factors and target displacements from the Idealized capacity curves of each frame.

The analyses showed that all the frames were able to developed an overall ductile mechanism and a stable non-linear behavior under SD limit state, most of the frames remain in the elastic behavior for Operational Level (OL) and Damage limitation (DL). The pushover capacity curves confirmed the average ratio V_p/V_y obtained for the frames as equal or higher than α_u/α_1=1.30 recommended by EN1998-1. For EC8 and DP-B frames, pushover analyses showed overall overstrength factors Ω_{ov} larger than the design behavior factor (q = *6.5*). For EC8 frames, this result is ascribable to the codified design procedure, which leads to increase the member size to satisfy the drift limitations as well to local and global verification for ULS limit state to satisfy hierarchy criteria. A similar case occurs for DP-B MRFs, due to the design requirements for ULS, columns need to be increased in order to fulfill hierarchy criteria for the dissipative connections methodology.

The seismic performance of the MRFs obtained from the non linear time history analysis i.e. incremental dynamic analysis (IDA) was investigated in terms of the maximum and minimum inter-storey drift distribution through the height of the structure, for transitory (TID) and residual (RID) inter-storey drift, as well as the peak acceleration of each storey (PSA). Results showed a similar performance for the the three design methodologies in terms of seismic demand (namely, transient and residual drift ratios) with values fairly below the proposed limit for DL, SD and NC states. In particular, at SD limit state the most of frames behave in elastic field. This result is mainly due to the design oversizing.

The comparison of RID demand for the three design methodologies showed significantly small values for all the frames, thus easily repairing may be expected after the earthquake. Investigation of the storey acceleration amplification factors reveal that DP-A and DP-B frames designed considering friction connections showed a significantly reduction when compared to EC8 frames.

Finally, material consumption comparison between design methodologies in terms of steel density was quantified and it was observed that frames designed with DP-B approach shown a higher steel density than those designed for EC8 and DP-A cases. This result is attributed to the need to provide adequate lateral stiffness and stronger requirements for local and global verification hierarchy criteria due to the design approach for the Friction connections, thus compelling the designer to select heavy profiles, as it result for columns steel sections for DP-B frames with higher weight than for the other two of the design methodologies. The comparison between steel density showed that the lowest material density obtained for all the frames was for DP-A frames, from an economical point of view, the former solution can turn to be more effective, only considering beams and columns steel sections.

Contents

List of Figures

List of Tables

1 Introduction and objectives

We have big, big problems - flooding, earthquake and many foolish things which now people are doing - I mean, these self-made catastrophes. If as engineers we are able to give to every man on the street the possibilities to help himself, to fight for this was one of my duties.

Frei Otto

1.1 Introduction

In highly active seismic zones structures need to be designed considering frequent earthquakes and they must withstand the seismic events with a low level of damage and remain safe and operable. Therefore, limiting damage in buildings has been a topic of constant research through the years.

Basically there are two procedures that can achieve this objective: (i) by applying additional damping devices (passive or active dampers) connected to certain members of the structure or (ii) by reducing the seismic input energy that the building has to withstand by means of base isolation systems that can decouple the structure of direct ground acceleration.

The Moment Resisting Frames (MRFs) are one of the most commonly used lateral force resisting system due to their high dissipation capacity, straight forward design, architectural versatility and simplicity of construction. Their main characteristic is to resist lateral loads by the principle of rigid frame action by developing bending moment and shear force both in beams and columns. Steel MRFs tend to be very flexible due to the high strength/weight

ratio of the material, therefore, they are prone to stability problems. With particular regard to seismic design, these systems require to fulfill higher stiffness demands and often the designer is forced to use larger members in order to satisfy code drift limits, since stiffness and strength are equal correlated, the bigger the members become the more the structures are over-designed, hence the higher the demands transferred to the foundation system, leading to heavy structures with an economic disadvantage in comparison to other systems like braced frames or shear walls systems.

In the capacity design philosophy of MRFs, the designer must choose the locations of yield zones in the frame i.e. the location of so called: plastic hinges, which for MRFs usually are located at beams ends while the rest of the members, columns, and connections remain elastic. This traditional design philosophy of MRFs leads to irrecoverable plastic deformation in the beams or joints, leading to costly post-earthquake repair or no chance to repair at all. For this reason, the current tendency in practice is to reduce the damage that the building will sustain during a seismic event and not only prevent collapse and keep the building operational, but mitigate and localize the damage, ideally, immediately after a major earthquake just minor damage will be localized in parts of the structure that are specifically chosen, easy to replace and less costly with respect to traditional MRF repair strategies.

Basically, in a capacity based design philosophy design the energy dissipation is provided through yielding of sacrificial elements, like the beams in the MRFs are taken as fusible in a strong-column-weak-beam approach, taking measures to keep the connections elastic (such as over-strengthening the joint with respect to the adjoining members or using a reduced beam section to help direct the plastic hinge formation). The European practice for the seismic design of MRFs dictates that the joint has to be rigid and robust enough to be effective in ensuring a ductile structural behavior i.e. the formation of a global mechanism with plastic hinges at the end of all beams, preventing thus brittle failure modes that lead to sudden structural collapse and important life safety risks.

The main concern nowadays is to develop low-damage buildings, either by a design conception where all members remain elastic or by introducing seismic isolation, damping devices or other techniques.

Innovative systems for earthquake-resistant building has been proposed in the last decades

and they have been thoroughly investigated and even implemented in practice with success. Modern structural systems, the traditional-improved or the innovative ones are able to limit their level of structural and nonstructural damage by controlling their lateral deformation. Steel MRFs can be converted in a low damage system by including beam to column capable of dissipate energy with minor damage while the members remain elastic. This mechanism can be achieved by using friction dampers that dissipate energy trough relative slip between the interfaces of bolted plates, controlled by a predetermined friction force based on level of clamping force and friction coefficient of the surfaces.

As mention by Clifton et al. (2007) the main characteristics of an innovative sliding Hinge Joint for MRFs are: 1) the structure should be provided with a ”non tearing slab”, due to the change in dimension (shortening or expansion) of the beam, the so called ”beam growth” that can lead to a change in distance between centerlines of columns after a major earthquake, leading to significant demands on columns, beams and tension tearing of the slab. 2) damage should be minimized during major events and 3) there must be a comparable cost with traditional connections.

According to Khoo et al. (2013) the advantages of using a Slide Hinge Joint (SHJ) over welded connections are: 1) decoupled moment frame strength and stiffness, 2) confinement of inelastic demand to the bolts which are easily replaced following an earthquake, (3) improved seismic-dynamic recentering ability, and (4) lower cost.

Summarizing for the current design codes, Moment Resistant Steel Frames under seismic actions are designed adopting full-strength beam-to-column joints with adequate over-strength with respect to the flexural resistance of the connected beam, aiming to ensure the engagement of the beam ends in the plastic range and the complete development of their plastic rotation capacity. Traditional joint typologies have heavily over designed welds because, these elements are characterized by a brittle failure. Precisely this brittleness, is the reason why bolted connections and more recently, partial-strength double split tee (DST) or friction connections (FFD) are been studied from both behavioral and economical point of view, the use of the mentioned connections is particularly appropriate because in such connection typologyies the dissipative components can be clearly established and easily replaced.

The current work deals with new approach for designing MRFs with dissipative joints i.e. friction joints, in particular, with the comparison of the traditional EN 1998-1 design methodology (from now on named as EC8 design methodology) with the design methodology developed and tested at University of Naples "Federico II", hereafter called *Design Procedure A* (DP-A) and University of Salerno in Italy, in this paper named *Design Procedure B* (DP-B). Several frame configurations (varying number of bays, span length, seismic hazard, etc.) are studied and compared with the aim of defining a straightforward design methodology consistent with the current design procedure for MRFs of EC8 and study the advantages of this innovative joint typology.

1.2 Objectives

The main objectives of the thesis are:

1. Understand how a friction joint dissipates energy and compare the behavior with typical joints configurations for MRFs, in terms of advantages, materials and design approach.

2. Design several types of Moment Resisting Frames (MRFs) according to the methodology available EN 1998-1 and review all compliant rules.

3. Define a procedure to design or adapt the current design of MRFs for the case of Free From Damage Frames (FFD), both for the methodology developed by University of Naples "Federico II' (DP-A) and University of Salerno in Italy (DP-B).

4. Analyze the seismic performance of the MRFs using Seismostruct software for the three design methodologies with a non-linear static (pushover) and non-linear dynamic incremental (Time-History) analysis (IDA) for several strong motion records.

5. Compare and discuss the overall behavior of the MRFs according to results obtained from the analysis carried out.

2 State of the Art

2.1 Seismic Design of Moment Resisting Frames According to Eurocode 1998-1

The European Committee of Standardization, under the European Union supervision, published and reviewd a set of standards known as Eurocodes that contain several rules for structural design for countries within European Union. Eurocode 8 (EC8), denoted as EN 1998: "Design of structures for earthquake resistance", applies for the design and construction of structures (buildings and other civil engineering works) in seismic regions.

EC8 consists of six parts covering: buildings, bridges, assessment and retrofitting of buildings, tanks, silos and pipelines, foundations, geotechnical aspects and retaining walls, towers, masts and chimneys; in this context Part 1 (General Rules, Seismic Actions and Rules for Buildings), which is of relevance to the current study, describes seismic design rules for buildings, section 6 contains specific Rules for Steel Buildings, from which, and for the present report, Moment Resisting Steel Frames (MRF's) rules are studied.

Two fundamental seismic design levels are considered in EC8:

- No collapse Requirement: as Ultimate Limit State (ULS), corresponds to seismic action based on a recommended probability of exceedance of 10% in 50 years, or a return period of 475 years and the requirement is to withstand the design seismic action without local or global collapse, therefore retain structural integrity and residual strength in the aftermath of the seismic event. In operational terms the balance between

resistance and energy-dissipation capacity is characterized by the so called "behavior factor, q" and its associated ductility classification. An important factor to take into account for this compliance criteria is also regarding nonstructural elements, they shouldn't represent risks to persons and must not have a detrimental effect on the response of the structural elements, therefore important detailing should be specified in structural drawings in order to fulfill this requirement.

- Damage Limitation Requirement: as Damage Limitation State (DLS), damage-limitation relates to a recommended probability of exceedance of 10% in 10 years, or a return period of 95 years. As expected, capacity design is directly associated with large events, but several checks are included to ensure compliance with serviceability, a key factor of this requirement is related to limit high repair costs after seismic events. According to EC8 design approach, the damage control is made by satisfying the deformation limits, as inter-storey drift limits, rotation of joints or global lateral deformation control, which in traditional MRFs turns to be a control criteria for selection of steel sections.

Regarding the seismic action, EC8 characterizes the earthquake motion at a given point on the surface by an elastic ground acceleration response spectrum, called *Elastic Response Spectrum*. In EC8 the so called *Reference elastic acceleration response spectra (S_e)* is defined as function of the period of vibration (T) and design ground acceleration (a_g) on rock (firm ground) (EN1998-1, Section 3.2.2, equations 3.2 to 3.5). The spectrum depends on the following factors:

- Soil factor (S)
- Damping correction factor (η)
- Pre-defined spectral periods (T_B, T_C and T_D) which vary with soil type and seismic source characteristics

For ultimate limit design (ULS), inelastic performance is incorporated through the *behavior factor (q)* to obtain an acceleration design spectrum (S_d) (EN1998-1, section

3.2.2.5, equations 3.13 to 3.16), therefore design will be checked against smaller seismic forces than those corresponding to a linear elastic response. To avoid inelastic analysis, elastic spectral accelerations are divided by the behavior factor (excepting some modifications for T $< T_B$ to account for inherent properties) to reduce the design forces in accordance with the structural configuration and expected ductility, obtaining a *Design Spectrum*, an example of this spectrum is shown in figure 2.1.

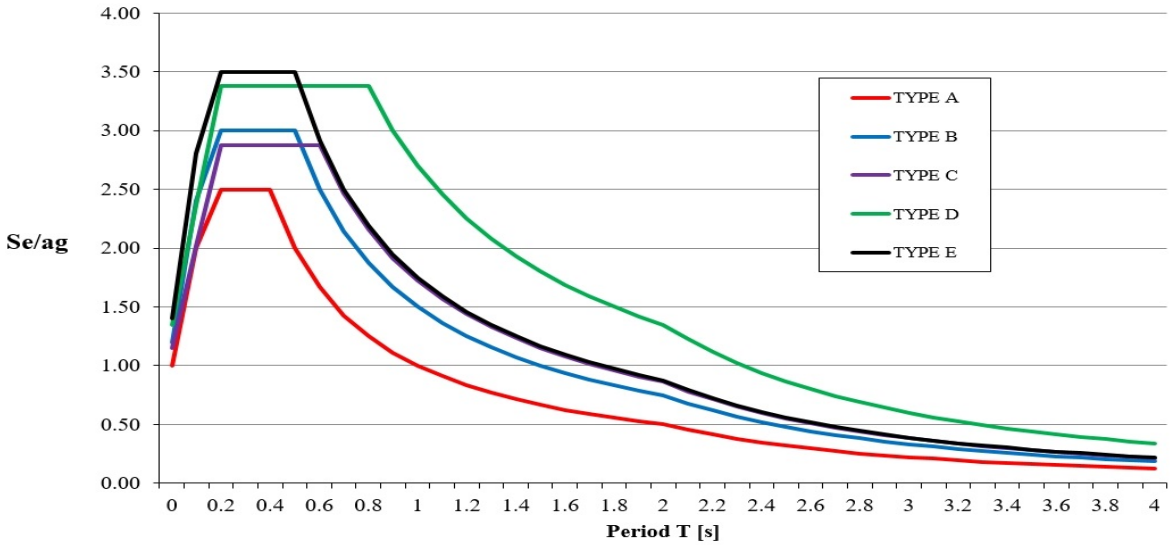

Figure 2.1 Recommended Type 1 response spectra for ground Type A to E with 5% damping ratio.

2.1.1 behavior factors

To take into account a dissipative design, Eurocode 8 describes rules for the consideration of values for the behavior factor (described in sections 6.1 to 6.5), which can be listed in table 2.1 for different structural types. For Moment Resisting Frames (MRFs) the limits of q are 4 and $5\alpha_u/\alpha_1$ for DCM (Ductility Class Medium) and DCH (Ductility Class High) respectively. The multiplier α_u/α_1 depends on the ultimate-to-first plasticity resistance ratio, related to the redundancy of the structure. This may be estimated from nonlinear static *push-over* analysis, but should not exceed 1.6 (EN 1998-1:2004 section 6.3.2 (6)). In the absence of detailed evaluation, α_u/α_1 may be assumed as 1.1, 1.2 and 1.3 for single portal, single-

span multi-storey and multi-span multi-storey frames, respectively as can be seen in figure 2.2

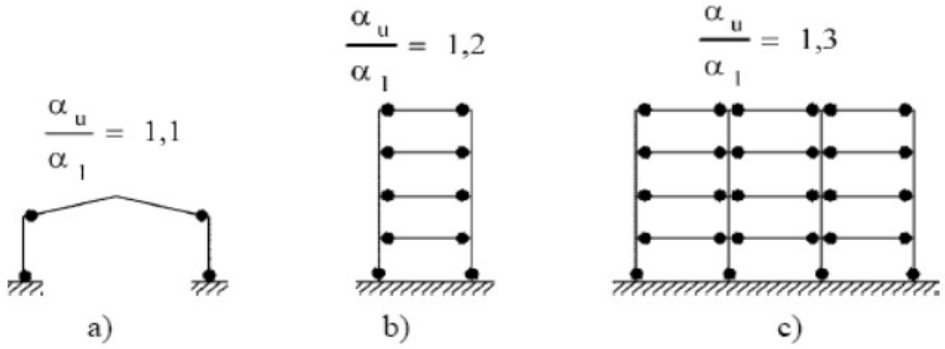

Figure 2.2 Recommended values for α_u/α_1 ratio (EN 1998:2004 section 6.3.1)

Table 2.1 Upper limit of reference values of behavior factors for systems regular in elevation (EN 1998-1:2004, Table 6.2)

STRUCTURAL TYPE	Ductility Class	
	DCM	DCH
a) Moment resisting frames	4	5 α_u/α_1
b) Frame with concentric bracings	-	-
Diagonal bracings	4	4
V-bracings	2	2.5
c) Frame with eccentric bracings	4	5 α_u/α_1
d) Inverted pendulum	2	2 α_u/α_1
e) Structures with concrete cores or concrete walls	Section 5	Section 5
f) Moment resisting frame with concentric bracing	4	4 α_u/α_1
g) Moment resisting frames with infills	-	-
Unconnected concrete or masonry infills, in contact with the frame	2	
Connected reinforced concrete infills	Section 7	Section 7
Infills isolated from moment frame	4	5 α_u/α_1

For regular structures in areas of low seismicity, a q value of 1.5 or 2 may be adopted without using dissipative procedures, recognizing the presence of inherent over-strength and ductility as described in EN 1998:2004 section 6.1.2. For the previous case the structure is classified as DCL (Ductility Class Low), the action effects can be calculated using a global

elastic analysis and the resistance of members and connections evaluated according to EC3 (Eurocode-3, 2005) without additional requirements. The application of q>1.5 requires the capability of parts of the structure (known as dissipative zones) to resist earthquake actions trough inelastic behavior and to provide them with sufficient ductility.

Dissipative zones should satisfy cross-section classification requirements depending on the value of q, which includes cross sections class 1, 2 or 3 for DCM and $1.5 < q \leq 2.0$; Class 1 or 2 for DCM and $2.0 < q \leq 4$, and Class 1 for DCH and q>4.0. As described in EN 1998:2004 section 6.3.1, the predetermined location of dissipative zones is also clearly identified. For moment resisting frames, plastic hinges are located at beam ends or beam-clumn joints, but column hinges are allowed at the base and in the top storey. In the case of typical braced frames, dissipative zones are assumed mainly in the tension diagonals. The advantage of the adoption of q values, enables the use of standard elastic analysis tools for the seismic design of regular structures, using a set of reduced forces.

For Serviciability requirement, although reduced forces are used to verify the capacity of the elements, drifts obtained from elastic analysis need to be amplified to account for inelastic deformations. In EC8, the same force-based behavior factors (q) are proposed as displacement amplification factors (q_d), although these differ in other seismic codes, drift and stability requirements are significantly more strigent, due to the fact that Moment resisting frames are more sensitive to those effects and usually are the governing criteria for the design of initial cross sections, leading to considerable over-strength, especially for higuer values of q (Elghazouli, 2010).

2.2 Free From Damage Connections (FFD, connections with friction pads)

Even though the development of supplemental damping devices started in New Zealand about 40 years ago (Latour et al., 2014; Mualla and Belev, 2002), the definition of design rules for buildings using connections with friction pads is still not codified, therefore the aim of this report is to clarify some rules for designers that apply this type of connections to Moment Resisting Frames (MRFs), in the following are described some of the experimental work and

parametrical analysis for material, type of connections and behavior for Free from Damage connections (FFD) and MRFs equipped with the so called friction connections.

FFD connections are rigid under serviceability conditions and under design earthquake actions they dissipate energy, by means of a friction mechanism, that accommodates the rotation of the beam through sliding. At local scale, FFDs are composed by beam-to-column connections equipped with friction pads; therefore, the dissipative zones are constituted by damping devices located at the beam ends. At global scale the prevention of column hinging that is necessary to achieve FFD structures, can be ensured by an elaborate design methodology based on the theorems of plastic collapse to guarantee the desired energy dissipation mechanism, in figure 2.3 is shown a typical configuration for this type of FFD connection (Latour et al., 2015), (Piluso et al., 2014).

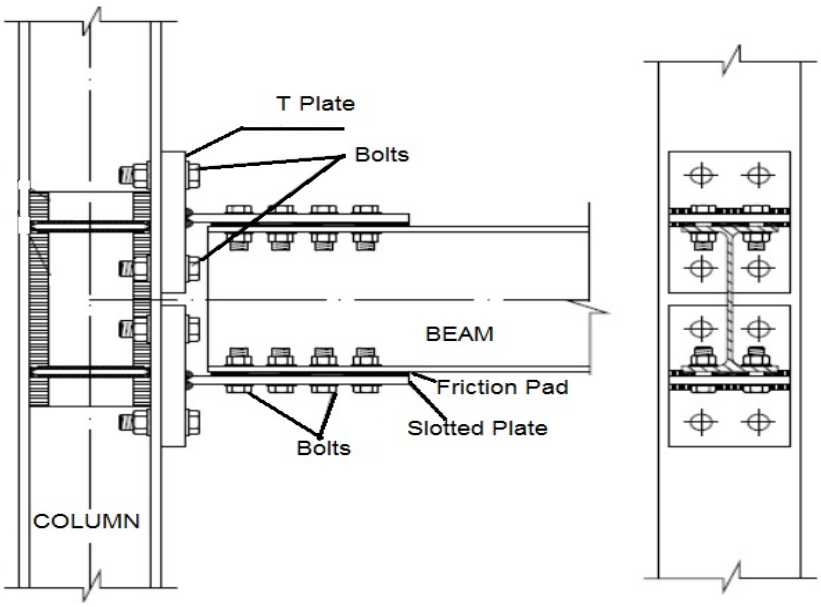

Figure 2.3 Description of typical configuration of FFD.

Alternative devices that are incorporated in the structures with the purpose of absorbing the kinetic energy generated in the structure by seismic events, and in this way, reduce the local and global damage were studied around the early 70's. One of the first works of characterization of the hysteretic behavior of sliding metallic surfaces with different treatments and configurations, clamped by high strength friction bolts to be used as dissipative links (mainly for braces) were developed by Kelly et al. (1972). The authors

tested three different mechanisms and studied the load displacement relations, the energy absorption capacity and the fatigue resistance in all cases.

In the years that followed, friction dampers were often applied for passive control systems, due to their high energy-dissipation potential at relatively lower costs compared to other systems avaiable at the time, and also due to its easy installation and maintenance. Tests of friction devices were carried out also by Pall and Marsh (1982), Grigorian et al. (1993), Mualla and Belev (2002) and many others in the early 2000's. Particularly Mualla and Belev (2002) tested a new friction damper device for chevron bracing systems, the device is composed by the combination of two side plates and one central plate connected by pre-tightened bolts that allows to control the compression force applied on the interfaces of the friction pad discs and steel plates, a similar concept to the FFD connections used in the current work for the MRFs.

The overall concept in a friction damper, is that basically the energy is dissipated by slippage between two or more surfaces in contact, and is directly related to the type of materials it is composed of and the pressure normal to the surfaces. These surfaces can be campled by using hydraulic pressure or as it is for the case of Friction connections, by high strength bolts where the key parameters are the magnitude of the tighten torque, number and diameter of bolts.

The slip force is proportional to the normal force and the friction coefficient μ, a key parameter in friction connections that is dependent on the sliding surface materials. As demonstrated by Mualla and Belev (2002) in their investigation with passive response control systems based on the FDD, this type of systems present an stable hysteretic behavior when a proper friction pad material is used. According to Amontons laws (1699), for this type of devices, the frictional force is independent of the apparent surface of contact and is proportional to the normal applied action, therefore the classical Coulomb friction equation can be applied $F = u \cdot N$, where u represents the friction coefficient and N the normal force to calculate the slipping force F (figure 2.4).

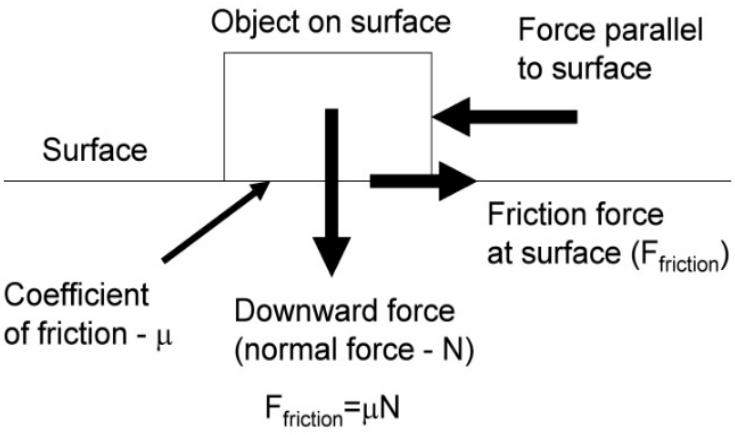

Figure 2.4 Basic scheme of friction coefficient.

The friction coefficient of the material is defined by experimental tests only, due to its dependency to different phenomena. The experimental work carried out by Latour et al. (2015) testing a set of 4 types of materials resulted in the finding that even though materials like steel can provide a high coefficient of friction, the behavior can be quite unstable. On the other hand materials like a hard rubber can develop a very stable behavior and high energy dissipation capacity even though they have a lower friction coefficient. Another experimental study carried out by Latour et al. (2014) investigated friction materials to be used as for supplemental damping devices clamped by high strength bolts under cyclic loading to be used in dissipative beam to column joints in Moment Resisting Frames, for six different interfaces: Steel-Steel interface, Brass-steel interface, sprayed aluminum-steel and three rubber based materials as friction pads between plates made of S275 steel. Aiming to obtain the static and dynamic friction coefficients, cyclic response under cyclic loads and energy dissipation capacity, the authors used different layouts of the sub-assemblies varying: the interface, tightening torque (200-550 Nm), the number of tightened bolts and type of bolt washers (flat washers or cone annular disc springs), the general scheme of the assembly used for all the tests is shown in figure 2.5.

For the steel based materials they found out that, the thermally sprayed aluminum on steel interface achieved a high value of friction coefficient and a cyclic response with small degradation as it is shown in figure 2.6. The rubber friction pads M0, a rubber based material used for automotive applications, exhibited a very stable behavior and high energy

dissipation capacity even for high levels of pre-loading as well as the hard rubber based material (M2), with the difference that in this case a lower value of the friction coefficient was measured. On the basis of all experimental results the authors concluded that three interfaces types seem more appropriate: *steel-steel, sprayed aluminum-steel and material M0-steel* those characterized by the higher values of the friction coefficient. For such interfaces, mathematical models to predict their cyclic response has been developed and compared with experimental test results indicating their accuracy. It was pointed out that use of friction pads made of steel plates with thermally sprayed aluminum could demonstrate a reasonable solution to improve the bending performance and the cyclic response of beam to column joints since it gives the highest initial friction coefficient and provides quite stable hysteresis loops with only small degradation.

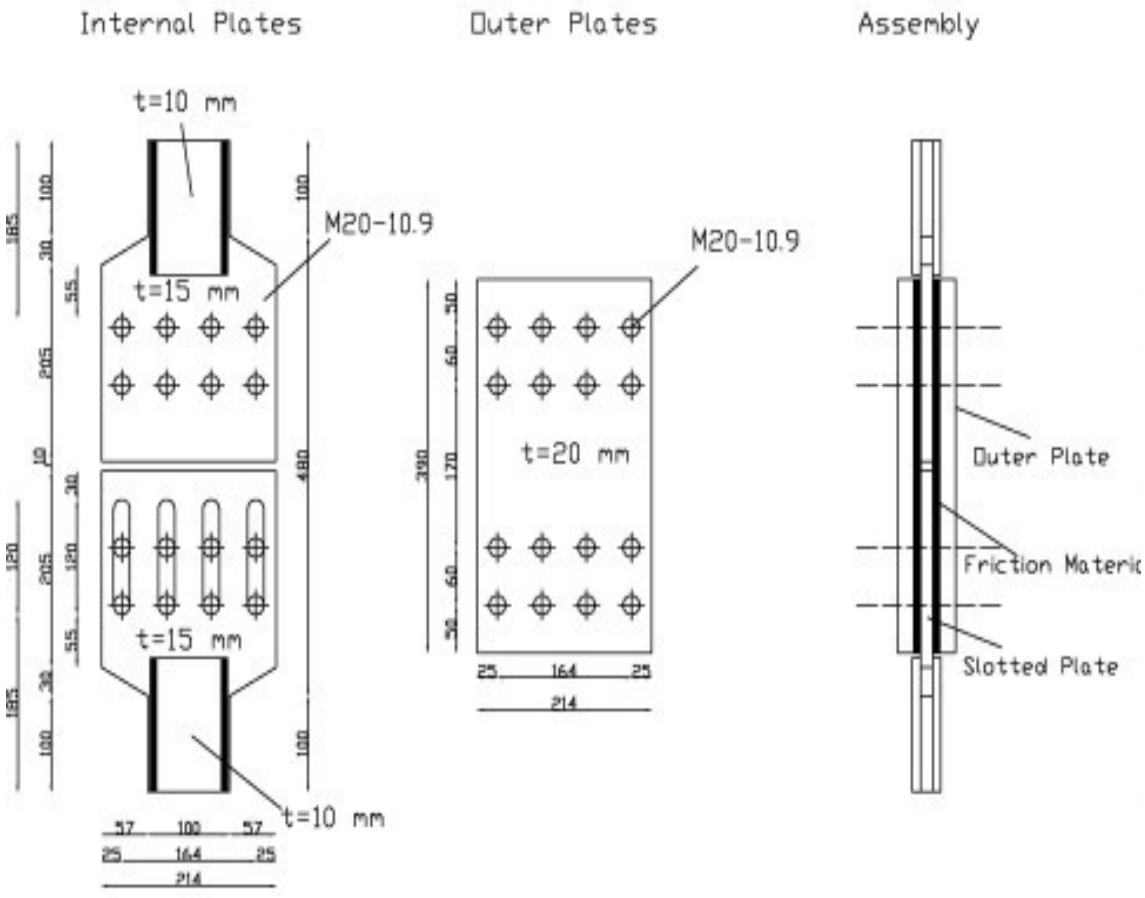

Figure 2.5 Scheme of the damping device tested, from Latour et al. (2014).

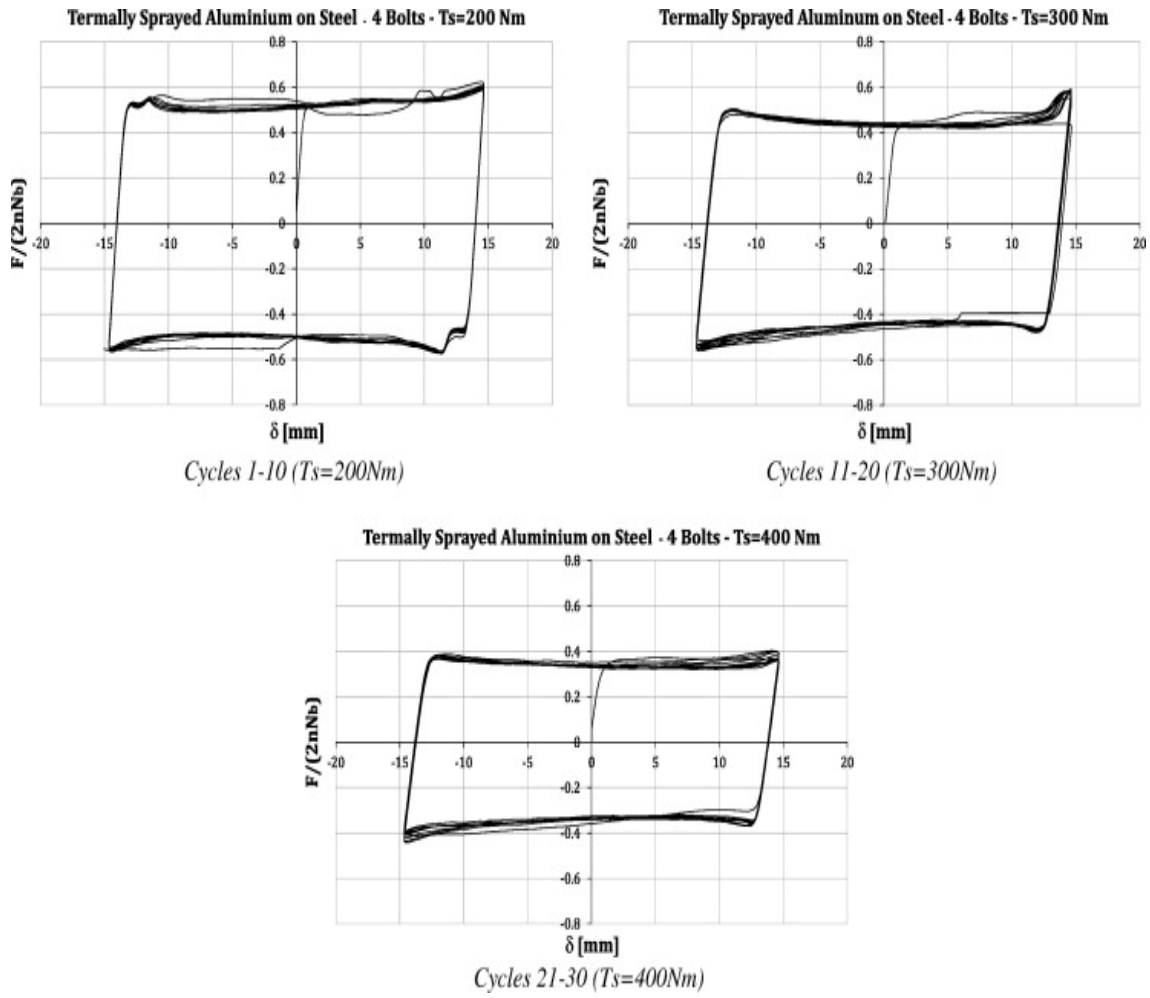

Figure 2.6 Friction coefficient-displacement curves for sprayed aluminum-steel interface, from Latour et al. (2014).

Experimental work done by Latour et al. (2011) studied two innovative solutions for double split tee beam-to-column connections (DST): by yielding devices and friction devices. They concluded that despite the different hardening behavior, the energy dissipation capacity of this joint typology is greater than that of both traditional T-stubs and dissipative T-stubs with an hourglass shape, up to the displacement range corresponding to the first 34 cycles.

Dissipative DST connections with interposed friction layers are characterized by stable hysteresis loops with low hardening, provided that the friction material is properly selected and the structural detail is properly designed, as can be seen in figure 2.7. In addition, the amount of the energy dissipation capacity of this innovative connection can be properly calibrated by acting on the friction resistance. Dissipative joints with friction material, after

inelastic cyclic rotations up to 0.06 rad, did not show any structural damage

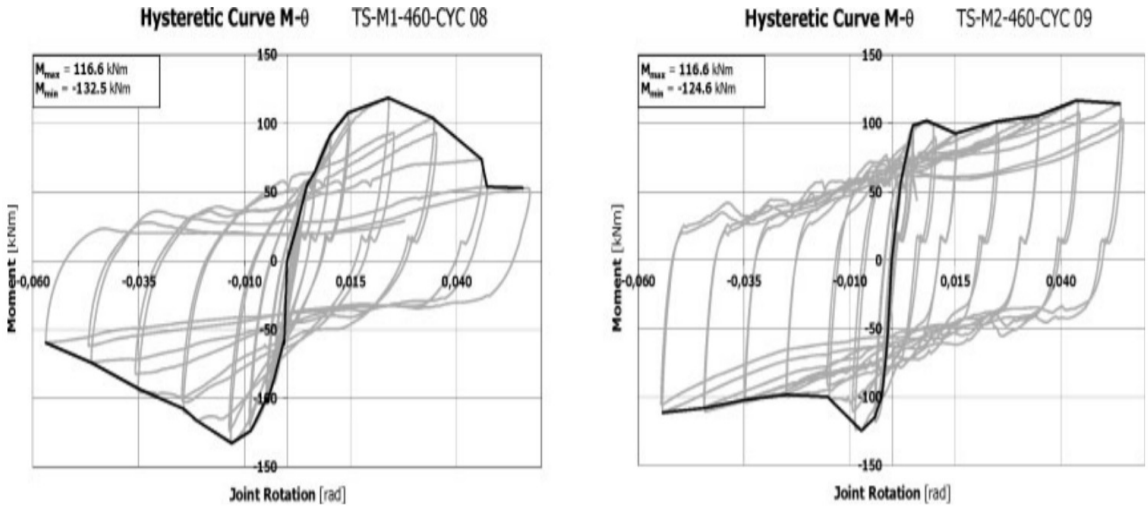

Figure 2.7 Moment-rotation curves of dissipative DST connections with friction pads, from Latour et al. (2011).

The hysteresis cycles obtained are similar to those of elastic-plastic dampers with high initial stiffness. This is the great advantage of friction devices, which can be designed to remain within the elastic range under the loading conditions corresponding to the serviceability limit states and to slip when energy dissipation is needed, the goal is to limit or avoid any damage in any joint component, with the exception of the friction pad. This means that this connection typology can be subjected to repeated cyclic rotation histories, i.e. to repeated earthquakes, by a simple replacement of the friction pad and, if needed, interposed friction pads are characterized by less hardening.

Another important issue that has been studied, is the preloading level of the bolts, therefore a key factor is to maintain, during its lifetime, the adequate preloading level. An inadequate preload in bolts can lead to unstable hysteresis loops and unpredictable dissipated energy (Latour et al., 2015). The experimental programs developed by Latour et al. (2015) evaluate the cyclic behavior of DST joints designed for dissipating the energy from seismic action in a couple of friction dampers located at the beam flanges level, the authors tested real scale external beam to column joints that were controlled by displacement in the experiment, a scheme of the tested joint is shown in figure 2.8

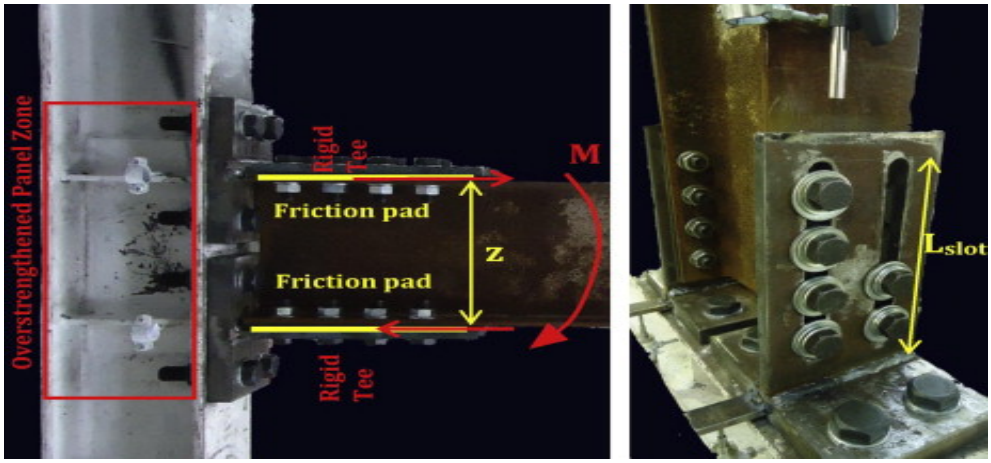

Figure 2.8 Scheme of the tested joint, from Latour et al. (2015).

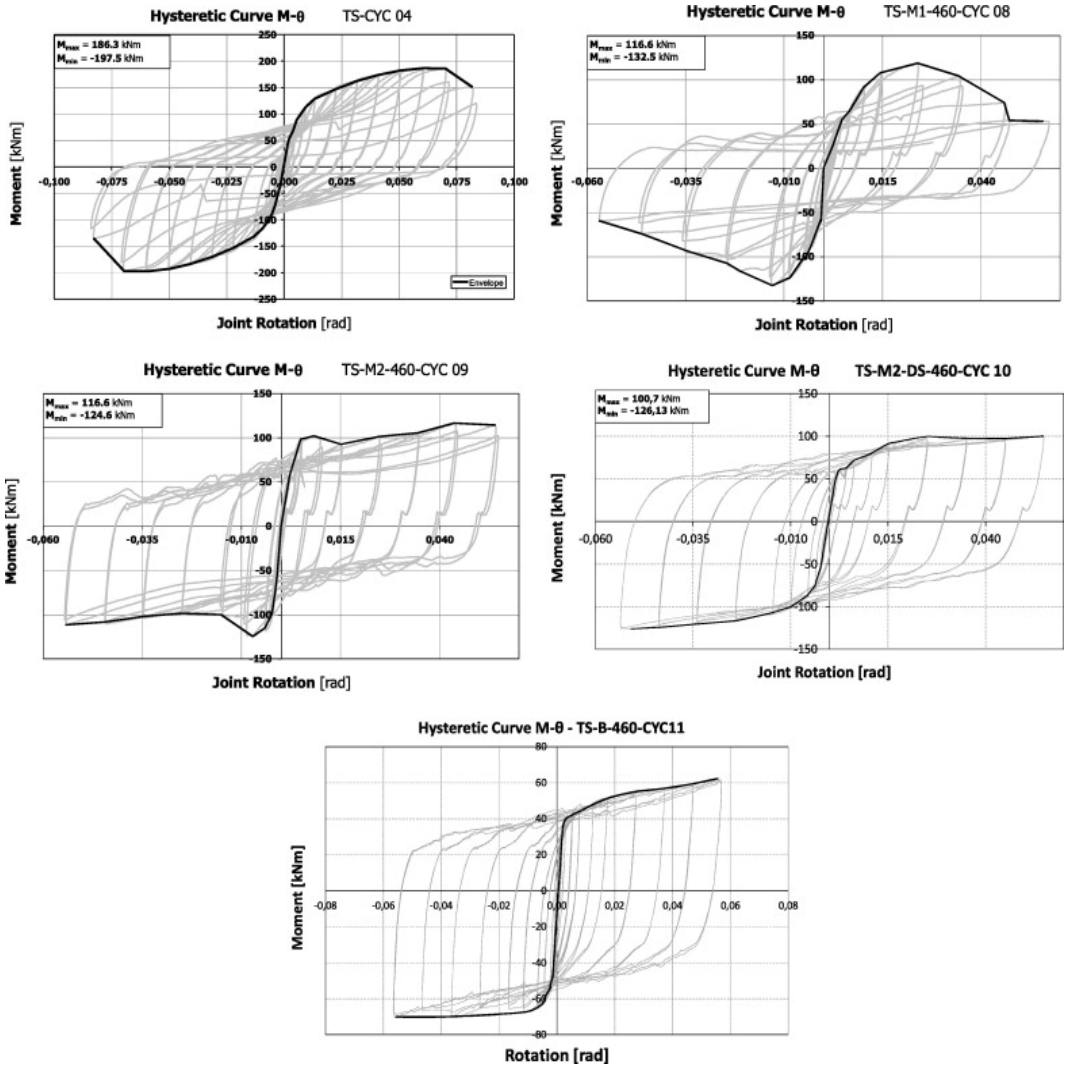

Figure 2.9 Hysteretic curves for tested joints, from Latour et al. (2015).

Authors have made comparison between this proposed innovative DST connection with friction pads and traditional DST connection, in terms of hysteretic characteristics under cyclic loading conditions. Figure 2.9 depicts the hysteretic behavior of the tested joints, where is possible to observe that some joints, after the slippage of the friction dampers, experienced pinching and strength degradation phenomena due to the reduction of the bolt preloading force after the fracture of the rubber plate.

Clifton et al. (2007) presented a Sliding Hinge Joint (SHJ) with an Asymmetric double sliding surface that is able to produce a non-rectangular hysteresis loop and study the behavior of the components influencing the sliding resistance and present a design model that is compared with the subassembly tests. In this joint typology the deformation occurs as shown in figure 2.10 with rotation about the top flange plate. Movements are largest at the bottom of the beam. The system dissipates energy by friction between the web-plate and the shims on either side of it, as well as between the bottom flange-plate and the shims either side of it. The beam shear force is carried in the bolts at the top of the web.

The design methodology presented in comparison with the test results showed that the calculated strength tends to be lower than the measured strength indicating that it may be suitable for design, but that an over strength factor of about 1.5 may be required for capacity design considerations. After comparing the behavior of the designed joint with the experimental tests, the authors found that the sliding hinge joint is a cost-effective solution for earthquakes-resistant structures, with little damage to the connection or the rest of the frame. A method to estimate the strength of the connection has been developed and when applied it gave results that compare well with both experimental tests.

Khoo et al. (2012) studied a Sliding Hinge Joint (SHJ), asymmetric friction connection (AFC) and selfcentering SHJ (SCSHJ). The later presents besides the property of the SHJ i.e. a low damage beam- column connection that rotates under design level earthquake through sliding ring springs as a self-centering component. The disc springs are designed for a percentage of total joint moment capacity, and have the role of reducing the residual displacement. This connection is known as the Self centering Sliding Hinge Joint (SCSHJ) and is depicted in 2.11.

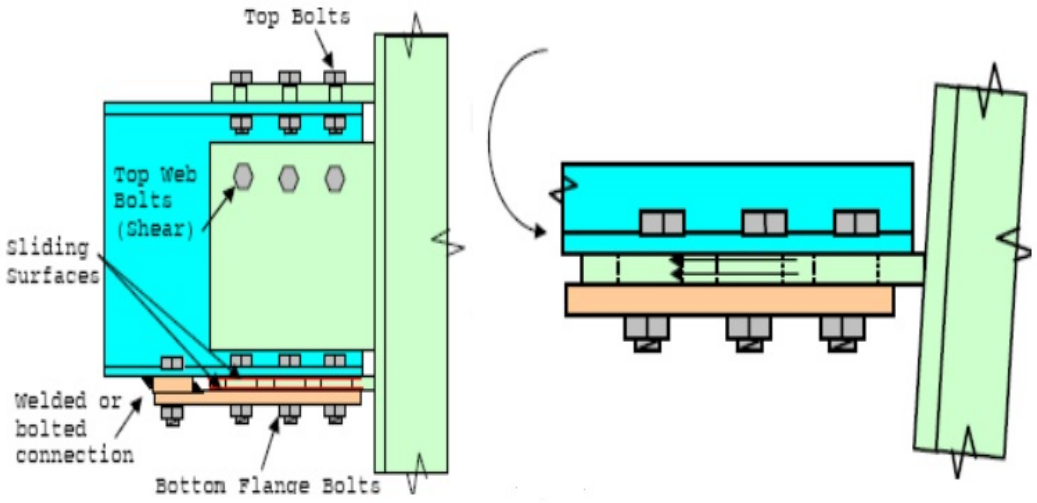

Figure 2.10 The Sliding Hinge Joint Details and Deformations (from Clifton et al. (2007)).

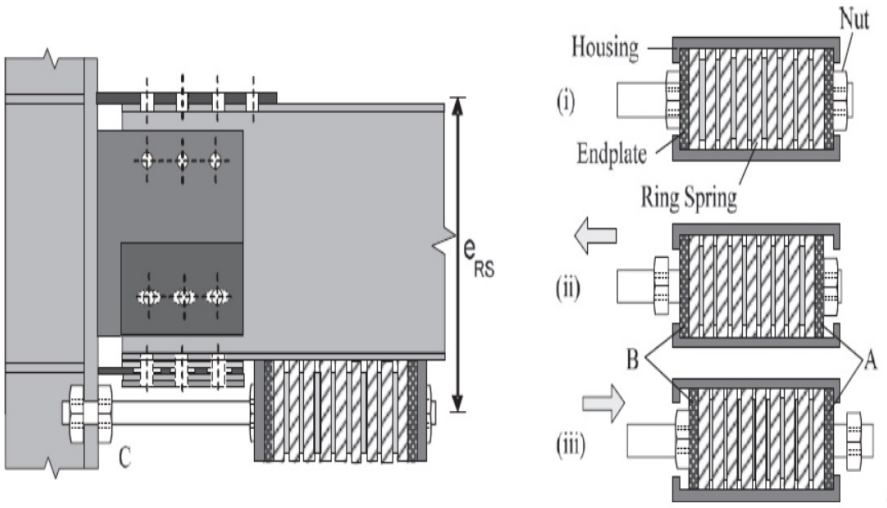

Figure 2.11 (Right) SCSHJ layout and (left) ring spring assembly (from Khoo et al. (2012)).

The SCSHJ aims to ensure the building is fully operational following a DLE shaking, through the use of friction damping ring springs manufactured by Ringfeder, Germany. In the SCSHJ the ring spring is designed as a percentage of total joint moment capacity (*Prs*), the aim is to reduce the frame residual drifts, after developing the experimental studies the authors found that there is an improvement in the flag-shape response (Moment rotation curves) while increasing the percentage of *Prs*, also the results showed that the rotational behavior about the top flange plate was shown to be effective in isolating the floor slab with minimal damage.

Few years later, Ramhormozian et al. (2014) showed that the Sliding Hinge Joint (SHJ) is capable of decouple joint strength and stiffness, limiting inelastic demands on both beams and columns and confining the yielding to bolts. This type of connection consists of 5 main components: the beams bottom flange, a bottom flange plate, cap plate and two shims all clamped by pre-tensioned bolts as is shown in figure 2.12. In the investigation, the authors used an improved washer called *Belleville*, along with disk springs and conical compression washers with the aim of investigate their effectiveness in keeping the pre-tension force in the bolts and avoid the relaxation of bolts during the sliding of the connection. It was shown that the washer was able to maintain most of the installed level of tension by pushing the bolts during sliding.

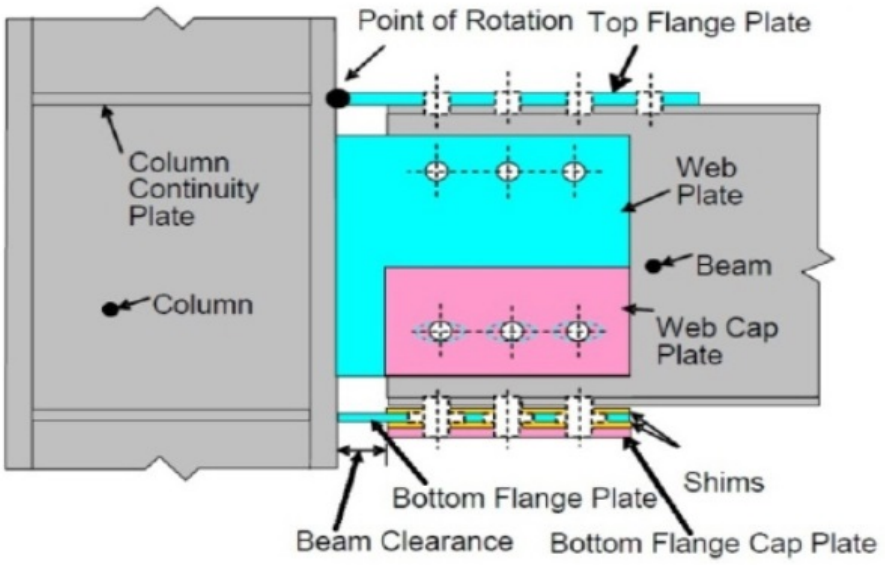

Figure 2.12 SHJ Setup with AFC components (Ramhormozian et al., 2014).

Later on, Khoo et al. (2013) studied the performance of the bottom and top flange components under multiple earthquakes, the components studied were the welds and plates which are subjected to inelastic demand during joint rotation under Design Level Earthquake (DLE). The authors found out that considering a clearance between column face and the beam end (SHJ), as developed by Clifton (2005), the SHJ can undergo at least 6 design level earthquakes events before the top flange plate fail in low-cycle fatigue, the current recommendations for design the top flange assure that there is no net elongation during joint

rotation in order to function as an effective pin and limit damage in the floor slab, as properly designed detailed and connected flange plates are not prone to low-cycle fatigue failure.

In an Asymmetric Friction Connection (AFC), able to develope non linear behavior through sliding between bolted plates while confining inelastic demand to the bolts, the sliding friction forces developed are dependent on the clamping force in the connection which is provided by fully tensioned bolts which pass through slotted holes. During a seismic event those bolts are subjected to moment and shear as well as axial force which reduces the clamping force on the sliding interfaces thereby reducing the sliding shear resistance (V_{ss}).

In order to investigate methodologies to evaluate the moment-shear-axial force interaction to calculate the sliding shear strength of the bolts, Khoo et al. (2015) proposed two design approaches: *Bolt model* and *Effective Coefficient of Friction method (ECoF)*, the authors evaluated and compared the results of 60 tests developed to improve the methodologies available, the tests were focused on bolts M16 to M24 and cleat thicknesses of 12 mmm to 25 mm, concluding that both methods can lead to similar results as those observed in the experimental tests and both can be used to calculate the V_{ss} (Slide shear capacity) for design purposes, the authors proposed to use a strength reduction factor of AFC of 0.75 and an over-strength factor of ?o,AFC of 1.4, the equations of both methodologies are shown in figure 2.14.

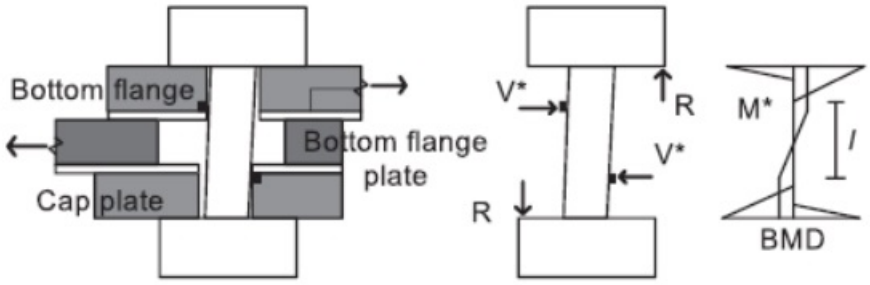

Figure 2.13 AFC idealised bolt deformation, external forces and bending moment distribution (from Khoo et al. (2015)).

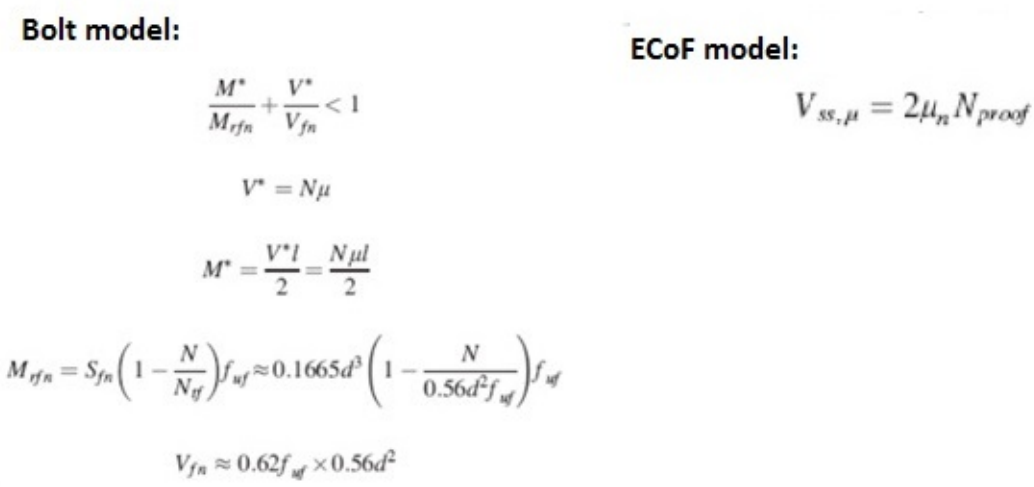

Figure 2.14 AFC sliding shear capacity calculation for Bolt model and ECoF method (from Khoo et al. (2015)).

One of the first investigations focused on applying this new Free From Damage (FFD) typology of connections, was developed by Piluso et al. (2014). FFD connections were applied to a MRFs aiming the goal of obtain free from damage structures, using beam to column connections equipped with friction pads, with the dissipative devices located at the end of the joints and dampers located at column base, looking to assure a damage prevention even when a global mechanism is completely developed, the goal of the proposed design procedure is the activation of all the friction dampers aiming the development of an energy dissipation mechanism characterized by the activation of friction dampers while the rest of the structures members remain in elastic range. By a rigorous design procedure based on second-order rigid plastic analysis in comparison with a Pushover and Incremental Dynamic Analysis, the authors concluded that the development of free from damage structures even for high seismic intensity values can be achieved. It is important to mention that the permanent lateral displacement is another issue to be studied although no structural damage is reached in the structures.

The behavior of the structures is not only rigid-plastic, displacements from elasto-plastic behavior should be taken into account, i.e. increase of second order effects that causes the increment of top sway displacement will result in decrease of horizontal force multiplier. Therefore, the design conditions should be realized to account for second order effects, thereby avoiding type-1-2-3 mechanisms as shown in figure 2.15

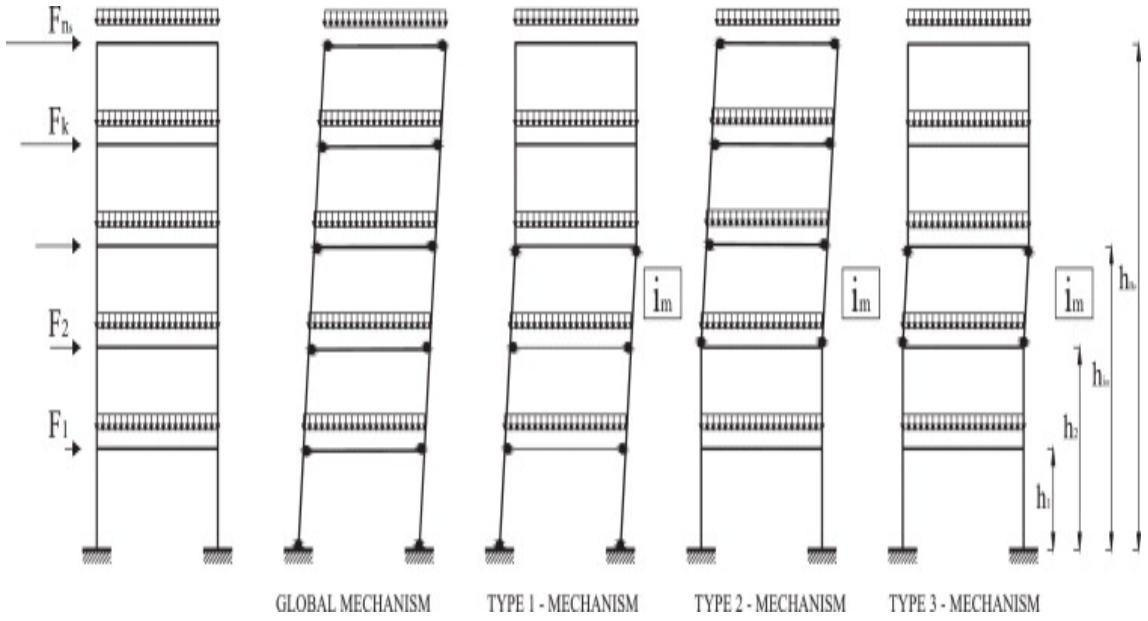

Figure 2.15 Collapse mechanism typologies (from (Piluso et al., 2014)).

The results obtained by the Push-over analyses reveal that the pattern of energy dissipation mechanism is in agreement with the global mechanism and softening behavior of Push-over curves correspond to mechanism equilibrium curve. In figure 2.16 (left) it is depicted the distribution of the *equivalent plastic hinges* which practically point out the activation of the corresponding friction dampers at the design displacement and in figure 2.16 (right) can be noted both the push-over curve that confirm the global mechanism.

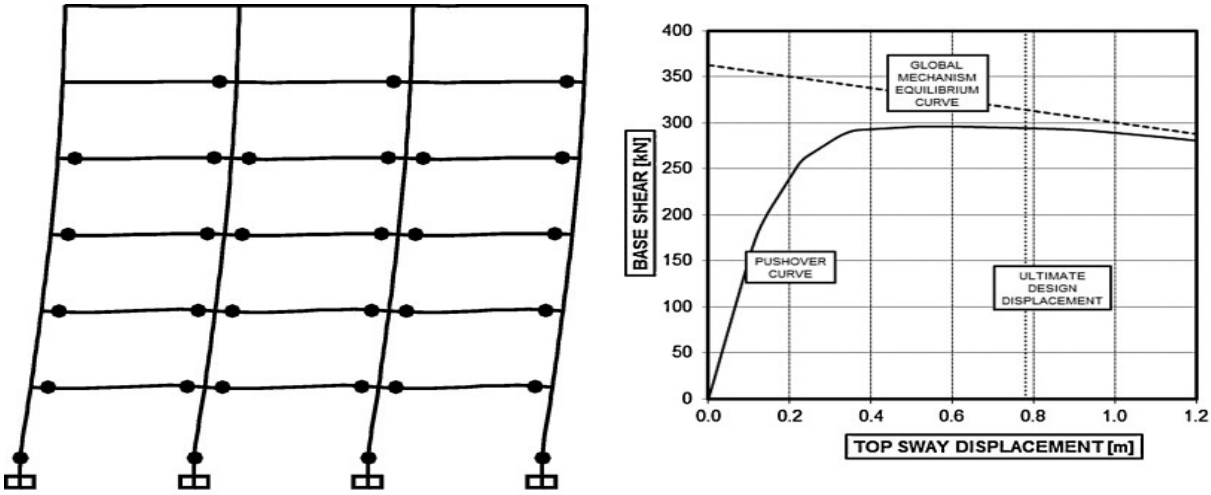

Figure 2.16 (R) Activation of friction dampers at the design displacement. (L) Push over curve (from Piluso et al. (2014)).

Later, Borzouie et al. (2015) developed an experimental test in order to apply base strong axis-aligned friction connection (SAFC) to evaluate the low damage requirement, considering modes of deformation involved in 2D horizontal deformation, in plane and out of plane loading. According to the experiment results columns have shown a stable behavior after several cycles for a drift of 4% in strong and weak axis directions without significant damage, requiring few or no replacement. Nevertheless another type of torsional demand developed, due to the alignment of the column base with the applied shear force, causing a twisting moment that can lead to floor twisting if many seismic columns deform in a similar way.

2.3 Innovative Moment Resisting Frame systems

Steel Moment Resisting Frames (MRFs) have long been recognized as effective earthquake resistant systems. As describe in the previous sections, the conventional design philosophy look for reliable mechanisms and stable energy dissipation capacities of the system. Consequently, beam ends, column bases and connections in a structure are allowed to develop inelastic deformations even simultaneously to balance the energy input of a strong ground motion in order to utilize the ductility of the steel MRFs. Although the life-safety goal can be achieved under intense earthquake events, a structure designed following the current philosophy may sustain inelastic deformations in most members, and significant unavoidable residual deformations. Hence, substantial economic loss due to repairing or demolishing work are expected. Another disadvantage of conventional MRFs is associated to its vulnerability to intense earthquakes, since the positive post-yielding stiffness cannot be ensured up to the maximum expected drift, especially when P- *Delta* effect is significant, leading to a possible collapse of the structure.

Many efforts have been dedicated to innovative MRFs for seismic performance enhancement. For instance, to reduce the residual deformation, self-centering MRFs structures implemented with post-tensioned connections (Lin et al., 2012; Reyes-Salazar et al., 2016) or other devices were developed, and their re-centering behavior was validated by experimental investigations. In parallel with these studies, innovative compound steel MRFs installed with various energy dissipation devices or fuses were investigated extensively, and

they were able to achieve the expected damage-control behavior and controllable failure modes when subjected to an earthquake event. Some of this works include a combination of systems, to mention some, Tzimas et al. (2016) highlighted the benefit of combining the post-tensioning and supplemental viscous damping technologies in the near-source fault by achieving significant reductions in collapse risk and probability of exceedance of residual story drift threshold values compared to the conventional MRFs. Rules for capacity design for this innovative systems have been studied in order to achieve the desired behavior of the frames, for instance the work of Karavasilis (2016) highlighted the importance to differentiate the design capacity rules for high-performance steel MRFs with viscous dampers when drift performance is assumed different as for typical steel MRFs.

Other type of innovative MRFs include the use of High Strength Steel in combination with dissipative members or connections, the experimental work of Ke and Chen (2016) studying MRFs composed of high strength steel (HSS) members and energy dissipation bays (EDBs) showed that those systems can exhibit damage-control behavior and insignificant increase of residual drift in the damage-control stage, verifying an improvement in the damage-control when compare with conventional steel MRF systems. A more common system known as *dual-steel* frames was studied by Tenchini et al. (2014), using High Strength Steel (HSS) in non-dissipative members and Mild Carbon Steel (MCS) in dissipative zones, with the aim of controlling the global frame behavior into a ductile overall failure mode. The authors showed that the use of HSS in EC8 compliant MRFs is effective to provide overall ductile mechanism, but it may lead to inefficient and uneconomical structures characterized by limited plastic demand due to the large design overstrength achieved by fulfilling the codified drift requirements, but highlighting the improvement of dual steel frames to guarantee a better control of plastic mechanism than single grade steel frames at near collapse limit state.

Friction devices adopted in combination with MRFs were studied by Güneyisi et al. (2014), with friction damped tension-compression diagonal braces, the authors pointed out that the application of friction damped braces allowed a reduction of damages to the main structural elements, thus significantly improving the seismic behavior of the frame. Many other studies are been developed in order to improve conventional MRFs systems with excellent outcomes, as this work may be part of those innovative structural developments.

3 Design Methodologies for Moment Resisting frames

3.1 Steel Moment Resisting Frames and compliance criteria according to EN 1998-1 section 6

For a regular moment frame (regularity conditions are described in EN 1998-1 section 4.2.3), the seismic design scenario can be summarized in an elastic analysis that incorporates lateral story forces determined according to the *Base Shear (V_b)*, which is a function of:

- Spectral design acceleration $S_d(T)$ in function of the natural period of the structure according to the soil type (EN 1998-1 section 3.2.2), type of elastic spectra and behavior factor (q).

- Seismic mass (m) consisting in the unfactored dead load (self weight and additional dead loads in the structure) and a portion of the imposed load (EN 1998-1 section 4.2.4).

After obtaining the results from the elastic analysis, EN 1998-1 specifies a set of code checks to ensure that capacity design is satisfied. Code requirements are describe in the following sections.

3.1.1 Capacity Design of members

Besides a number of required verifications for dissipative zones at beam ends, the main concept of capacity design criteria in a Moment-Resisting Frame is related to the so called

Weak beam -Strong Column behavior, therefore a typical application of this rule used in most of the seismic codes has the following form:

According to section 6.6.3 of EC8, the design bending moment ($M_{Ed,col}$) for columns can be obtained from the equation 3.1

$$M_{Ed,col} = M_{Ed,G} + 1.1 \cdot \gamma_{ov} \cdot \Omega \cdot M_{Ed,E} \tag{3.1}$$

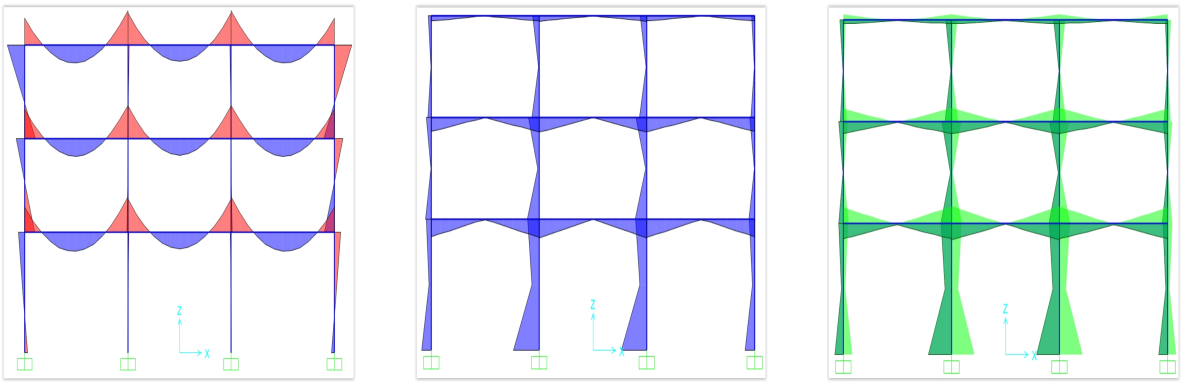

(a) Gravity loads ($M_{Ed,G}$). **(b)** Lateral Load ($M_{Ed,E}$). **(c)** Resultant moment (M_{Ed}).

Figure 3.1 Moments due to gravity and lateral loading components in the seismic situation.

Where:

- $M_{Ed,G}$ and $M_{Ed,E}$ are the bending moments due to the gravity loads and seismic forces respectively as shown in figure 3.1.
- Ω is the beam over-strength factor, calculated as the minimum value of $\Omega_i = M_{pl,Ed,i}/M_{Ed,i}$ for all the beams in which dissipative zones are located where $M_{Ed,i}$ is the total design moment, as a combination of gravity and seismic loads, for the i beam and $M_{pl,Ed,i}$ is the corresponding plastic moment.
- The material over-strength factor γ_{ov} represents the ratio of actual to design yield strength of steel, EC8 recommends a value of 1.25 in the absence of measurements.
- The 1.1 magnification factor takes into account other material effects such as strain hardening and strain rate.

3.1.2 Stability and Drift criteria

EC8 requirements for deformation are based on *second order effects* and *inter story drifts*, which is related to the damage limitation (serviceability) condition described in section 2.1. In EN 1998-1 section 4.4.2.2(2), second - order (P-Δ) effects are specified through an inter-storey drift sensitivity coefficient (θ) given as:

$$\theta = \frac{P_{tot} \cdot d_r}{V_{tot} \cdot h} \tag{3.2}$$

where:

- P_{tot} and V_{tot} are the total cumulative gravity load and seismic shear, respectively, at the storey under consideration.
- h is the storey height.
- d_r is the design inter-storey drift as a product of elastic inter-storey drift from analysis and behavior factor (q).

According to EN 1998-1 section 4.4.2.2(3) and (4), instability is assumed beyond $\theta = 0.3$ and is considered as an upper limit. If $\theta \leq 0.1$, second-order effects could be ignored, but for $0.1 < \theta \leq 0.2$, $P - \Delta$ may be approximately accounted for in seismic action effects through the multiplier $\alpha = \frac{1}{1-\theta}$.

For serviceability verifications, d_r is limited proportionally to h, in the general form, equation 3.3 should verify:

$$d_r \cdot \nu \leq \psi \cdot h \tag{3.3}$$

EN 1998-1 section 4.4.3.2 specifies a set of different values for ψ, suggested as 0.5%, 0.75% and 1% for brittle, ductile or non-interfering non-structural components, respectively; ν is a reduction factor which accounts for the smaller more-frequent earthquakes associated with serviceability (10% of probability of occurrence in 10 years, or a return period of 95 years), recommended as 0.4-0.5 depending on the importance class.

The deformation criteria stipulated in EC8 covers all types of buildings, for the case of Moment Resisting Frames, due to their inherent flexibility, it becomes particularly important when designing cross sections of columns and beams. The above deformation criteria are

indicate for all building types but, as expected, they are particularly important in moment frames due to their inherent flexibility. This has direct implications on seismic design as discussed below. It is worth noting that EC8 requirements for θ are quite stringent in comparison with other codes; the same applies to inter-storey serviceability drift, particularly if the lower limit of 0.5% is adopted in design.

3.2 Design Methodology for Moment Resisting Frames with Friction Connections

3.2.1 Free From Damage Connections - Design procedure A for steel MRFs (compliance criteria)

A step by step design procedure for Moment Resisting Frames (MRFs) is presented for frames equipped with friction joints considering the design procedure developed by the University of Naples "Federico II", hereafter named Design Procedure a (DP-A). A general design procedure can be summarized as follows:

1. Modelling the frame, using frame elements for a 3D or 2D simplified model, considering additional masses due to the geometrical configuration of the building (number of MRFs in plant, direction of secondary beams and gravity loads).

2. Design the initial sections considering Drift limits, EN 1998-1 Damage Limitation requirements may be take into account, EN 1998-1 section 4.4.3.

3. Evaluate the design forces for the seismic combinations, considering different factors for seismic loads according to the type of friction joint, namely consider the over-strength factor (Ω_u) for the design of non-dissipative elements.

4. Design of joints as dissipative elements, direct loads obtained for seismic and gravitational combinations may be take into account.

5. Strength and stability verification of structural elements may be reviewed according to EN 1991-1 as for the traditional design of MRF's.

For the current design approach, the dissipative element is the joint, hence the connection will be design with the forces obtained form the seismic combination. Therefore, beams and columns as non-dissipative elements will be design with an over-strength with respect of the joint considering two main sources of over-strength for this type of connection:

- High pre-tension in bolts at the early stages of the connection, right after the pre-stressing of bolts and for a short period of time the tension in the bolts is higher than the amount of tension that will remain for the life time of the building.

- Hardening of the friction pad, experimental results showed that when cyclic loads are developed in the connection, the dynamic friction coefficient of the pad can vary than the value for a static friction, usually the static friction coefficient is higher than the cyclic value, therefore, it becomes a source of over-strength to take into account for the non-dissipative elements.

Considering the previous phenomena in a friction connection, the over-strength factor for non-dissipative elements known as Ω_u takes a value of 2 to take into account in the verification of sections for the MRF. The seismic load may be take into account as described in section 2.1 (EN 1998-1 section 3.2) as well as the behavior coefficient q (EN 1998-1 section 6.3.2). Permanent and live loads may be take into account with their respective load combination coefficients ($\psi_{2,i}$) and seismic mass participation factors ($\Psi_{E,i}$) according to EN 1990 Annex A and EN 1998-1 section 4.2.4 respectively. Seismic combinations for ULS verifications according to EN 1990 can be considered in the general form as:

$$\sum G_{k,i} + \sum \Psi_{2,i} \cdot Q_{k,i} + A_{Ed} \tag{3.4}$$

The strength and stability regular verifications for beams and columns are conducted according to EN 1993-1. For serviciability verifications, the load combinations are as shown in eq. 3.5 considering the design seismic actions multiplied by $\upsilon \cdot q$ to verify the inter-storey drift:

$$\sum G_{k,i} + \sum \Psi_{2,i} \cdot Q_{k,i} + \upsilon \cdot q \cdot A_{Ed} \tag{3.5}$$

P-Δ effects must be take into account as described in section 3.1.2, considering the limits for $0.1 < \theta \leq 0.2$ and the magnification factor for seismic loads $\alpha = \frac{1}{1-\theta}$; also torsional

effects may be take into account as described in EN 1998-1 section 4.3.3.2.4.

Joints are designed as dissipative elements using the forces obtained directly from the elastic analysis for the seismic combinations, therefore the conditions shown in equations 3.6, 3.7, 3.8 need to be satisfy to fulfill this criteria:

$$\frac{M_{Ed}}{M_{j,Rd}} \leq 1 \tag{3.6}$$

$$\frac{V_{Ed}}{V_{j,Rd}} \leq 1 \tag{3.7}$$

$$\frac{N_{Ed}}{N_{j,Rd}} \leq 0.15 \tag{3.8}$$

Where M_{Ed}, V_{Ed}, N_{Ed} are the design bending moment, shear force and axial force for the seismic combination and $M_{j,Rd}, V_{j,Rd}, N_{j,Rd}$ are the design resistance for bending, shear and axial force of the joint. In order to involve the beam in the energy dissipation mechanism, the condition shown in eq. 3.9 should be satisfied in order to verify that the bending moment developed in the joint is less than 80% of the beam plastic capacity ($M_{j,Rd}$):

$$\frac{M_{b,Rd}}{M_{j,Rd}} \geq 1.25 \tag{3.9}$$

Global verification for capacity design for both Beams and Columns must satisfy equations 3.10, 3.11 and 3.12:

$$N_{Ed} = N_{Ed,G} + \Omega_u N_{Ed,E} \tag{3.10}$$

$$M_{Ed} = M_{Ed,G} + \Omega_u M_{Ed,E} \tag{3.11}$$

$$V_{Ed} = V_{Ed,G} + \Omega_u V_{Ed,E} \tag{3.12}$$

Where:

- $M_{Ed,G}$ and $M_{Ed,E}$ are the bending moments due to the gravity loads (considering seismic combination factors) and seismic forces respectively, seismic forces are calculated considering the magnification factors due to torsional effects and stability verification in the necessary case.
- Ω_u is the joint over-strength factor as discussed before, calculated considering the two main sources of over-strength in the join taking a value of 2.

For columns, special consideration must be take into account to control the level of shear

force at 50% of its capacity avoiding the possibility of a brittle failure.

Local verification for hierarchy requirements must be fulfill for the column- joint, the later is described in eq. 3.13. Figures 3.3 and 3.4 summarize the design procedure.

$$\sum M_{Rc} \geq \Omega_u \sum M_j + \sum (V_i \cdot \frac{d_c}{2}) \tag{3.13}$$

where:

- $\sum M_{Rc}$ is the sum of the design values of the resistance moments of the columns at the node.
- $\sum M_j$ the sum of the design moments of the connections, directly taken from the seismic combinations as a result of the static analysis.
- $\sum (V_i \cdot \frac{d_c}{2})$, is the design shear force of the connection directly taken from the seismic combination and d_c is the distance from the axis of the column to the face of the joint as shown in figure 3.2.

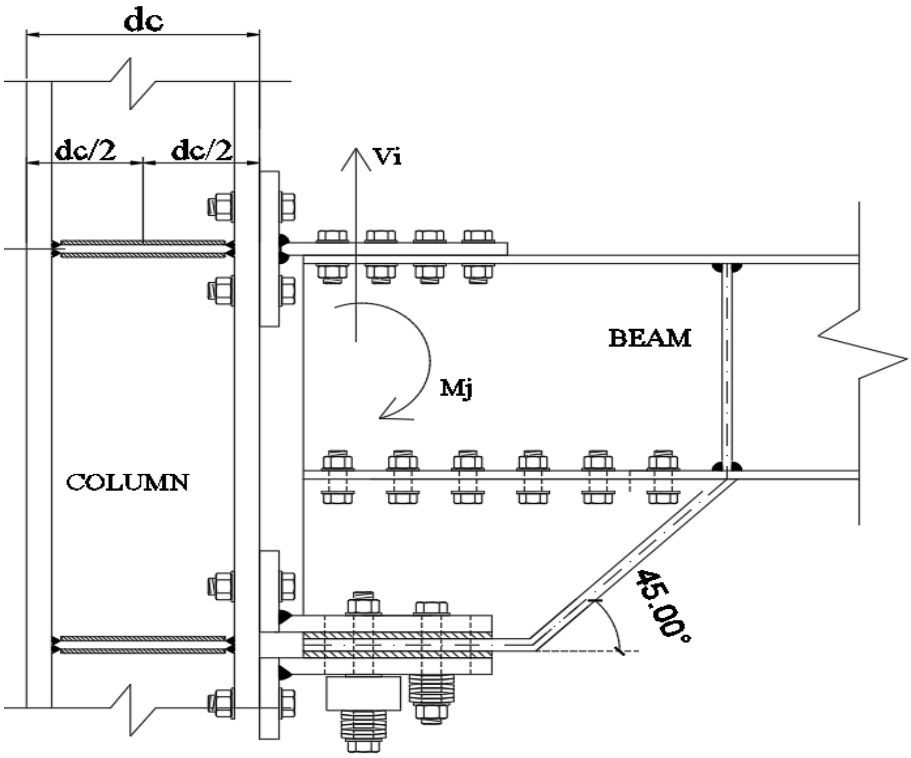

Figure 3.2 Joint forces configuration for local verification for hierarchy requirements.

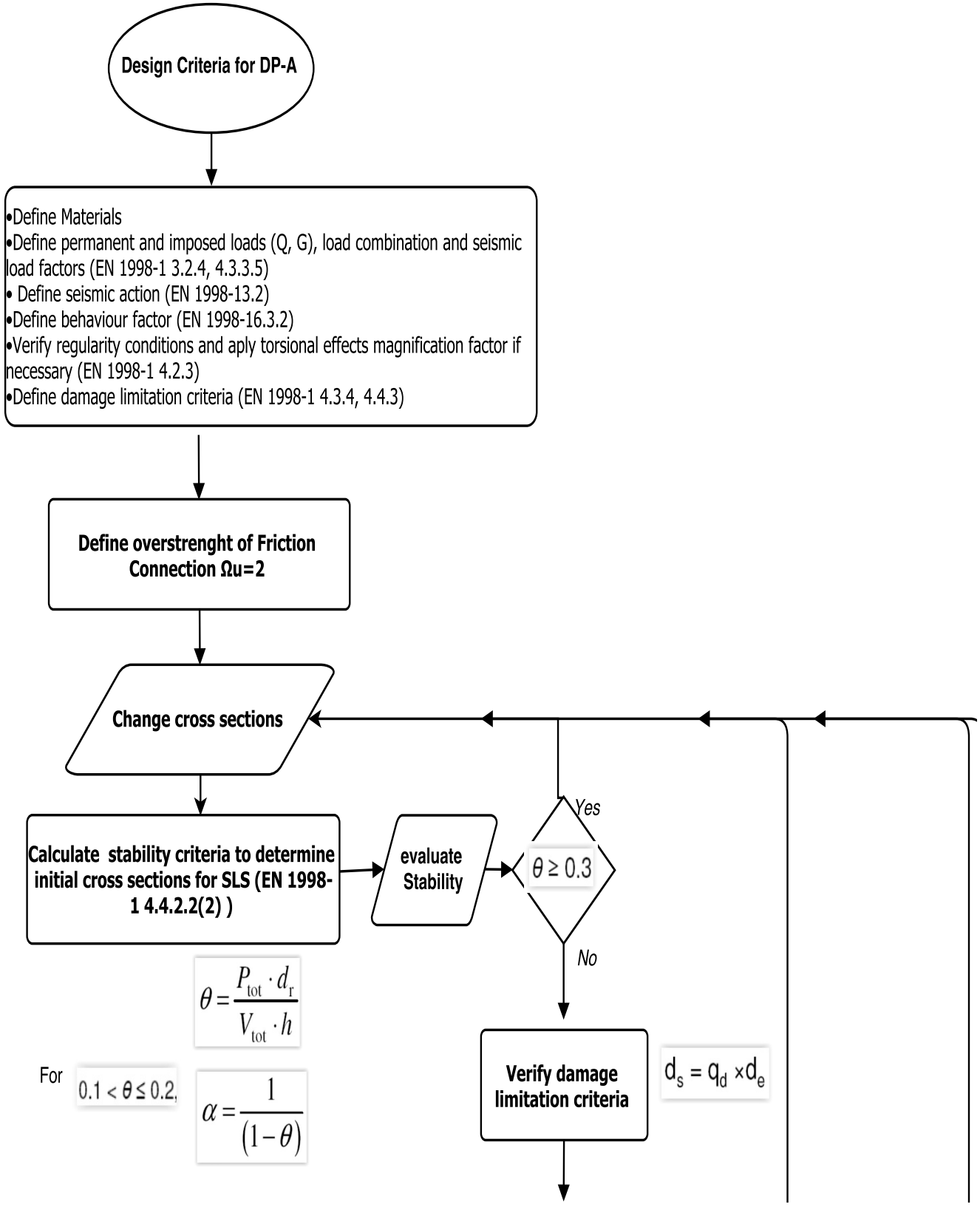

Figure 3.3 Design methodology for FFD-Naples Workflow

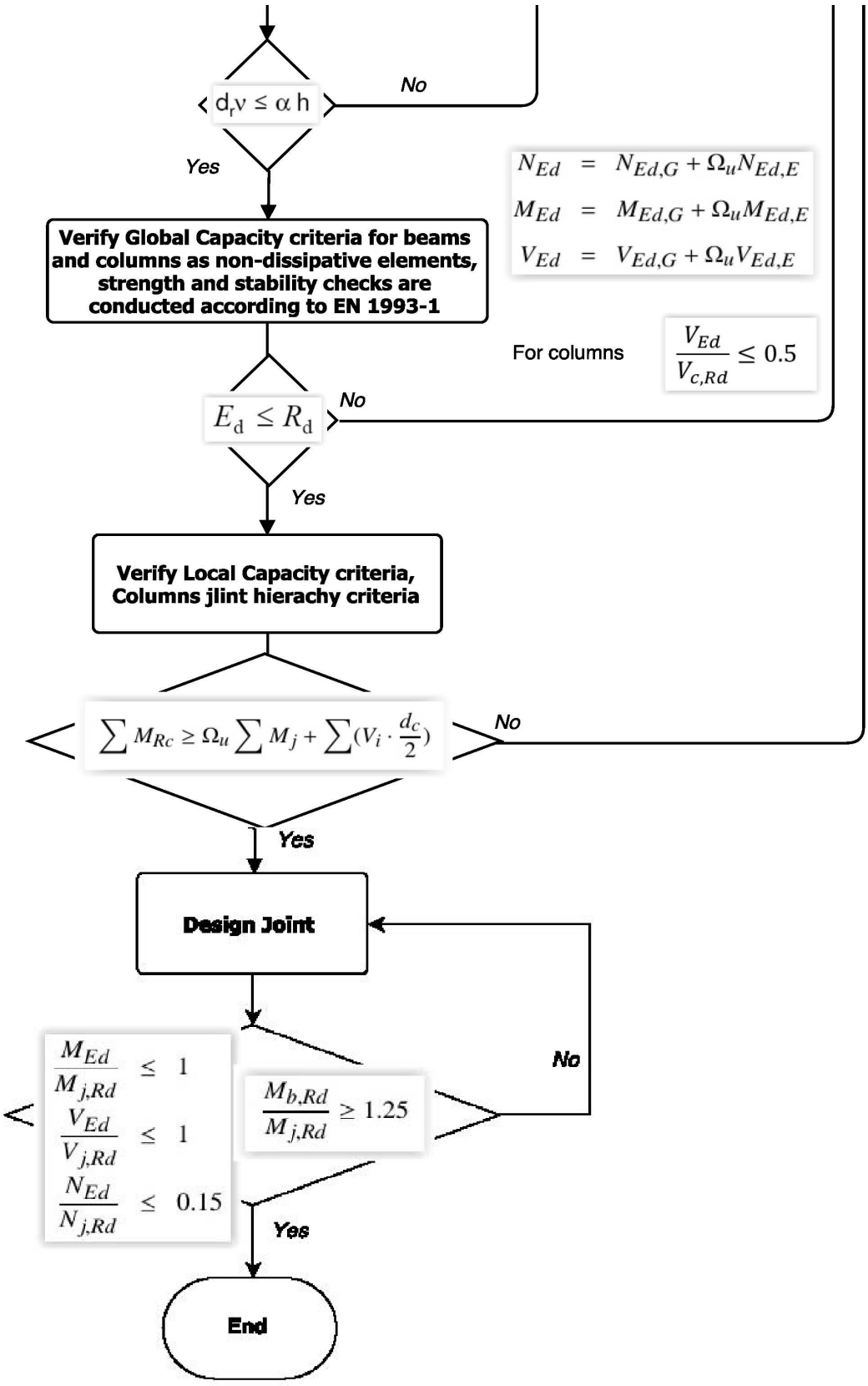

Figure 3.4 Design methodology for FFD-Naples Workflow.

3.2.2 Free From Damage Connections - Design Procedure B for steel MRFs (compliance criteria)

The initial consideration for the Design approach for DP-A for Seismic load, combination, torsional effects and stability verifications must be followed for Serviciability Limit State, the difference with the previous design approach is for the Capacity design (ULS) i.e. Global and local verifications of the frame, for both beams and columns, that must satisfy equations 3.14, 3.15 and 3.16:

$$N_{Ed,c} = N_{Ed,c,G} + \Omega_u \cdot \Omega_b N_{Ed,c,E} \tag{3.14}$$

$$M_{Ed,c} = M_{Ed,c,G} + \Omega_u \cdot \Omega_b M_{Ed,c,E} \tag{3.15}$$

$$V_{Ed,c} = V_{Ed,c,G} + \Omega_u \cdot \Omega_b V_{Ed,c,E} \tag{3.16}$$

Where:

- $M_{Ed,c,G}$ and $M_{Ed,c,E}$ are the bending moments due to the gravity loads (considering seismic combination factors) and seismic forces respectively for the column, seismic forces are calculated considering the magnification factors due to torsional effects and stability verification in the necessary case.

- Ω_u is the joint over-strength factor as discussed before, calculated considering the two main sources of over-strength in the join taking a value of 2.

- Ω_b is a beam over-strength factor, calculated as the minimum value of $\Omega_b, i = M_{pl,Ed,b,i}/M_{Ed,b,i}$ for all the beams part of the MRF system $M_{Ed,b,i}$ is the total design moment, as a combination of gravity and seismic loads, in beam i and $M_{pl,Ed,b,i}$ is the corresponding plastic moment.

For columns, special consideration must be take into account to control the level of shear force at 50% of its capacity avoiding the possibility of a brittle failure.

For beams that form part of the MRF, the Global Capacity verification must satisfy

equations 3.17, 3.18 and 3.19:

$$N_{Ed,b} = N_{Ed,b,G} + \Omega_u \cdot N_{Ed,b,E} \quad (3.17)$$

$$M_{Ed,b} = M_{Ed,b,G} + \Omega_u \cdot M_{Ed,b,E} \quad (3.18)$$

$$V_{Ed,b} = V_{Ed,b,G} + \Omega_u \cdot V_{Ed,b,E} \quad (3.19)$$

Where:

- $M_{Ed,b,G}$ and $M_{Ed,b,E}$ are the bending moments due to the gravity loads (considering seismic combination factors) and seismic forces respectively for the column, seismic forces are calculated considering the magnification factors due to torsion effects and stability verification in the necessary case.

- Ω_u is the joint over-strength factor as discussed before, calculated considering the two main sources of over-strength in the join taking a value of 2.

Local verification for hierarchy requirements must be fulfill for the column- joint, the former implies eq. 3.20, 3.21, 3.22 and 3.23:

$$\sum M_{Rd,col} \geq \Omega_u \sum M_{con} \quad (3.20)$$

$$\sum M_{con} = \sum M_{j,node} + \sum (V_j \cdot (S_h + \frac{d_c}{2})) \quad (3.21)$$

$$M_{j,node} = 0.8 \cdot M_{pl,beam} \quad (3.22)$$

$$V_j = \frac{2 \cdot M_j}{L*} + V_{G,b} \quad (3.23)$$

where:

- $\sum M_{Rd,col}$ is the summation of the design values of the moments of resistance of the columns at the node.

- $\sum M_{con}$ is the summation of the connection moments at the node considering also shear force developed by joint connection.

- Ω_u is the joint over-strength factor as discussed before, calculated considering the two main sources of over-strength in the join taking a value of $\Omega_u = 2$.

- $\sum M_{j,node}$ the sum of the design moments of the connections, taken as a percentage, 80% for this case, of the Plastic Moment of the beams $M_{pl,beam}$ part of the MRF and the dissipative connection.

- V_j, is the design shear force of the connection, calculated as the summation of the design moments of the joint at both extremes of the beam divided by the length between the interior faces of the connection as shown in figure 3.5 and the shear force in the beam produced by the gravity loads ($V_{G,b}$).

- S_h is the lenght of the haunch and d_c is the distance from the axis of the column to the face of the joint as shown in figure 3.6.

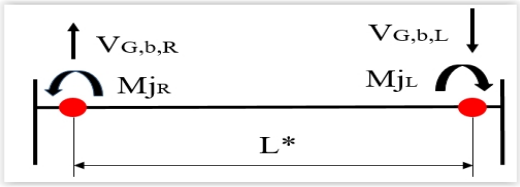

Figure 3.5 Sketch of beam and developed forces in the FD-Connection.

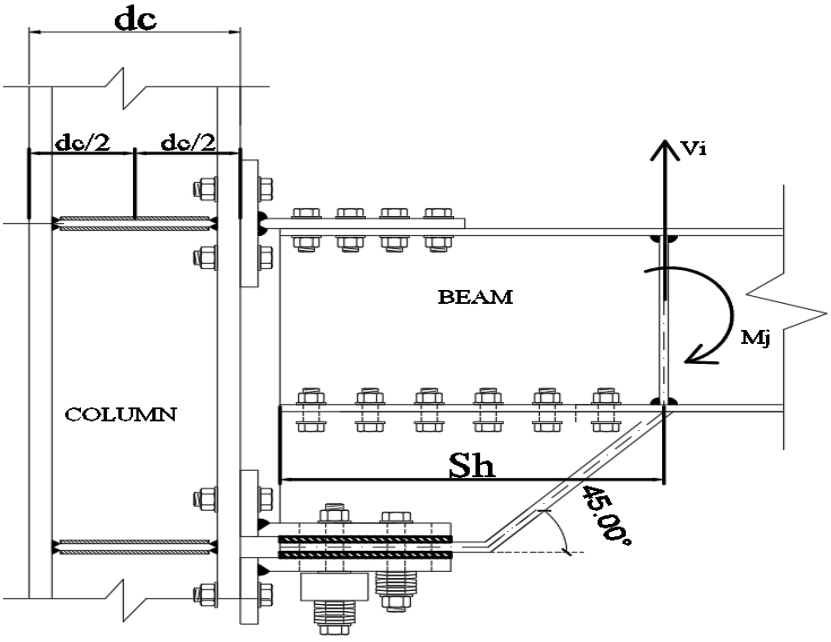

Figure 3.6 Joint forces configuration for local verification for hierarchy requirements.

Figures 3.7 and 3.8 summarize the design procedure.

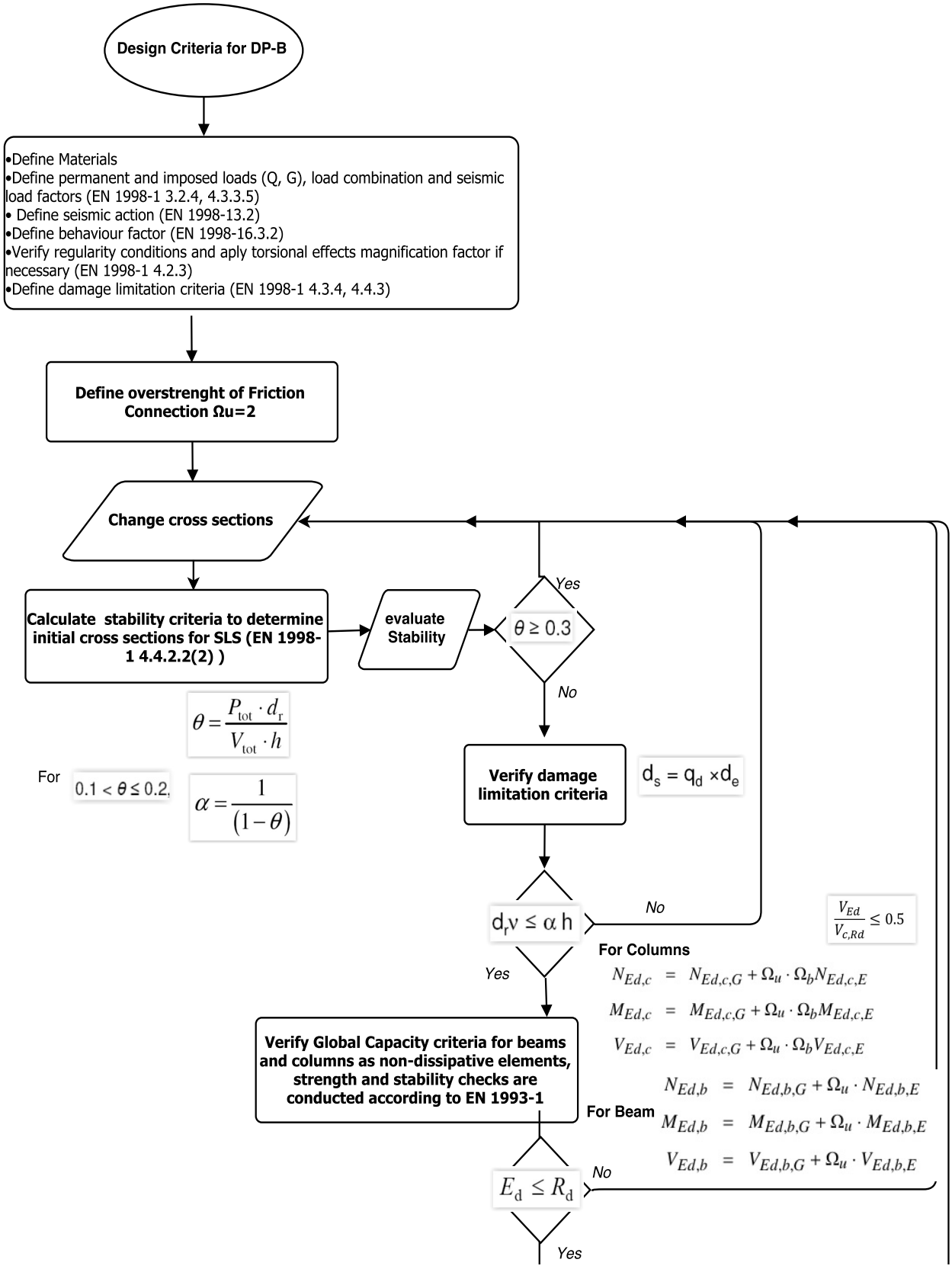

Figure 3.7 Design methodology for FFD-Salerno Workflow

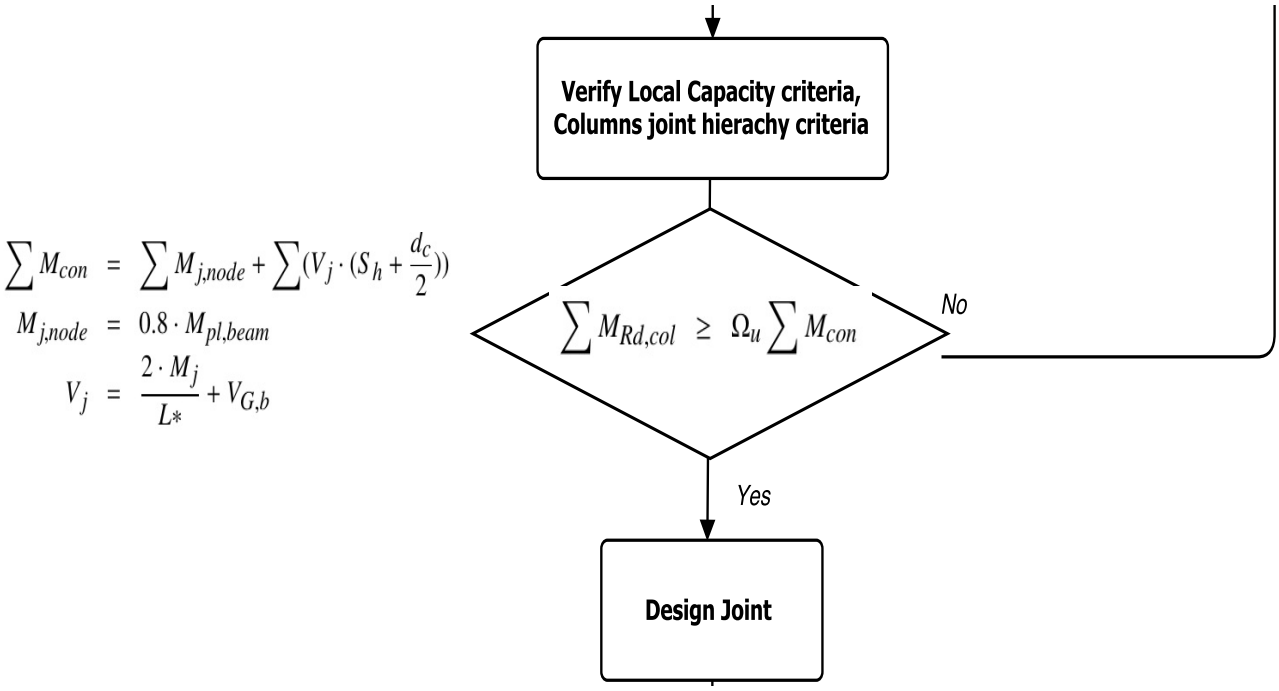

Figure 3.8 Design methodology for FFD-Salerno Workflow

4 Parametric Study

4.1 Moment Resisitng Frames characteristics and design parameters

In order to study the performance of the Moment Resisting Frames (MRFs) designed considering Friction Connections with the methodology developed by University of Naples "Federico II" hereafter called *Design Procedure A* (DP-A) and University of Salerno of Italy, in this paper named as *Design Procedure B* (DP-B), compared with the current design methodology described in EN 1998-1 (named as EC8), several frames were studied by Non-linear Static (Pushover) Analysis and non-linear Time History (IDA) analysis developed with SeismoStruct software. Initially the frames were design according to the requirements of the three design methodologies, as described in sections 2.1, 3.2.1 and 3.2.2.

The varying parameters for the investigated frame typologies are as follows:

- Three storeys MRFs.
- Two variations for the number of spans per frame are considered: 3 and 5.
- Two variations for the span length 6m and 8m.
- Two hazard levels are considered: a medium seismicity level (PGA = 0.25g) and a high seismicity level (PGA = 0.35g).
- The story height for all the frames is typically considered as 4.5 m for the first (ground) storey and 3.5 m for all upper storeys. No basements are considered and the bases of

ground, storey columns are assumed to be fully fixed.

The parameters for each frame typology are summarized in table 4.1. The storey plan is square with uniform span lengths in both principal directions for the case of 3-span frames and rectangular (5 by 3 bays) for the case of 5-span frames.

Table 4.1 Structural configuration for Moment Resisting frames of 3 storeys.

Structural configuration						
Frame Description -	**No. of stories**	**No. Bays**	**Span Length**	**PGA %g**	**Type of Connection**	**Design aproach**
MRF-3-3-6-MH-EC8	3	3	6	0.25	Rigid	EC8
MRF-3-3-6-HH-EC8	3	3	6	0.35	Rigid	EC8
MRF-3-3-8-MH-EC8	3	3	8	0.25	Rigid	EC8
MRF-3-3-8-HH-EC8	3	3	8	0.35	Rigid	EC8
MRF-3-5-6-MH-EC8	3	5	6	0.25	Rigid	EC8
MRF-3-5-6-HH-EC8	3	5	6	0.35	Rigid	EC8
MRF-3-5-8-MH-EC8	3	5	8	0.25	Rigid	EC8
MRF-3-5-8-HH-EC8	3	5	8	0.35	Rigid	EC8
MRF-3-3-6-MH-FD-NA	3	3	6	0.25	Dissipative	DP-A
MRF-3-3-6-HH-FD-NA	3	3	6	0.35	Dissipative	DP-A
MRF-3-3-8-MH-FD-NA	3	3	8	0.25	Dissipative	DP-A
MRF-3-3-8-HH-FD-NA	3	3	8	0.35	Dissipative	DP-A
MRF-3-5-6-MH-FD-NA	3	5	6	0.25	Dissipative	DP-A
MRF-3-5-6-HH-FD-NA	3	5	6	0.35	Dissipative	DP-A
MRF-3-5-8-MH-FD-NA	3	5	8	0.25	Dissipative	DP-A
MRF-3-5-8-HH-FD-NA	3	5	8	0.35	Dissipative	DP-A
MRF-3-3-6-MH-FD-SA	3	3	6	0.25	Dissipative	DP-B
MRF-3-3-6-HH-FD-SA	3	3	6	0.35	Dissipative	DP-B
MRF-3-3-8-MH-FD-SA	3	3	8	0.25	Dissipative	DP-B
MRF-3-3-8-HH-FD-SA	3	3	8	0.35	Dissipative	DP-B
MRF-3-5-6-MH-FD-SA	3	5	6	0.25	Dissipative	DP-B
MRF-3-5-6-HH-FD-SA	3	5	6	0.35	Dissipative	DP-B
MRF-3-5-8-MH-FD-SA	3	5	8	0.25	Dissipative	DP-B
MRF-3-5-8-HH-FD-SA	3	5	8	0.35	Dissipative	DP-B

In order to identify each frame, a name code has been given as follows:

MRF_ Storey-Number of span-Span length(m)-Design Methodology

Where:

- Number of span: 3 or 5 .
- Span length: 6 m or 8 m.
- Design Methodology: EC8 for Eurocode 1998-1 design methodology, DP-A for design methodology developed at University of Naples “Federico II” and DP-B for the design methodology developed by University of Salerno in Italy.

The lateral force resisting system is placed at the perimeter of the plan of the building. The interior frames are assumed to be gravity frames and their lateral load resisting capacity is neglected. Two-dimensional frame models are used for the design, with appropriate selection of the tributary areas for gravity and seismic loads. In figure 4.1 a schematic plan view is presented with the position of the lateral load resisting system for the case of a 3-bay plan layout and in figure 4.2 a vertical schematic cut is presented.

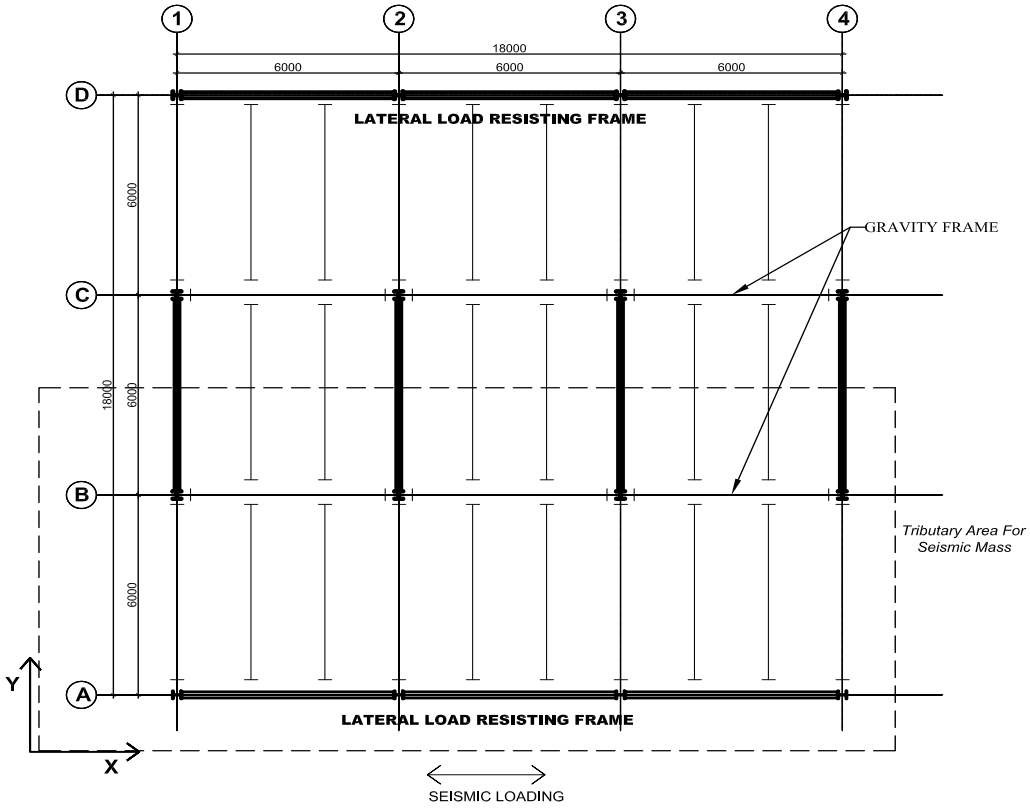

Figure 4.1 Plan view of the buildings MRF

All the frames were designed according to Eurocode 1993 (EC3) and Eurocode 1998-1 (EC8). The material for all frame elements is S355 steel with an over-strength factor γ = 1.25. The maximum behavior factor q allowed by EN 1998-1 is used for MRFs, namely, a value of q=6.5 is used.

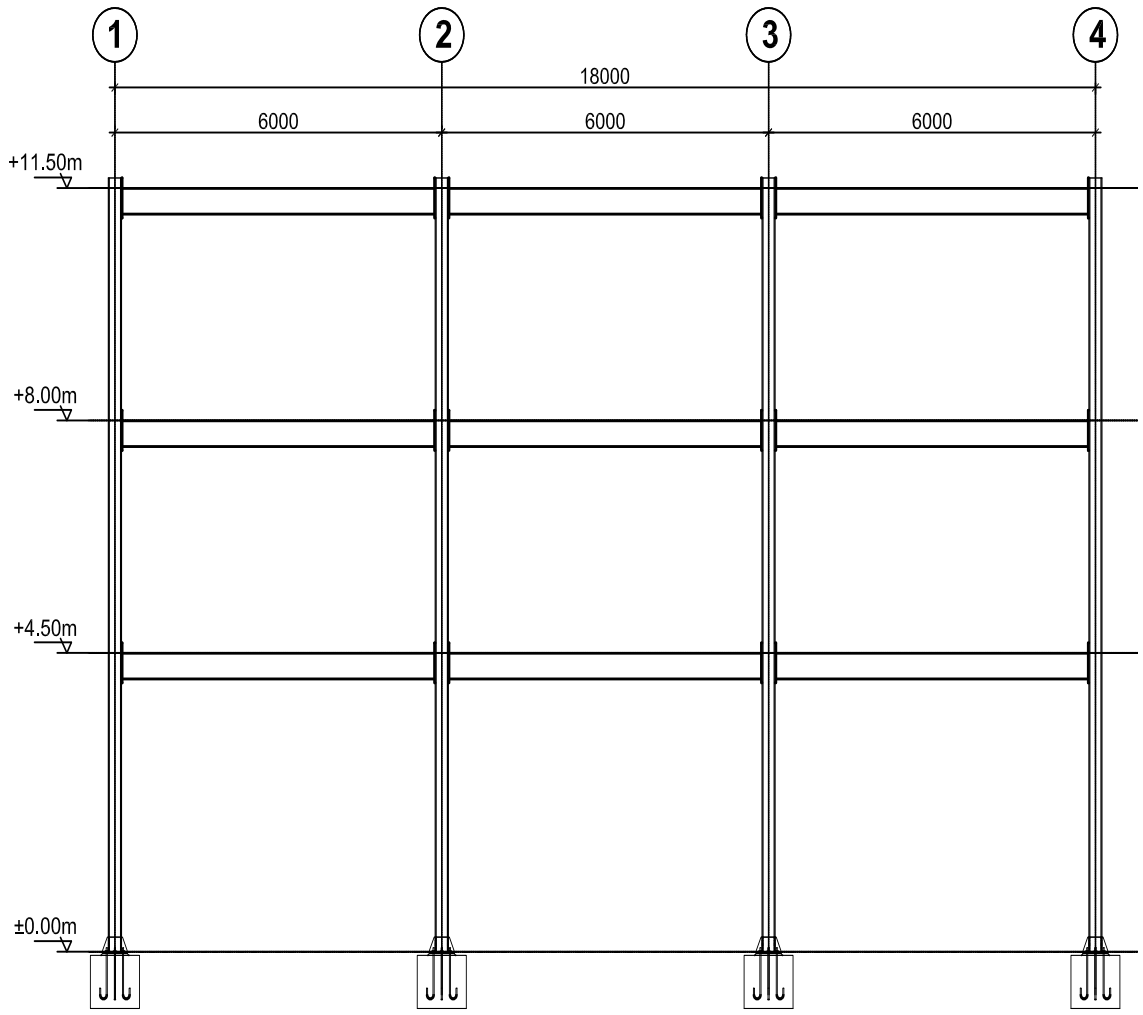

Figure 4.2 Vertical section of the MRF system

A design spectra Type 1 for Soil Type C is used for calculating the seismic loads both in the medium seismicity (MH, PGA=0.25g) and high seismicity (HH, PGD=0.35g) cases, in figure 4.3.

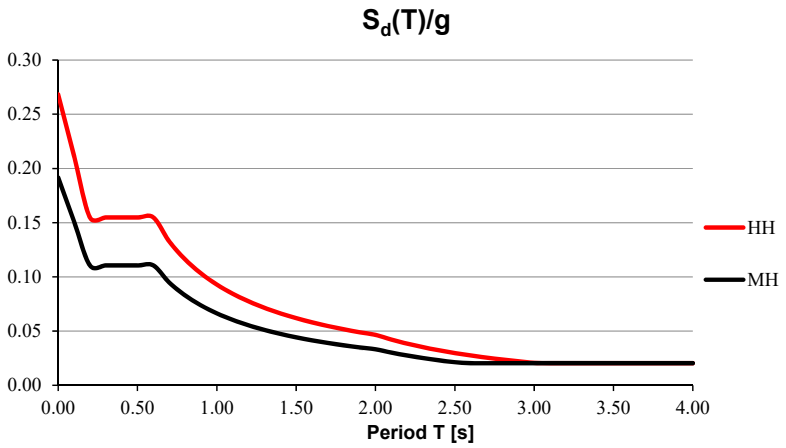

Figure 4.3 Design spectrum for Medium and High seismicity.

The lateral force method of analysis was employed for calculating the seismic action effects, disregarding the torsional effects. The permanent loads, the imposed loads and the relevant combination factors were selected according to the destination (residential/office building), in table 4.2 are shown the load values for Roof and Intermediate Storeys used in all cases. Inter-storey drifts were limited to 0.75% of the storey height (implying ductile non-structural elements connected to the frames) and the inter-storey drift sensitivity coefficient θ was limited to < 0.1, as for this condition P-Δ effects are not considered in the analysis and design. If the condition $\theta < 0.1$ leads to impractical design solutions, then it was relaxed to $0.1 < \theta < 0.2$, with appropriate multiplication of the seismic action effects by the factor $\frac{1}{1-\theta}$. The seismic masses per floor are shown in table 4.3 for the different frame types.

Table 4.2 Surface design loads for all frames (vertical loads)

Vertical Design Loads	**Load (kN/m^2**	
Location	**Permanent**	**Imposed**
Intermediate Storeys	4.5	2
Roof	4.5	2

Table 4.3 Seismic mass for the MRFs.

Seismic Mass (tons)	**MRF 3-3-6**	**MRF 3-3-8**	**MRF 3-5-6**	**MRF 3-5-8**
Intermediate floor	79.27	140.92	132.11	234.86
Roof	82.24	146.20	137.06	243.67

The frames were modeled using the structural analysis software SAP2000, with rigid joints, seismic masses are assigned to one joint node at each floor, all the nodes per storey are connected by a rigid diaphragm, for the calculation of modes and eigen-periods. As described in section 3.1 member strength and stability checks are performed according to EN 1993-1 and for seismic compliance criteria EN 1998-1, section 6.6. Excel spreadsheets were created for the calculation and verification of interstorey drift, second-order effects sensitivity parameter θ and α parameter, as well as the calculation for the appropriate Ω beam overstrenght factor as required in EN 1998-1, Section 6.6. Beam - column resistance ratio checks were performed for all joints as required for global verification in EN 1998-1, Section 4.4.2.3.

The design criteria that governed most of the design of the MRFs, as expected, is the Inter-storey drift limitation and sensitivity to second-order (P-Δ) effect limitation, an iterative procedure was followed in some cases in order to fulfill those requirements. The final sections for columns are type HEB, HEM and HD, and for beams IPE steel sections. In tables 4.4 and 4.5 are summarized the final sections for each frame type and design methodology.

Table 4.4 Element sections for each designed MRF for Medium seismic Hazard (MH).

MRF-MH-EC8					MRF-MH-DP-A					MRF-MH-DP-B				
-	Storey	Ext. Col.	Int. Col.	Beam	-	Storey	Ext. Col.	Int. Col.	Beam	-	Storey	Ext. Col.	Int. Col.	Beam
MRF-3-3-6	3	HE260B	HE360B	IPE300	MRF-3-3-6	3	HE260B	HE360B	IPE300	MRF-3-3-6	3	HE280B	HE400B	IPE300
	2	HE280B	HE400B	IPE400		2	HE280B	HE400B	IPE400		2	HE300B	HE500B	IPE400
	1	HE280B	HE400B	IPE450		1	HE280B	HE400B	IPE450		1	HE300B	HE500B	IPE400
MRF-3-3-8	3	HE360B	HE450B	IPE400	MRF-3-3-8	3	HE360B	HE450B	IPE400	MRF-3-3-8	3	HE400B	HE450M	IPE400
	2	HE400B	HE550B	IPE500		2	HE400B	HE550B	IPE500		2	HE400B	HE550M	IPE500
	1	HE400B	HE550B	IPE550		1	HE400B	HE550B	IPE550		1	HE400B	HE550M	IPE550
MRF-3-5-6	3	HE280B	HE400B	IPE330	MRF-3-5-6	3	HE280B	HE400B	IPE330	MRF-3-5-6	3	HE280B	HE400B	IPE300
	2	HE300B	HE450B	IPE400		2	HE300B	HE450B	IPE400		2	HE300B	HE500B	IPE400
	1	HE300B	HE450B	IPE400		1	HE300B	HE450B	IPE400		1	HE300B	HE500B	IPE400
MRF-3-5-8	3	HE360B	HE500B	IPE400	MRF-3-5-8	3	HE360B	HE500B	IPE400	MRF-3-5-8	3	HE360B	HD400X287	IPE400
	2	HE400B	HE600B	IPE500		2	HE400B	HE600B	IPE500		2	HE400B	HD400X382	IPE500
	1	HE400B	HE600B	IPE550		1	HE400B	HE600B	IPE550		1	HE400M	HD400X382	IPE550

Table 4.5 Element sections for each designed MRF for High seismic Hazard (HH).

MRF-HH-EC8					MRF-HH-DP-A					MRF-HH-DP-B				
-	Storey	Ext. Col.	Int. Col.	Beam	-	Storey	Ext. Col.	Int. Col.	Beam	-	Storey	Ext. Col.	Int. Col.	Beam
MRF-3-3-6	3	HE360B	HE500B	IPE360	MRF-3-3-6	3	HE360B	HE500B	IPE360	MRF-3-3-6	3	HE340B	HE400M	IPE360
	2	HE400B	HE600M	IPE500		2	HE400B	HE550B	IPE500		2	HE400B	HD400X634	IPE500
	1	HE400B	HE600M	IPE550		1	HE400B	HE550B	IPE550		1	HE400B	HD400X634	IPE500
MRF-3-3-8	3	HE450B	HD400X677	IPE450	MRF-3-3-8	3	HE450B	HD400X421	IPE500	MRF-3-3-8	3	HE450B	HD400X347	IPE450
	2	HE500B	HD400X677	IPE600		2	HE500B	HD400X592	IPE600		2	HE450M	HD400X677	IPE750X147
	1	HE500B	HD400X677	IPE750X147		1	HE500B	HD400X592	IPE750X147		1	HE450M	HD400X677	IPE750X147
MRF-3-5-6	3	HE360B	HE400M	IPE360	MRF-3-5-6	3	HE360B	HE400M	IPE360	MRF-3-5-6	3	HE360B	HE400M	IPE360
	2	HE400B	HD400X592	IPE500		2	HE400B	HD400X463	IPE500		2	HE400M	HD400X592	IPE500
	1	HE400B	HD400X592	IPE500		1	HE400B	HD400X463	IPE500		1	HE400M	HD400X592	IPE500
MRF-3-5-8	3	HE360B	HE400M	IPE450	MRF-3-5-8	3	HE360B	HD400X287	IPE450	MRF-3-5-8	3	HE360M	HD400X347	IPE450
	2	HE450B	HD400X421	IPE750X147		2	HE400B	HD400X421	IPE750X147		2	HE360M	HD400X634	IPE750X147
	1	HE450M	HD400X421	IPE750X147		1	HE400B	HD400X421	IPE750X147		1	HE360M	HD400X634	IPE750X147

In tables 4.6 and 4.7 area shown the fundamental period, design base shear and total weight of each frame.

Table 4.6 Design Base shear and fundamental period for MRF's.

	Base Shear (Vd)	Fundamental period (s)	Weight (ton)
MRF-3-3-6-HH-DP-B	365.65	0.59	19.6
MRF-3-3-8-HH-DP-B	650.04	0.586	25.7
MRF-3-5-6-HH-DP-B	609.42	0.58	33.9
MRF-3-5-8-HH-DP-B	1083.41	0.591	45.1
MRF-3-3-6-MH-DP-B	181.52	0.866	9.8
MRF-3-3-8-MH-DP-B	336.24	0.831	16.2
MRF-3-5-6-MH-DP-B	305.80	0.857	15.8
MRF-3-5-8-MH-DP-B	550.09	0.847	31.1

Table 4.7 Design Base shear and fundamental period for MRF's.

	Base Shear (Vd)	Fundamental period (s)	Weight (ton)
MRF-3-3-6-HH-EC8	386.80	0.58	13.9
MRF-3-3-8-HH-EC8	677.87	0.615	28.1
MRF-3-5-6-HH-EC8	658.01	0.591	32
MRF-3-5-8-HH-EC8	1073.62	0.64	40.15
MRF-3-3-6-MH-EC8	178.89	0.91	9.1
MRF-3-3-8-MH-EC8	327.81	0.88	14.2
MRF-3-5-6-MH-EC8	309.09	0.88	15.7
MRF-3-5-8-MH-EC8	566.13	0.85	23.4
MRF-3-3-6-HH-DP-A	368.15	0.63	12.5
MRF-3-3-8-HH-DP-A	665.70	0.623	25.2
MRF-3-5-6-HH-DP-A	634.79	0.62	29
MRF-3-5-8-HH-DP-A	1032.12	0.665	35.8
MRF-3-3-6-MH-DP-A	178.53	0.912	9.1
MRF-3-3-8-MH-DP-A	327.88	0.88	14.3
MRF-3-5-6-MH-DP-A	309.09	0.88	15.7
MRF-3-5-8-MH-DP-A	572.79	0.84	23.4

4.2 Non-Linear Static (Push-over) Analysis

After the design of the MRFs according to the three design methodologies, final element sections and internal forces are used in order to define the models for a Non-Linear Static Analysis (NLSA), known also as Push-over analysis. The models were developed with the structural software SeismoStruct (2016) developed by SeismoSoft under an academic license for research studies. SeismoStruct allows the user to run not only NLSA models but also Incremental Dynamic Analysis which were used as a second phase in this work.

To develop the models in SeismoStruct, the following parameters were used:

- A Stress-Strain Material model based on the relationship proposed by Menegotto (1973), coupled with the isotropic hardening rules proposed by Filippou et al. (1983).

Defined by:

- Modulus of elasticity, E_s=210 MPa.
- Yield strength, F_y=443 MPa, considering the overstrenght of material S355.
- Strain hardening parameter, μ=0.0025.
- Specific weight, γ=78 kN/m3.

- Geometry and steel sections (for beams and columns) are defined in SeismoStruct as designed with the methodologies presented in sections 3.1, 3.2.1 and 3.2.2. The force-based (infrmFB) distributed inelasticity elements were used for the elements in the 2-D models. The later account for distributed inlestacity through integration of material response over the cross section and integration of the section response along the length of the element. The cross-section behavior is reproduced by means of the fiber approach, assigning an uniaxial stress-strain relationship at each fiber, therefore fiber meshing is important according to the type of analysis and the importance of the element.

- Concentrated seismic mass per floor defined in one node of each diaphragm per floor.

- For EC8 MRFs, beam column joints are defined as rigid connections, therefore no plastic hinges are defined in the structural model, but rigid elements to simulate the rigid haunched connection as shown in figure 4.4, the rigid elements are placed at both sides of the center of the intersection node, also above and below the intersection node, as shown in figure 4.5, the so called *rigid elements* are defined with an infinite rigidity and no self weight material.

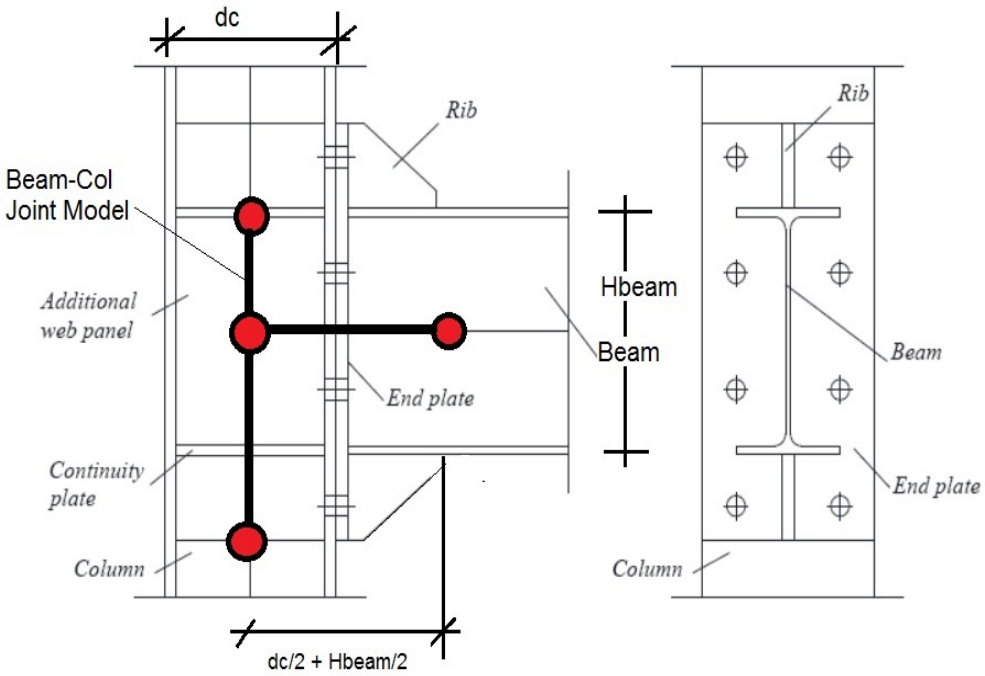

Figure 4.4 Scheme of a Rigid Beam-column connection for MRFs design with EC8 approach.

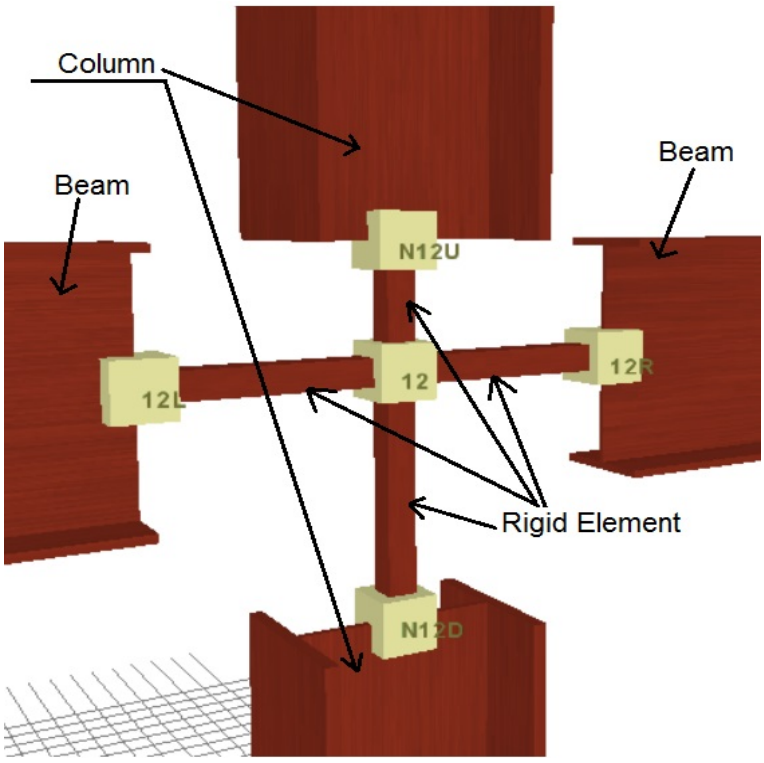

Figure 4.5 Joint structural model defined in SeismoStruct software.

- For MRFs design with DP-A, the beam-column joints are defined with plastic hinges, with a bilinear-kinematic model shown in figure 4.8, defined by the initial Stiffness K_0, yield force F_y as the internal moment for the seismic combination taken from the results of each frame designed in SAP2000v15, and the Post-yield hardening ratio *r* as a small value to resemble a perfect plastic behavior. The structural model of the beam-column joint is defined with 4 nodes, *N1* at the intersection of central axis of beam and column, two nodes placed on the vertical axis, *N1U* at the top of the beam flange and *N1D* at the bottom of the haunch element (which height is taken as one half of the height of the beam), and two nodes placed in the horizontal axis, *N1L* at the left side of the face of the column and *N1R* at the right side of the face of the column, in figures 4.6 and 4.7 are shown the scheme of the beam-column joint for a Friction connection and the structural model defined in SeismoStruct respectively.

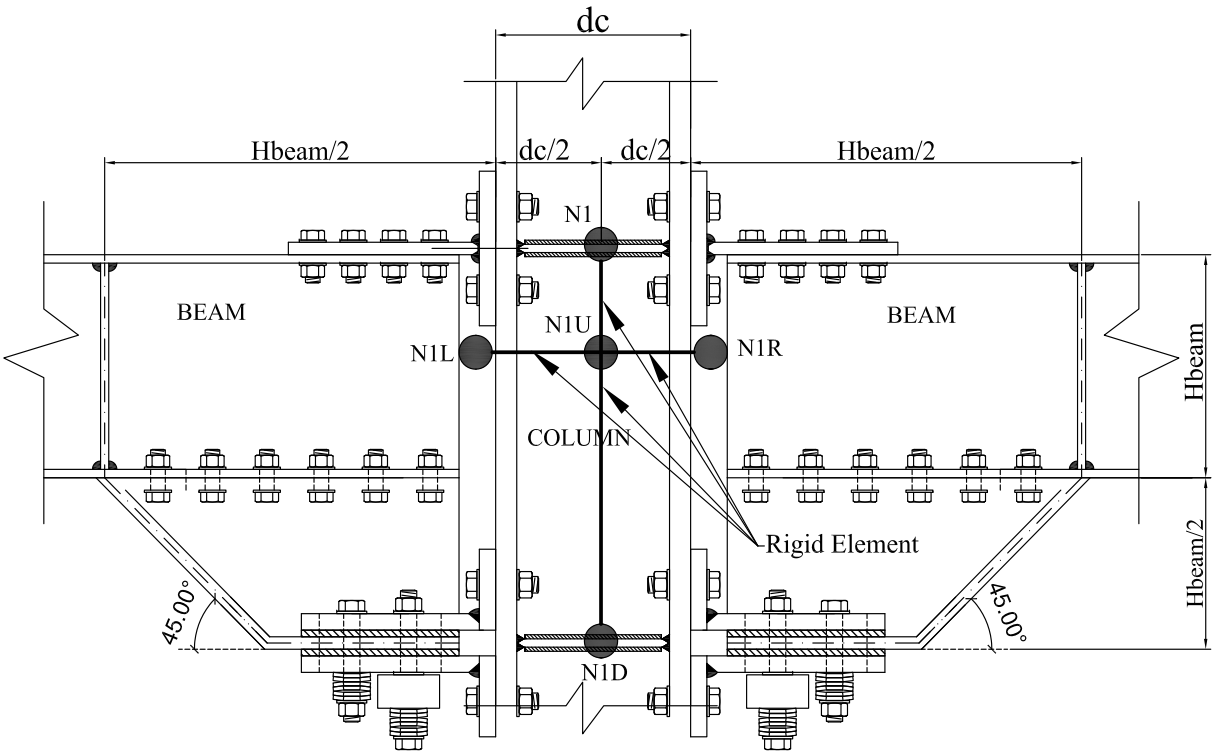

Figure 4.6 Scheme of a Rigid Beam-column connection for MRFs design with DP-A approach.

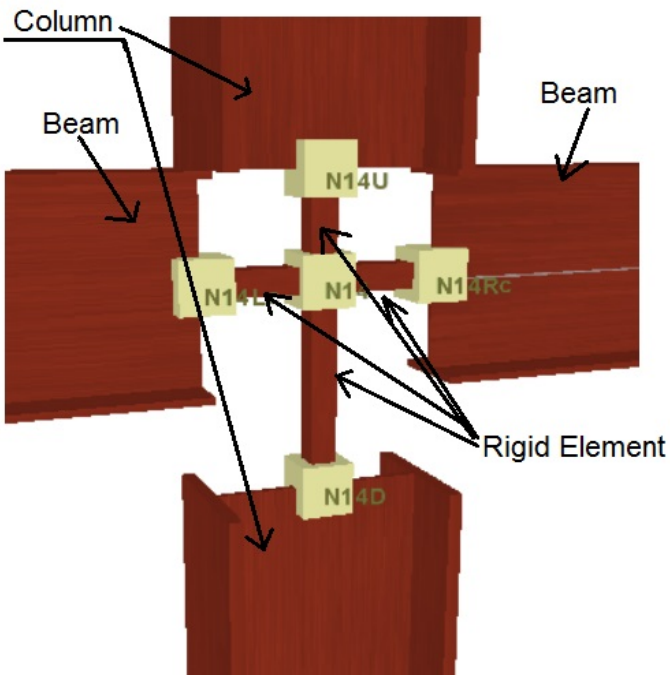

Figure 4.7 Joint structural model defined in SeismoStruct software for MRFs-DP-A and MRFs-DP-B.

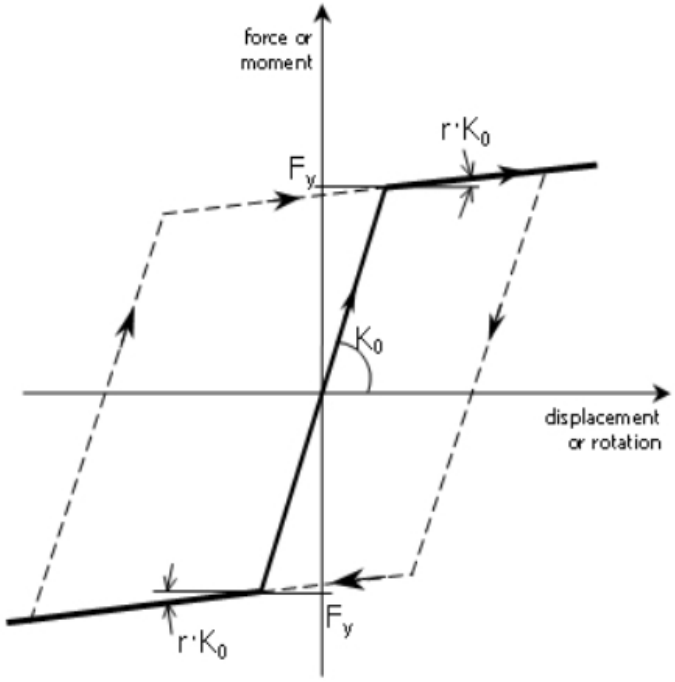

Figure 4.8 Bilinear kinematic model for plastic hinges.

- For the MRFs design with DP-B methodology, the beam-column joints are defined with plastic hinges, with the same bilinear-kinematic model as for MRFs-DP-A, shown in

figure 4.8, defined by the initial Stiffness K_0, yield force F_y, defined as 80% of the plastic moment of the beams ($0.8 \cdot Mb_{pl}$), and the Post-yield hardening ratio r as a small value to resemble a perfect plastic behavior. The structural model of the beam-column joint is the same as described for the MRFs-DP-A with the appropriate hinge parameters, in figures 4.6 and 4.7 are shown the scheme of the beam-column joint for a Friction connection and the structural model defined in SeismoStruct respectively.

- The base of the columns were defined with appropriate restrain definitions, all the base nodes were restrain in both displacement and rotation, the rest of the nodes were restricted in the out of plane displacement and rotation, only a 2-D analysis was performed for all the MRFs studied.

- For the load pattern, two types of lateral load distribution were defined as required for the Non-linear static analysis defined in EN 1998-1 section 4.3.3.4.2.2 : a) *Uniform load pattern* based on lateral forces that are proportional to the masses along the frame height; b) a *Modal or Triangular load pattern* proportional to lateral forces consistent with the first mode of the structure considering a lateral force distribution, of the horizontal direction, determined in the elastic analysis according to EN 1998-1 section 4.3.3.2 and 4.3.3.3.

- The control node was defined in the upper right corner of each MRF, considering minimum of 500 steps for increasing the load pattern until reach a top displacement of 1m. In order to study the Over-strength factors for the frames an idealized elasto-plastic force-displacement curve was defined based on the capacity curve of each MRF following the procedure shown in EN1998-1 Annex B.3. Three limit states were studied for the calculation of the target displacements: Limit state of Damage Limitation (DL) with a probability of exceedance of 20% in 50 years or a return period of 225 years, Significant Damage (SD) with a probability of exceedance of 10% in 50 years or a return period of 475 years and Near Collapse limit state (NC) with a probability of exceedance of 2% in 50 years or a return period of 2475 years.

- In order to take into account $P - \Delta$ effects for the 2-D model, a *Leaning Column* that

carries the gravity loads in the building not directly acting on the MRFs i.e. carries the gravity load of the gravity frames not considered in a simplified 2-D model was used. This additional column elements are connected to the moment frame by pinned joints at each end, for this consideration, *Truss* element type are defined for vertical and horizontal elements with infinite stiffness and null self weight, ensuring the columns are hinged at both top and bottom ends. This type of methodology allows inducing only additional overturning moment from lateral displacement to the simplified 2-D model.

4.3 Incremental Dynamic Analysis (IDA)

In order to investigate the behavior of the MRFs under recorded seismic events, a Non-linear Time history analysis i.e. Incremental Dynamic Analysis (IDA) was performed for all the frames. One set of 14 natural earthquake acceleration records were used to carry out the nonlinear time history analyses of the investigated structures. The records match the elastic acceleration spectra of EC8 corresponding to a seismic hazard level of 10% probability of exceedance in 50 years, for a High seismic Hazard scenario (HH) i.e. $PGA_0 = 0.35g$, EN 1998-1 Type 1 Soil type C target spectrum.

The comparison between the design code spectra and 5% damped accelerations are given in figure 4.9. The properties of the selected natural ground acceleration such as the date of the seismic event, the recorded station name and country, the Moment Magnitude (M_w), and the type Fault mechanism are summarized in Table 4.8

Table 4.8 Basic data of the selected ground motions.

Earthquake name	Date	Station Name	Station Country	Magnitude Mw	Fault mechanism
Alkion	24.02.1981	Xylokastro-O.T.E.	Greece	6.6	Normal
Montenegro	24.05.1979	Bar-Skupstina Opstine	Montenegro	6.2	Reverse
Izmit	13.09.1999	Yarimca (Eri)	Turkey	5.8	Strike-Slip
Izmit	13.09.1999	Usgs Golden Station Kor	Turkey	5.8	Strike-Slip
Faial	09.07.1998	Horta	Portugal	6.1	Strike-Slip
L'Aquila	06.04.2009	L'Aquila - V. Aterno - Aquila Park In	Italy	6.3	Normal
Aigion	15.06.1995	Aigio-OTE	Greece	6.5	Normal
Alkion	24.02.1981	Korinthos-OTE Building	Greece	6.6	Normal
Umbria-Marche	26.09.1997	Castelnuovo-Assisi	Italy	6	Normal
Izmit	17.08.1999	Heybeliada-Senatoryum	Turkey	7.4	Strike-Slip
Izmit	17.08.1999	Istanbul-Zeytinburnu	Turkey	7.4	Strike-Slip
Ishakli	03.02.2002	Afyon-Bayindirlik ve Iskan	Turkey	5.8	Normal
Olfus	29.05.2008	Ljosafoss-Hydroelectric Power	Iceland	6.3	Strike-Slip
Olfus	29.05.2008	Selfoss-City Hall	Iceland	6.3	Strike-Slip

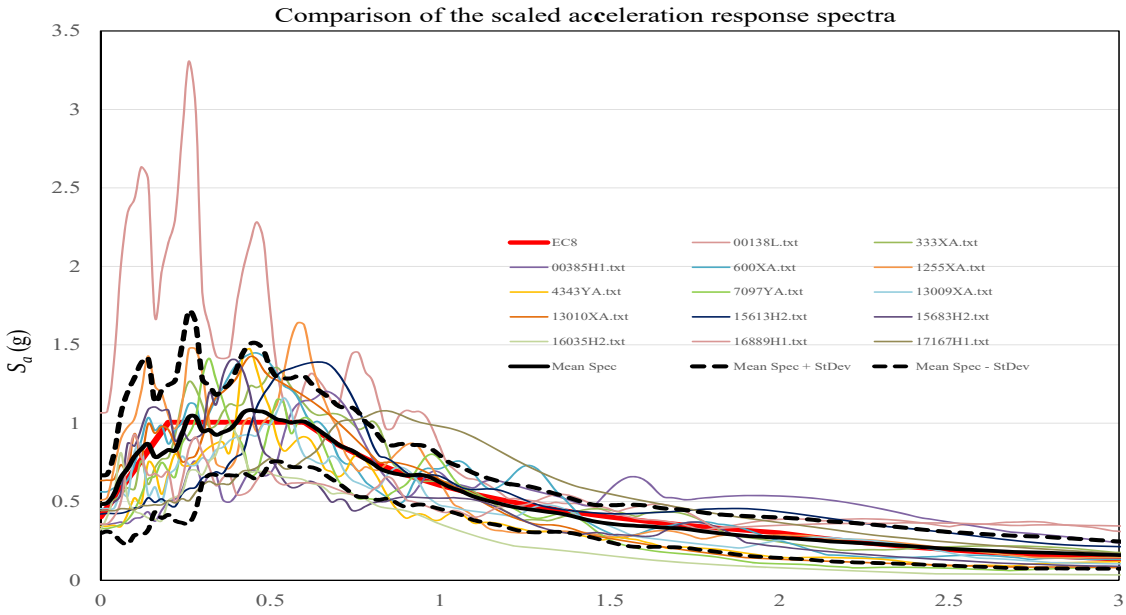

Figure 4.9 Comparison of the scaled acceleration response spectra of the 14-record high-hazard (HH) set with the 5% damped Type 1, Soil C design spectrum of EN 1998-1 with PGA = 0.35 g.

In figures 4.10 to 4.12 are presented the acceleration time histories for the 14 records used for the IDA of the frames. It should be noted that each record was fictitiously extended by 10 seconds with a zero acceleration in order to allow the frames experience 10 seconds of free vibrations around the final post-quake configuration, which are necessary to calculate the residual inter-storey drift ratios from the nonlinear time history analyses.

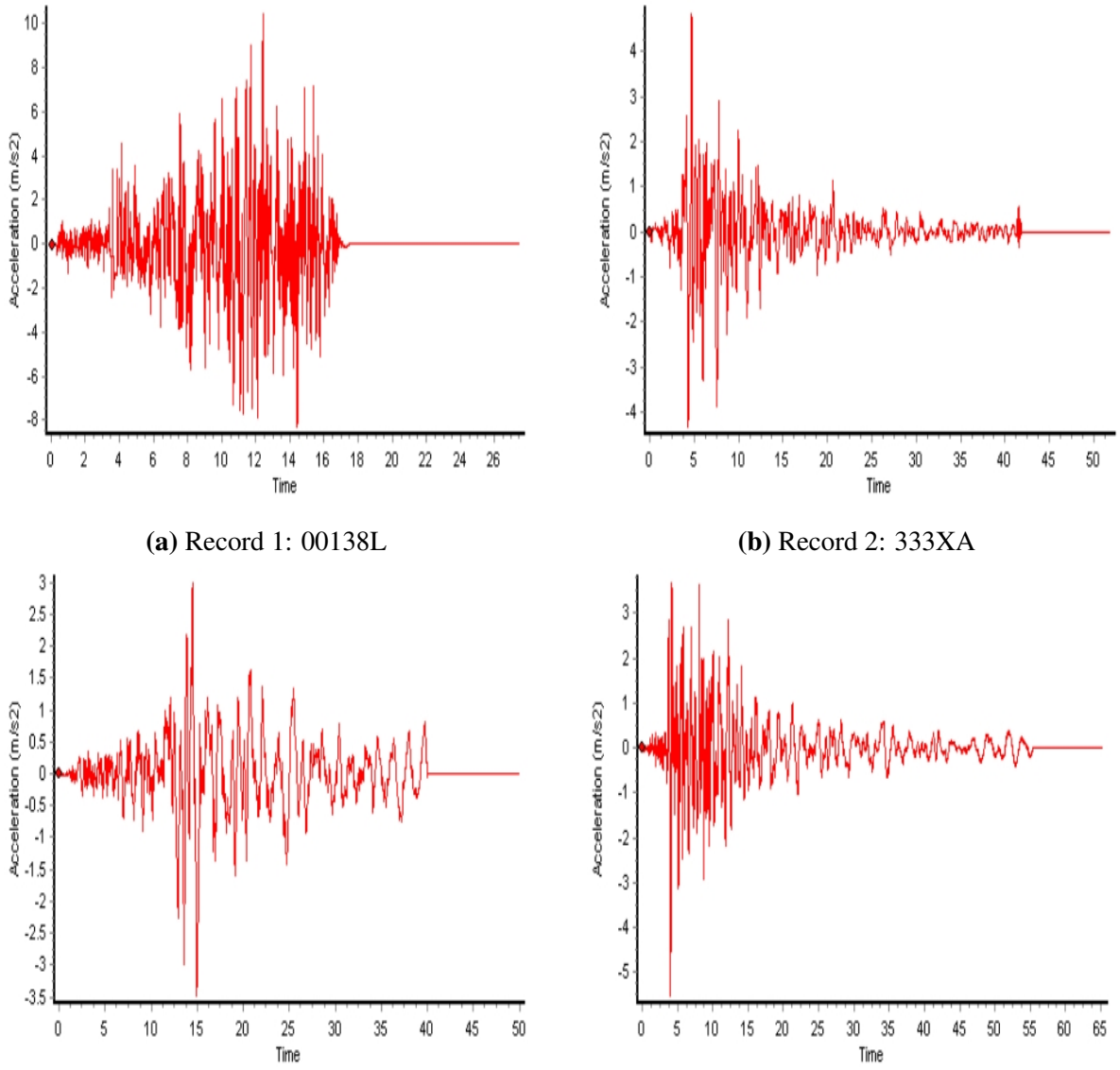

(a) Record 1: 00138L

(b) Record 2: 333XA

(c) Record 3: 00385H1

(d) Record 4: 600XA

Figure 4.10 Original Acceleration time histories.

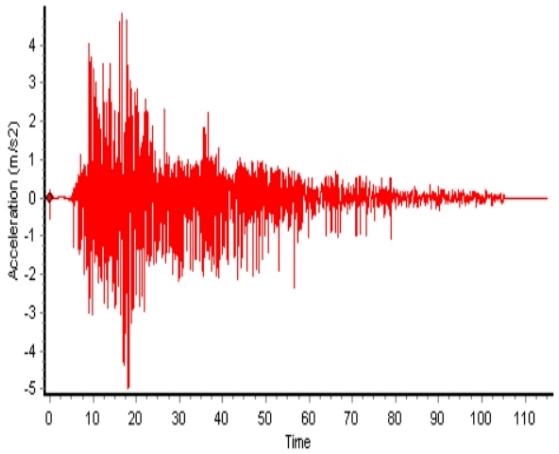

(a) Record 5: 1255XA

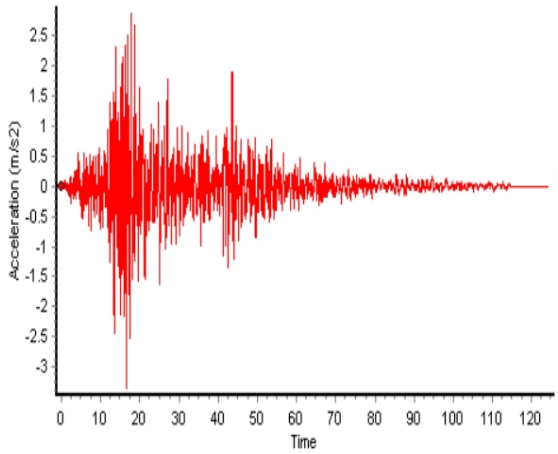

(b) Record 6: 4343YA

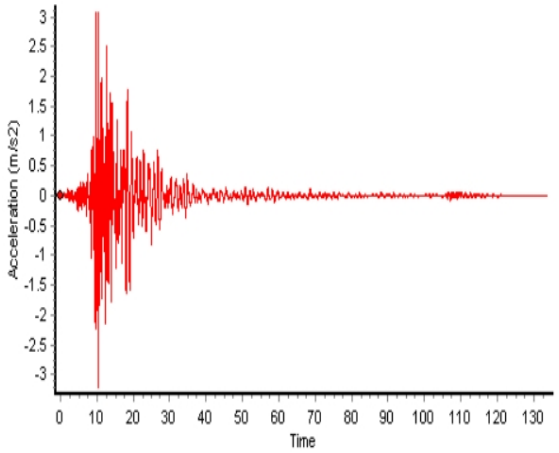

(c) Record 7: 7097YA

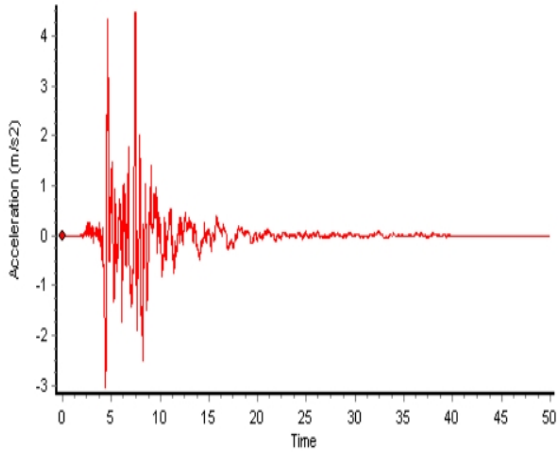

(d) Record 8: 13009XA

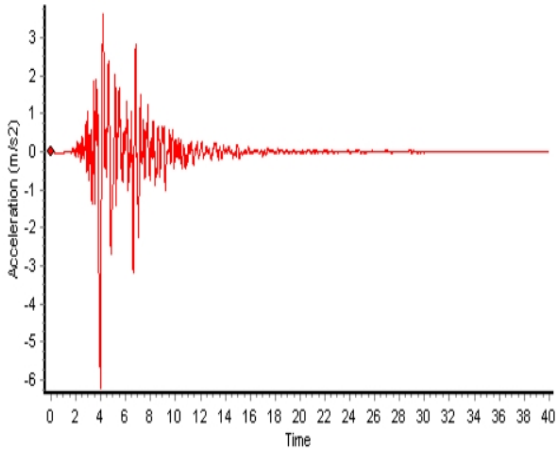

(e) Record 9: 13010XA

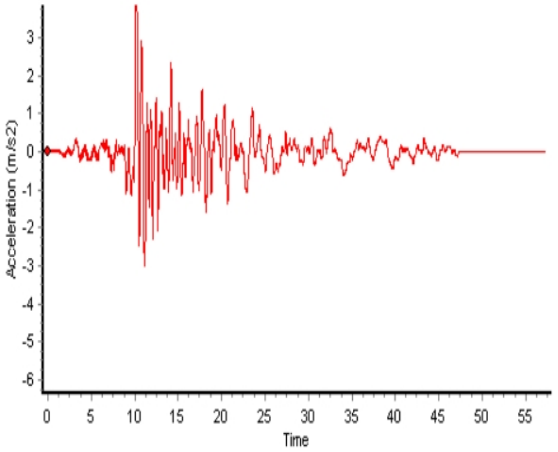

(f) Record 10: 15613H2

Figure 4.11 Original Acceleration time histories (continuation).

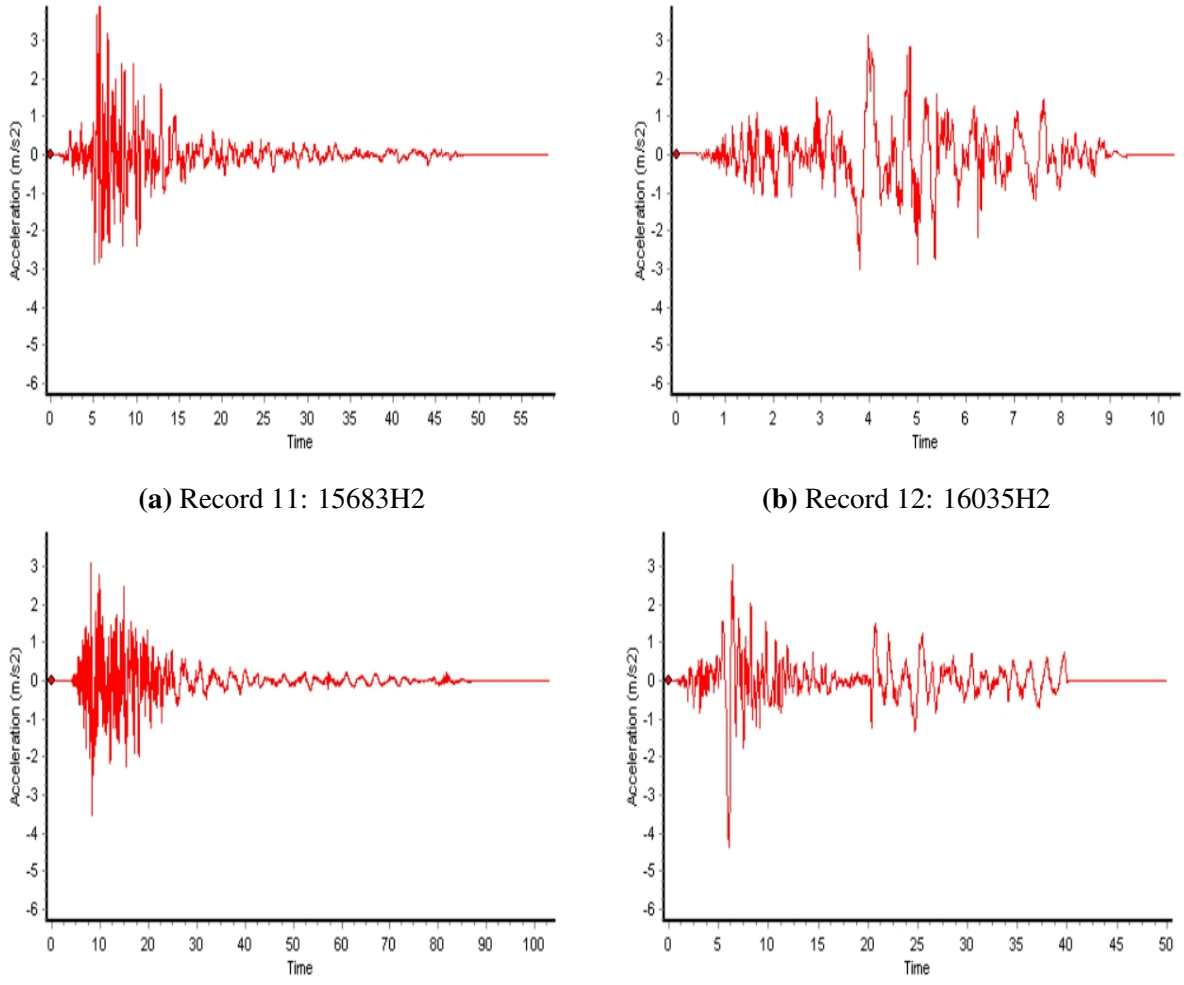

(a) Record 11: 15683H2

(b) Record 12: 16035H2

(c) Record 13: 16889H1

(d) Record 14: 17167H1

Figure 4.12 Original Acceleration time histories (continuation).

SeismoStruct (2016) Software was used to perform the 2-D analysis considering the following parameters:

- Geometry and frame sections were taken the same as for the Non Linear Static (pushover) analysis, Incremental Dynamic Analysis scenario is defined in the software in order to provide the corresponding parameters and records for the analysis.
- The 14 records were defined and scaled, with the proper scaling factors previously calculated to match the design spectrum, for Medium and High Hazard levels.
- Rayleigh tangent stiffness damping has been used, defined by the first and second

periods of each frame, both with with a 2 % of damping ratio.

- Each record includes a minimum of 10 seconds, at the end of the record, with null acceleration in order to study the Residual inter-storey drift under free vibration.
- The time step for all the records is considered as $t = 0.005s$, taken as half of the time step of the records, and the load is applied at the base of each column.
- The seismic performance is evaluated for three performance levels, associated to different annual rate of exceedance according to Eurocode-8 (2005):

  a) Damage Limitation limit state (*DL*), the building is subjected to earthquakes with probability of exceedance 20% in 50 years (return period T=225 years). For this limit state the structure is only lightly damaged and no limitation of use is accounted, the corresponding structural performance should be verified with an inter-storey drift limitation of 0.75%.

  b) Significant Damage Limit state (*SD*) with a probability of exceedance 10% in 50 years (return period T=475 years) where the structure shall have no local or global collapse under the design seismic action, nevertheless the structure is strongly damaged but has some residual lateral strength and stiffness and vertical elements are capable of sustaining vertical loads, thus providing the strength to sustain moderate after-shocks. To verify the effectiveness of the structural performance, a limit value for residual inter-storey drift of 1% has been used and a 2.5% transient inter-storey drift, as recommended by FEMA 356 for Steel Moment Frames.

  c) Near Collapse Limit state (*NC*) with a probability of exceedance 2% in 50 years (return period T=2475 years). For this limit state, structures are expected to be heavily damaged, with negligible residual lateral strength and stiffness, although vertical elements are still capable of sustaining vertical loads. Large permanent drifts are present. The structures are near collapse and are not able to resist to moderate earthquake after-shocks. A transient/residual inter-storey drift ratio of 5.0% has been assumed to characterize this damage scenario, as recommended by FEMA 356 for Steel Moment Frames..

- Plastic demand was studied for each limit state, in order to control the strain results of each structural element, beam and column, with three levels of performance: *Slight Damage* limit for $\varepsilon \leq 0.0021$ verifying elements that remain in the elastic range, *Serious Damage* limit for $0.0021 < \varepsilon \leq 0.016$, and *Very Serious Damage* limit for $\varepsilon > 0.032$ considering the ultimate strain of the material before failure.

Table 4.9 summarizes the performance levels used for the three limit states and the acceleration ratio a/a_g with a_g as the pick ground acceleration i.e. Scale Factors (SF) for the records content.

Table 4.9 Seismic Performance limitation criteria for IDA.

Limit state	Return period (years)	SF	Failure criteria
Damage limitation (DL)	225	0.59	0.75% Transient inter-storey drift ratio
Significant Damage (SD)	475	1	1% Residual interstorey drift ratio
			2.5% Transient inter-storey drift ratio
Near collapse (NC)	2475	1.73	5% Residual interstorey drift ratio
			5% Transient inter-storey drift ratio

5 Results and Discussion

Overall twenty-four MRFs were designed with the three design methodologies investigated in this work: the first set of eight frames designed according to EN1998-1, the second and third set of eight frames with the methodologies developed and tested at University of Naples "Federico II" - *Design Procedure A* (DP-A) and University of Salerno in Italy - *Design Procedure B* (DP-B). The comparison between these set of frames allows to study the benefits of the use of friction connections to MRFs and the performance verification of the design methodologies.

The seismic performance of the frames was evaluated by a Non-linear Static (Pushover) Analysis and non-linear Time History (IDA) analysis, both nonlinear static and dynamic analyses were performed using the structural software SeismoStruct V2016 (SeismoStruct, 2016).

5.1 Non-Linear Static (Pushover) Analysis results and discussion

Non-linear static (pushover) analysis (NLSA) was performed for all the frames considering two cases for the lateral load distribution, as specified by EN 1998-1 4.3.3.4.2.2, hereafter named : *Uniform* and *Triangular load pattern*. Capacity curves i.e. top displacement against base shear were obtained for all the frames. According to the methodology of EN 1998-1 Annex B, target displacements for three levels of performance were calculated:

- Limit state of Damage Limitation (DL) with a probability of exceedance of 20% in 50

years or a return period of 225 years.

- Significant Damage (SD) with a probability of exceedance of 10% in 50 years or a return period of 475 years.
- Near Collapse limit state (NC) with a probability of exceedance of 2% in 50 years or a return period of 2475 years.

5.1.1 Capacity curves

The response parameters monitored by the performed pushover analyses are shown in figure 5.1. For each frame results, V_y refers to the base shear that corresponds to the formation of the first plastic hinge,V_b corresponds to the design base shear and V_p refers to the Ultimate shear capacity of the frame. For top displacement control, d_y corresponds to the top displacement corresponding to the formation of the first plastic hinge and d_u is the top displacement at the ultimate shear capacity of the frame. In figures 5.2 to 5.7 are shown the resultant capacity curves for all the frames studied for NLSA for both patterns of lateral load i.e. *Triangular* and *Uniform*, for each design methodology. In the capacity curves, the top displacement was monitored against the base shear of the structure, in vertical axis the base shear is normalized with the design base shear (V_c/V_d) of each frame.

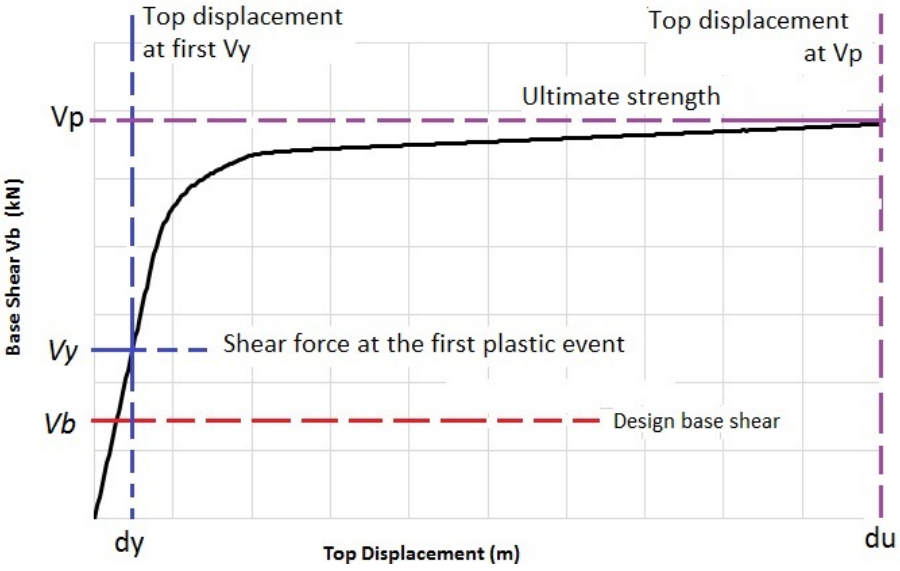

Figure 5.1 Parameters monitored in pushover analysis.

As it can be noted from the capacity curves, all the frames showed an actual capacity considerably higher than that assumed in the design. The later might be due to the design procedure which is governed by the requirements to satisfy both inter-storey drift limits and to control stability coefficients. Regarding the span length influence, frames with shorter span lengths for EC-8 and DP-B cases, shown slightly overstrength, and the contrary case result for DP-A frames. This result is related to the design procedure as longer beams imply larger beam depth that is correlated with stiffer and stronger columns to satisfy capacity design criteria.

For what concerns to the influence of number of spans frames with 5 spans experienced higher V_c/V_d ratios than frames with 3 spans, and the same increase in V_c/V_d is observed for frames designed for High seismic Hazard (HH), both cases are due to the higher rigidity of the frames that leads to stiffer structures, therefore higher overstrength elements. Regarding the lateral load distribution pattern, no significant influence is observed, it can be noticed that for EC-8 frames higher V_c/V_d ratios are for a *Triangular* load pattern, and for DP-A and DP-B frames higher ratios were found for a Uniform load pattern.

The higuest V_c/V_d ratios are for EC-8 frames, an average ratio of 8 for both Uniform and Triangular load patters was obtain. Regarding DP-B designed frames, an average V_c/V_d ratio of 6 for *Triangular* load pattern and around 7 for a *Uniform* load pattern was obtained. Observing the curves for DP-A frames, is noticeable that V_c/V_d ratio is smaller, around 3 for *Triangular* load pattern and 4 for a *Uniform* load pattern, the later shows that FD-NA frames have a smaller over-design criteria than the other methodologies. All the frames presented stable capacity curves, with a perfect elasto-plastic behavior. Only two frames from FD-NA results shown a reduction of capacity from the average frames, MRF-3-3-6-HH-DP-A and MRF-3-5-8-HH-DP-A.

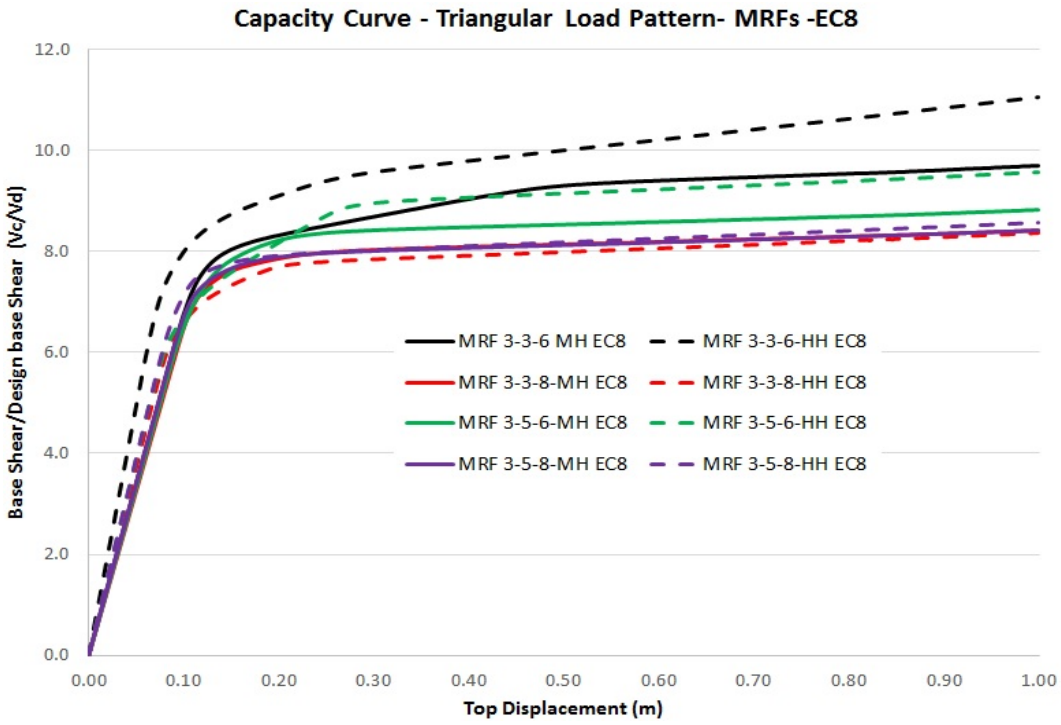

Figure 5.2 Capacity curves for frames designed with EC8 for Triangular load pattern.

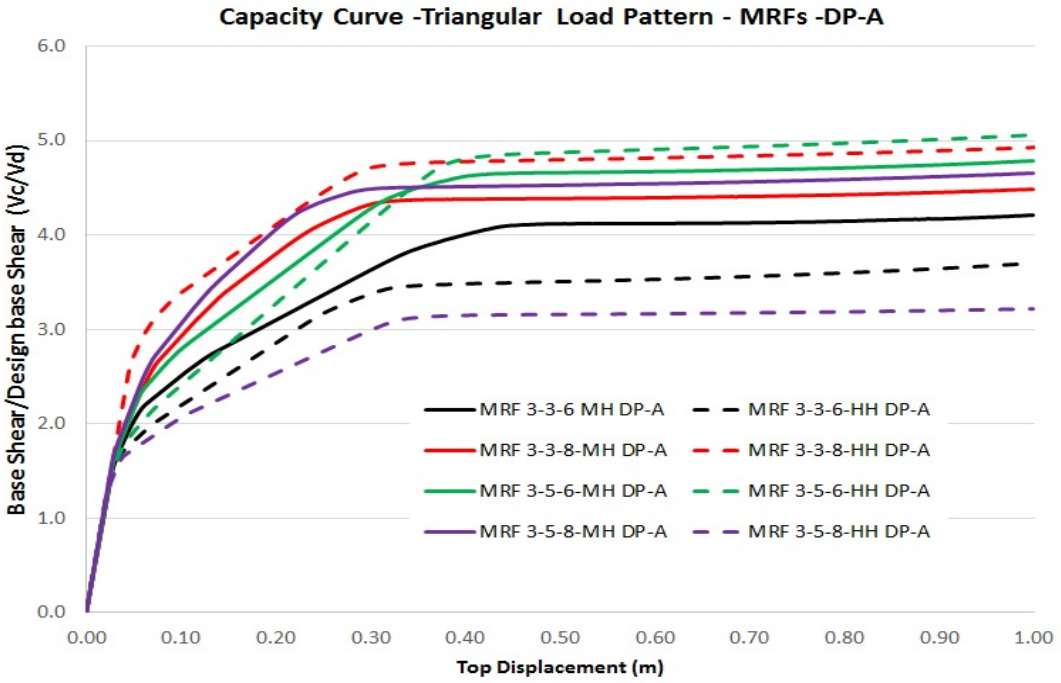

Figure 5.3 Capacity curves for frames designed with DP-A design methodology for Triangular load pattern.

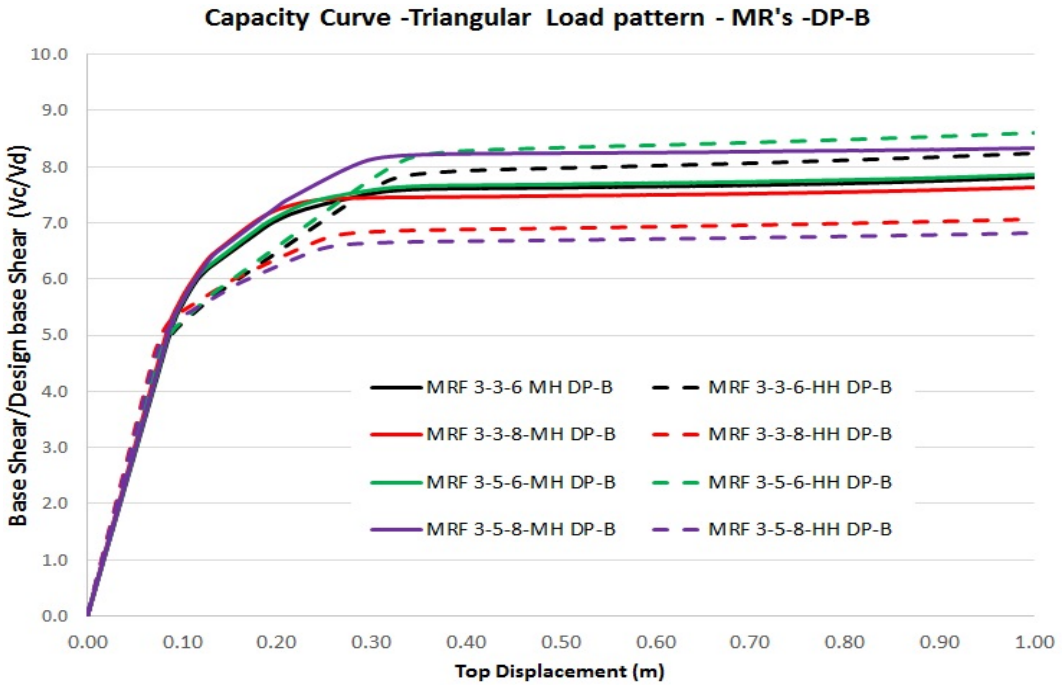

Figure 5.4 Capacity curves for frames designed with DP-B design methodology for Triangular load pattern.

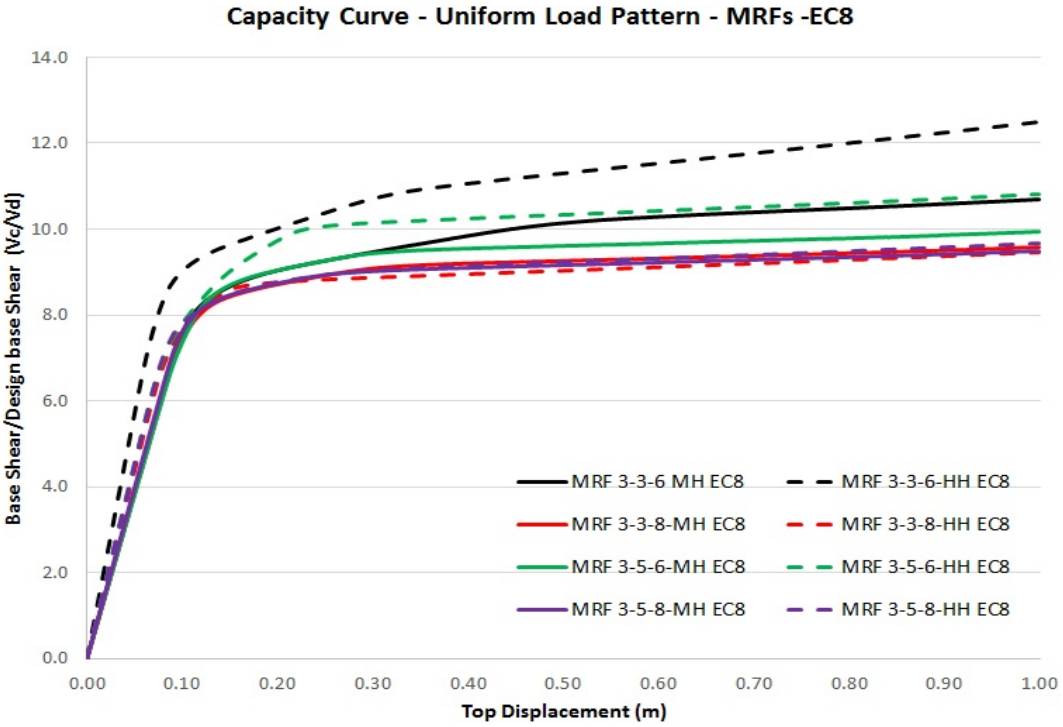

Figure 5.5 Capacity curves for frames designed with EC8 for Uniform load pattern.

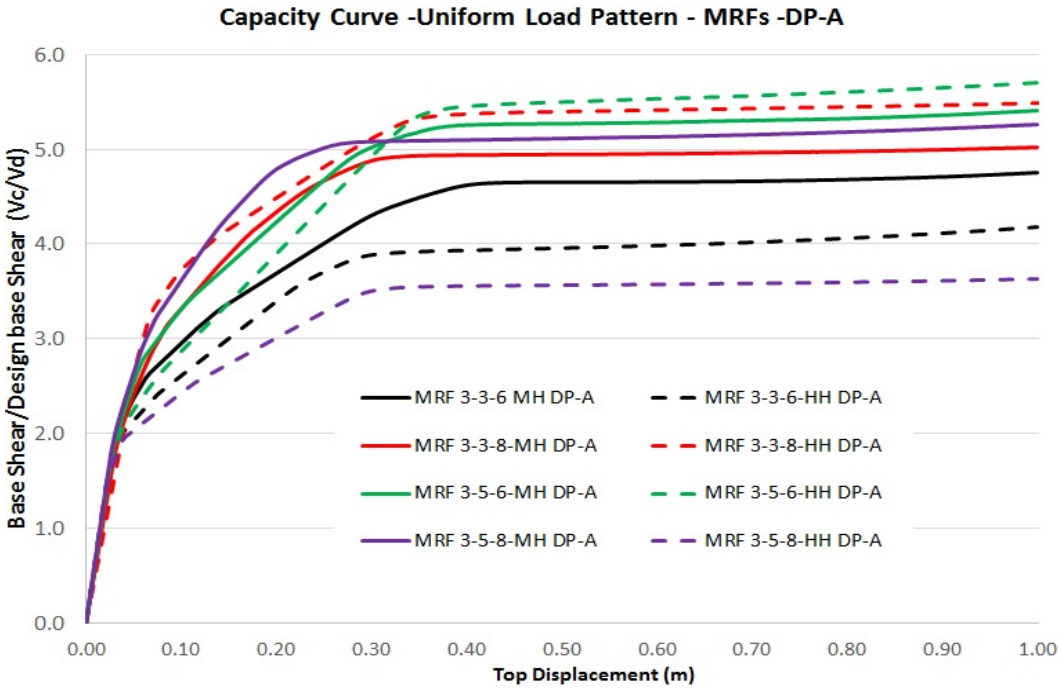

Figure 5.6 Capacity curves for frames designed with DP-A design methodology for Uniform load pattern.

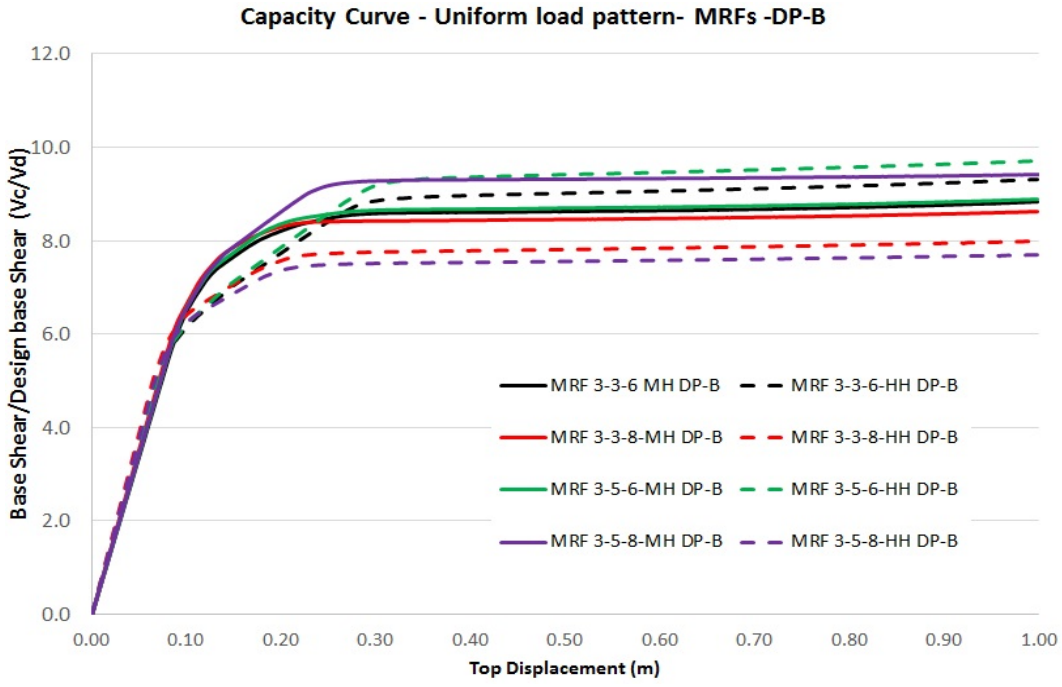

Figure 5.7 Capacity curves for frames designed with DP-B design methodology for Uniform load pattern.

5.1.2 Overall Overstrength factor investigation

The *overall overstrength factor* (Ω_{ov}) factor was investigated for all the frames, this factor can be defined as the ratio between the base shear corresponding to the ultimate capacity of the frame and the design base shear as shown in equation 5.1.

$$\Omega_{ov} = \frac{V_p}{V_b} \tag{5.1}$$

Two important shear ratios can be extracted from equation 5.1:

$$\Omega_{ov} = \frac{V_p}{V_y} \cdot \frac{V_y}{V_b} \tag{5.2}$$

Where:

- Peak base shear (V_p) and Yield base shear (V_y): $\Omega_1 = V_p/V_y$, also known as *Redundancy factor* that corresponds to α_u/α_1 defined in EN 1998-1 4.3.3.4.2.4, as the Ultimate shear capacity of the frame V_p and the base shear value at which the structure reach the first beam plastic resistance V_y. This ratio depends on the frame configuration, formation of the collapse mechanism, redistribution capacity and gravity loading.

- Yield base shear (V_y) and Design base shear (V_b): $\Omega_2 = V_y/V_b$, known as *Overdesign factor*, calculated for all the frames as the base shear value at which the structure reach the first beam plastic resistance V_y and the base design V_b shear of the structure according to its level of seismicity and fundamental period.

In figures 5.8 to 5.16 are summarized the performance parameters from pushover analysis for all the frames. For the redundancy factor $\Omega_1 = V_p/V_y$ and the overdesign factor $\Omega_2 = V_y/V_b$ minimum values from the two lateral load patters are depicted, and a trend line is presented for each design methodology. The pushover curves obtained under *Triangular* load distribution, for the majority of the cases, gave the lower values with a mean value for V_p/V_y within the range of 1.16 and 2.53 for all the frames.

For the design of the frames, according to EN-1998-1 6.3.1 and 6.3.2(3), a recommended value for Moment Resisting Frames typology of α_u/α_1= 1.3 was considered. For EC-8 frames, MRF-3-3-6-MH, MRF-3-3-8-MH, MRF-3-5-8-MH and MRF-3-5-8-HH shown the

lowest values but equal 1.3, while MRF-3-3-8-HH and MRF-3-5-6-HH resulted in an equal or higher value than the maximum recommended value of 1.6 according to EN-1998-1 6.3.2(6).

For the DP-B frames, four frames result in a ratio of 1.3 and MRF-3-5-6-HH higher that the recommended limit with Ω_1=1.7, the remain frames are in between 1.3 and 1.6 limits. For DP-A frames, all the frames exceed the maximum factor of 1.6 according to EN 1998-1. When trend lines are compared for each design methodology, is clear to notice that DP-A frames experienced a higher ultimate capacity compared to the other two cases with an average tendency higher than 2.5 for the redundancy factor, DP-B frames with 1.4 and EC8 frames with 1.35, slightly larger than recommended factor by EN 1998-1.

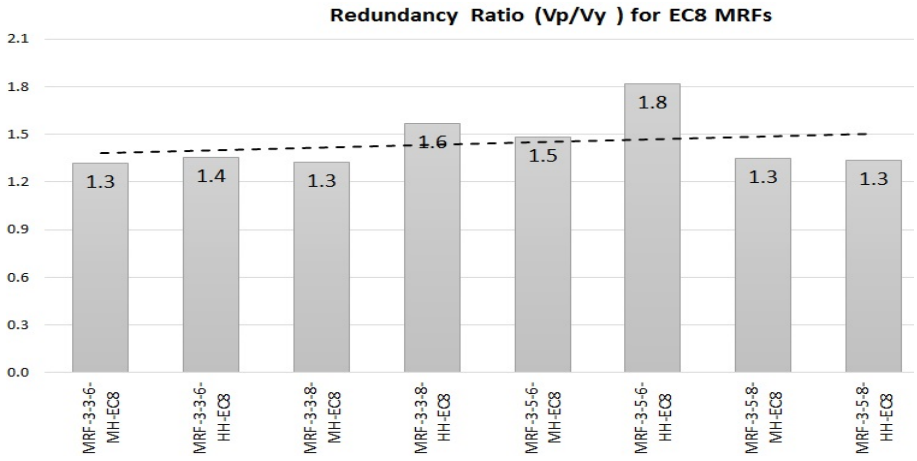

Figure 5.8 Redundancy factor V_p/V_y for MRFs designed with EC8.

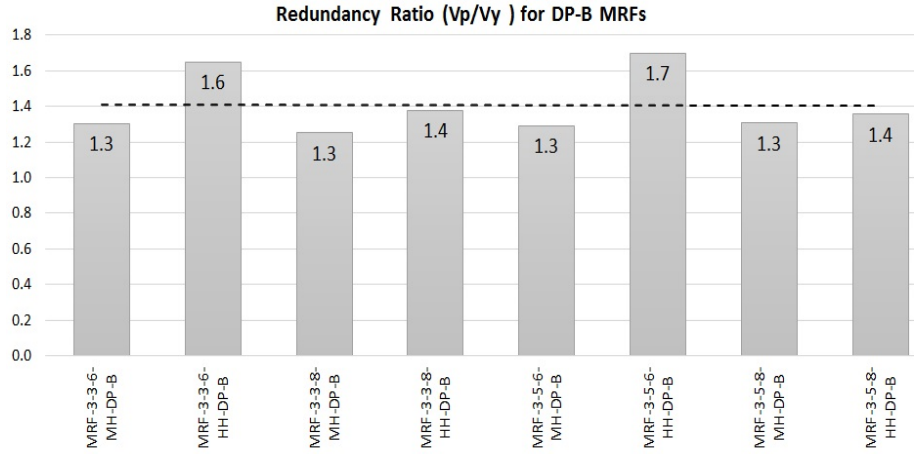

Figure 5.9 Redundancy factor V_p/V_y for MRFs designed with DP-B.

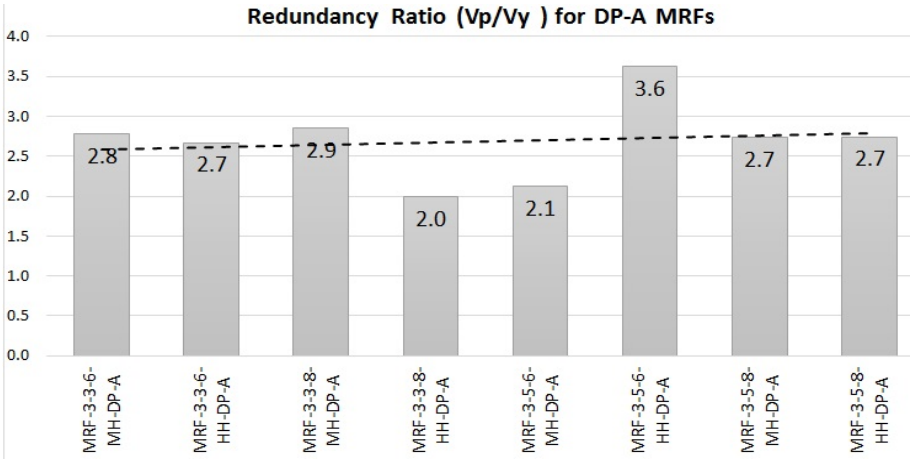

Figure 5.10 Redundancy factor V_p/V_y for MRFs designed with DP-A.

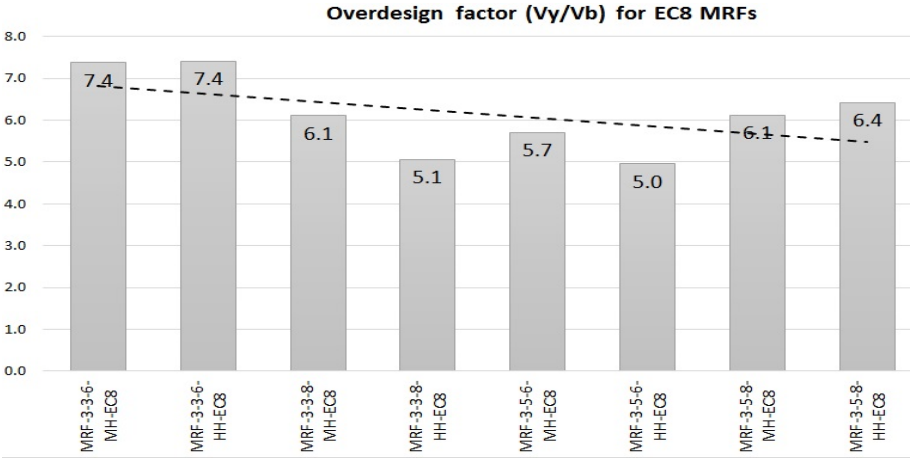

Figure 5.11 Over-design factor V_y/V_b for MRFs designed with EC8.

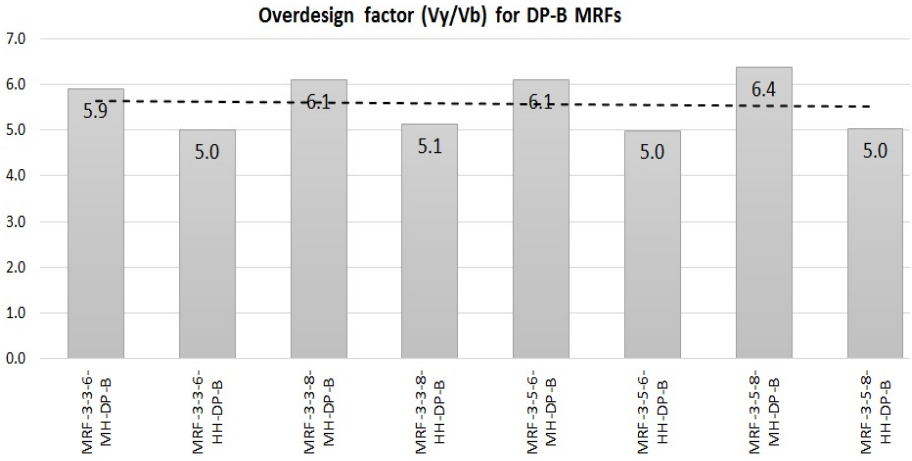

Figure 5.12 Over-design factor V_y/V_b for MRFs designed with DP-B.

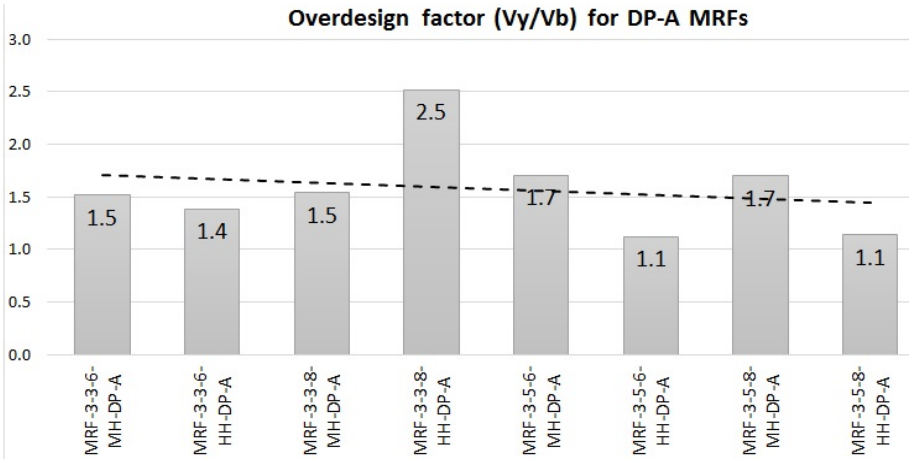

Figure 5.13 Over-design factor V_y/V_b for MRFs designed with DP-A.

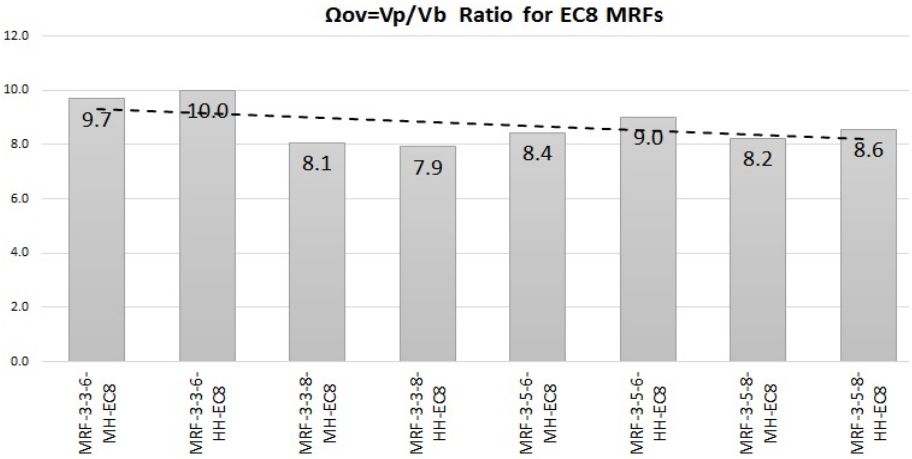

Figure 5.14 Overall Overstrength factor Ω_{ov} for MRFs designed with EC8.

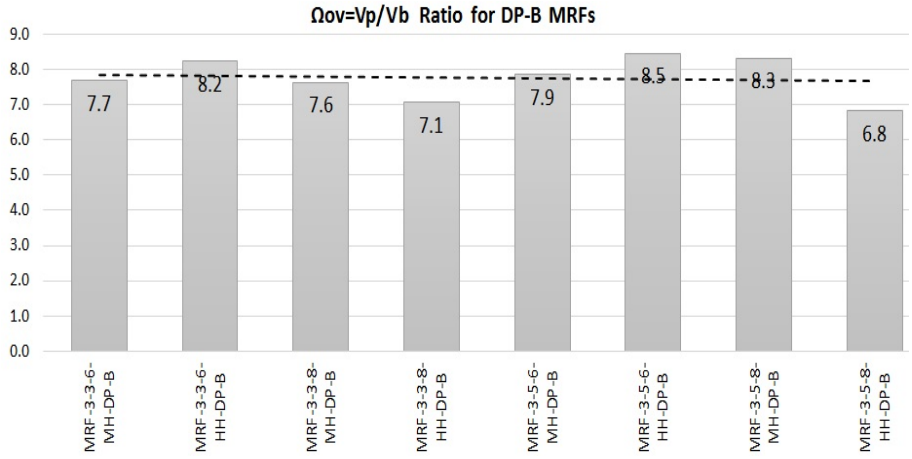

Figure 5.15 Overall Overstrength factor Ω_{ov} for MRFs designed with DP-B.

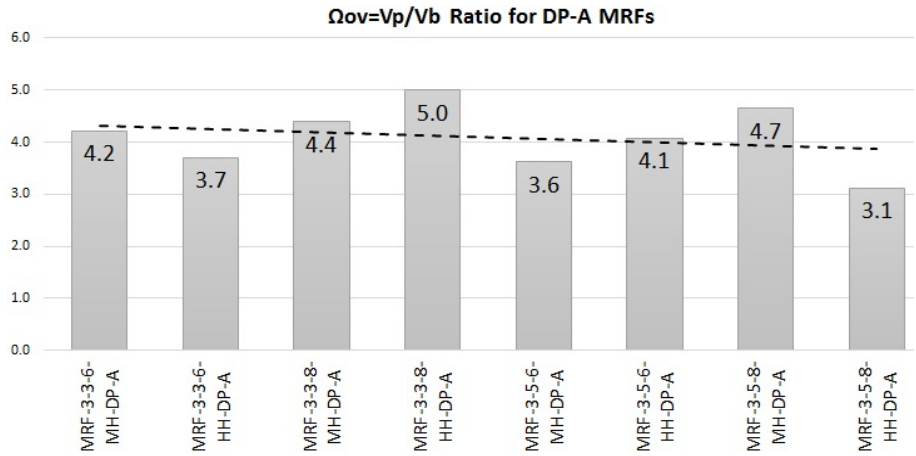

Figure 5.16 Overall Overstrength factor Ω_{ov} for MRFs designed with DP-A.

Regarding the overdesign factor ($\Omega_2 = V_y/V_b$), the pushover curves obtained with the modal distribution show the lowest Ω_2 ratio. Larger values have been obtained for the EC8 and DP-B frames, average value ranges from 5.1 to 6.7, values closer to *q=6.5* factor used in the design. This might be due to the oversize of the elements in order to fulfill the code drift requirements. There is no significant difference regarding the span length of number of bays in between frames. In the other hand, for DP-A frames the overdesign factor result in lower values within the range 1.1 a and 2.5, this corresponds to the design methodology which considers directly the forces form the seismic combination for the local and global hierachy verifications, rather than expected forces, although code drift requirements are still verified.

As it can be observed from figures 5.14 to 5.16, the overall overstrength factors Ω_{ov} for all the frames show that, code drift requirements to provide adequate lateral stiffness, leads to highly overstrength frames, regardless the design methodology for resistance of the elements. Trend lines for each methodology show averages values of 8 for EC8 and DP-B frames, and 4 for DP-A frames.

When comparing the calculated Overall overstrength factors Ω_{ov} obtained from the pushover analysis with the design overstrength factors for global verification of columns according to each design methodology, it can be noted that all the frames result in higuer Ω_{ov} values that design assumptions, which is the ideal behavior of the frames. Nevertheless, for the case of EC8 frames, the difference between the factors is around 50%, that shows that

the real behavior of the frames is highly overstimated with the current design approach.

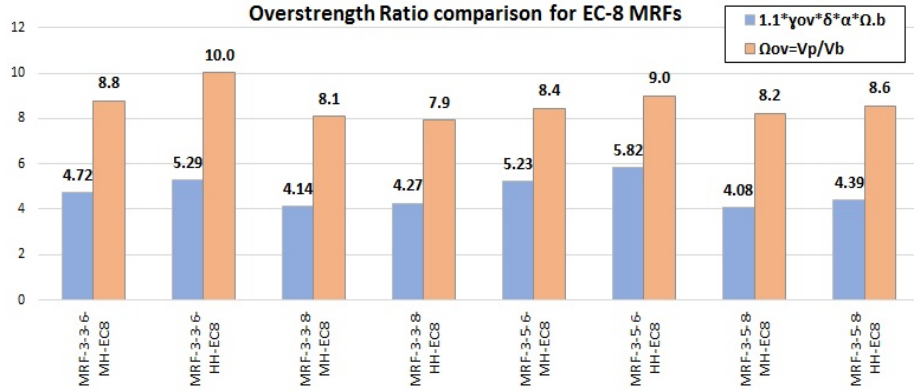

Figure 5.17 Overstrength factors comparision for MRFs designed with EC-8.

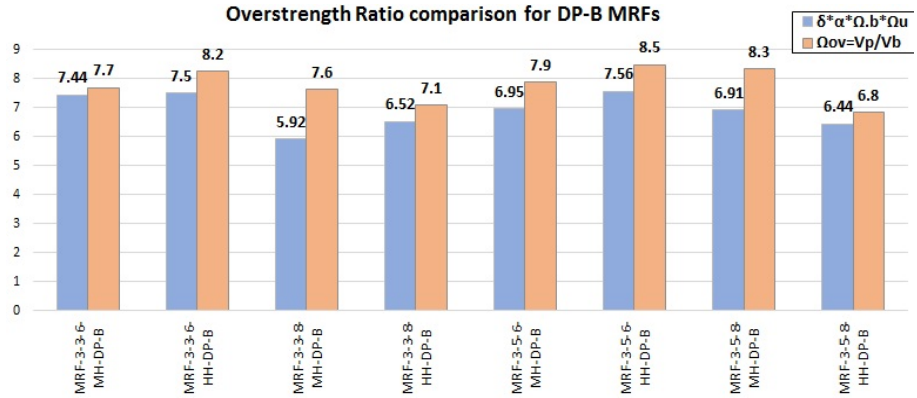

Figure 5.18 Overstrength factors comparision for MRFs designed with FD-SA design methodology.

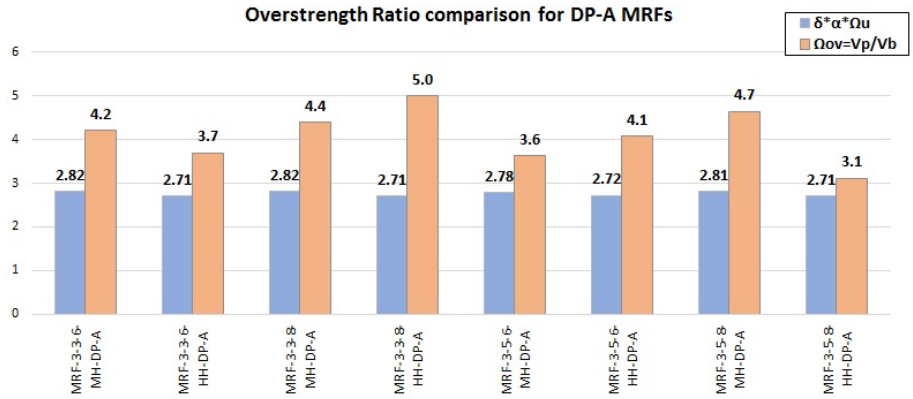

Figure 5.19 Overstrength factors comparision for MRFs designed with FD-NA design methodology.

5.1.3 Ductility factor investigation

The ductility factor (μ) has been computed for all frames in order to evaluate the plastic displacement capacity of the frames considering the ultimate displacement as a limit of 5% inter-storey drift ratio for Near Collapse (NC) performance level recommended by FEMA 356. The μ factor is defined as:

$$\mu = \frac{\delta_u}{\delta_y} \tag{5.3}$$

Where:

- δ_u is the top displacement for an inter-storey drift ratio of 5% ahieved at the top of the frame.
- δ_y is the top displacement for the formation of the first plastic hinge occurs.

In figures 5.20 and 5.22 are pictured the overall ductility factors obtained as the minimum values from both *Triangular* mode and *Uniform* lateral load pattern for the pushover analysis. As it can be noted both EC8 and DP-B frames exhibit similar average values for all the frames, between the range of 5 to 6, and for FD-NA frames, μ values are higher with an average value of 15, except for MRF-3-5-6-MH. The later shows that NA frames with smaller overstrength factors can develop larger ductility factors.

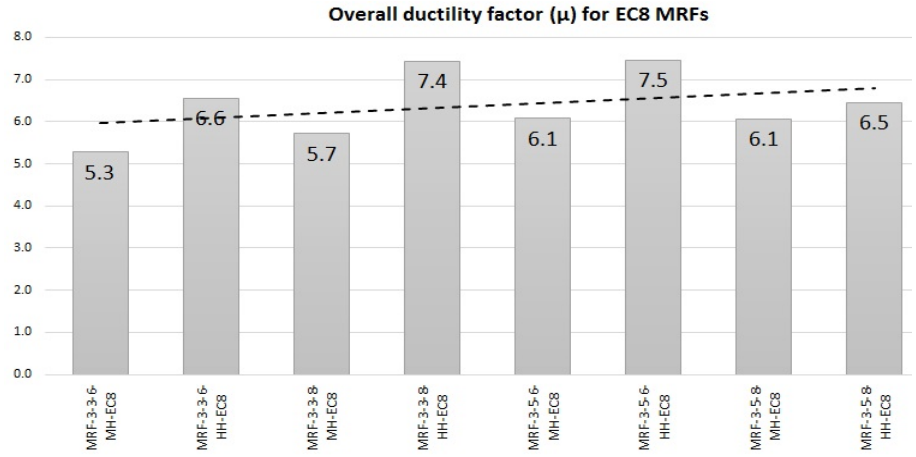

Figure 5.20 Ductility factors μ for MRFs designed with EC-8.

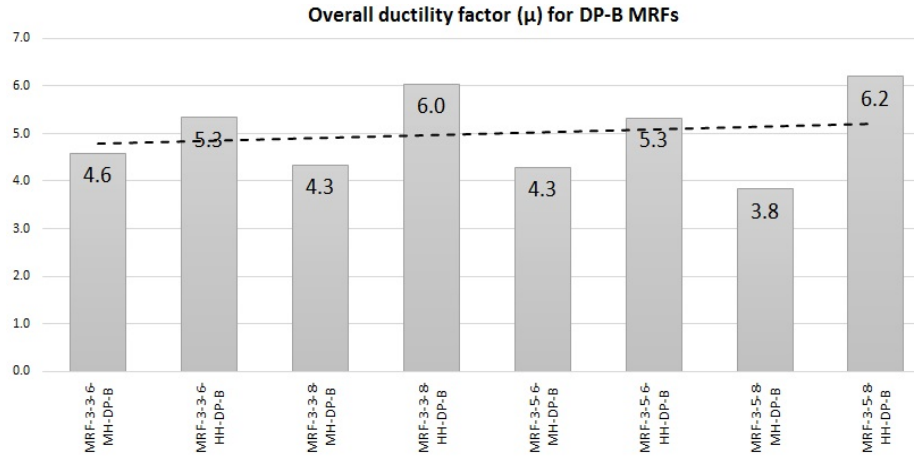

Figure 5.21 Ductility factors μ for MRFs designed with DP-B.

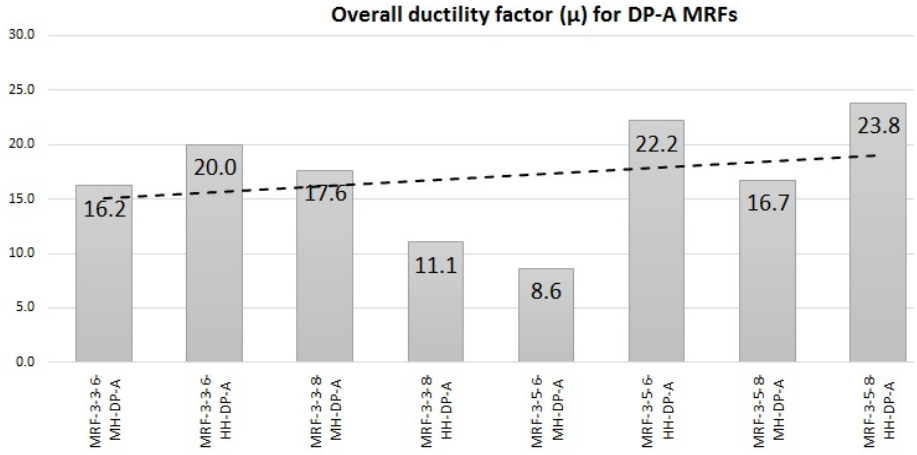

Figure 5.22 Ductility factors μ for MRFs designed with DP-A.

5.1.4 Idealized capacity curves

The results presented in figures 5.23 and 5.27 show the Idealized capacity curves along with the calculated capacity curves for MRF-3-3-6-MH for each design methodology and both lateral load patterns. For the rest of the frames, results are depicted in Annex A.

Target displacements for three limit states, Operational Level (OP), Damage Limitation (DL) and Significant Damage (SD), are calculated according to the procedure of EC-8 Annex B and described in the Idealized capacity curves of each frame. First observation to be made is that most of the frames remain in the elastic behavior for Operational Level (OL) Limit state and also for Damage limitation (DL) for the case of EC-8 and DP-B approach, for the first case, only MRF-3-3-8-MH experienced a non-linear behavior for OL limit state, the rest

of the frames for both design methodologies developed a plastic behavior for a Significant Damage (SD) limit state as it is expected.

For the case of DP-A designed frames, all remained elastic under Operational Level (OP) limit state, frames with 8 m span experienced non-linear behavior for OL limit state. All the frames developed a stable non-linear behavior under SD limit state as expected.

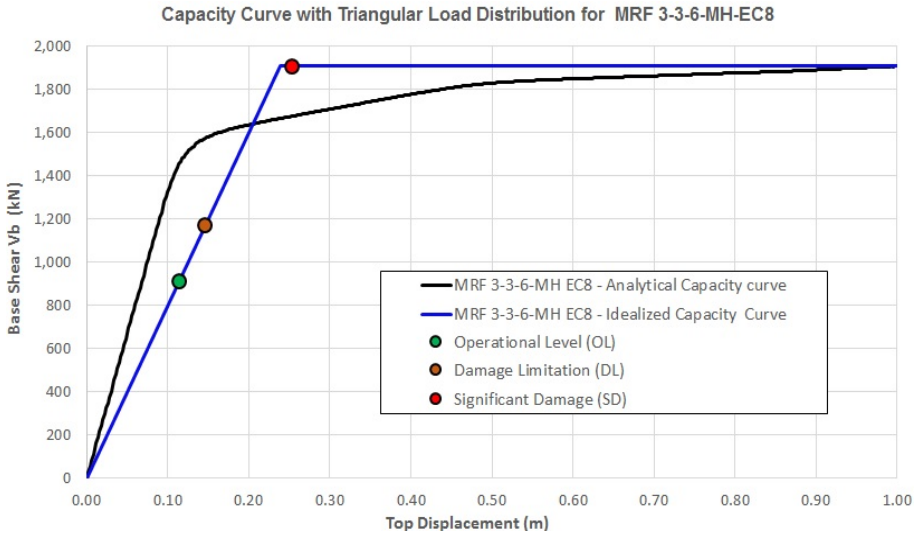

Figure 5.23 Calculated and Idealized Capacity Curve for MRF-3-3-6-MH-EC8 for Triangular load pattern, T=0.91s.

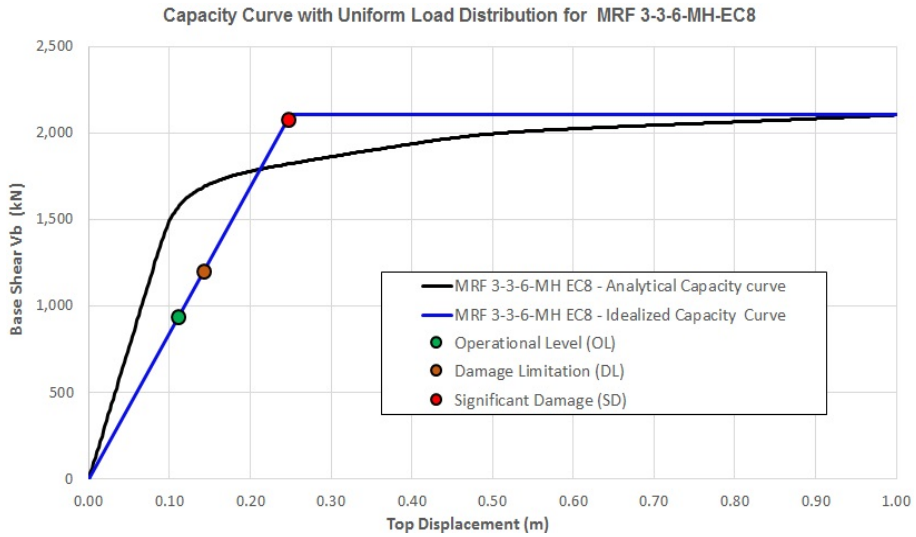

Figure 5.24 Calculated and Idealized Capacity Curve for MRF-3-3-6-MH-EC8 for Uniform load pattern, T=0.91s.

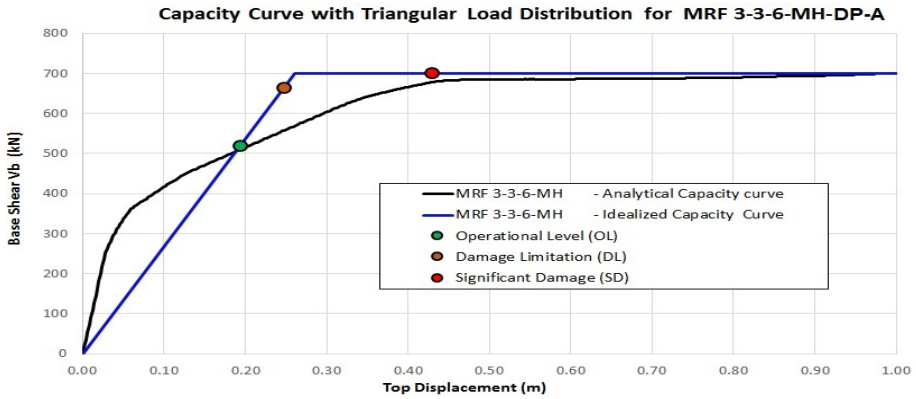

Figure 5.25 Calculated and Idealized Capacity Curve for MRF-3-3-6-MH-DP-A for Triangular load pattern, T=0.91s.

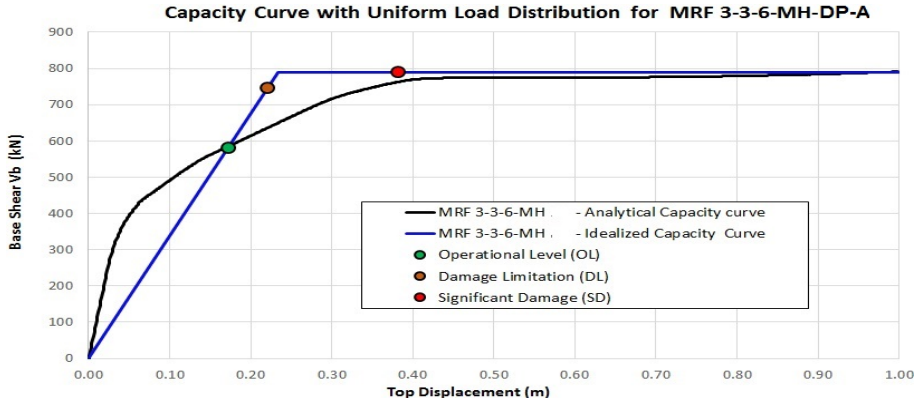

Figure 5.26 Calculated and Idealized Capacity Curve for MRF-3-3-6-MH-DP-A for Uniform load pattern, T=0.91s.

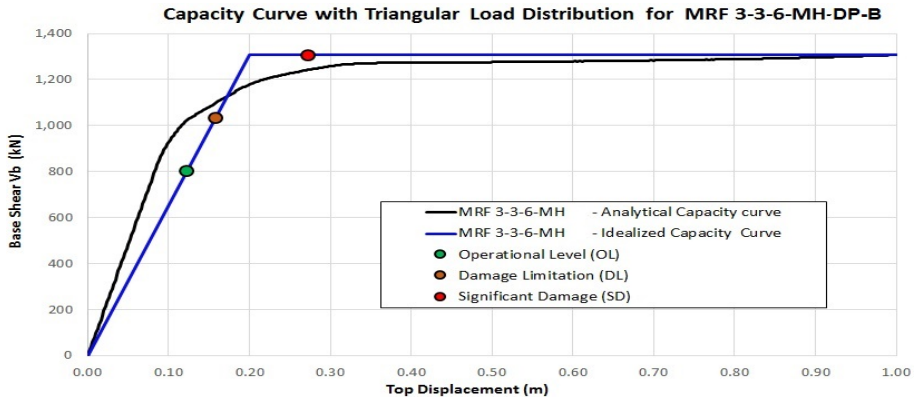

Figure 5.27 Calculated and Idealized Capacity Curve for MRF-3-3-6-MH-DP-B for Triangular load pattern, T=0.87s.

5.2 Incremental Dynamic Analysis results and discussion

The seismic response of the Moment Resisting Frames obtained from the non linear time history analysis i.e. incremental dynamic analysis (IDA) was investigated in terms of the maximum and minimum inter-storey drift distribution through the height of the structure, for transitory (during the strong motion of the accelerograms) and residual (for the last 10s with zero acceleration i.e. free vibration) inter-storey drift, as well as the peak acceleration of each storey.

Three performance levels were investigated i.e. i) Damage Limitation limit state (*DL*) with a probability of exceedance 20% in 50 years (return period T=225 years) defined by a scale factor of 0.59 for the acceleration of the records, ii) Significant Damage Limit state (*SD*) with a probability of exceedance 10% in 50 years (return period T=475 years) and a scale factor of 1, iii) Near Collapse Limit state (*NC*) with a probability of exceedance 2% in 50 years (return period T=2475 years) and a scale factor of 1.73. Plastic demand of each element in the structure as a maximum strain measured for the 14 records was investigated for each frame, results are presented in Annex B, where is possible to observe that most of the frame elements reach *Slight Damage* performance level at Near Collapse (NC) limit state i.e. with a measured strain equal or close to the steel yield strain.

5.2.1 Transient Inter-storey drift investigation

Figures 5.28 to 5.30 picture the maximum and minimum median value of the Transient Interstorey Drift (TID) for DL, SD and CP limit states for all the MRFs design with EC-8, the *TID* is presented along the building height. A decreasing tendency along the height is visible for all the frames, this is clear due to the larger height of the first storey with respect the other storeys.

According to EN 1998-1 4.4.3. For a DL performance level, considering that non-structural elements are not attached to the main structure, a limit of 0.75% for lateral inter-storey drift was considered for the initial design, none of the frames reach this limit under this performance level. For DL, MRF-3-5-8-HH and MRF-3-3-6-MH shown the maximum values of *TID* with approximate 0.45% for the first storey. Although the seismic design of the

frames has been influenced by drift limitation, the maximum values of TID are significantly lower than the limit of 0.75%

For SD limit state only MRF-3-3-6-MH exceeds 0.75% and for NC limit state MRF-3-3-6-MH for the first storey result in a maximum inter-storey drift of ±0.98% and MRF-3-5-8-HH with -0.91%, both cases are significantly lower than the limits of 2.5% and 5% respectively, showing that there is a very limited inelastic demand as was observed from the results of pushover analyses. Is clear to notice that MRFs designed with EC8 result, in most of the cases, into inefficient and uneconomical structures due to the severe requirements for both drift limitations and stability criteria.

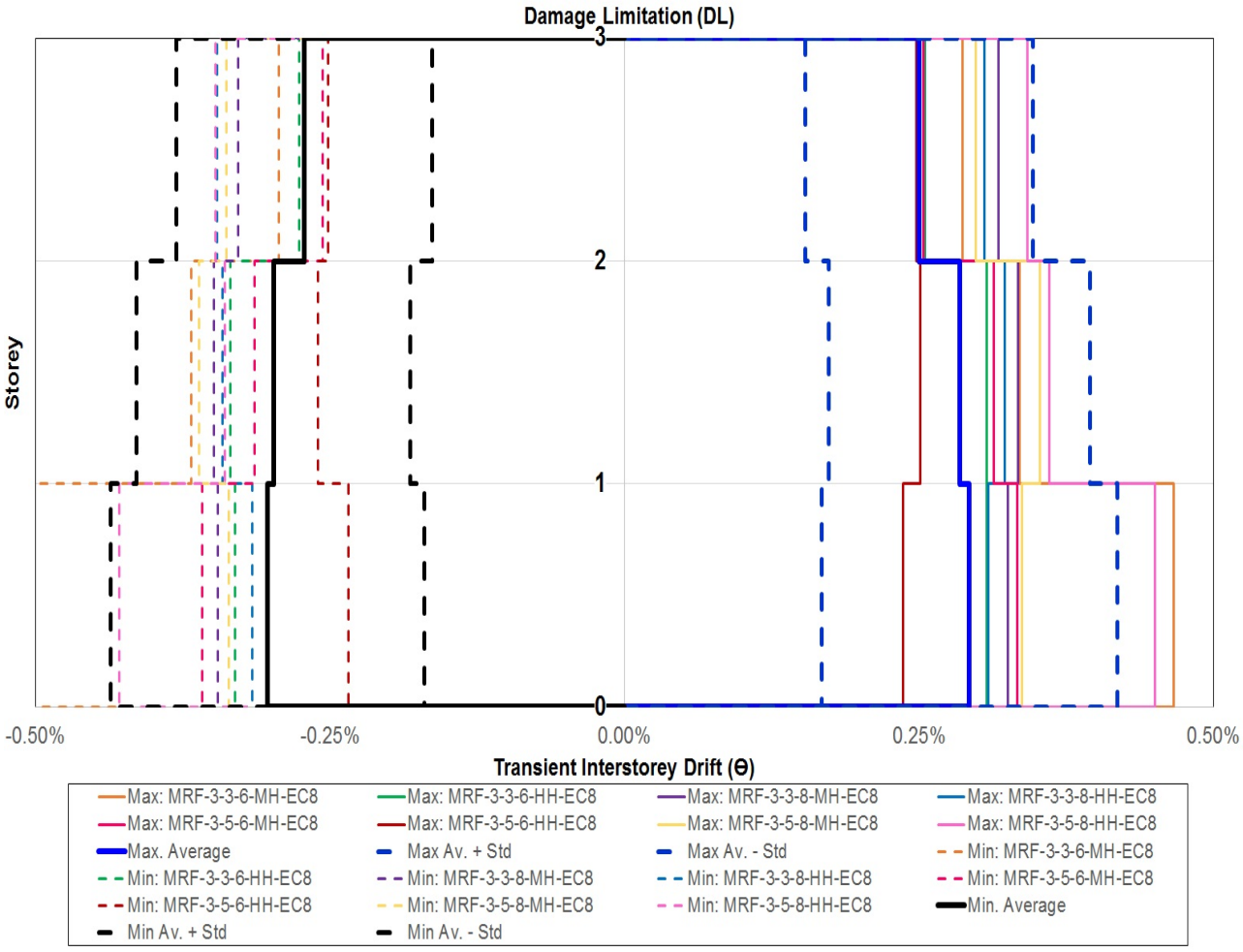

Figure 5.28 Maximum and minimum Transient inter-storey drift for EC8 frames under Damage Limitation (DL) limit state.

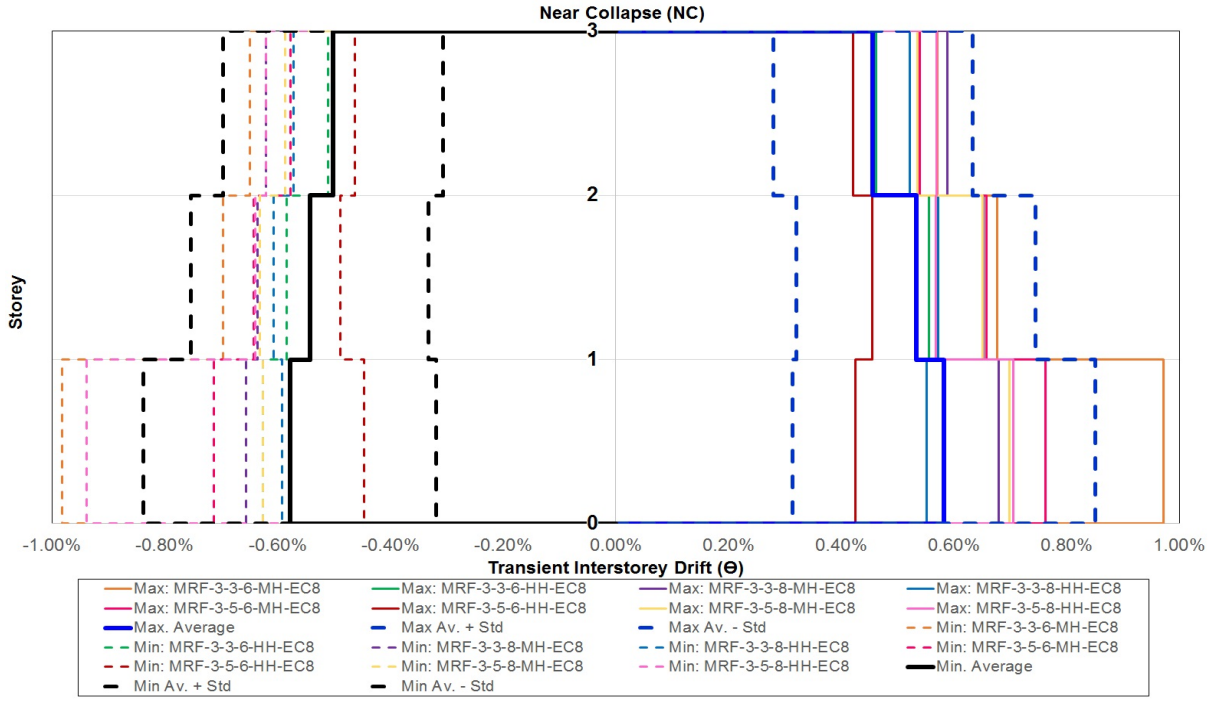

Figure 5.29 Maximum and minimum Transient inter-storey drift for EC8 frames under Significant Damage (SD) limit state.

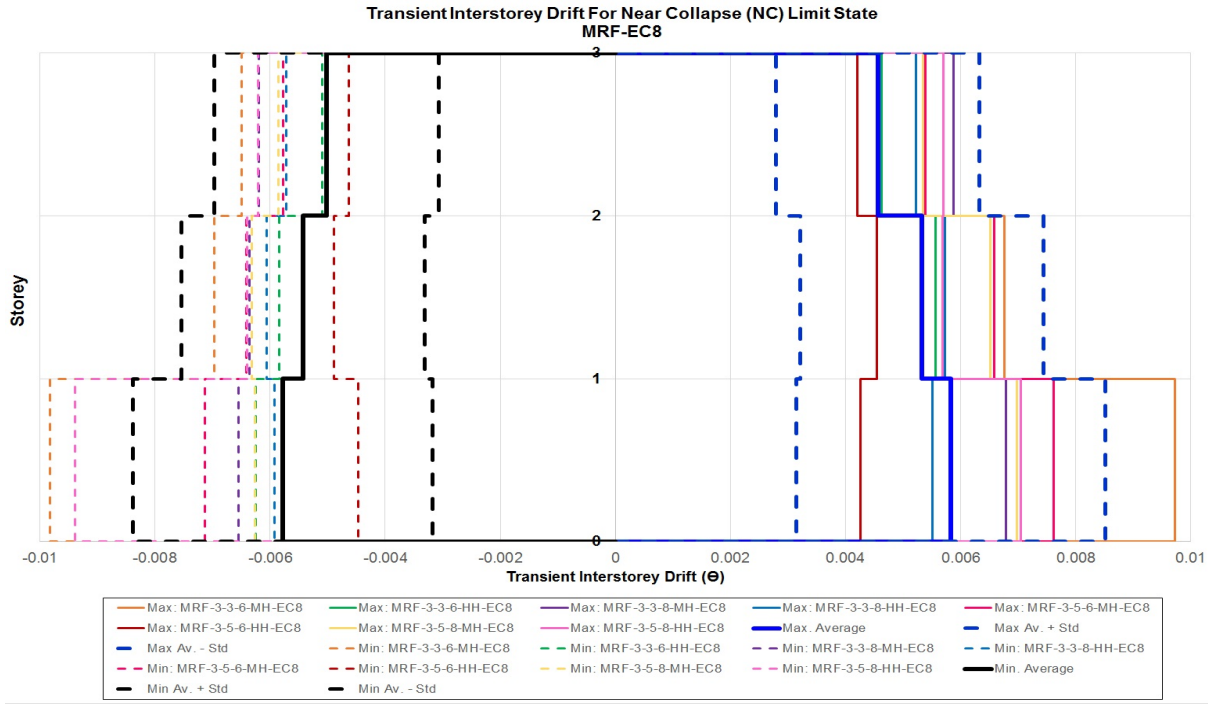

Figure 5.30 Maximum and minimum Transient inter-storey drift for EC8 frames under Near Collapse (NC) limit state.

In figures 5.31 to 5.33 are plotted the results for Transient Inter-storey Drift (*TID*) for DL, SD and NC limit states the frames designed with *Design Procedure A* (DP-A), along the height of the structure. For a DL limit state, same inter-storey drift limit of 0.75% was considered as for EC8 frames, none of the frames reached the limit criteria, neither for SD limit state, although the last limit state allows a higher inelastic demand with 2.5% inter-storey drift limit. For NC limit state, frames MRF-3-3-6-MH and MRF-3-5-8-HH exceeded the 0.75% inter-storey drift with ±0.85%, but significantly lower than the 5% limit criteria.

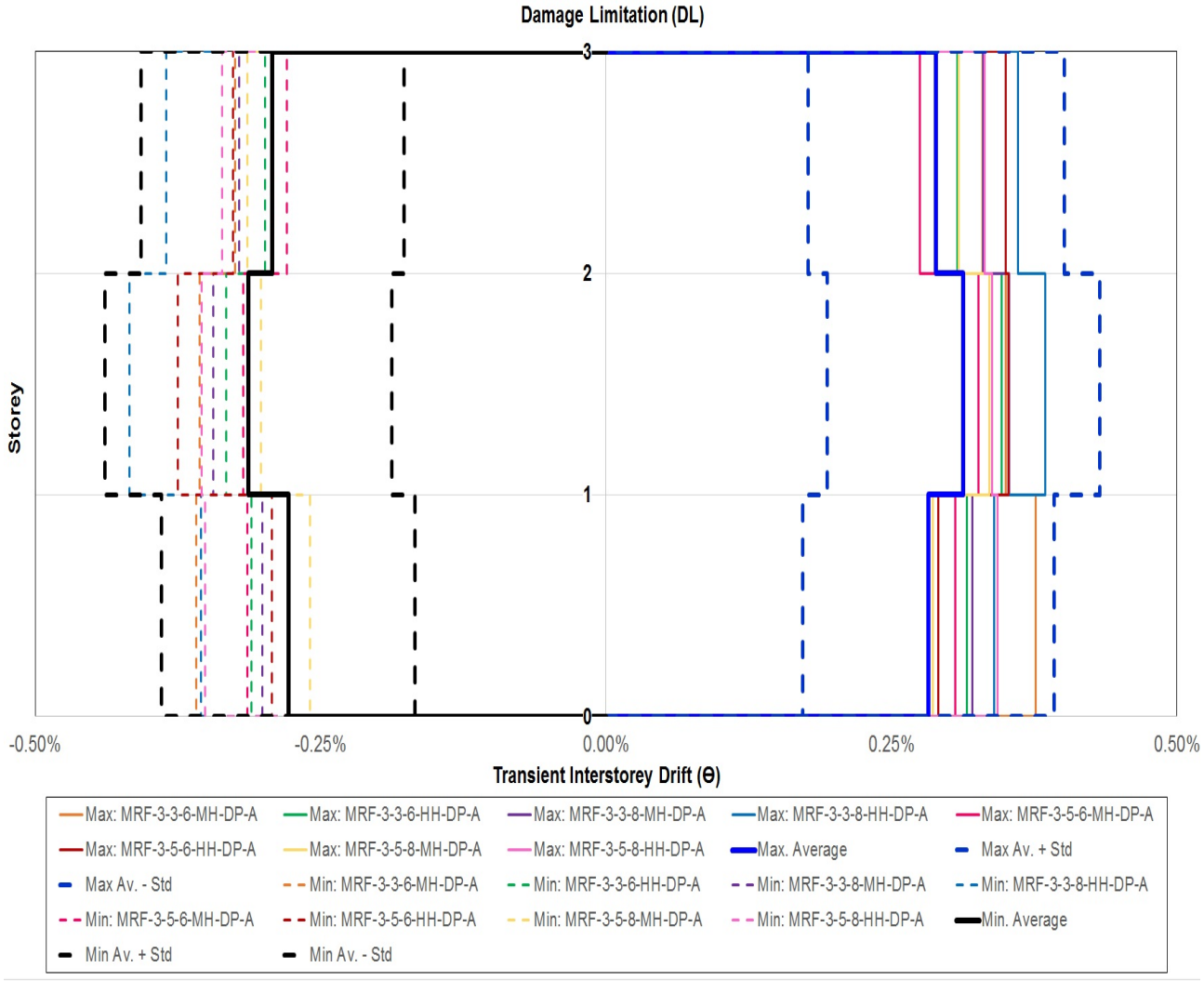

Figure 5.31 Maximum and minimum Transient inter-storey drift for DP-A under Damage Limitation (DL) limit state.

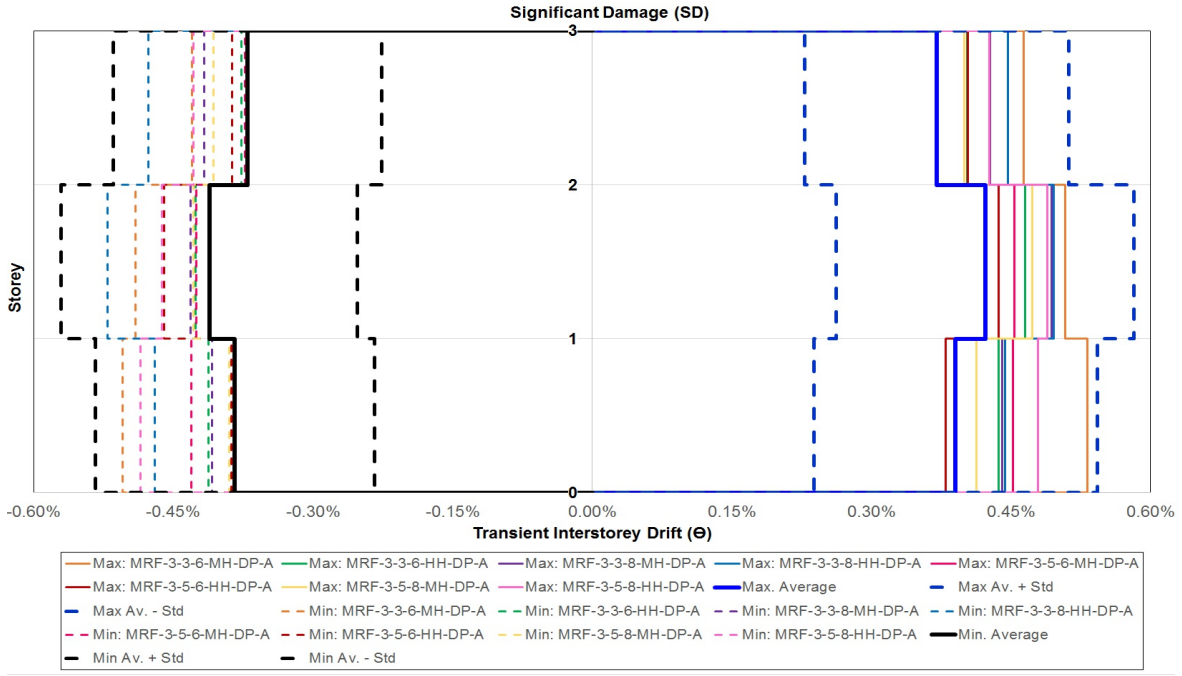

Figure 5.32 Maximum and minimum Transient inter-storey drift for DP-A under Significant Damage (SD) limit state.

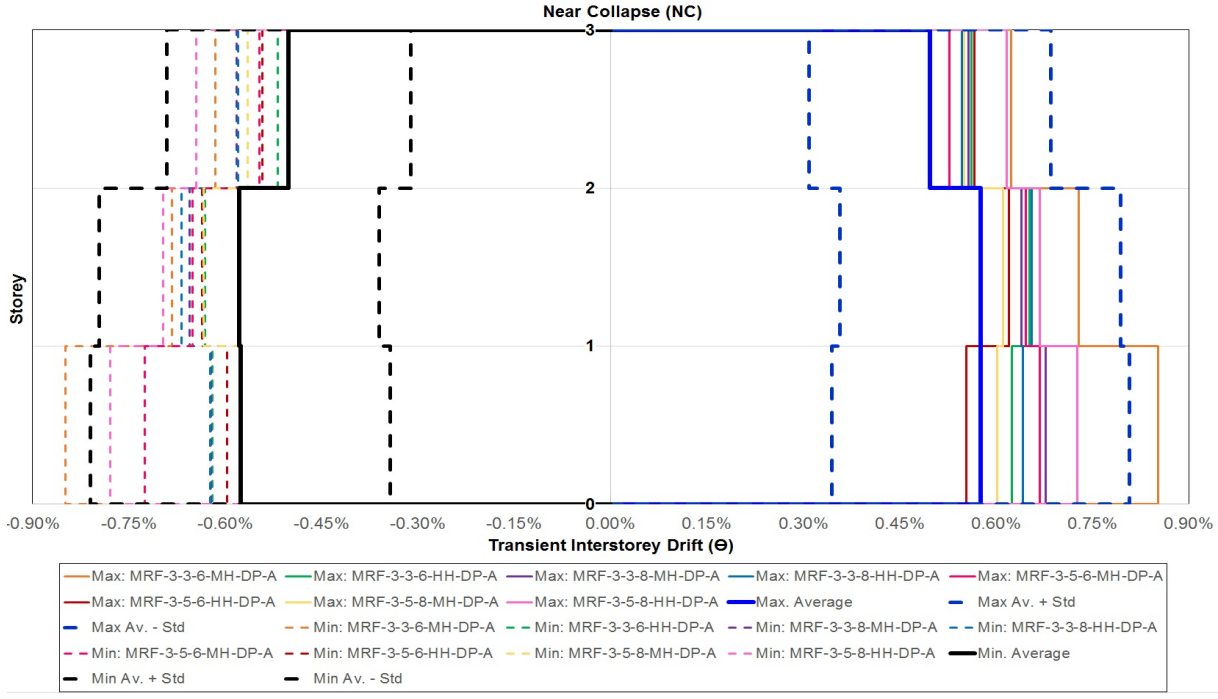

Figure 5.33 Maximum and minimum Transient inter-storey drift for DP-A under Near Collapse (NC) limit state.

Figures 5.34 to 5.36 show the results for Transient Interstorey Drift (*TID*) for DL, SD and CP limit states for the frames design with *Design Procedure B* (DP-B). None of the frames reach the inter-storey drift limit of 0.75% at any of the studied limit states. This clearly shows the highly restrictive performance of the frames due to the large lateral rigidity requirements of the design procedure.

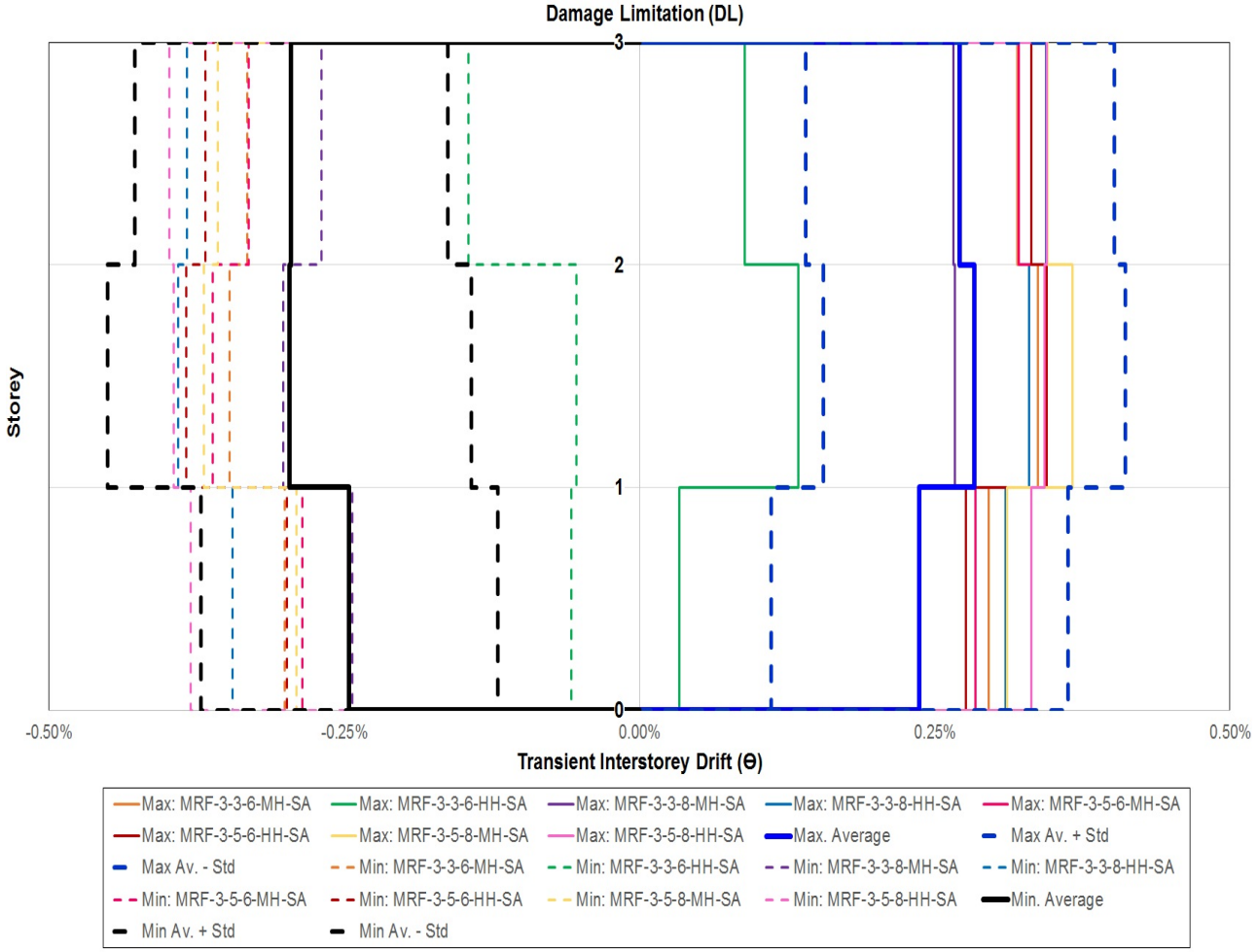

Figure 5.34 Maximum and minimum Transient inter-storey drift for DP-B under Damage Limitation (DL) limit state.

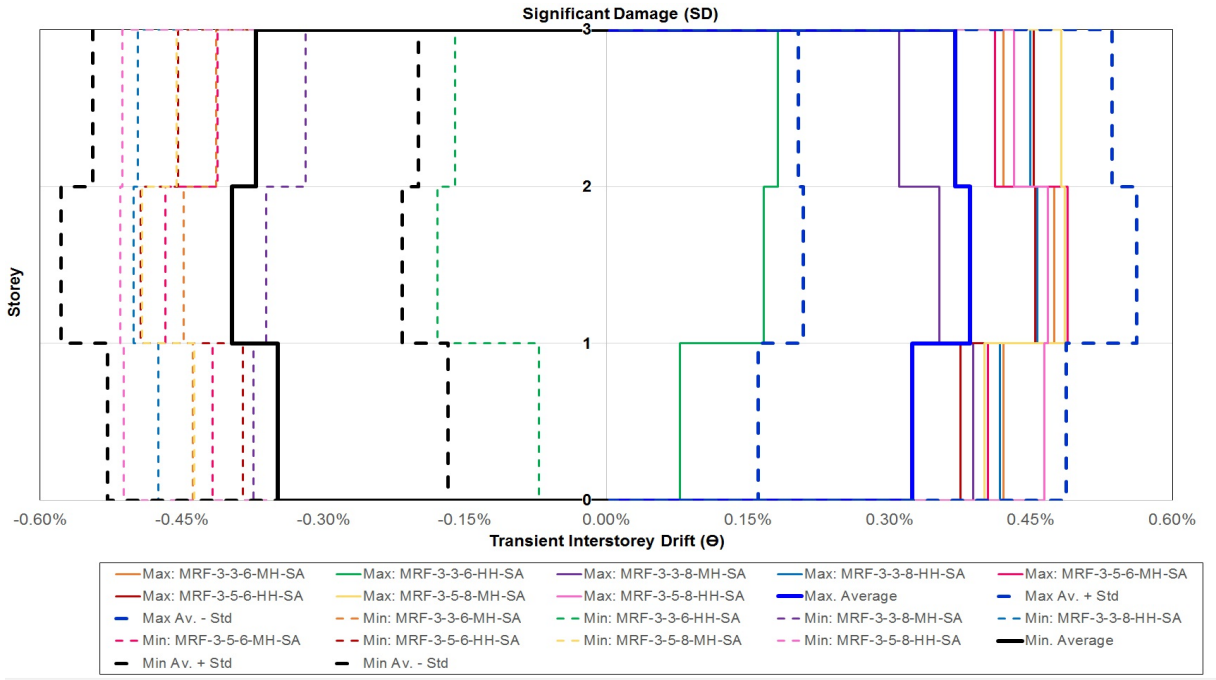

Figure 5.35 Maximum and minimum Transient inter-storey drift for DP-B under Significant Damage (SD) limit state.

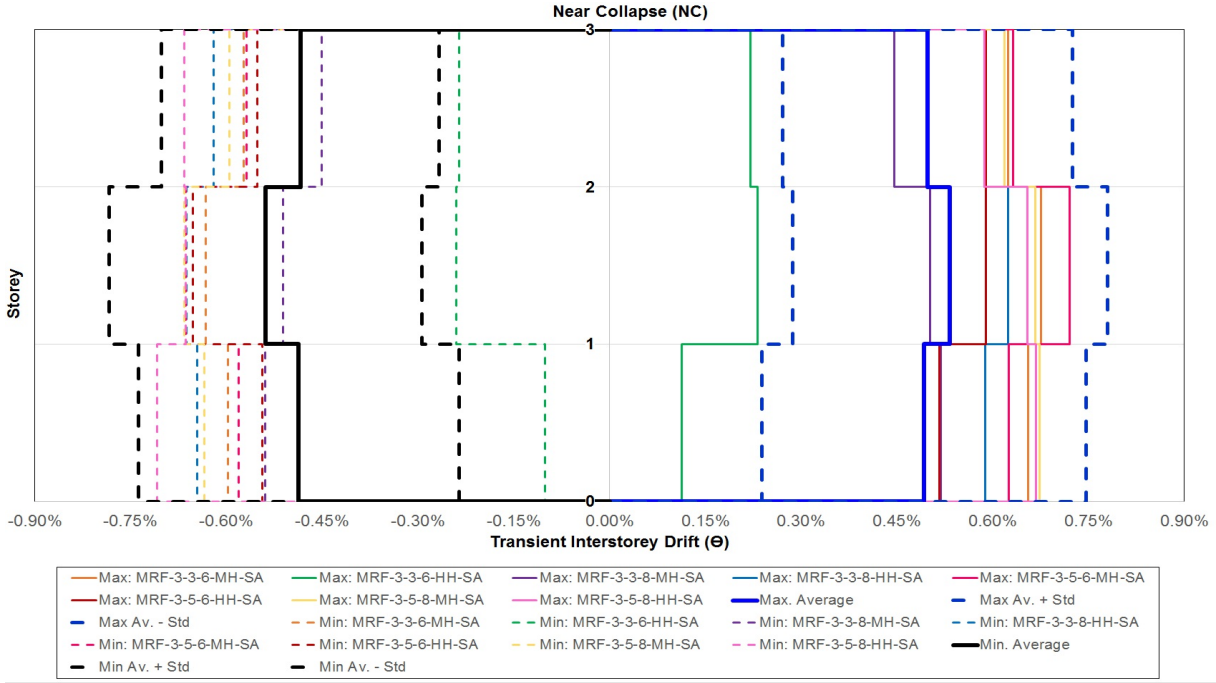

Figure 5.36 Maximum and minimum Transient inter-storey drift for DP-B under Near Collapse (NC) limit state.

5.2.2 Residual Inter-storey drift investigation

The residual inter-storey drift ratios (RID) has been monitored at each limit state, these factors can provide an important data regarding the damage distribution and post-earthquake possible reparability for the structures. Figures 5.37 to 5.39 show the Residual Interstorey Drift (RID) for DL, SD and CP limit states for all the MRFs designed with EC8, distributed along the height of the frames and increased by a 1000 scale due to its small values.

As it was observed for the pushover results, at DL limit state all the frames behave elastically, therefore RID values for this limit state are expected to be close to zero. The last is noticeable from the results of EC8 frames where average values are within the range of 0.002% and 0.006%. For SD and NC limit states, small RID were found, with maximum values lower than 1% limit criteria for SD limit state. Maximum RID values are around 0.012% and 0.024% at SD and NC limit state respectively.

In order to compare the final configuration of the frames post-quake with the global initial sway imperfections limit criteria according to EN-1991 5.3.2, a value of Φ=2.331 was calculated and compare to the RID of the frames for SD and NC limit states. It can be recognized that none of the frames reached the limit criteria at any limit state studied, is possible to expect that the frames will not experience permanent inter-storey drifts after the seismic events that will reduce its resistance to buckling, leading to complex P-Δ effects.

Figures 5.40 to 5.42 show the Residual Inter-storey Drift (RID) for DL, SD and CP limit states for the MRFs designed with DP-A. For DL limit state, small values were obtained with maximum values within the range of 0.01% and 0.012%, as it is expected for this limit state where all the frames remain elastic. For SD and NC limit states, maximum values of 0.02% and 0.04% were observed, values are smaller than limit criteria of 1%, it can be expected that those structures remain easily to repair after earthquake showing an economical advantage on repairing costs which can represent a high percentage of the overall cost of a structure in an initial benefit-cost analysis.

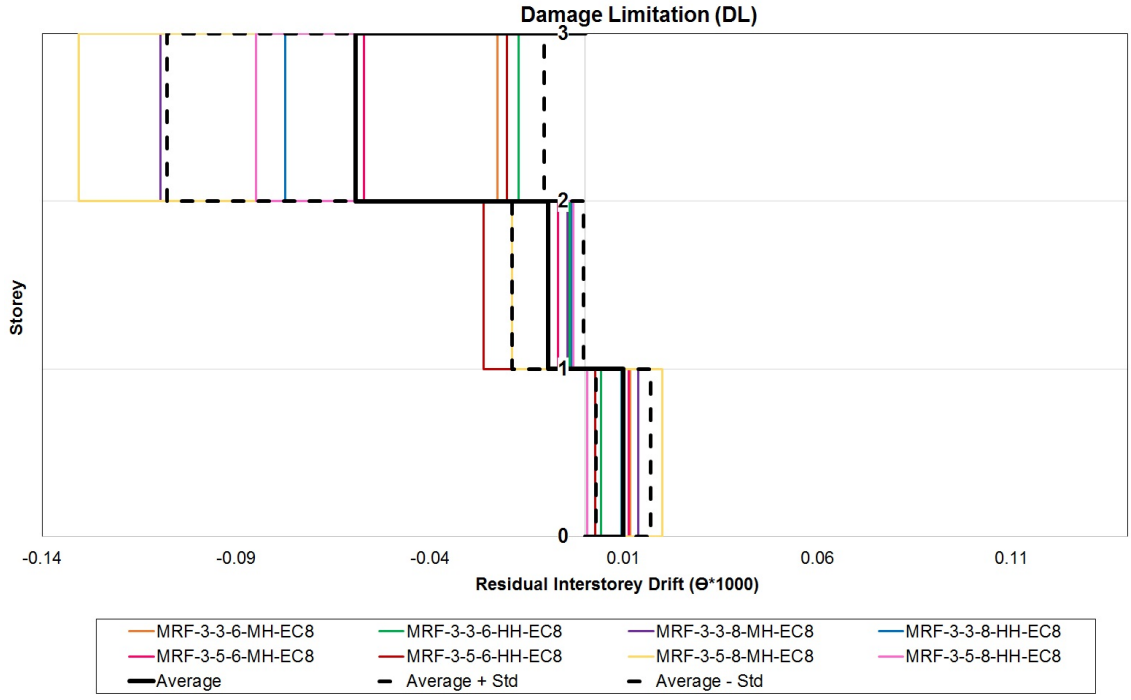

Figure 5.37 Residual inter-storey drift for EC8 frames under Damage Limitation (DL) limit state.

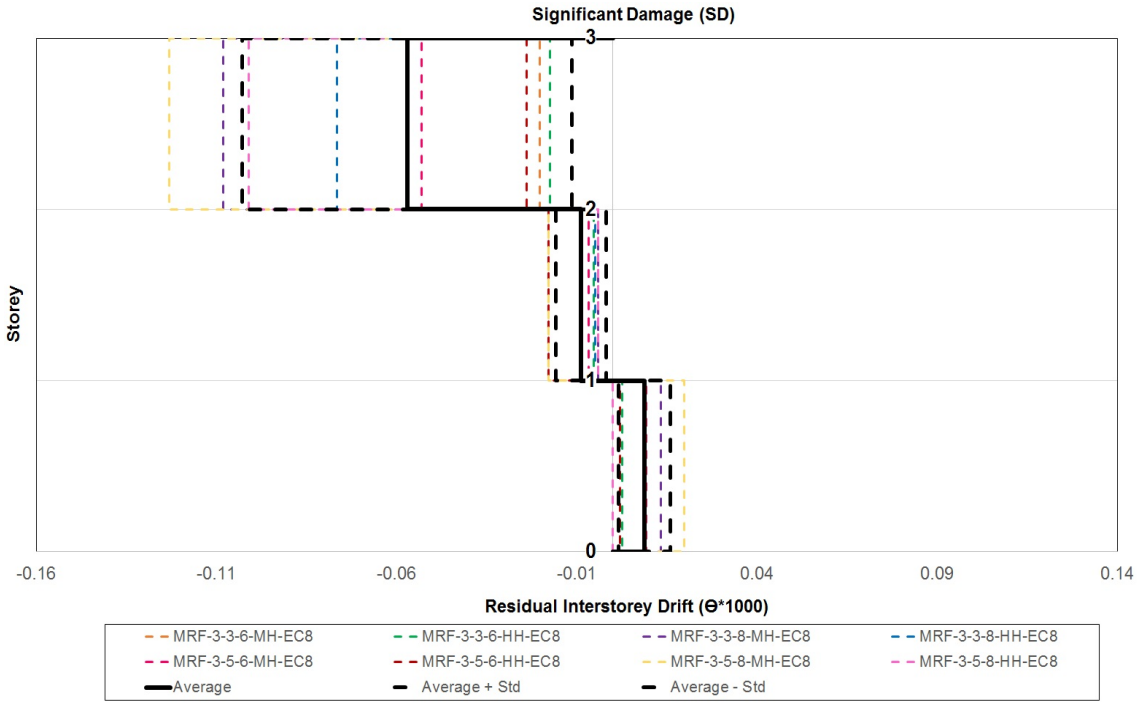

Figure 5.38 Residual inter-storey drift for EC8 frames under Significant Damage (SD) limit state.

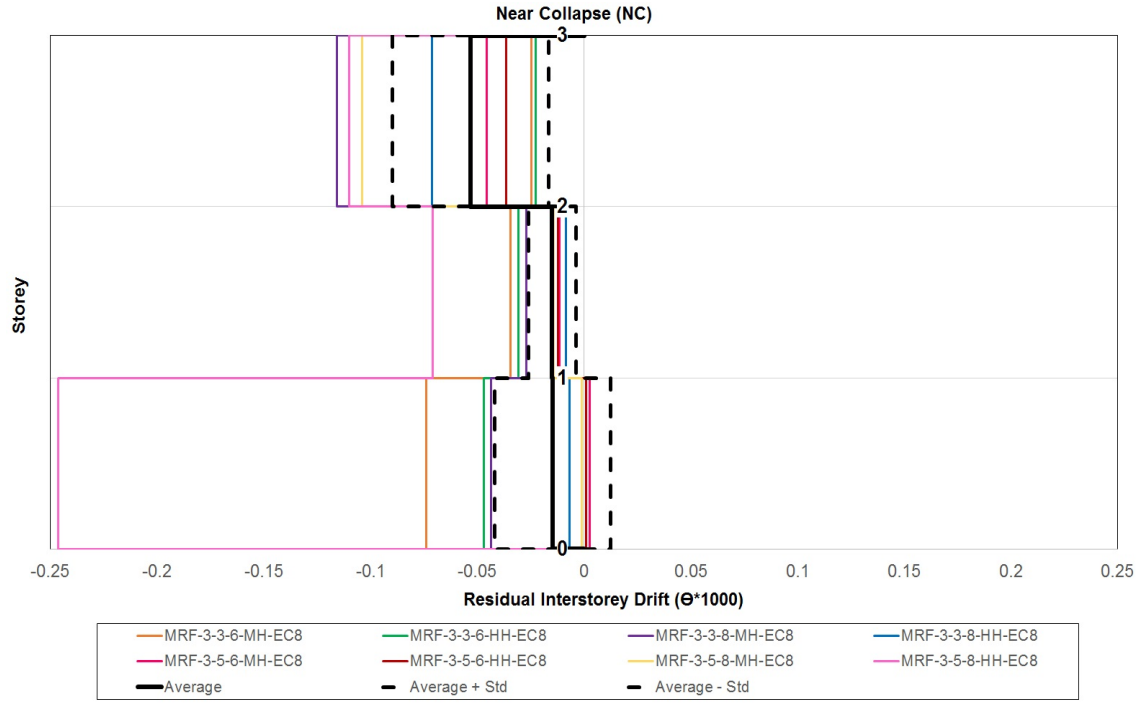

Figure 5.39 Residual inter-storey drift for EC8 frames under Near Collapse (NC) limit state.

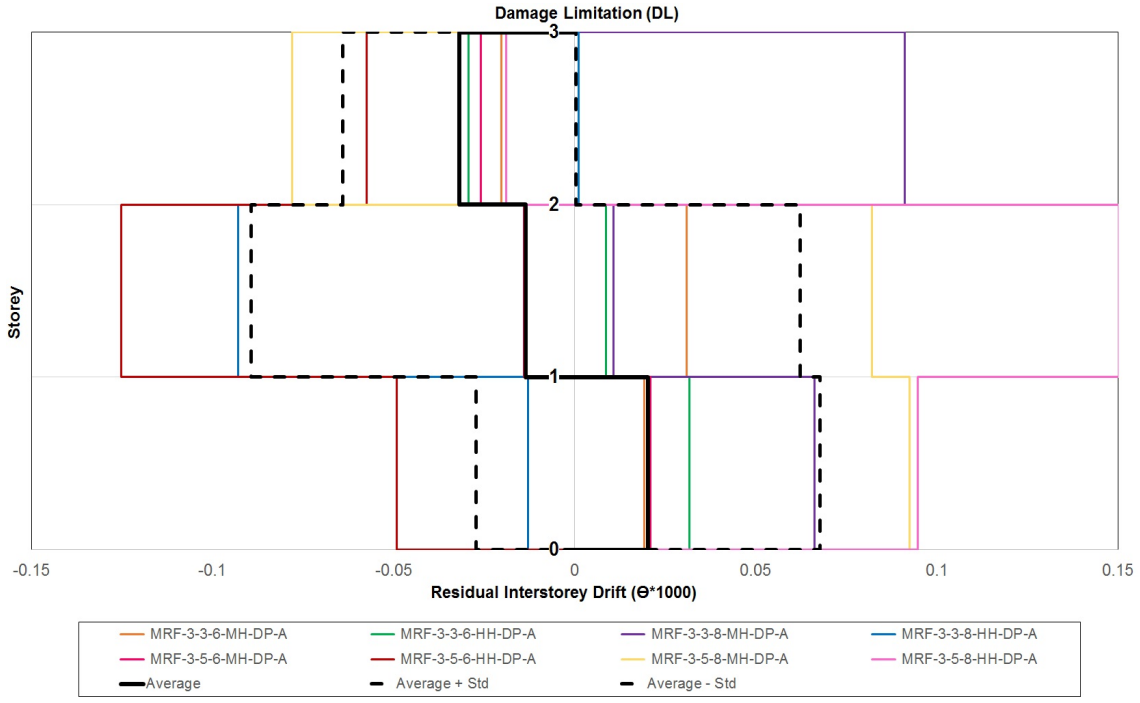

Figure 5.40 Residual inter-storey drift for DP-A under Damage Limitation (DL) limit state.

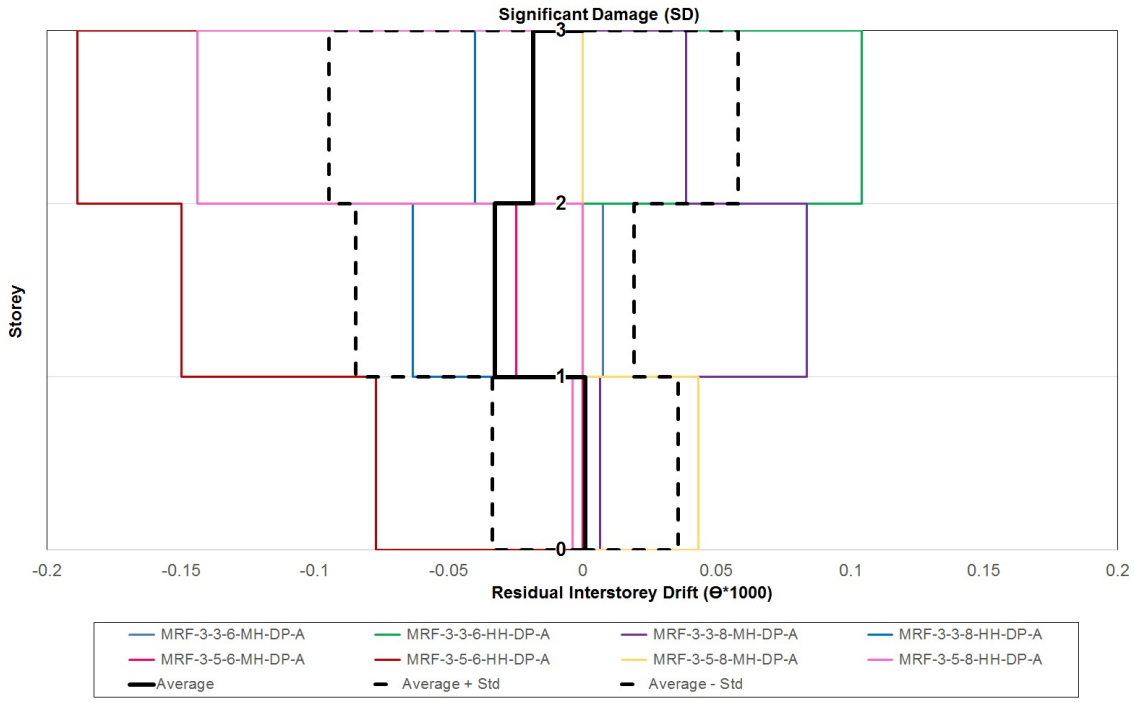

Figure 5.41 Residual inter-storey drift for DP-A under Significant Damage (SD) limit state.

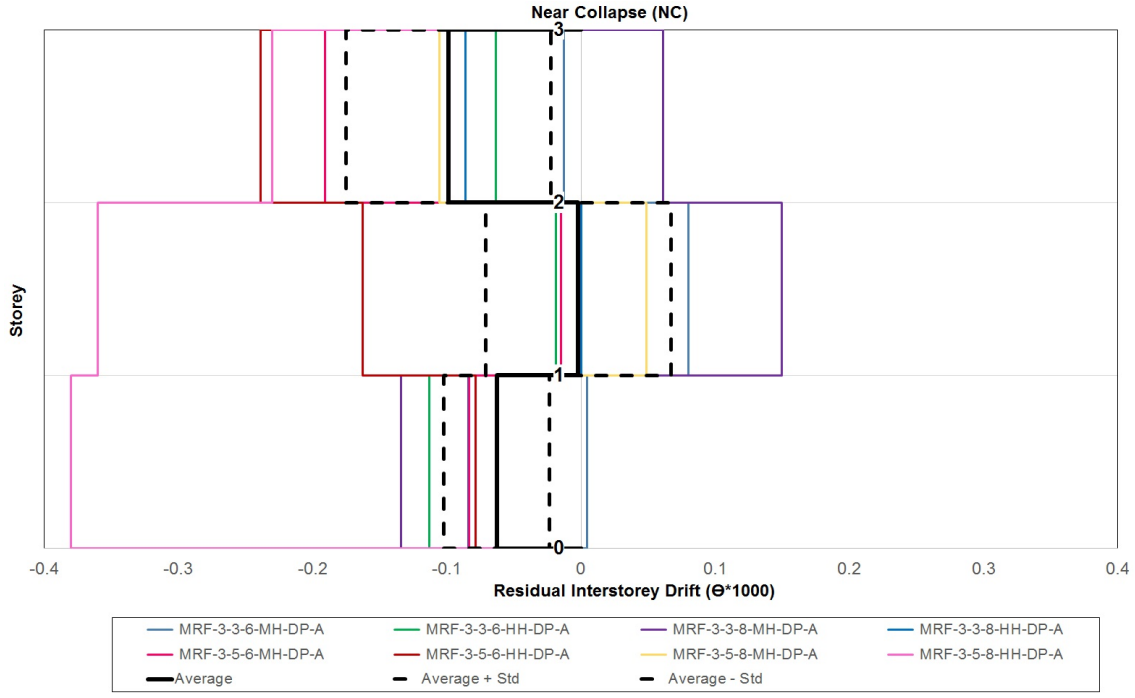

Figure 5.42 Residual inter-storey drift for DP-A under Near Collapse (NC) limit state.

From figures 5.43 to 5.45 we can see the RID results for the frames design with DP-B, for the three limit states previously defined. For DL limit state, a maximum value of 0.024%

was obtained with the majority of the frames in within the range of 0.006% and 0.011%, as it is expected under the elastic behavior of the frames. For SD and NC limit states, small values were observed ranging the average of 0.0085% and 0.025% respectively, values smaller than SD limit criteria of 1% and NC limit criteria of 5%.

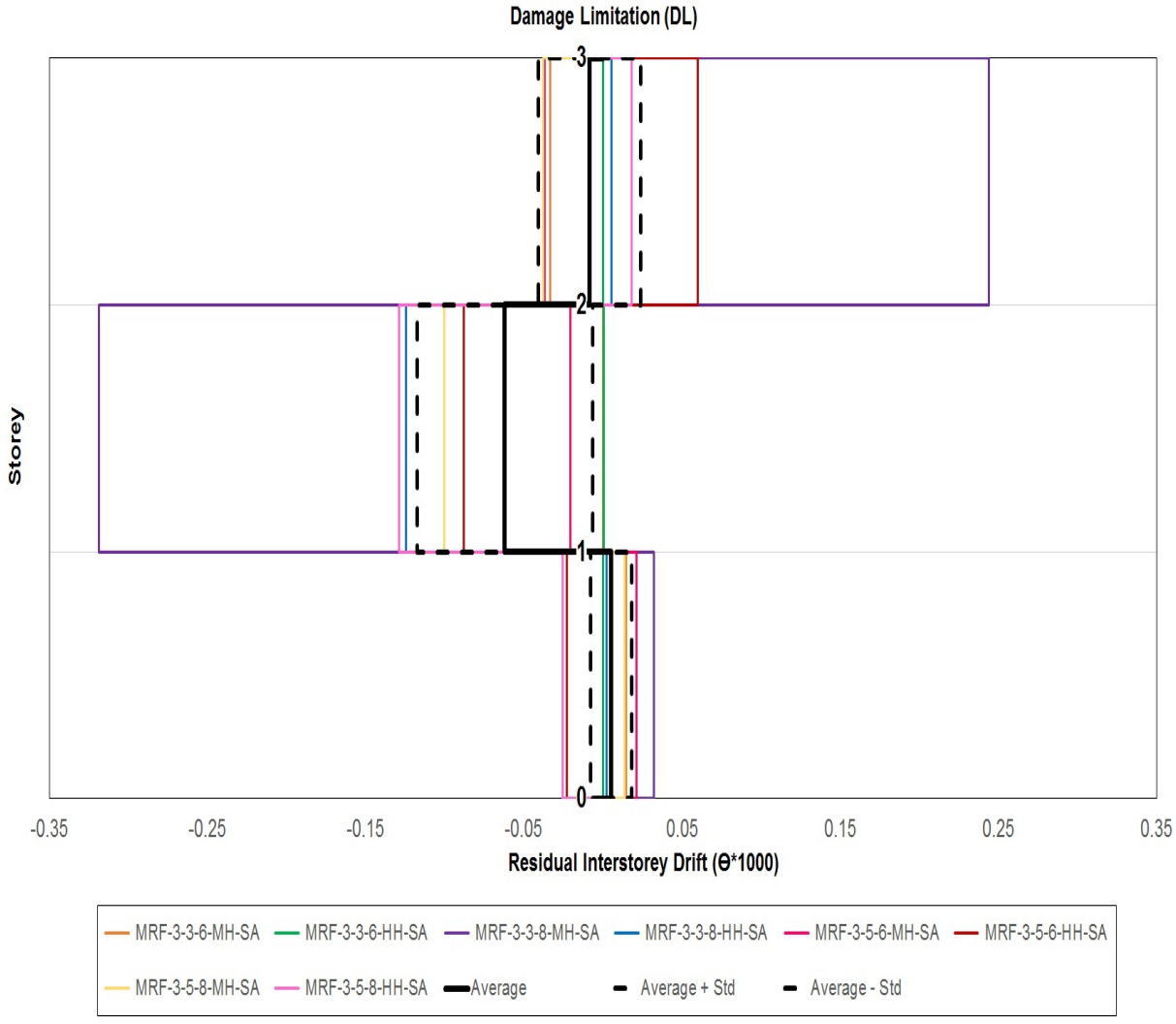

Figure 5.43 Residual inter-storey drift for DP-B under Damage Limitation (DL) limit state.

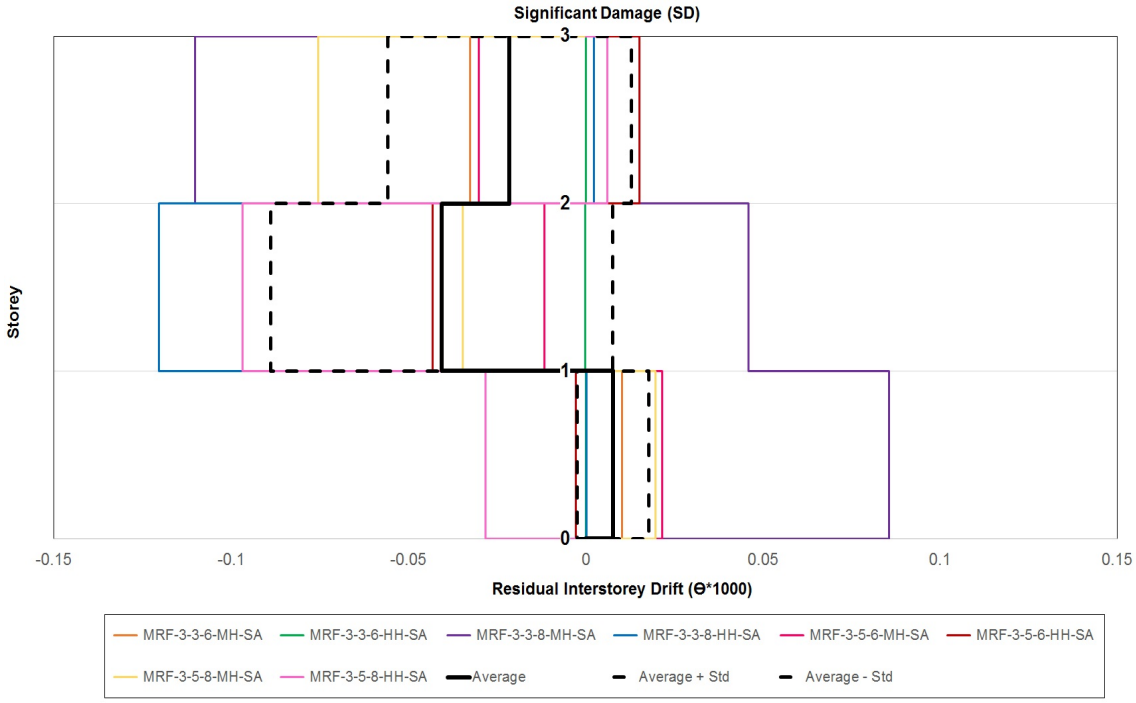

Figure 5.44 Residual inter-storey drift for DP-B under Significant Damage (SD) limit state.

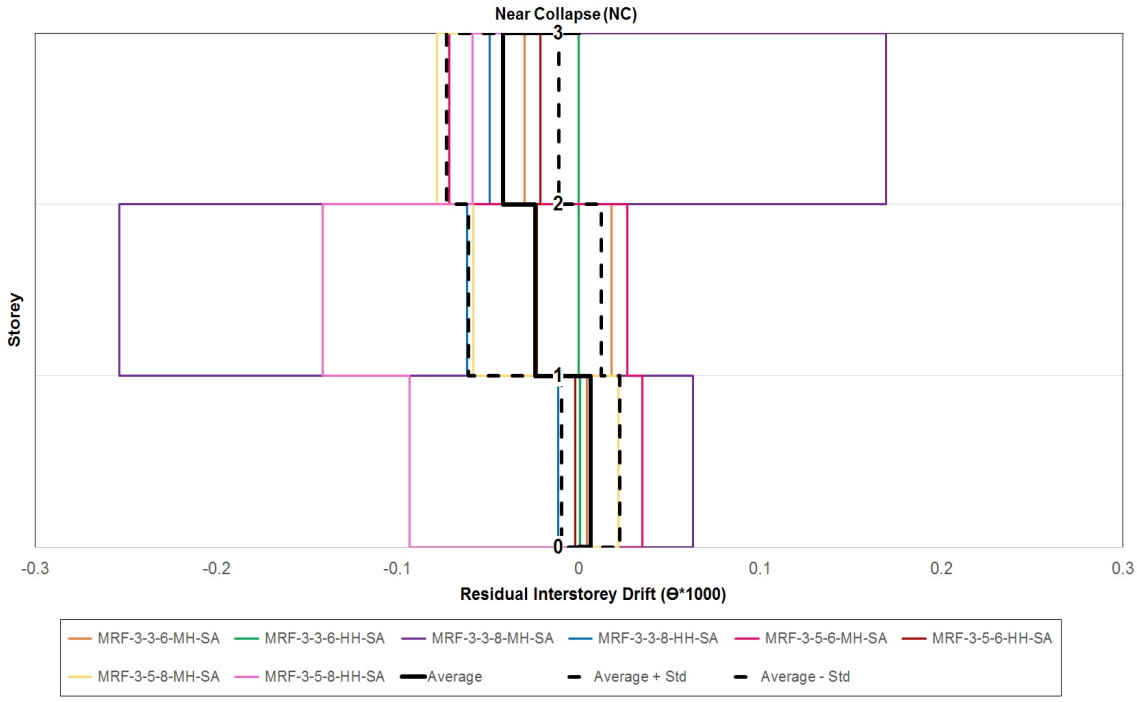

Figure 5.45 Residual inter-storey drift for DP-B under Near Collapse (NC) limit state.

5.2.3 Maximum acceleration per storey investigation

Conventionally, Peak Storey Accelerations (PSA) are related to non-structural damage, that can allow us to estimate the potential economic loss in a structure according on the type of facilities and non-structural elements present. PSA was evaluated as the maximum absolute acceleration value per storey (PSA) compared with the maximum absolute acceleration of the base (PSA_g), therefore amplification factors of base acceleration per storey are shown and studied in the next paragraphs for the three limit states studied before (DL, SD and NC), results are shown by each storey.

In figures 5.46 to 5.48 are shown the amplification factors for PSA for each storey in relation of the base maximum acceleration for DL, SD and CP limit states for the frames designed with EC-8. The highest amplification factors are for the first and second storeys with average values of 6 and 4 respectively, for the third storey, higher amplification factors appear for DL state. In figures 5.49 to 5.51 are depicted the amplification factors for maximum acceleration of each storey for the frames designed with DP-A. The highest amplification factors are for the second storey, up to average 10 times the base acceleration values for DL limit state. For the third and first storeys, average values for the three limit states are around 2. For the SD limit state of DP-A and EC8 frames under DL limit state, the significant dynamic magnification of storey accelerations is correlated with very severe non-structural damage.

For the frames designed with DP-B, the highest amplification factors are for MRF-3-5-6-MH for the second storey, average values for DL limit state are approximate 4. For the first storey average values remain constant for the three limit states within the range 0.5 and 3, while for the third storey average values are 0.8 to 3.2, with a constant distribution for the three limit states.

In the following pages all the results for the maximum accelerations amplification factors (PSA/PSA_g) per storey and design methodology are presented.

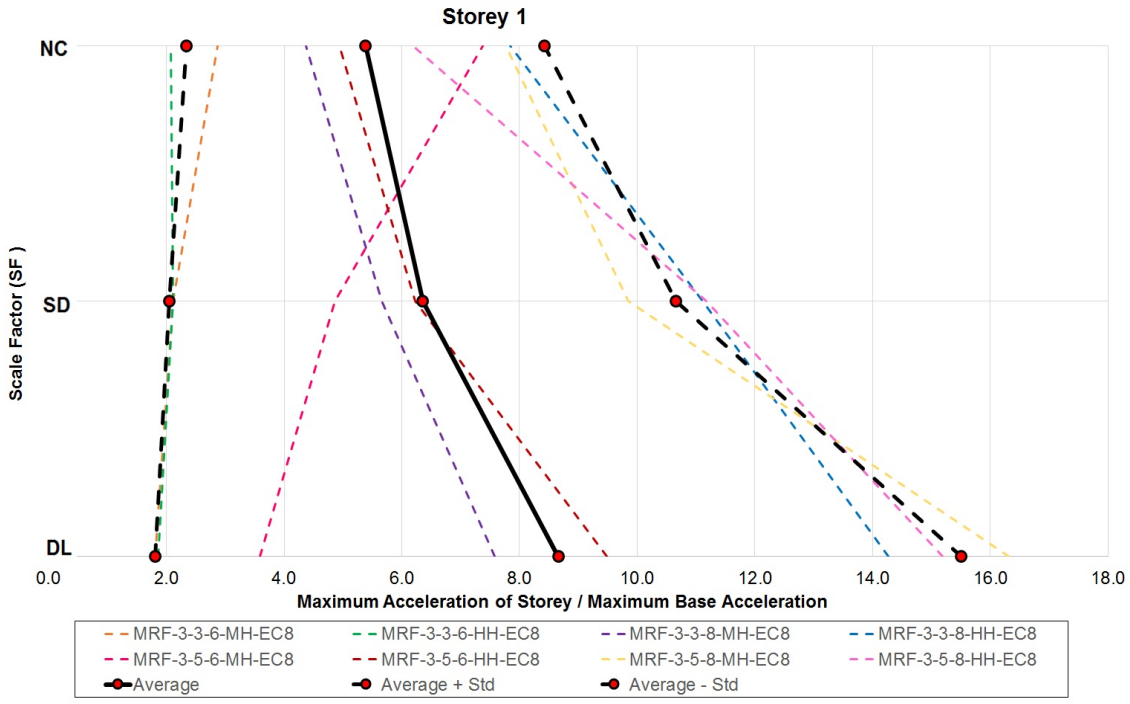

Figure 5.46 Maximum storey acceleration for DL, SD and NC limit states for the third storey of MRFs-EC8.

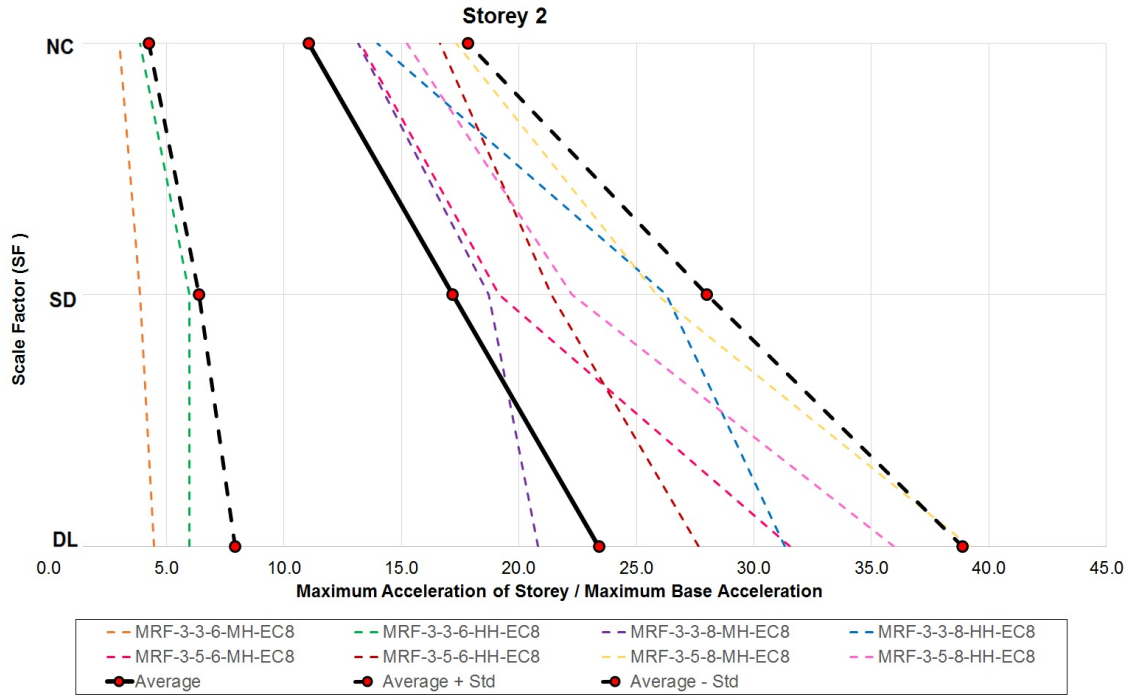

Figure 5.47 Maximum storey acceleration for DL, SD and NC limit states for the second storey of MRFs-EC8.

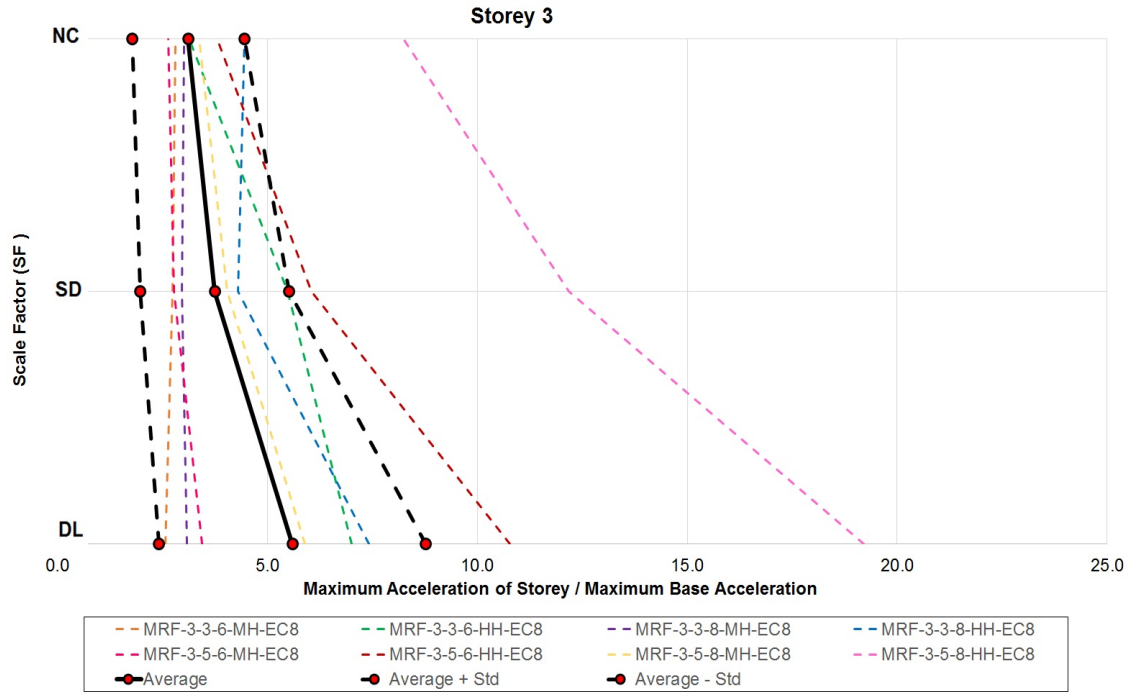

Figure 5.48 Maximum storey acceleration for DL, SD and NC limit states for the first storey of MRFs-EC8.

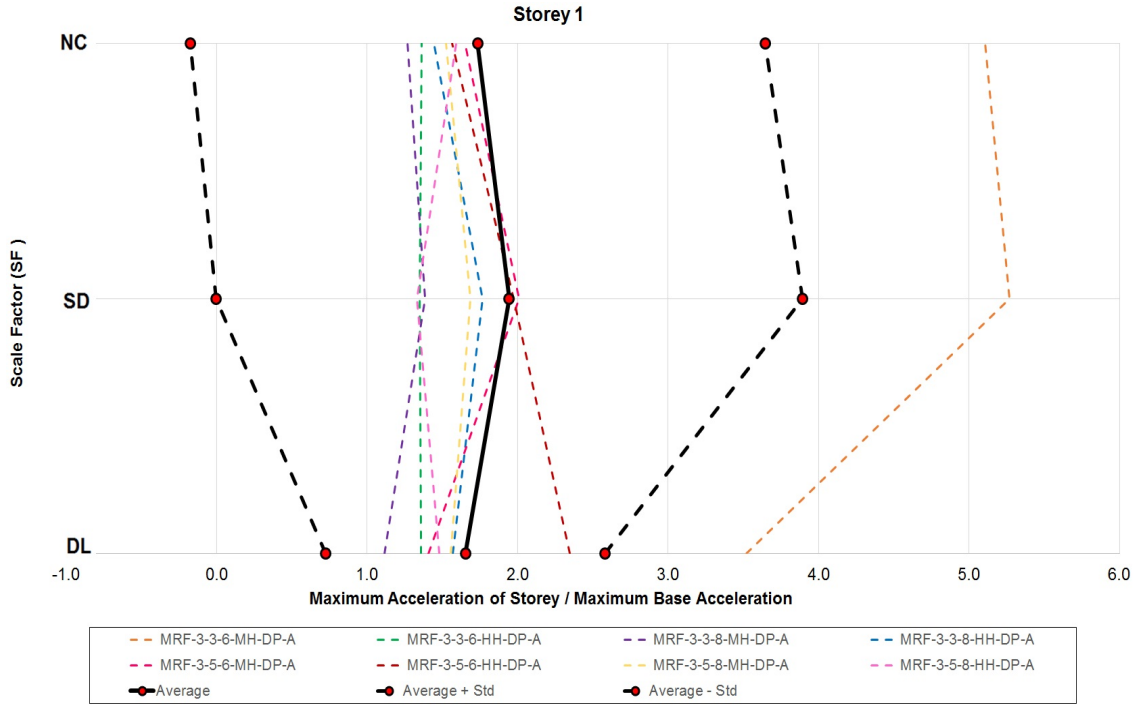

Figure 5.49 Maximum storey acceleration for DL, SD and NC limit states for the third storey of MRFs-DP-A.

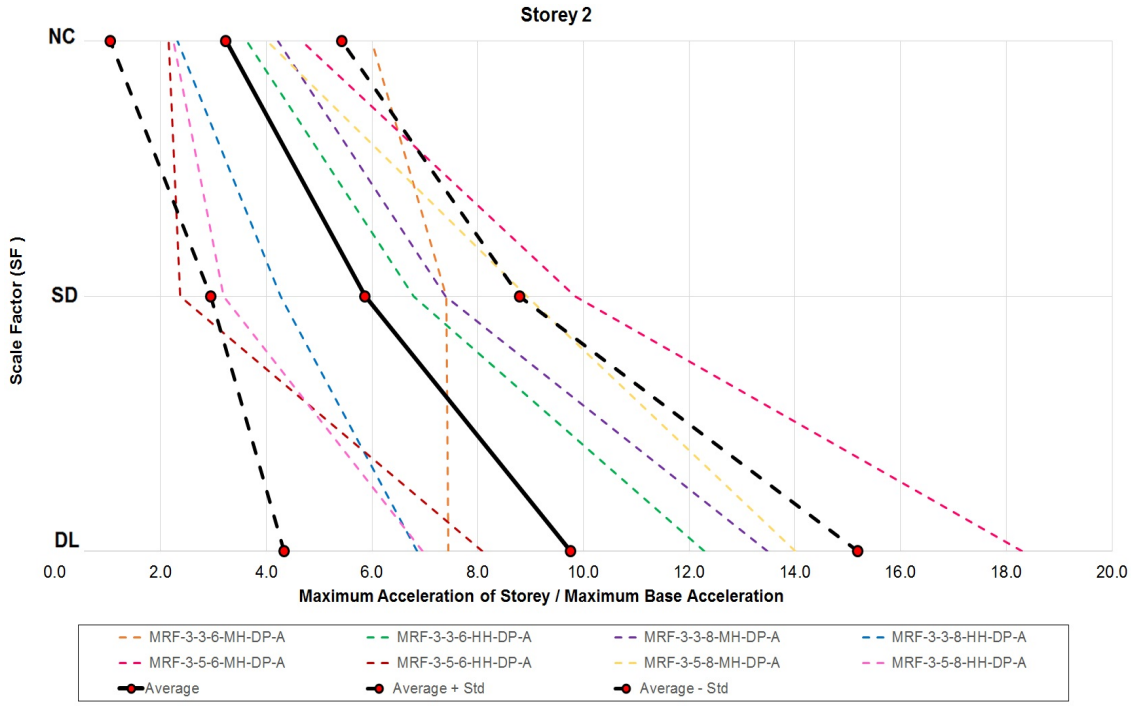

Figure 5.50 Maximum storey acceleration for DL, SD and NC limit states for the second storey of MRFs-DP-A.

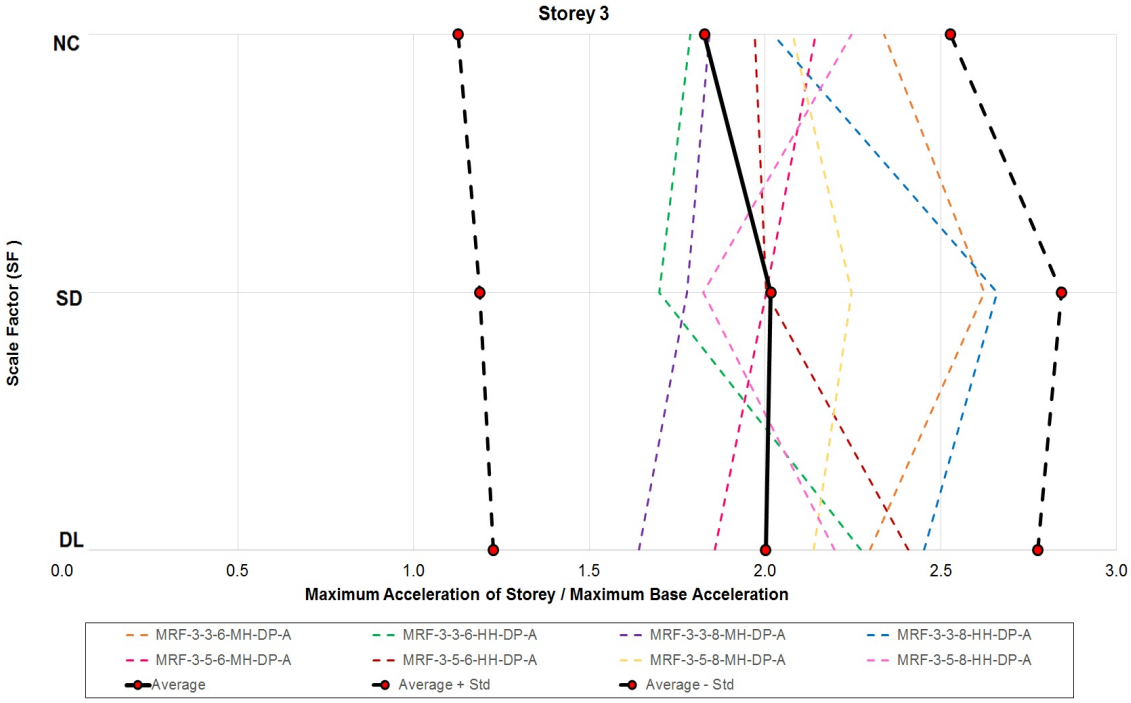

Figure 5.51 Maximum storey acceleration for DL, SD and NC limit states for the first storey of MRFs-DP-A.

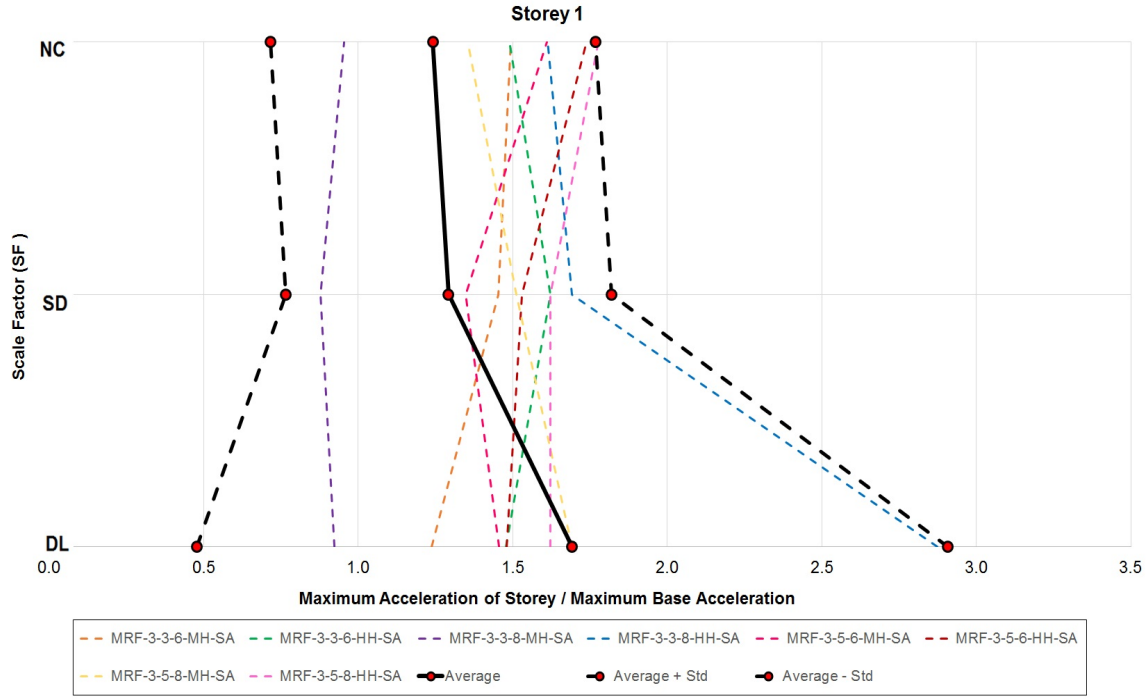

Figure 5.52 Maximum storey acceleration for DL, SD and NC limit states for the third storey of MRFs-DP-B.

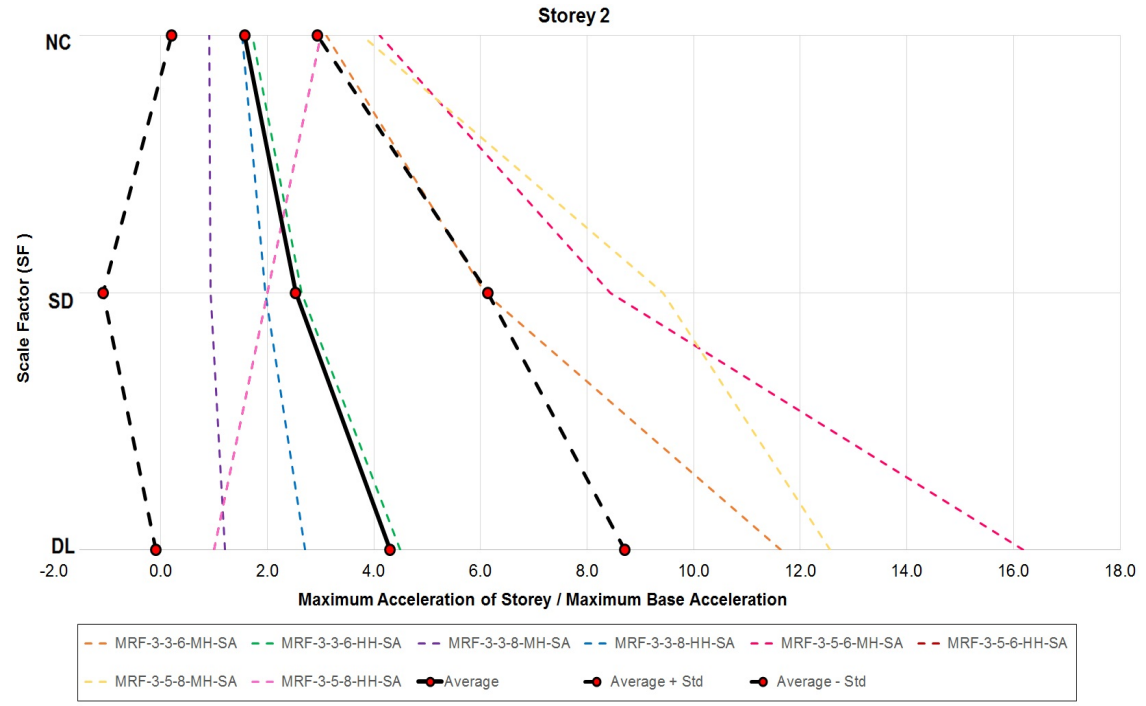

Figure 5.53 Maximum storey acceleration for DL, SD and NC limit states for the second storey of MRFs-DP-B.

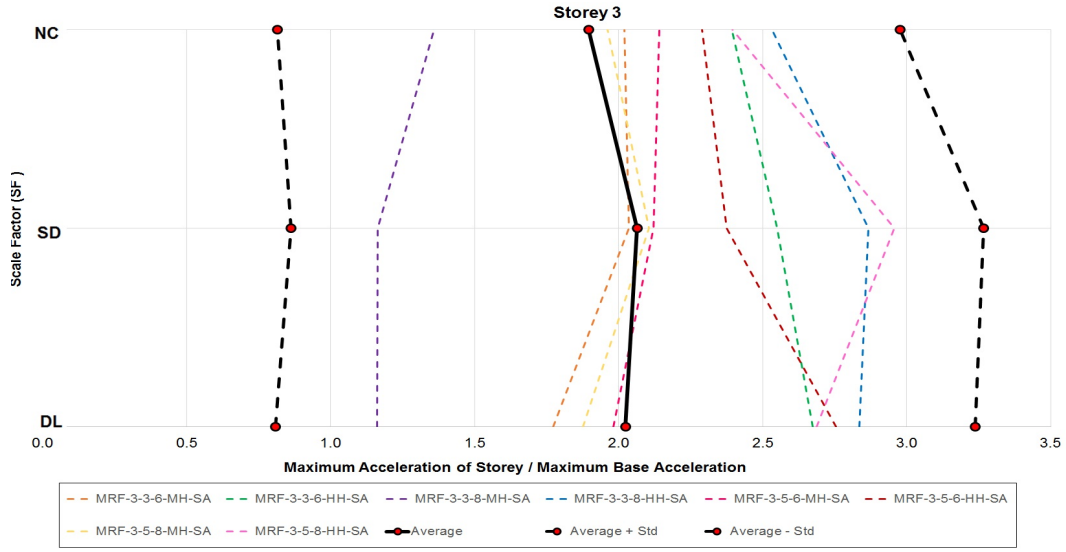

Figure 5.54 Maximum storey acceleration for DL, SD and NC limit states for the first storey of MRFs-DP-B.

5.2.4 Comparison of design methodologies

In figures 5.55 to 5.57 are depicted the average results of Transient Inter-storey Drift (TID) for all the frames design with the three different methodologies, for DL, SD and CP limit states. The TID is presented along the frame height. From the results is possible to see that none of average results of the three methodologies reach the 0.75% inter-storey drift limit at any Limit state. Is clear to notice that for the three methodologies, for DL limit state the structures remain elastic as expected. Considering that for SD and NC limit states, inter-storey drift limits are 2.5% and 5% respectively, results shown significantly lower values, within ranges 0.35% and 0.43% for SD and 0.48% and 0.57% for NC limit states. This might be due to the highly restrictive designed controlled by drift limits and stability criteria for all the cases.

For EC8 cases, maximum drift values are concentrated in the first storey, with a notorious difference of drift values with the second and third storeys. For DP-A and DP-B frames, maximum TID values are concentrated in the second storey. For DL limit state, a uniform and similar TID distribution along the frames height were obtain for the three methodologies, while differences between design methodologies can be observed for NC limit state, where maximum values and a more uniform distribution along height are for DP-A-MRFs.

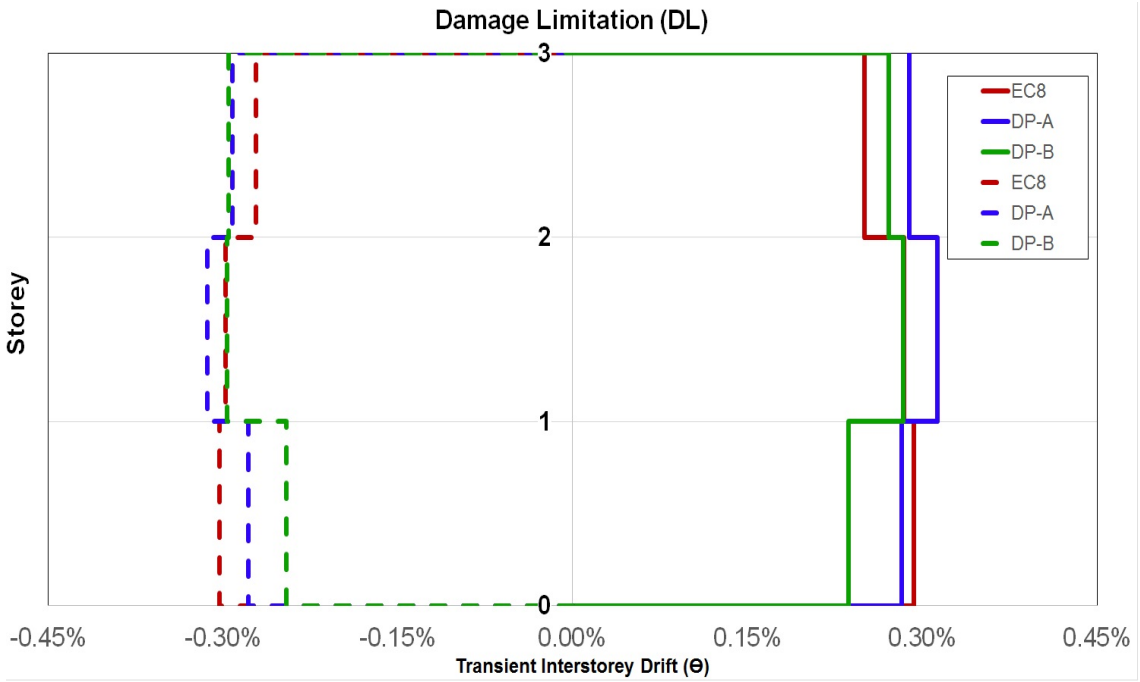

Figure 5.55 Transient Inter-storey Drift comparison of design methodologies for Damage Limitation (DL) limit state.

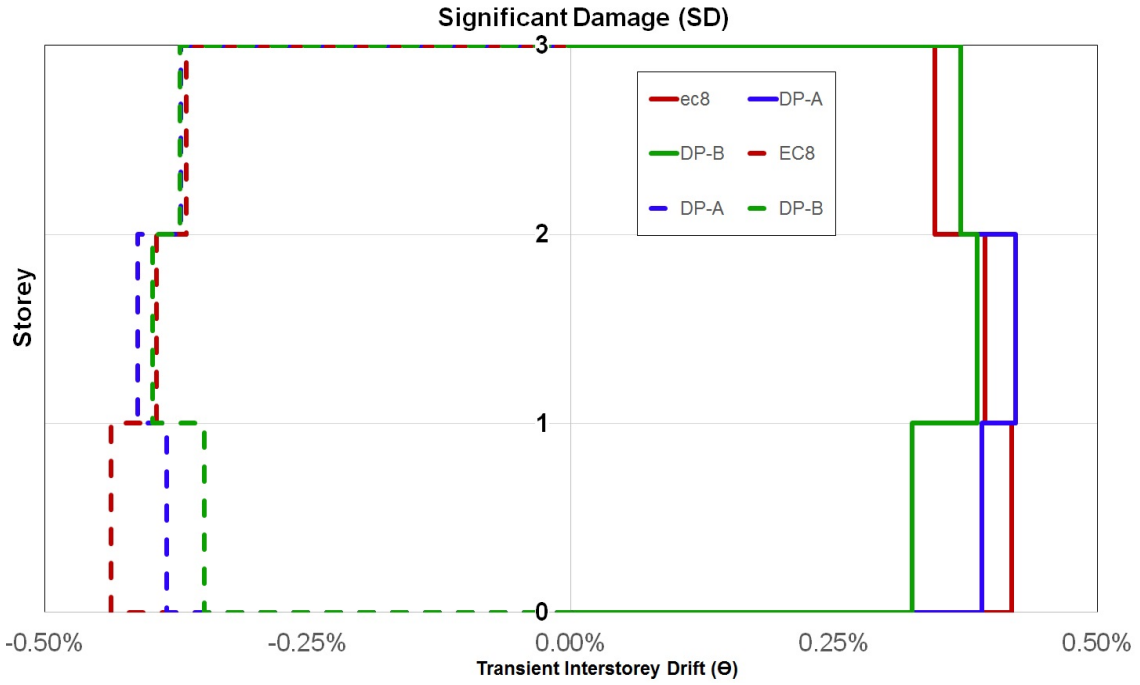

Figure 5.56 Transient Inter-storey Drift comparison of design methodologies for Significant Damage (SD) limit state.

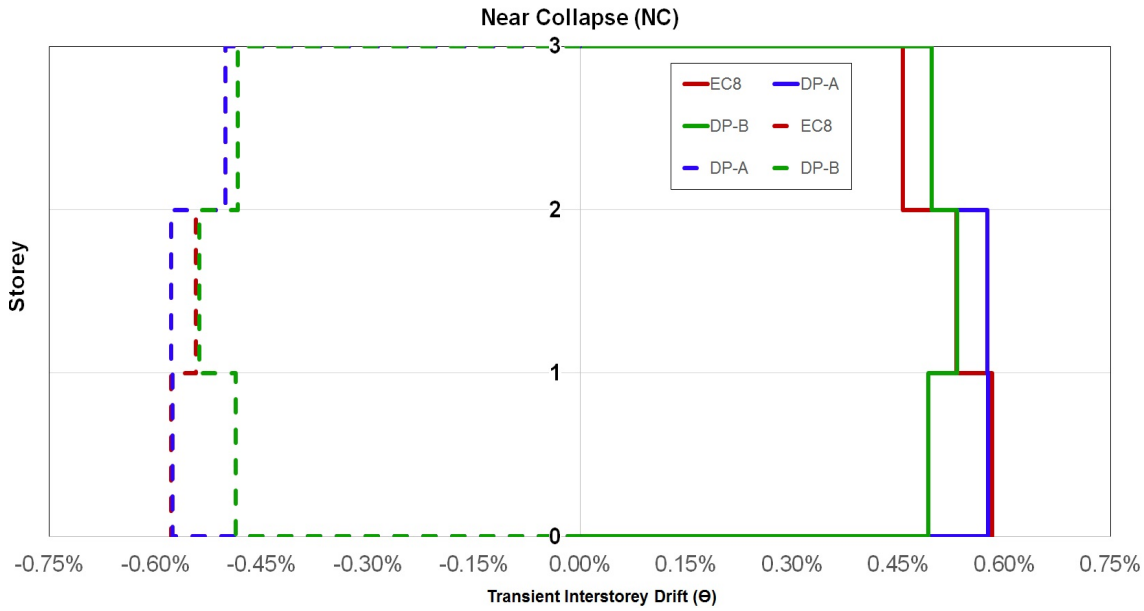

Figure 5.57 Transient Inter-storey Drift comparison of design methodologies for Near Collapse (NC) limit state.

Comparison of average results for Residual Interstorey Drift (RID) for the three design methodologies are presented in figures 5.58 to 5.60. For DL limit state, maximum RID values are for DP-B methodology for the second storey, with a -0.006% value, as it is expected maximum values for the three cases are close to zero due to the frames remaining in the elastic range under this limit state. For SD limit state, maximum RID values are for the 3rd Storey for the EC8 case, except for the second Storey where SA case is higuer. Maximum values are within the range 0.001% and 0.006% significantly lower than 1% limit. A similar result is observed for NC limit state, with maximum values for DP-A with maximum values of 0.0065% and 0.01%. DP-A frames showed a more uniform distribution of RID along the height of the frames for DL and SD limit states.

It can be noticed that the residual drifts demand is relatively small for all the cases, thus allowing easily the repair after the earthquake. Within the years the importance of this issue has been recognized, the repairing costs may overcome in some cases the constructional cost of the new building. Therefore, although the performance of the examined frames is limited in terms of incurring in an inelastic behavior, a cost-benefit analysis can turn the structures to be considered as cheaper taking into account the final repairing costs.

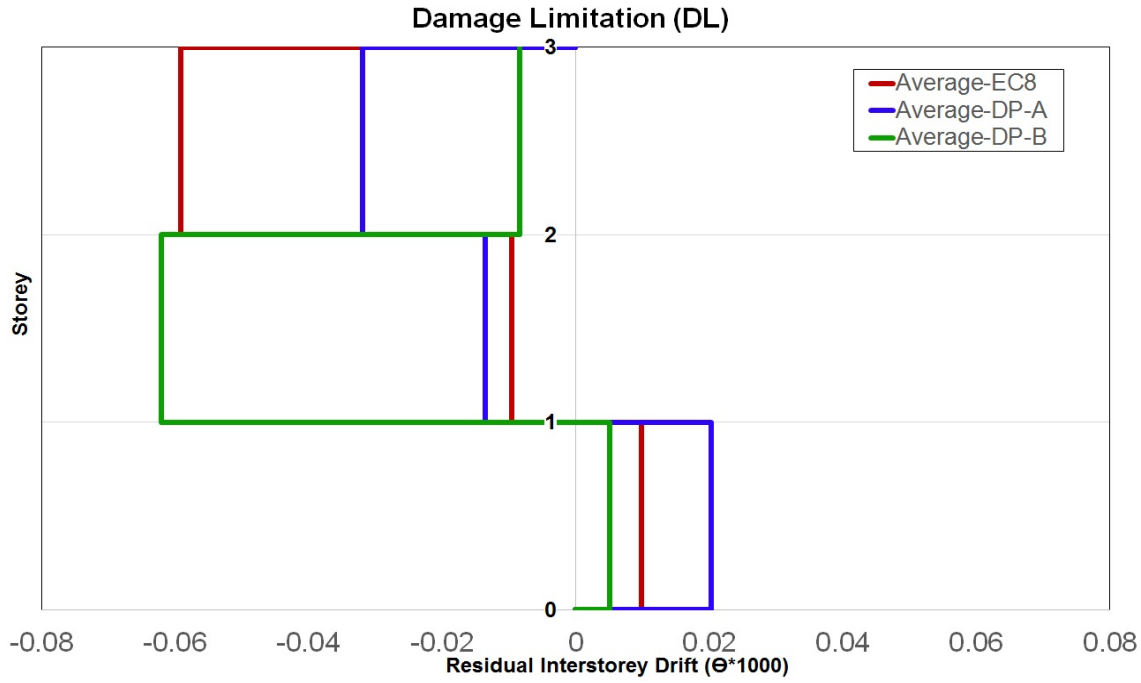

Figure 5.58 Residual Inter-storey Drift comparison of design methodologies for Damage Limitation (DL) limit state.

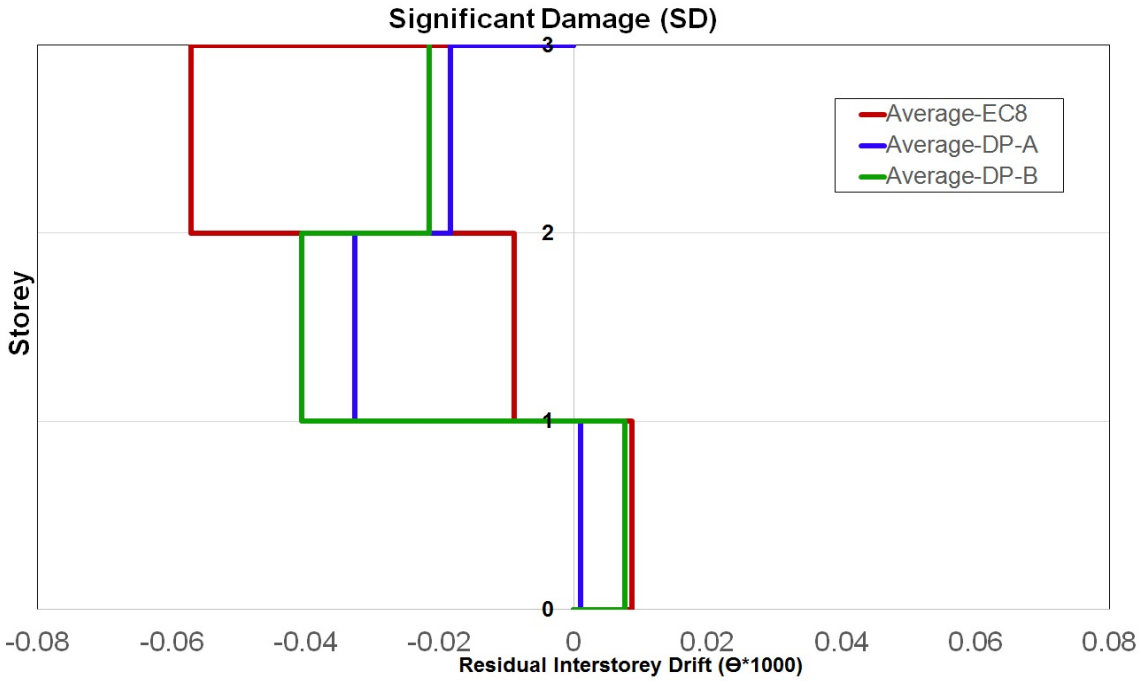

Figure 5.59 Residual Inter-storey Drift comparison of design methodologies for Significant Damage (SD) limit state.

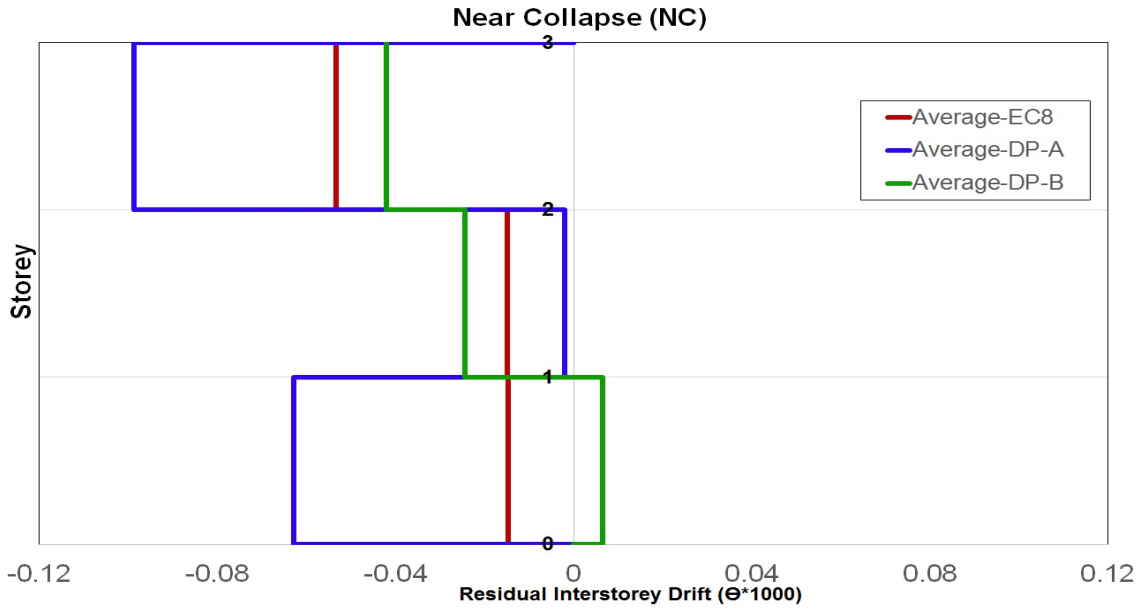

Figure 5.60 Residual Inter-storey Drift comparison of design methodologies for Near Collapse (NC) limit state.

As a last comparison parameter from the non-linear analysis, figures 5.61 to 5.63 show the average results of each design methodology for the amplification factors for Peak Storey Acceleration with ground peak acceleration (PSA/PSA_g) for DL, SD and CP limit states. The tendency for the three limit states is similar, EC8 amplification factors are the highest of the three methodologies. Regardless the limit state, DP-A and DP-B frames present similar values for the amplification factors for each storey: for the third Storey an average value of 2 is constant, for the second Storey amplification factors range from 5 to 10 and for the first Storey an average amplification factor of 1.7 remains almost constant.

For EC8, maximum amplification factors result for DL limit state and the second floor, and for the third and first floor result in factors higher than 10. The significant dynamic magnification of storey accelerations for the results of EC8 frames examined cases clearly highlights that very severe non-structural damage can be expected. Is important to notice that most of architectural components, mechanical and electrical equipment, building contents and inventory are prone to high amplitude of storey accelerations. Hence, it should be observed that such a kind of structural systems (MRFs) might be inappropriate for critical facilities, like hospitals or schools.

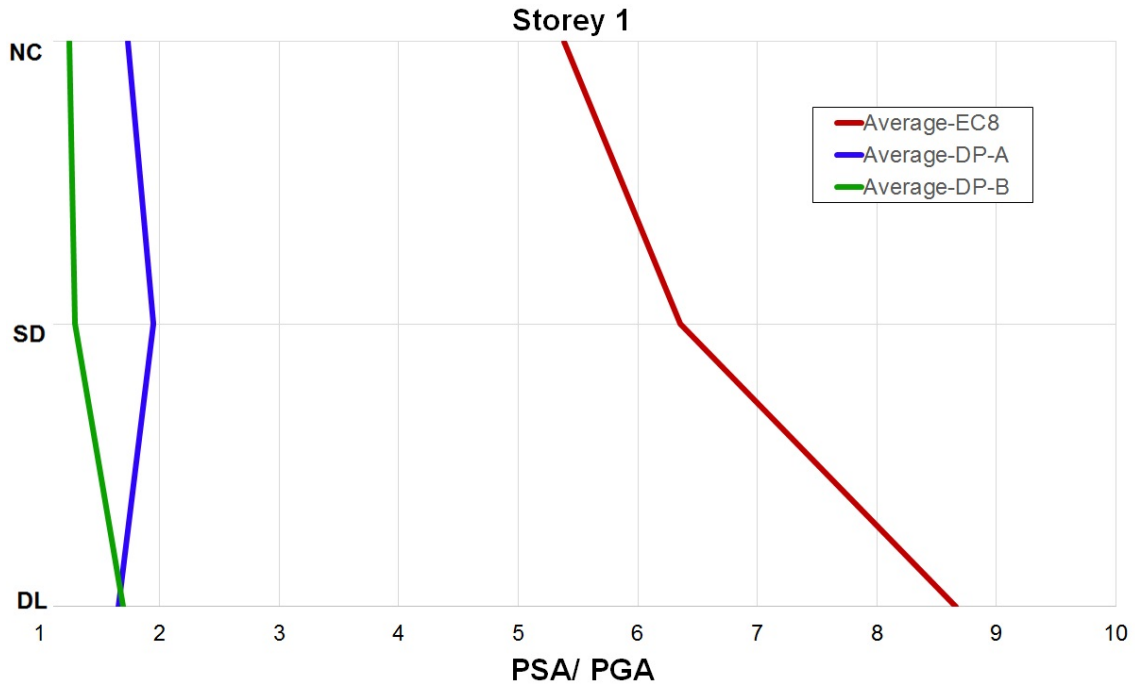

Figure 5.61 Peak Storey Acceleration comparison of design methodologies for the first storey.

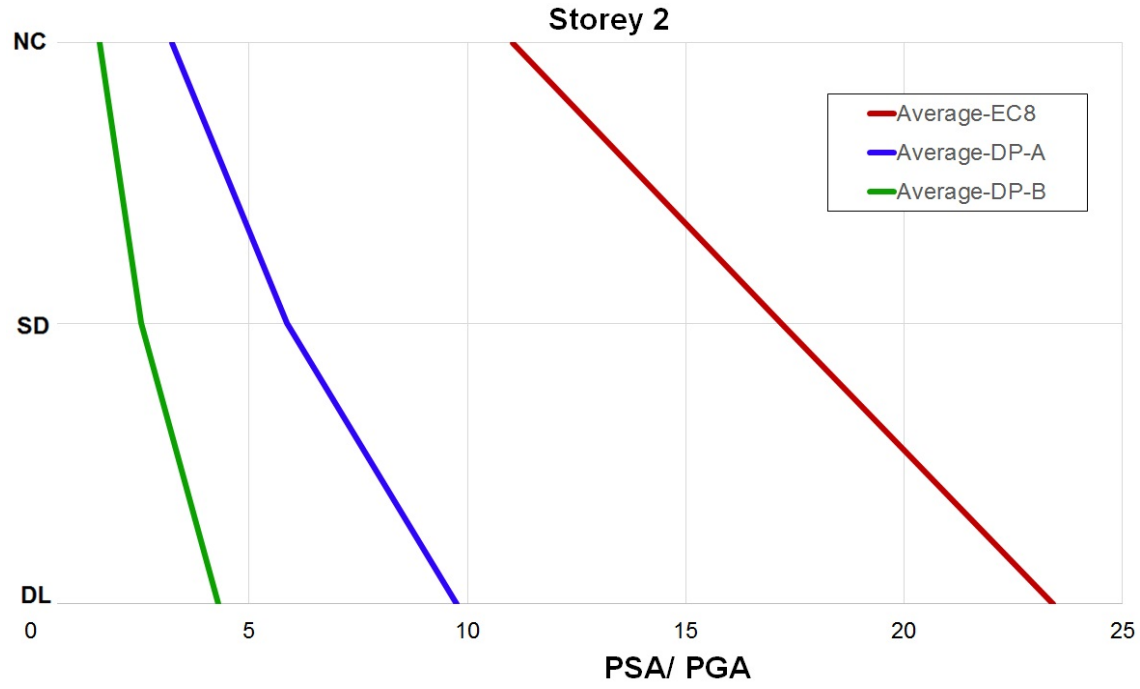

Figure 5.62 Peak Storey Acceleration comparison of design methodologies for the second storey.

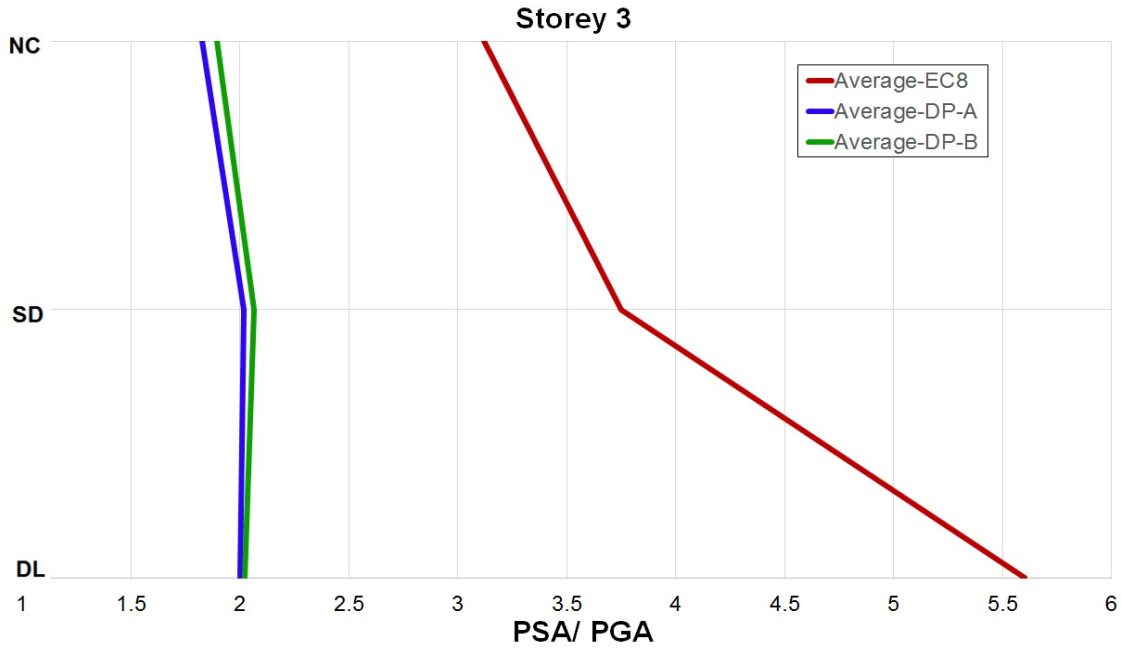

Figure 5.63 Peak Storey Acceleration comparison of design methodologies for the third storey.

In order to evaluate the influence of the design methodologies on the constructional costs, the material consumption has been calculated for all the frames designed for the three different methodologies. The steel consumption has been computed in terms of total weight of steel. In table 5.1 are presented the total weight per type of frame and design methodology, the steel quantification is also divided by Beams and columns.

Table 5.1 Total weight per type of element for the Moment Resisting Frames.

	Weight (kg)								
	EC8			DP-A			DP-B		
	Beam	Column	Total	Beam	Column	Total	Beam	Column	Total
MRF-3-3-6-MH	3348.7	5774.6	9123.3	3348.7	5774.6	9123.3	3146.7	6678.0	9824.7
MRF-3-3-6-HH	4557.7	9366.9	13924.6	4557.7	7980.5	12538.2	4303.5	15329.6	19633.0
MRF-3-3-8-MH	6299.0	7860.0	14159.0	6299.0	7962.0	14261.0	6299.0	9858.0	16157.0
MRF-3-3-8-HH	8319.7	19743.5	28063.2	8643.5	16585.8	25229.4	8903.5	16845.8	25749.2
MRF-3-5-6-MH	5451.7	10236.4	15688.1	5451.7	10236.4	15688.1	5244.4	10535.4	15779.8
MRF-3-5-6-HH	7172.4	24805.2	31977.6	7172.4	21818.5	28990.8	7172.4	26772.6	33945.0
MRF-3-5-8-MH	10498.4	12885.9	23384.3	10498.4	12885.9	23384.3	10498.4	20561.8	31060.1
MRF-3-5-8-HH	14839.0	21572.8	36411.8	14839.0	20920.4	35759.4	14839.0	30217.0	45056.1

To calculate the total amount of density of steel per frame, the total weight of the frame (for beams and columns) has been divided by the tributary area of the frame i.e. $3L^2$ multiplied by the number of storeys according to figure 4.1. In figures 5.64 and 5.65 are depicted the comparison of density of steel for each type of frame for the three design methodologies.

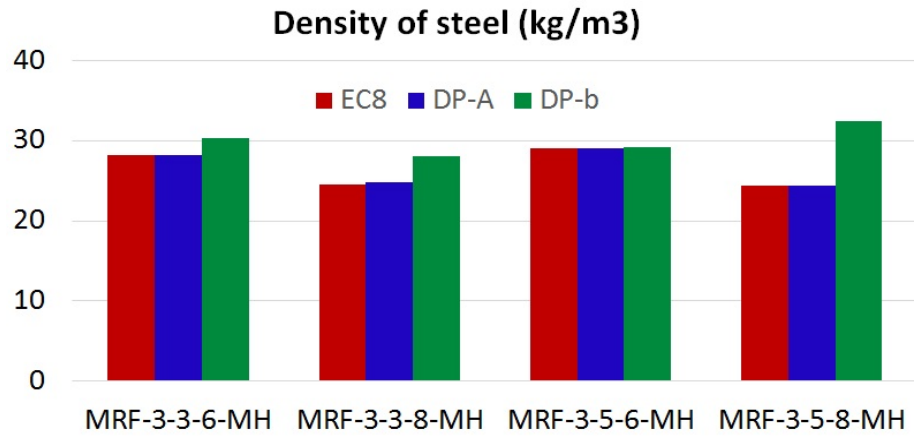

Figure 5.64 Density of steel MRFs with Medium Seismic Hazard, for the three design methodologies.

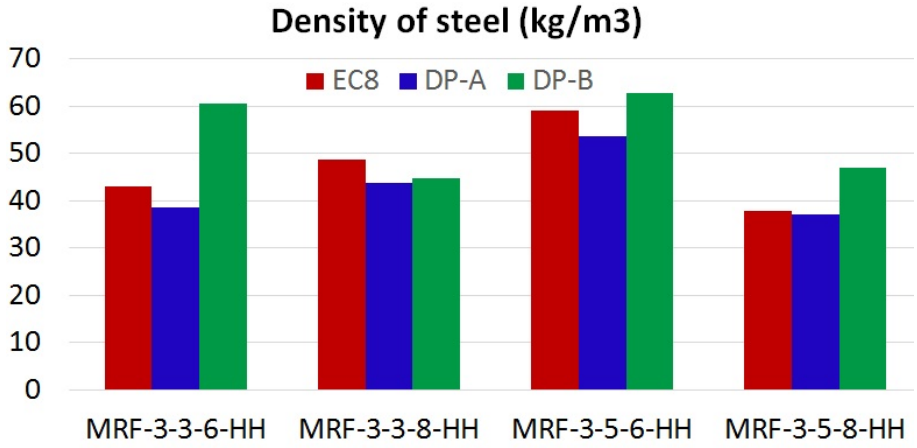

Figure 5.65 Density of steel MRFs with High Seismic Hazard, for the three design methodologies

As previously discussed, all the design procedure of the frames was influenced first to satisfy both drift and stability limitations, therefore differences in final element sections might be due to each design methodology criteria for local and global hierarchy requirements. From the steel consumption comparison we can notice that the frames designed with Design

Procedure B shown a higher steel density than those designed for EC8 and DP-A cases. This result is ascribable to the need to provide adequate lateral stiffness and stronger requirements for local and global verification hierarchy criteria due to the design approach for the Friction connections as described in section 3.2.2, thus compelling the designer to select heavy profiles, the later can be observed from table 5.1 where column weights are higher than for the other two of the design methodologies.

The lowest material density obtained for all the frames was for DP-A case, differences are more important for frames under High seismic Hazard i.e *MRF-HH* moment resisting frame cases.

6 Final Conclusions

Nature gave us earthquakes to keep us humble.
N. Ambraseys

The main aim of this dissertation work was to investigate the seismic performance of different arrangements of MRFs designed with the traditional methodology of EN 1998-1 in comparison with MRFs designed with dissipative joints, for two proposed design methodologies, developed and tested at University of Naples "Federico II" named as Design procedure A (DP-A) and University of Salerno in Italy, named as Design Procedure B (DP-B). To attain this purpose, a parametric study based on both nonlinear static and dynamic analyses has been presented, on the basis of the results described and discussed in the previous Chapters, the following conclusions can be drawn:

- The average redundancy ratio (V_p/V_y) obtained for the frames from pushover analysis, confirmed the assumed value of α_u/α_1=1.30 recommended by EN1998-1 for MRFs. Frames designed with procedure A exceeded the maximum recommended value of 1.6 given by EN1998-1.

- For EC8 and DP-B frames, pushover analyses showed overall over-design factors $\Omega_{ov} = \frac{V_p}{V_y} \cdot \frac{V_y}{V_b}$ larger than the design behavior factor ($q = 6.5$). For EC8 frames, this result is ascribable to the codified design procedure, which leads to increase the member size to satisfy the drift limitations as well to local and global verification for ULS limit state to satisfy hierarchy criteria. A similar case occurs for DP-B-MRFs,

due to the design requirements for ULS, columns need to be increased in order to fulfill hierarchy criteria for the dissipative connections methodology.

- The overall ductility factor (μ) was take into account considering as ultimate displacement the top displacement for a 5% inter-storey drift ratio as for NC limit state criteria, the results showed that the frames can develop high plastic deformation, average values for μ were around 5 and 6, and for frames designed with procedure A, a significant increase of μ was found out, with an average value of 11.

- The Idealized capacity curves allow us to identify the target displacements for three limit states: Operational Level (OP), Damage Limitation (DL) and Significant Damage (SD), according to the procedure of EC-8 Annex B. All the frames developed a stable non-linear behavior under SD limit state. The majority of frames remain in the elastic behavior for Operational Level (OL) and Damage limitation (DL) and developed a plastic behavior for a Significant Damage (SD) limit state as it is expected.

- When average inter-storey drift demand of each design methodology frames was examined comparatively, it was observed that the frames designed with DP-A shown a uniform inter-storey drift distribution along the height of the frame.

- The non-linear incremental dynamic analysis (IDA) and seismic performance-based evaluation has been carried out considering three limit states according to EN1998-3, i.e. damage limitation (DL), significant damage (SD) and near collapse (NC). Nonlinear dynamic analyses showed that the frames have a seismic demand (namely, transient and residual drift ratios) fairly below the proposed limit for DL, SD and NC states. In particular, at SD limit state most of the frames behave in the elastic field. This result is mainly due to the design oversizing.

- Residual Inter-storey Drifts demand is significantly small for all the frames designed with the three methodologies, thus allowing easily the repair after the earthquake. Although the performance of the examined frames is limited in terms of incurring in an inelastic behavior, a cost-benefit analysis can lead to consider the structures as economically favorable taking into account the final repairing costs.

- The median Peak Storey Accelerations/Peak Ground Acceleration amplification factors (PSA/PSA_g) where compared for each storey and the three design methodologies. DP-A and DP-B frames designed considering friction connections showed a reduction of the the storey acceleration amplification factors when compared to EC8 frames. The average values ofPSA/PSA_g for DP-A and DP-B frames range between 2 and 5 times, and for EC8 frames, factors higher than 10 were observed. Hence, significant amplification effects can occur and should be accounted for preserving the integrity of facilities and non-structural elements due to its sensitivity to damage according to the level of acceleration.

- Regarding material consumption comparison between design methodologies, steel density was quantified and from the results it was observed that frames designed with DP-B result with higher steel density than frames designed for EC8 and DP-A. This result is ascribable to the need to provide adequate lateral stiffness and stronger requirements for local and global verification hierarchy criteria, due to the design approach for the Friction connections, thus compelling the designer to select heavy profiles, as it is clear for the column sections for DP-B frames, with a higher column weight than for the other two of the design methodologies. The comparison between steel density showed that the lowest material density obtained for all the frames was for the frames designed with procedure A, from an economical point of view, the former solution can turn to be more effective, only considering beams and columns steel sections.

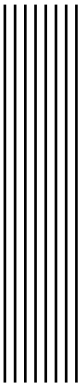

References

J. Borzouie, G. MacRae, J. Chase, G. Rodgers, and G. Clifton. Experimental studies on cyclic performance of column base strong axis–aligned asymmetric friction connections. *Journal of Structural Engineering*, 142(1):04015078, 2015.

G. Clifton, G. MacRae, H. Mackinven, S. Pampanin, and J. Butterworth. Sliding hinge joints and subassemblies for steel moment frames. In *Palmerston North, New Zealand: Proc of New Zealand Society for Earthq Eng Conf*, 2007.

G. C. Clifton. *Semi-rigid joints for moment-resisting steel framed seismic-resisting systems*. PhD thesis, ResearchSpace@ Auckland, 2005.

A. Elghazouli. Assessment of european seismic design procedures for steel framed structures. *Bulletin of earthquake engineering*, 8(1):65–89, 2010.

Eurocode-3. *Eurocode 3: Design of Steel Structures, Part 1.1: General Rules and Rules for Buildings, BS-EN1993-1-1-2005,*. European Committee for Standardization, CEN, Brussels, 2005.

Eurocode-8. *Eurocode 8: Design of Structures for Earthquake Resistance, Part 3: Assessment and retrofitting of buildings, EN1998-3-2005,*. European Committee for Standardization, CEN, Brussels, 2005.

Federal Emergency Management Agency . (FEMA). *FEMA 356, Prestandard and Commentary for the Seismic Rehabilitation of Buildings,*. Washington, DC., 2000.

F. C. Filippou, E. P. Popov, and V. V. Bertero. Effects of bond deterioration on hysteretic behavior of reinforced concrete joints. 1983.

C. E. Grigorian, T.-S. Yang, and E. P. Popov. Slotted bolted connection energy dissipators. *Earthquake Spectra*, 9(3):491–504, 1993.

E. M. Güneyisi, M. D'Aniello, and R. Landolfo. Seismic upgrading of steel moment-resisting frames by means of friction devices. *Open Construction and Building Technology Journal*, 8(1):289–299, 2014.

T. L. Karavasilis. Assessment of capacity design of columns in steel moment resisting frames with viscous dampers. *Soil Dynamics and Earthquake Engineering*, 88:215–222, 2016.

K. Ke and Y. Chen. Seismic performance of mrfs with high strength steel main frames and edbs. *Journal of Constructional Steel Research*, 126:214–228, 2016.

J. M. Kelly, R. Skinner, and A. Heine. Mechanisms of energy absorption in special devices for use in earthquake resistant structures. *Bulletin of NZ Society for Earthquake Engineering*, 5(3):63–88, 1972.

H. Khoo, G. Clifton, J. Butterworth, and G. MacRae. Developments on the sliding hinge joint. In *15 th World Conference on Earthquake Engineering. Lisboa*, 2012.

H.-H. Khoo, C. Seal, C. Clifton, J. Butterworth, and G. A. MacRae. Behaviour of the bottom and top flange plates in the sliding hinge joint. *Bulletin of the New Zealand Society for Earthquake Engineering*, 46(1):1–10, 2013.

H.-H. Khoo, C. Clifton, G. MacRae, H. Zhou, and S. Ramhormozian. Proposed design models for the asymmetric friction connection. *Earthquake Engineering and Structural Dynamics*, 44(8):1309–1324, 2015.

M. Latour, V. Piluso, and G. Rizzano. Experimental analysis of innovative dissipative bolted double split tee beam-to-column connections. *Steel Construction*, 4(2):53–64, 2011.

M. Latour, V. Piluso, and G. Rizzano. Experimental analysis on friction materials for supplemental damping devices. *Construction and Building Materials*, 65, 2014.

M. Latour, V. Piluso, and G. Rizzano. Free from damage beam-to-column joints: Testing and design of dst connections with friction pads. *Engineering Structures*, 85:219–233, 2015.

Y.-C. Lin, R. Sause, and J. Ricles. Seismic performance of a large-scale steel self-centering moment-resisting frame: Mce hybrid simulations and quasi-static pushover tests. *Journal of Structural Engineering*, 139(7):1227–1236, 2012.

M. Menegotto. Method of analysis for cyclically loaded rc plane frames including changes in geometry and non-elastic behavior of elements under combined normal force and bending. In *Proc. of IABSE symposium on resistance and ultimate deformability of structures acted on by well defined repeated loads*, pages 15–22, 1973.

I. H. Mualla and B. Belev. Performance of steel frames with a new friction damper device under earthquake excitation. *Engineering Structures*, 24(3):365 – 371, 2002. ISSN 0141-0296.

A. S. Pall and C. Marsh. Response of friction damped braced frames. *Journal of Structural Engineering*, 108(9):1313–1323, 1982.

V. Piluso, R. Montuori, and M. Troisi. Innovative structural details in mr-frames for free from damage structures. *Mechanics Research Communications*, 58:146–156, 2014.

S. Ramhormozian, G. Clifton, and G. MacRae. The asymmetric friction connection with belleville springs in the sliding hinge joint. *NZSEE, Auckland, New Zealand*, 2014.

A. Reyes-Salazar, M. D. Llanes-Tizoc, J. Bojorquez, E. Bojórquez, A. López-Barraza, and A. Haldar. Force reduction factors for steel buildings with welded and post-tensioned connections. *Bulletin of Earthquake Engineering*, 14(10):2827–2858, 2016.

SeismoStruct. *Version 2016, Release 5: Seismosoft-Earthquake Engineeting Software Solution*. 2016.

A. Tenchini, M. D'Aniello, C. Rebelo, R. Landolfo, L. S. da Silva, and L. Lima. Seismic performance of dual-steel moment resisting frames. *Journal of Constructional Steel Research*, 101:437–454, 2014.

A. S. Tzimas, G. Kamaris, T. L. Karavasilis, and C. Galasso. Collapse risk and residual drift performance of steel buildings using post-tensioned mrfs and viscous dampers in near-fault regions. *Bulletin of Earthquake Engineering*, 14(6):1643–1662, 2016.

Appendix A

Idealized Capacity Curves for MRFs with Target displacements

In the following pages all the idealized capacity curves are shown for the three design methodologies and both lateral load patterns.

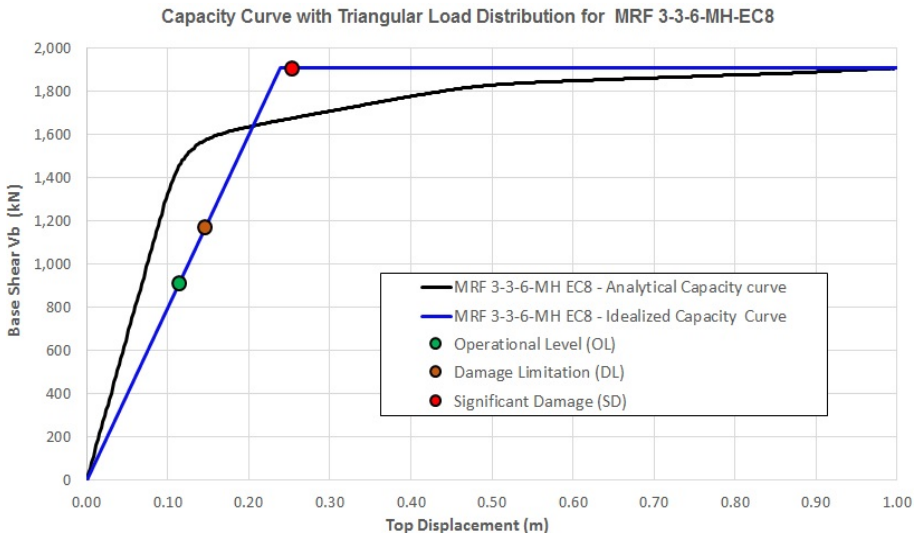

Figure A.1 Calculated and Idealized Capacity Curve for MRF-3-3-6-MH-EC8 for Triangular load pattern, T=0.91s.

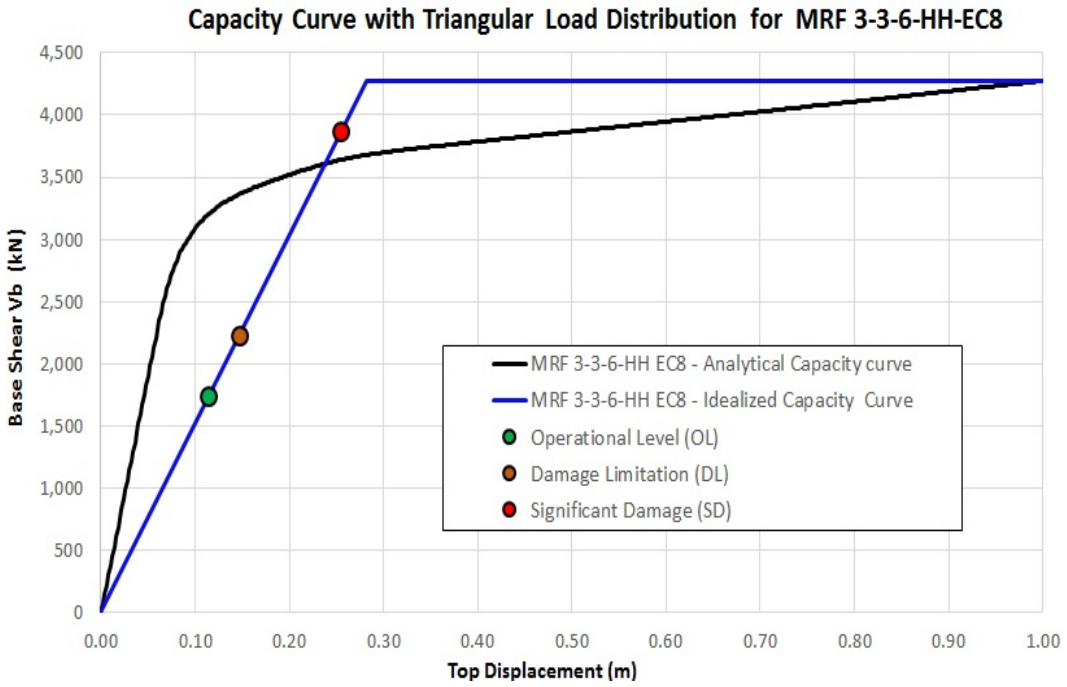

Figure A.2 Calculated and Idealized Capacity Curve for MRF-3-3-6-HH-EC8 for Triangular load pattern, T=0.58s.

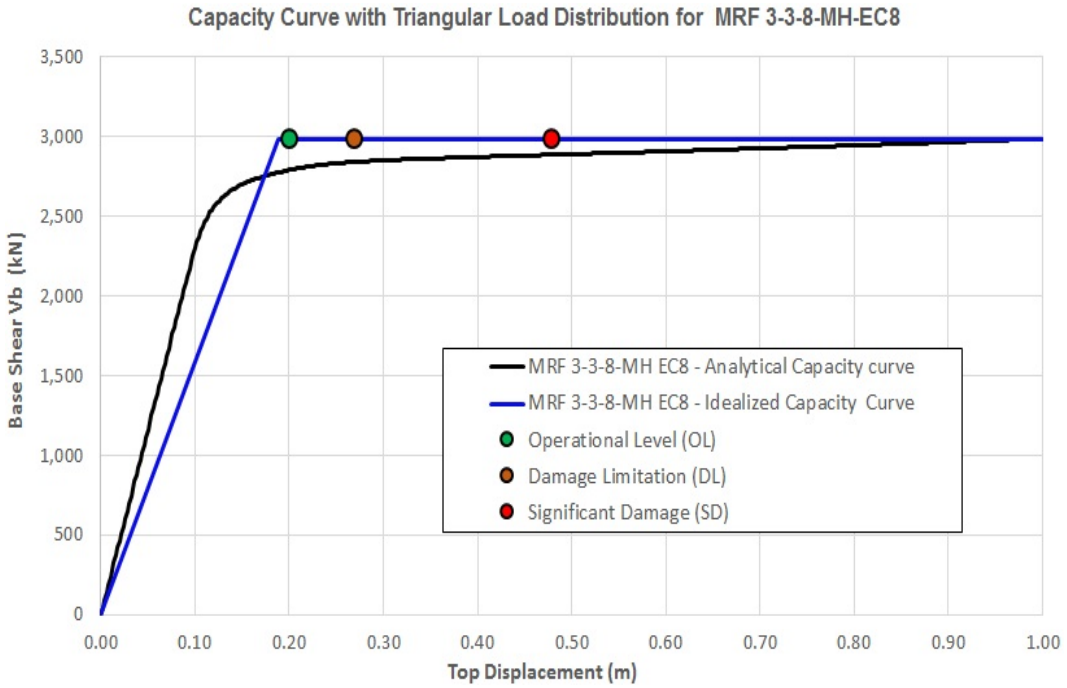

Figure A.3 Calculated and Idealized Capacity Curve for MRF-3-3-8-MH-EC8 for Triangular load pattern, T=0.82s.

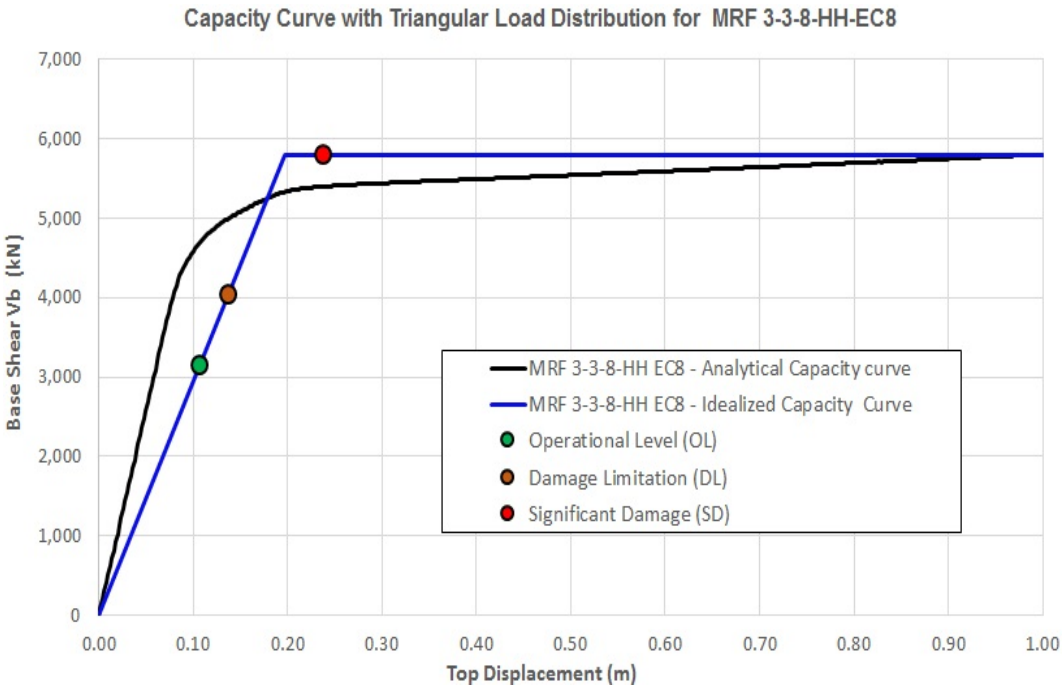

Figure A.4 Calculated and Idealized Capacity Curve for MRF-3-3-8-HH-EC8 for Triangular load pattern, T=0.615s.

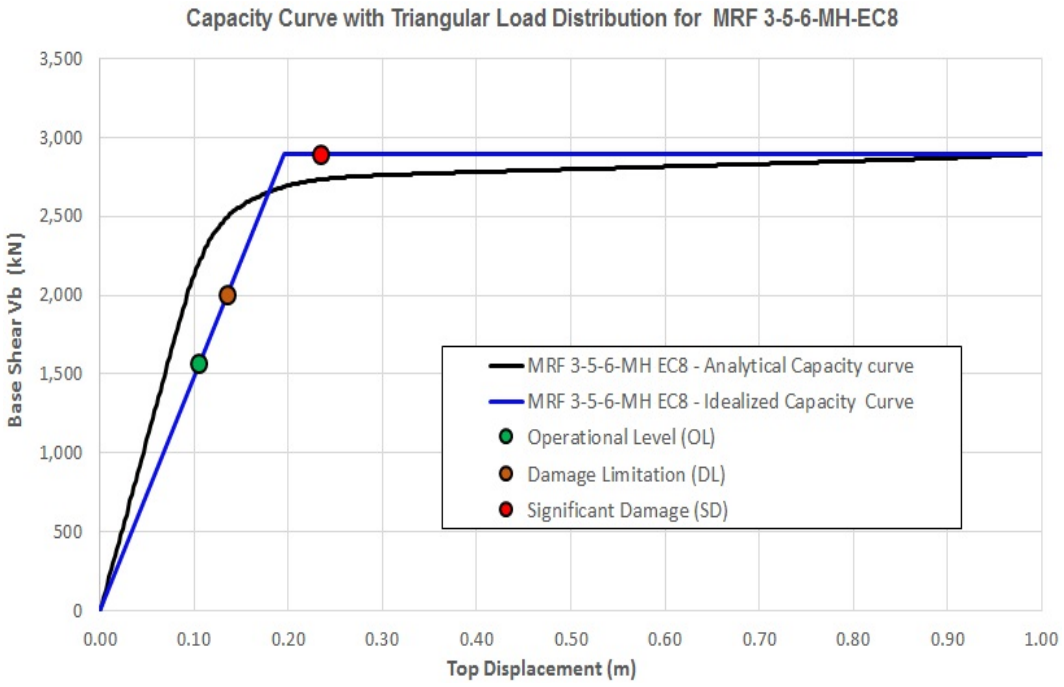

Figure A.5 Calculated and Idealized Capacity Curve for MRF-3-5-6-MH-EC8 for Triangular load pattern, T=0.87s.

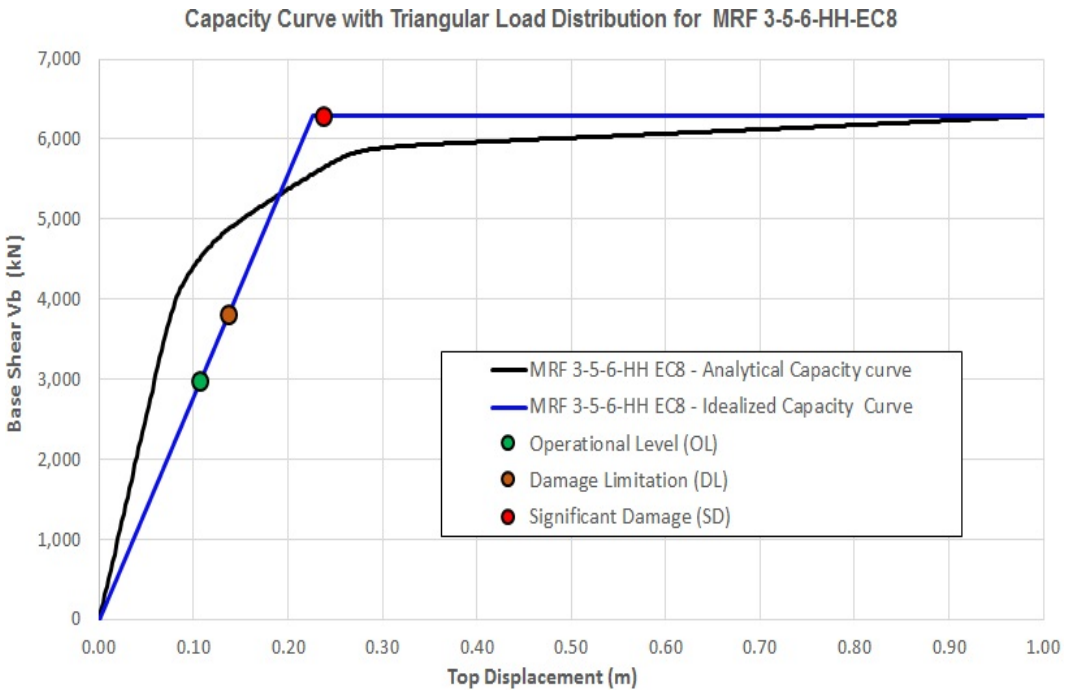

Figure A.6 Calculated and Idealized Capacity Curve for MRF-3-5-6-HH-EC8 for Triangular load pattern, T=0.59s.

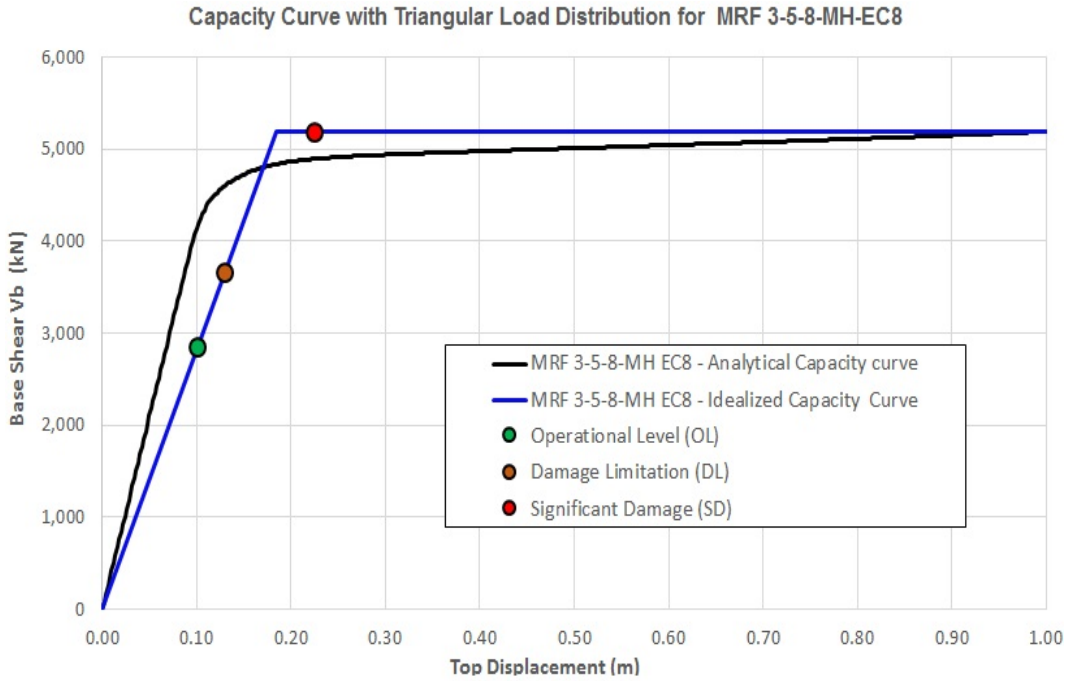

Figure A.7 Calculated and Idealized Capacity Curve for MRF-3-5-8-MH-EC8 for Triangular load pattern, T=0.845s.

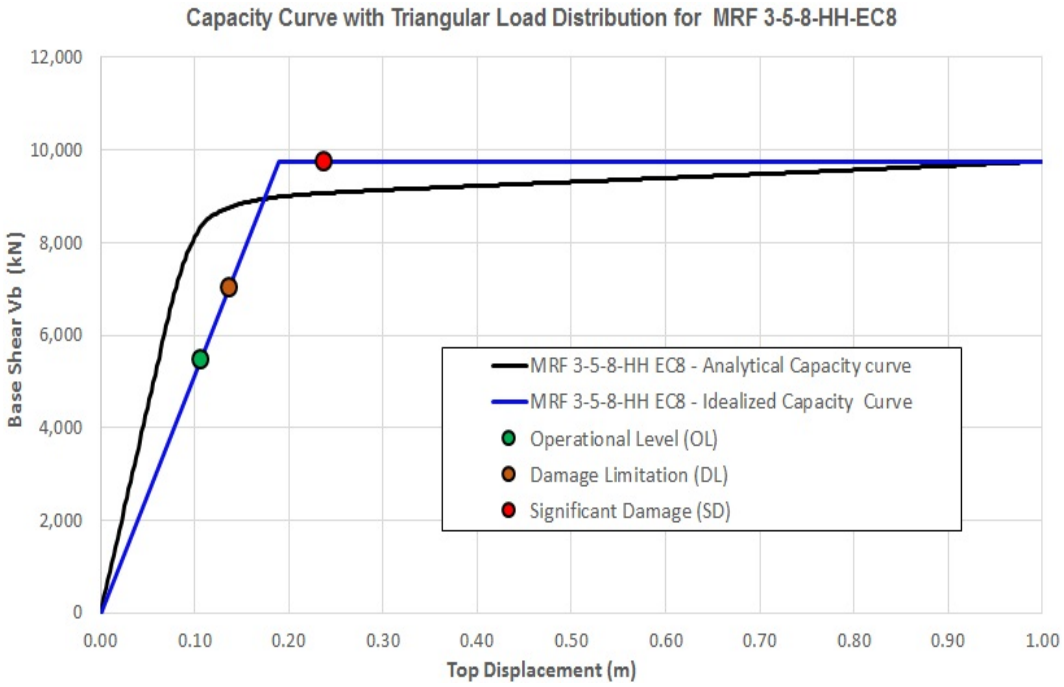

Figure A.8 Calculated and Idealized Capacity Curve for MRF-3-5-8-HH-EC8 for Triangular load pattern, T=0.64s.

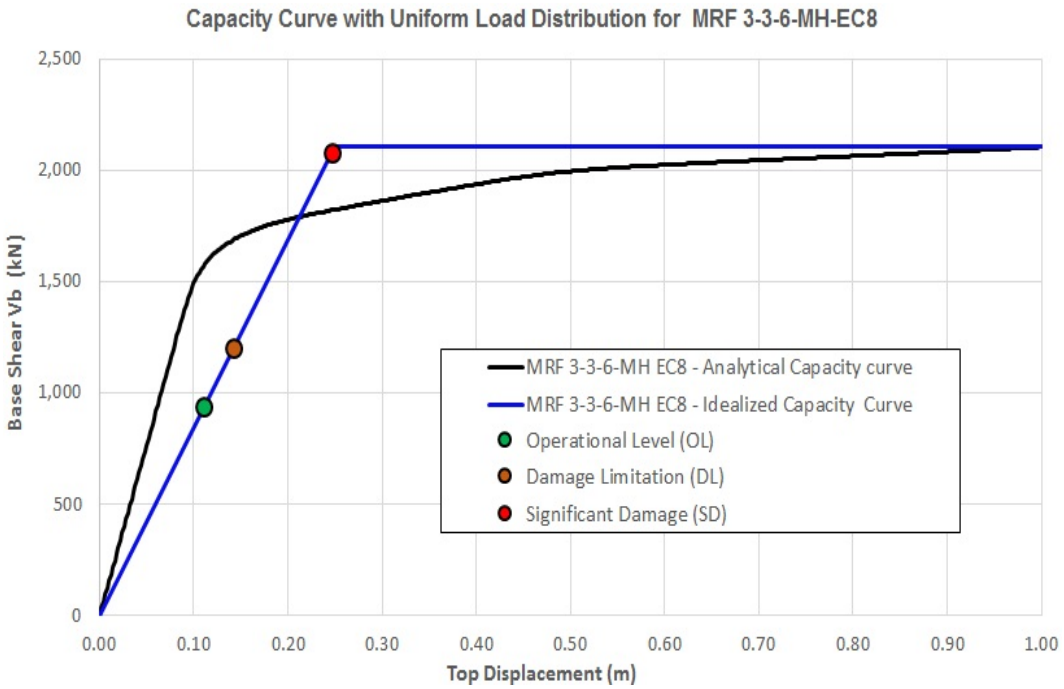

Figure A.9 Calculated and Idealized Capacity Curve for MRF-3-3-6-MH-EC8 for Uniform load pattern, T=0.91s.

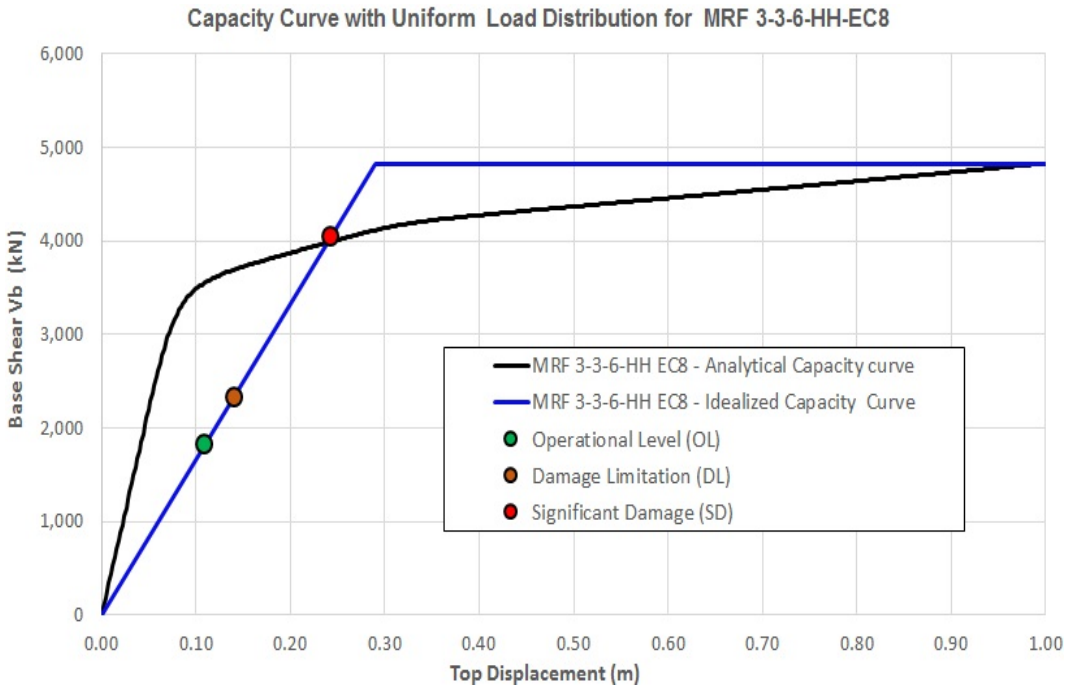

Figure A.10 Calculated and Idealized Capacity Curve for MRF-3-3-6-HH-EC8 for Uniform load pattern, T=0.58s.

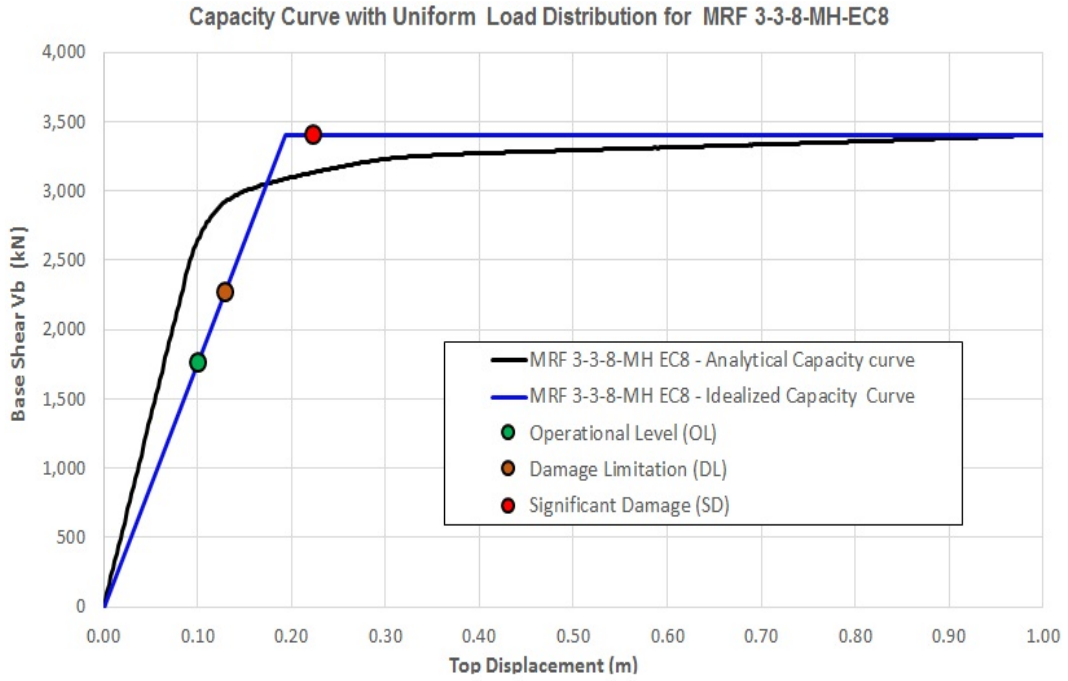

Figure A.11 Calculated and Idealized Capacity Curve for MRF-3-3-8-MH-EC8 for Uniform load pattern, T=0.82s.

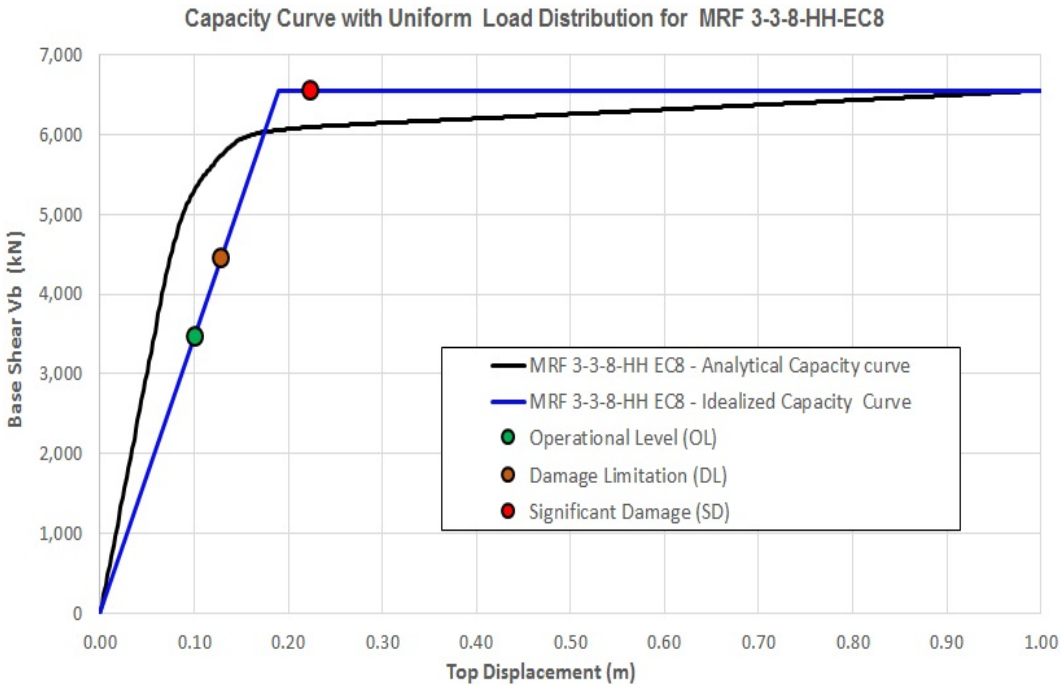

Figure A.12 Calculated and Idealized Capacity Curve for MRF-3-3-8-HH-EC8 for Uniform load pattern, T=0.615s.

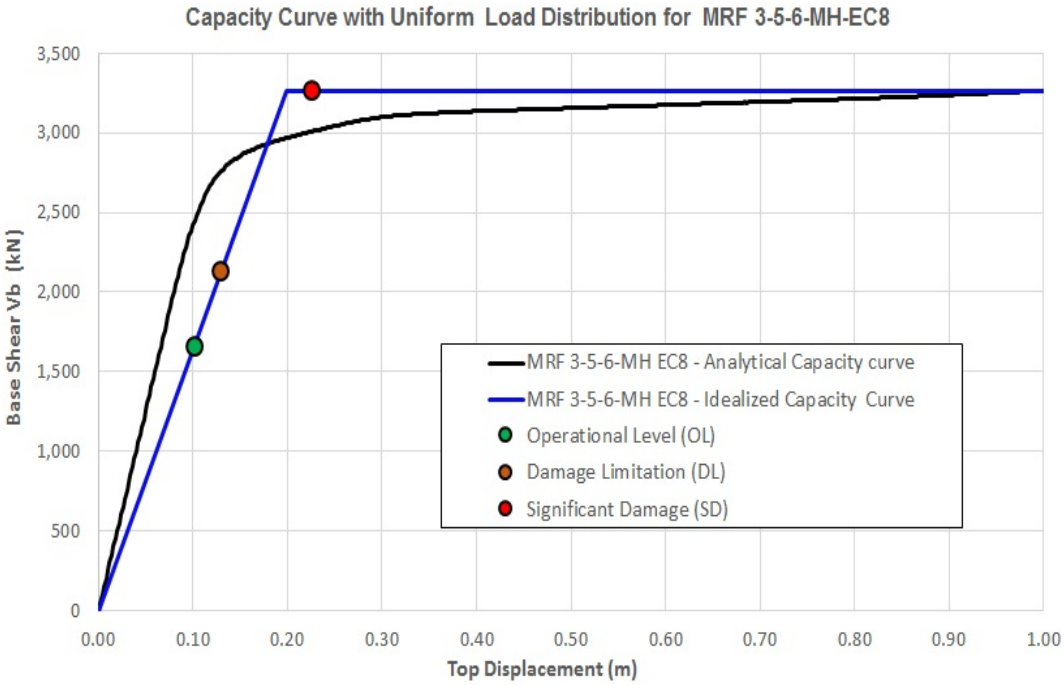

Figure A.13 Calculated and Idealized Capacity Curve for MRF-3-5-6-MH-EC8 for Uniform load pattern, T=0.87s.

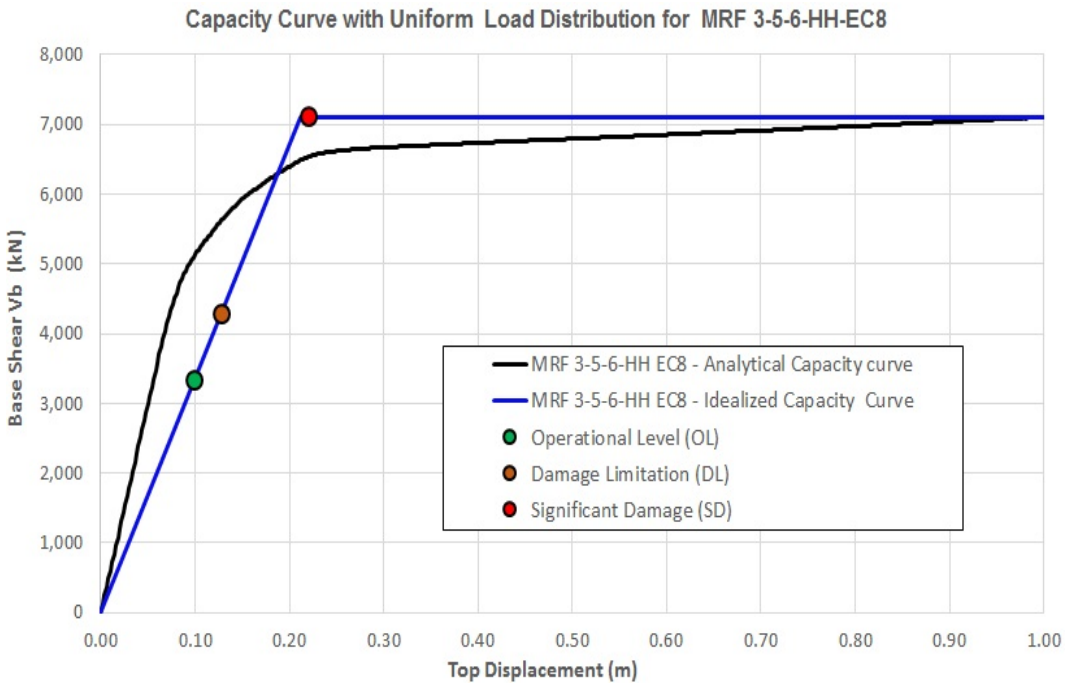

Figure A.14 Calculated and Idealized Capacity Curve for MRF-3-5-6-HH-EC8 for Uniform load pattern, T=0.59s.

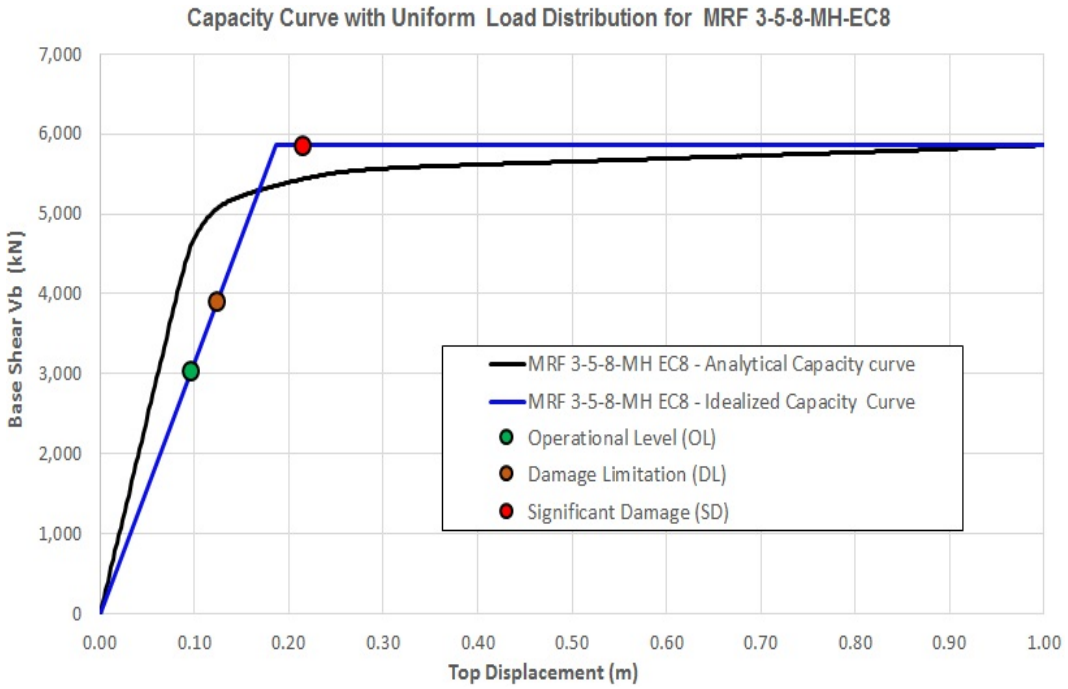

Figure A.15 Calculated and Idealized Capacity Curve for MRF-3-5-8-MH-EC8 for Uniform load pattern, T=0.845s.

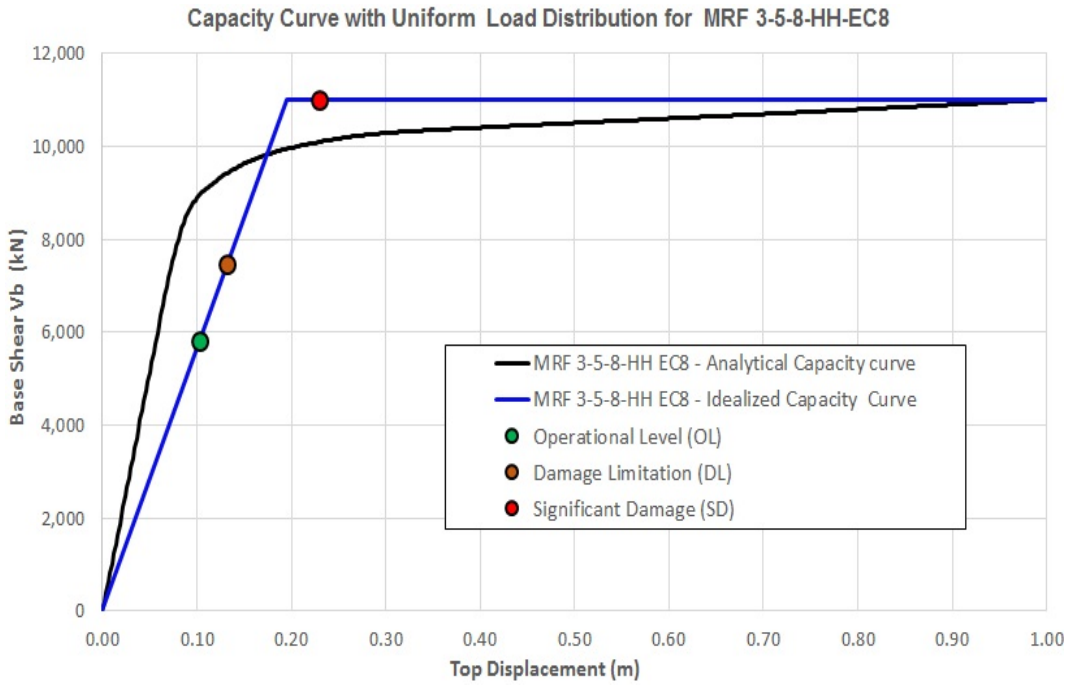

Figure A.16 Calculated and Idealized Capacity Curve for MRF-3-5-8-HH-EC8 for Uniform load pattern, T=0.64s.

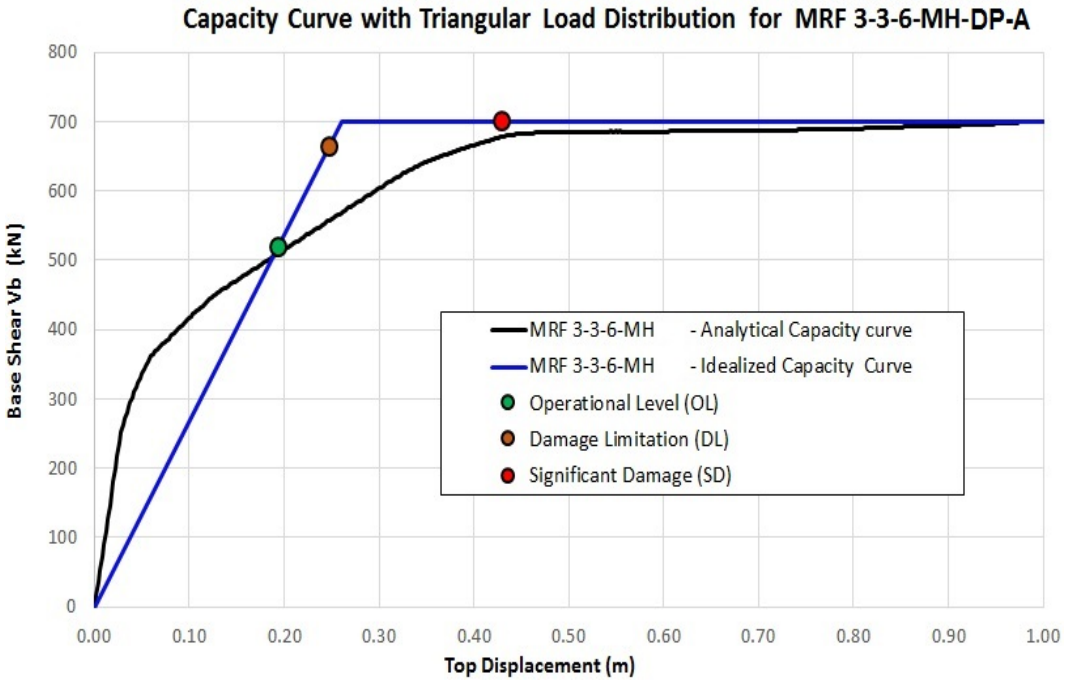

Figure A.17 Calculated and Idealized Capacity Curve for MRF-3-3-6-MH-DP-A for Triangular load pattern, T=0.91s.

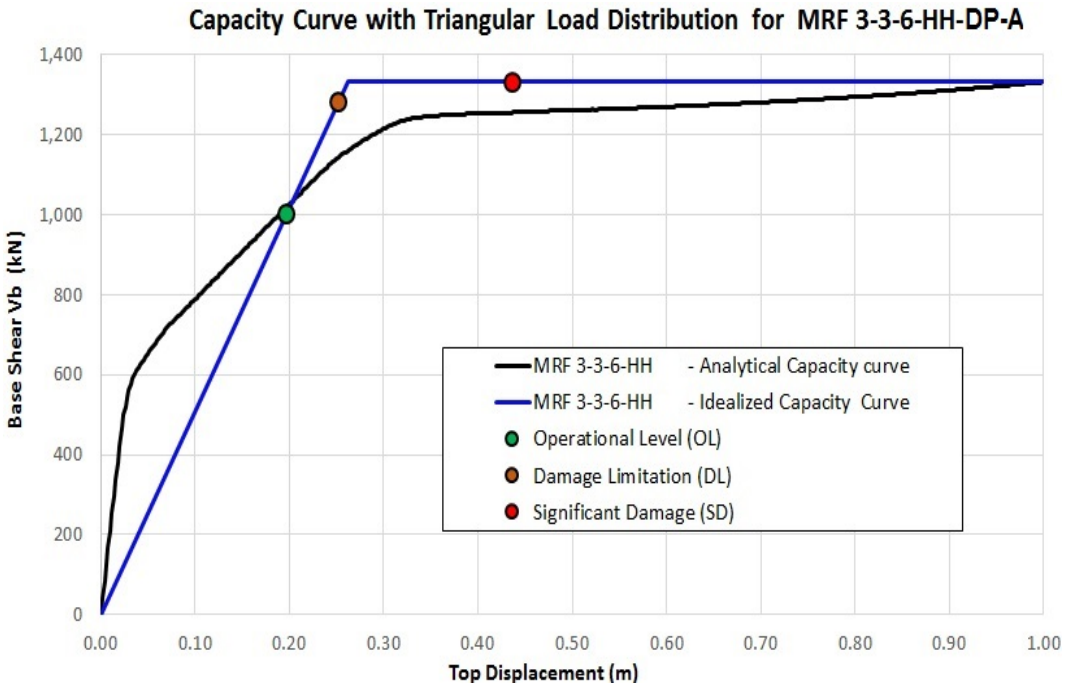

Figure A.18 Calculated and Idealized Capacity Curve for MRF-3-3-6-HH-DP-A for Triangular load pattern, T=0.625s.

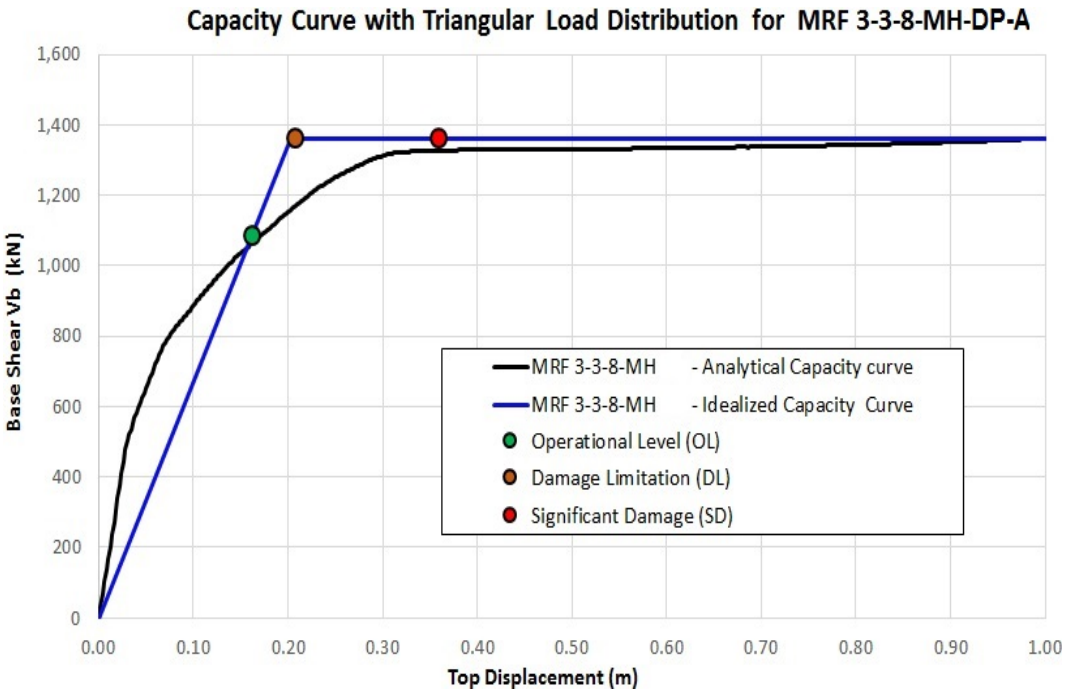

Figure A.19 Calculated and Idealized Capacity Curve for MRF-3-3-8-MH-DP-A for Triangular load pattern, T=0.879s.

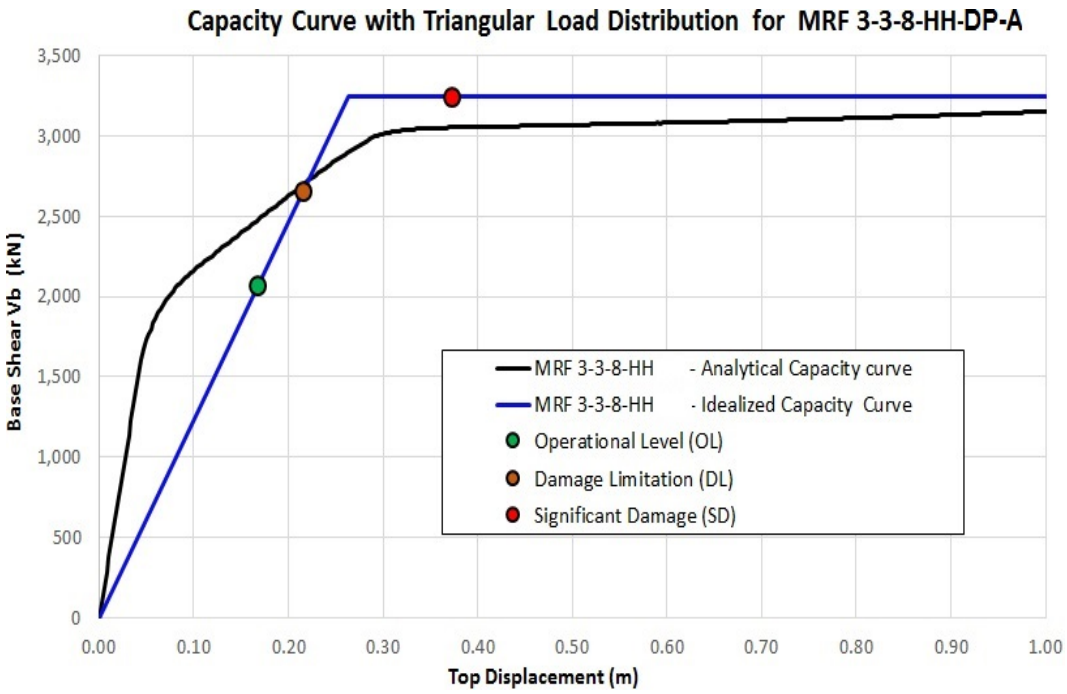

Figure A.20 Calculated and Idealized Capacity Curve for MRF-3-3-8-HH-DP-A for Triangular load pattern, T=0.623s.

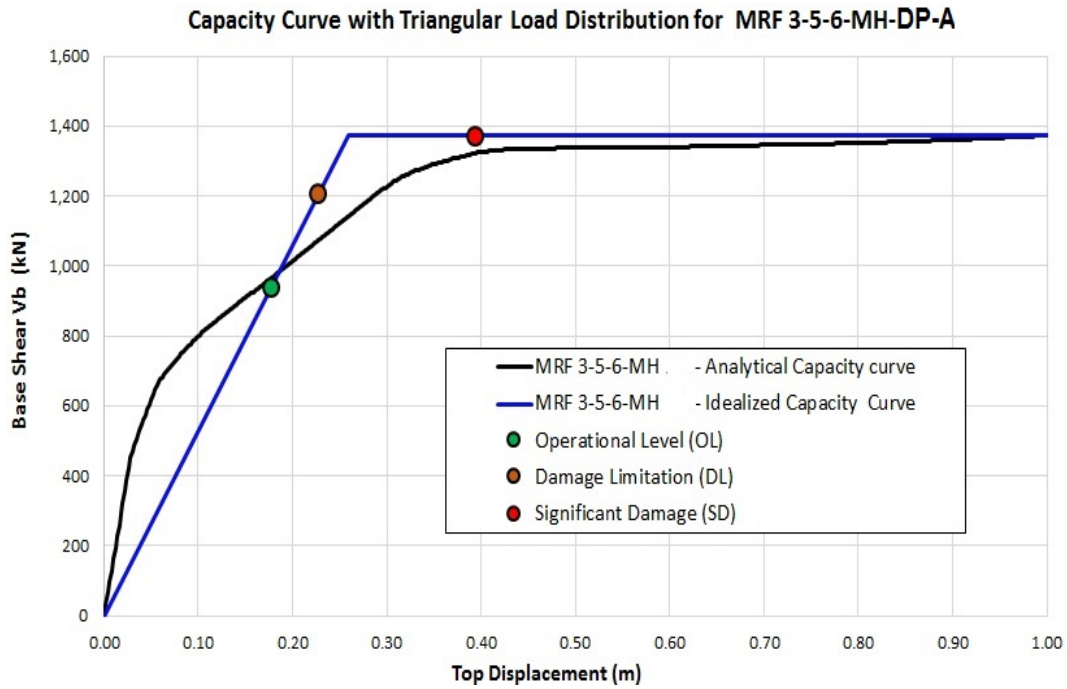

Figure A.21 Calculated and Idealized Capacity Curve for MRF-3-5-6-MH-DP-A for Triangular load pattern, T=0.87s.

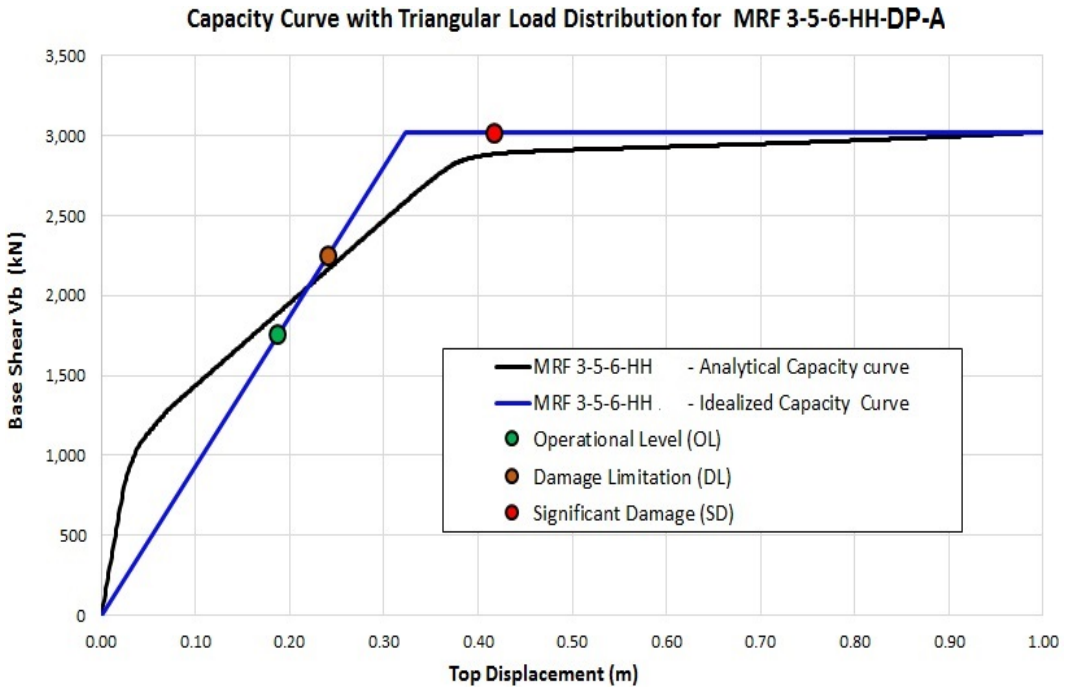

Figure A.22 Calculated and Idealized Capacity Curve for MRF-3-5-6-HH-DP-A for Triangular load pattern, T=0.62s.

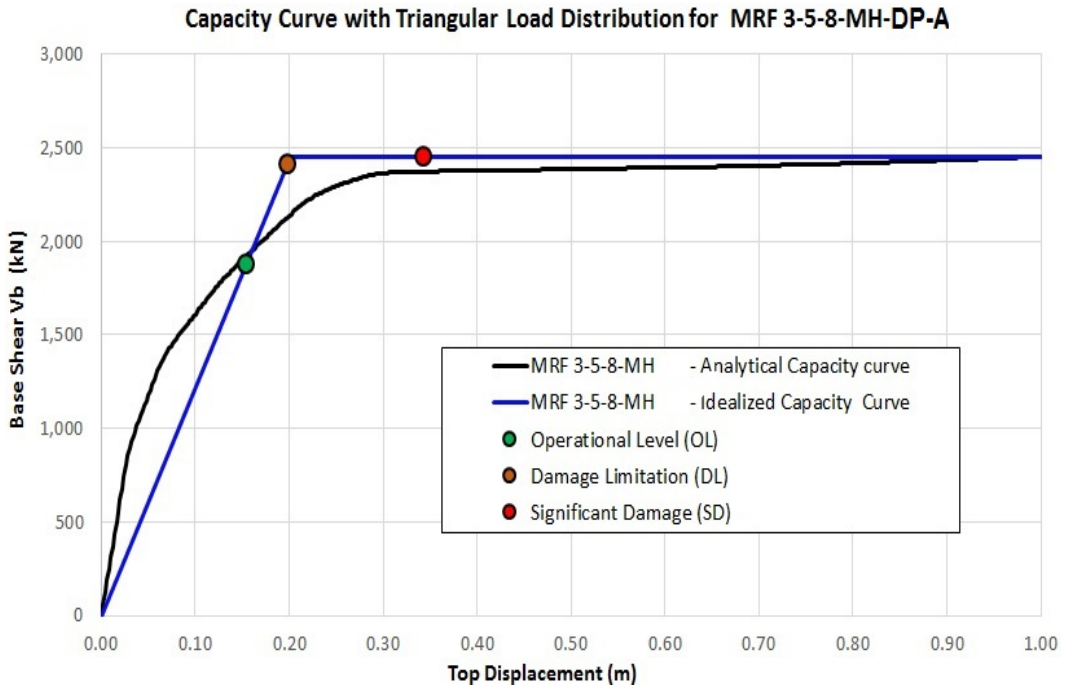

Figure A.23 Calculated and Idealized Capacity Curve for MRF-3-5-8-MH-DP-A for Triangular load pattern, T=0.84s.

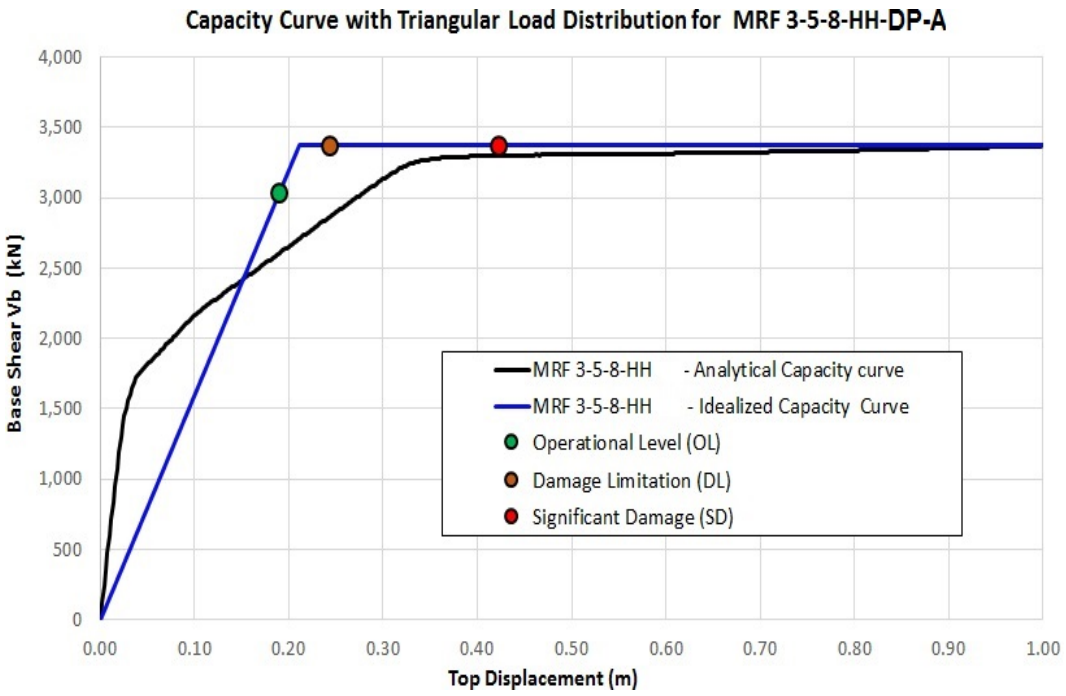

Figure A.24 Calculated and Idealized Capacity Curve for MRF-3-5-8-HH-DP-A for Triangular load pattern, T=0.665s.

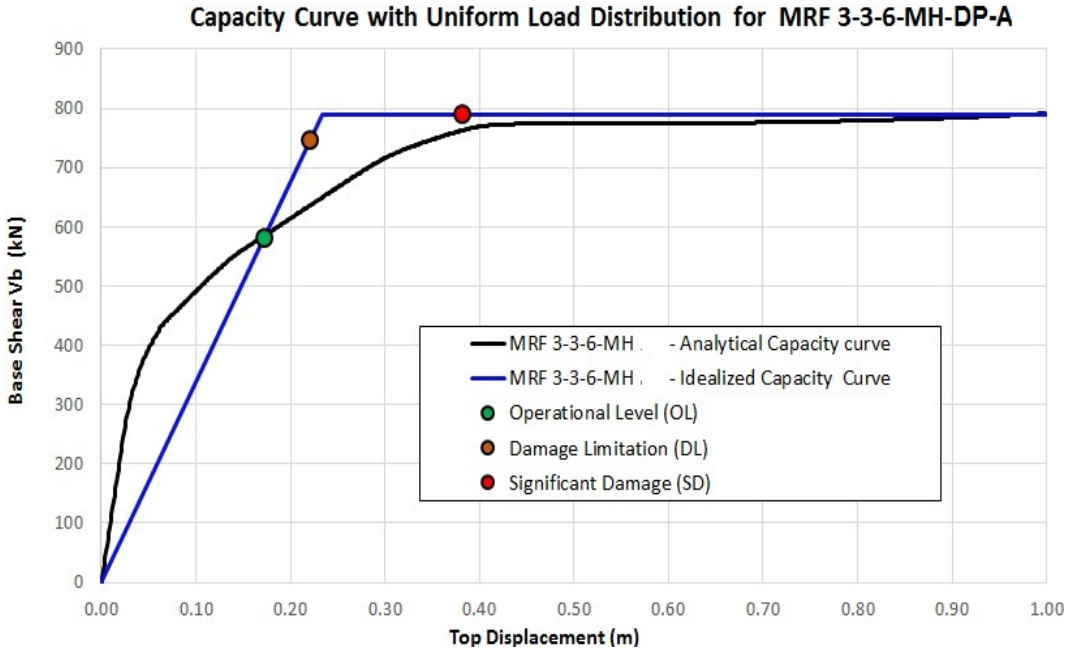

Figure A.25 Calculated and Idealized Capacity Curve for MRF-3-3-6-MH-DP-A for Uniform load pattern, T=0.91s.

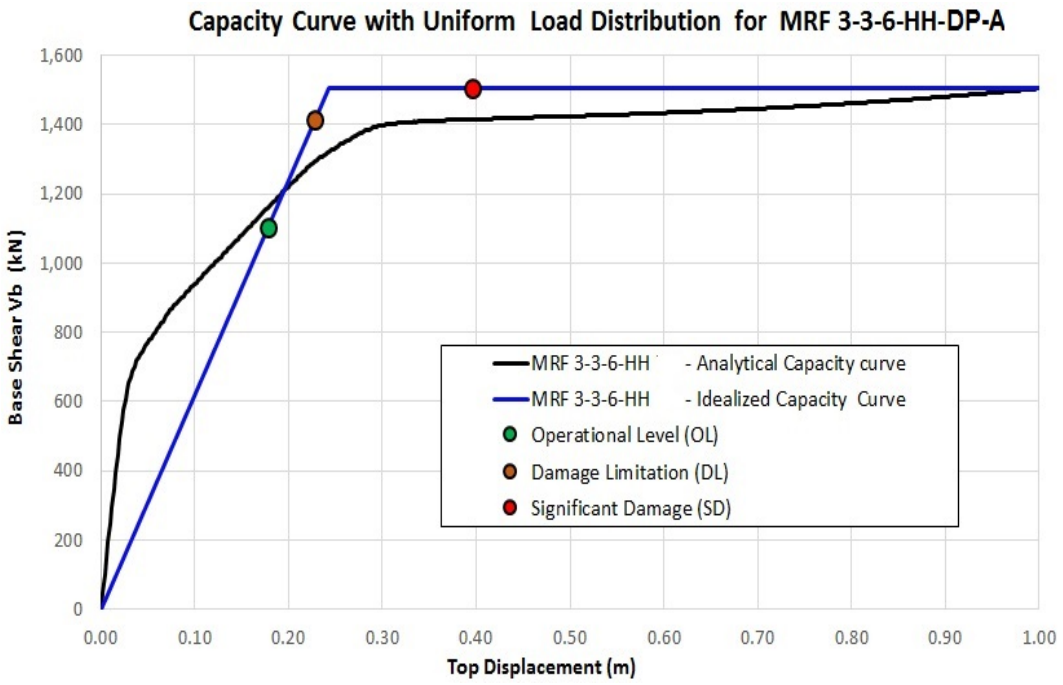

Figure A.26 Calculated and Idealized Capacity Curve for MRF-3-3-6-HH-DP-A for Uniform load pattern, T=0.625s.

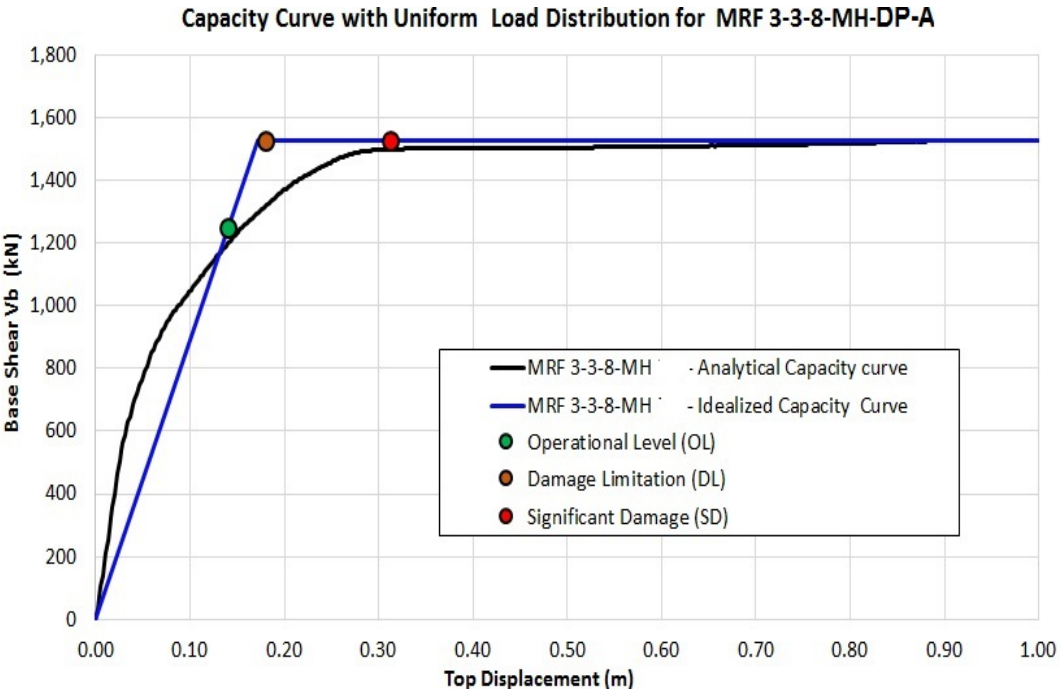

Figure A.27 Calculated and Idealized Capacity Curve for MRF-3-3-8-MH-DP-A for Uniform load pattern, T=0.879s.

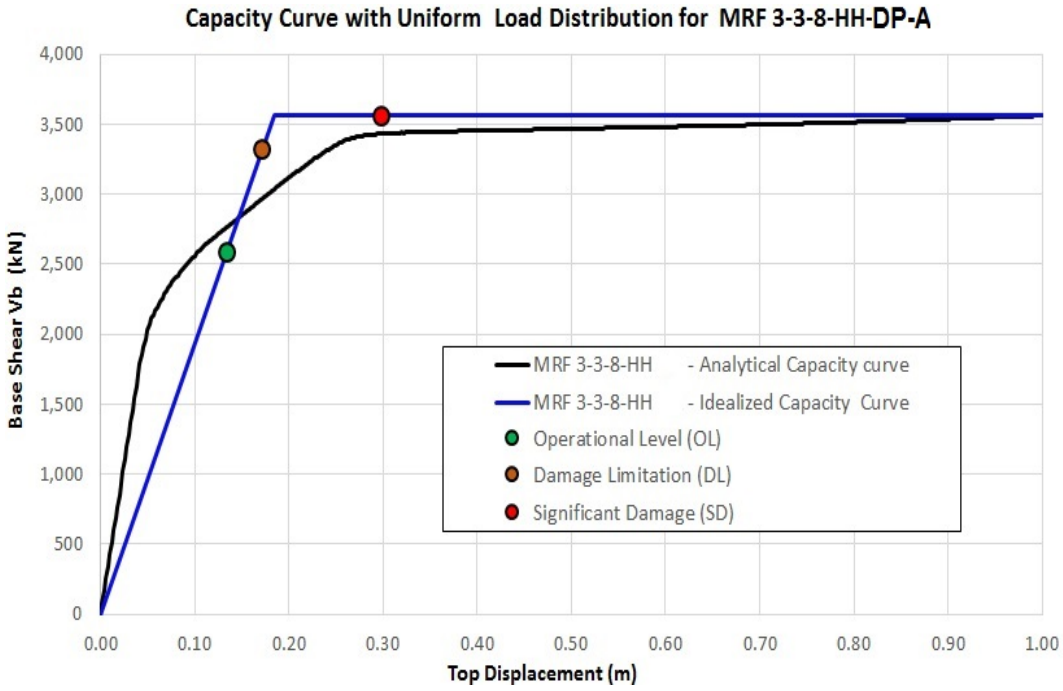

Figure A.28 Calculated and Idealized Capacity Curve for MRF-3-3-8-HH-DP-A for Uniform load pattern, T=0.62s.

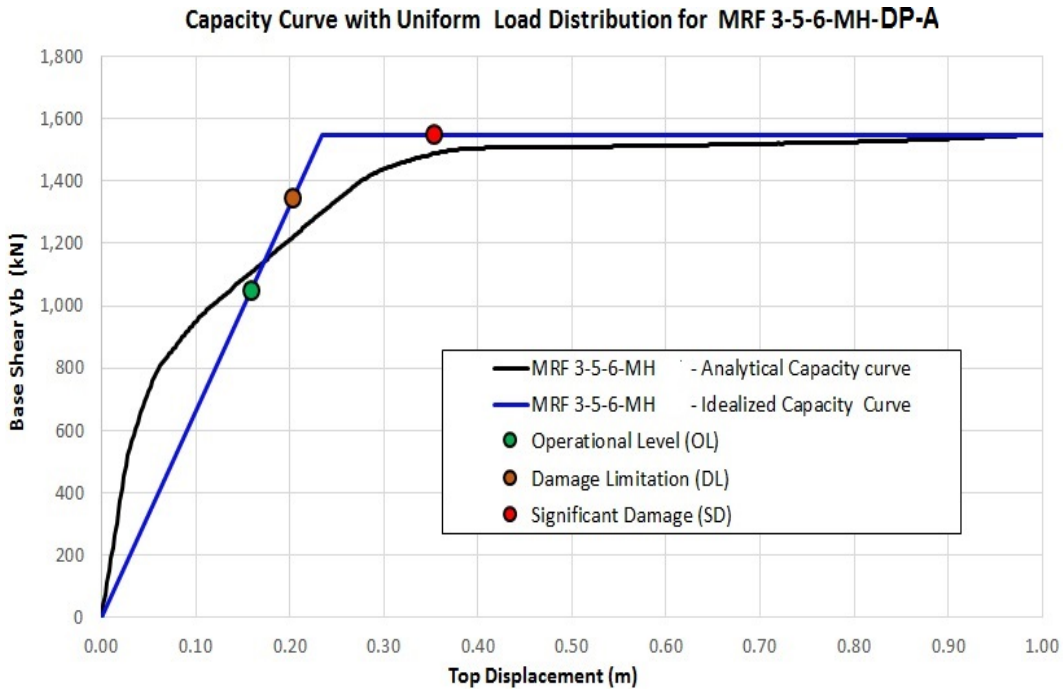

Figure A.29 Calculated and Idealized Capacity Curve for MRF-3-5-6-MH-DP-A for Uniform load pattern, T=0.87s.

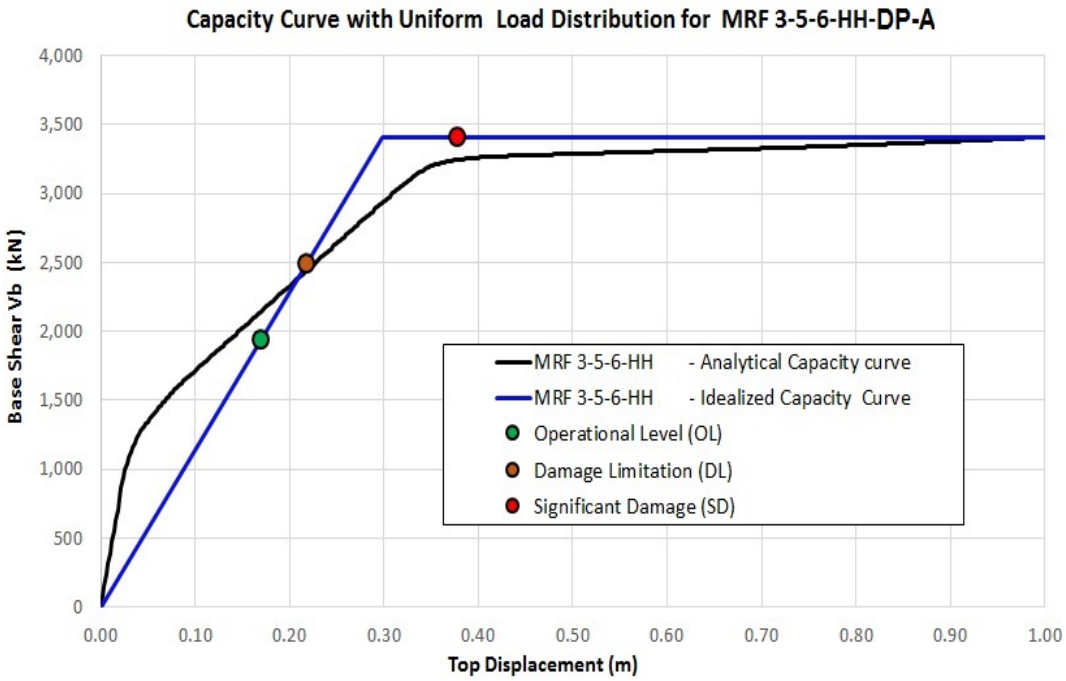

Figure A.30 Calculated and Idealized Capacity Curve for MRF-3-5-6-HH-DP-A for Uniform load pattern, T=0.62s.

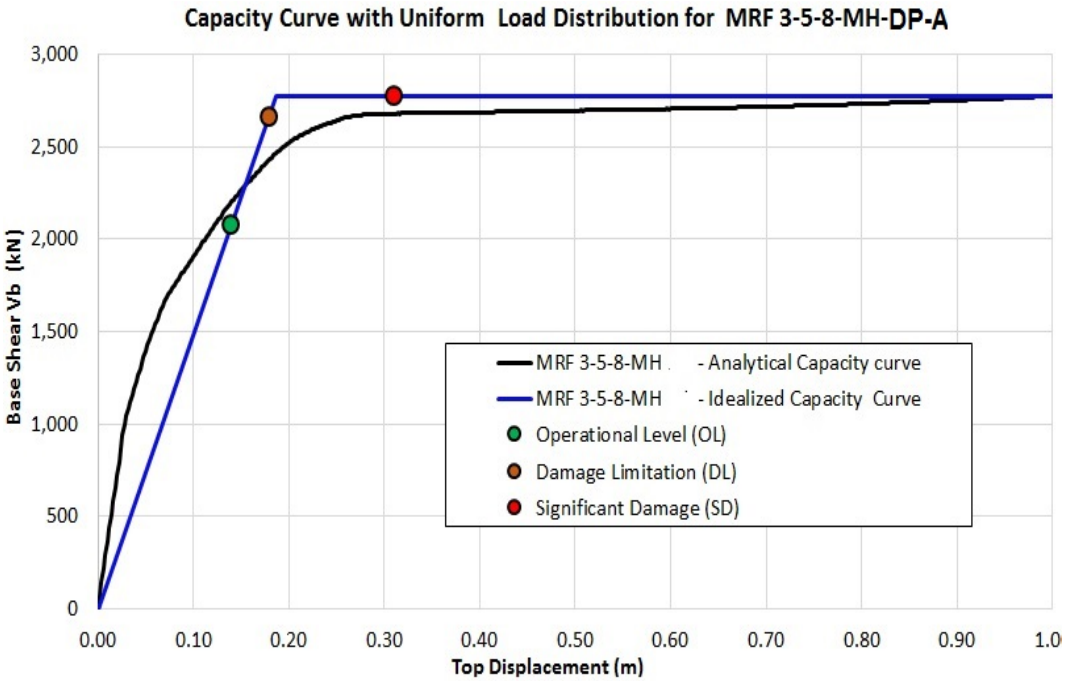

Figure A.31 Calculated and Idealized Capacity Curve for MRF-3-5-8-MH-DP-AA for Uniform load pattern, T=0.845s.

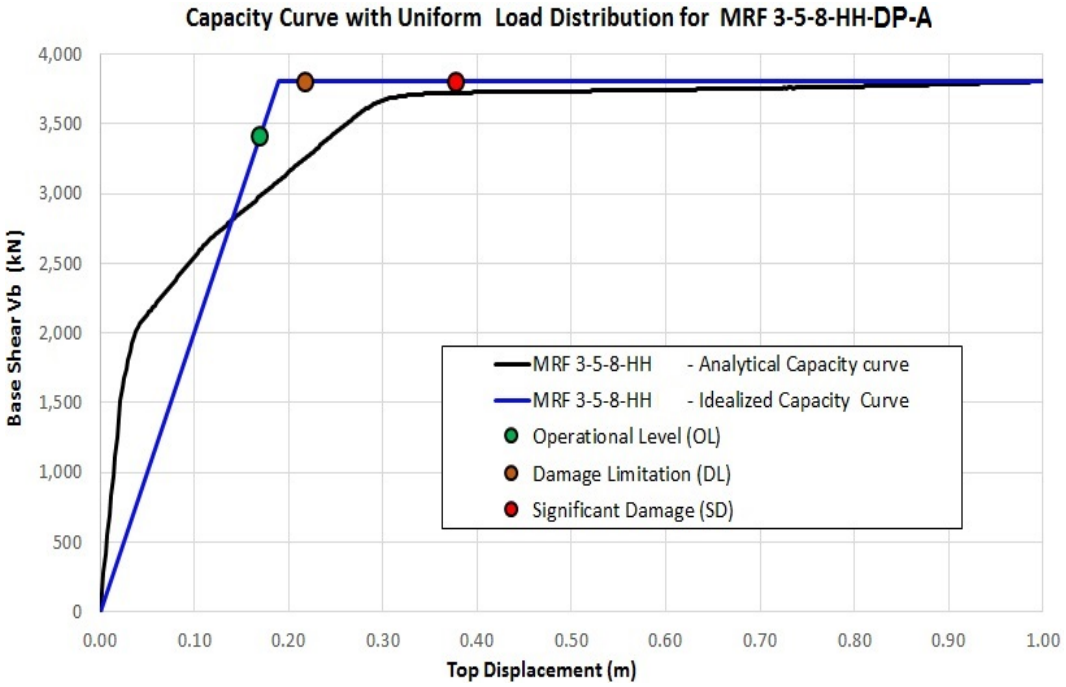

Figure A.32 Calculated and Idealized Capacity Curve for MRF-3-5-8-HH-DP-AA for Uniform load pattern, T=0.665s.

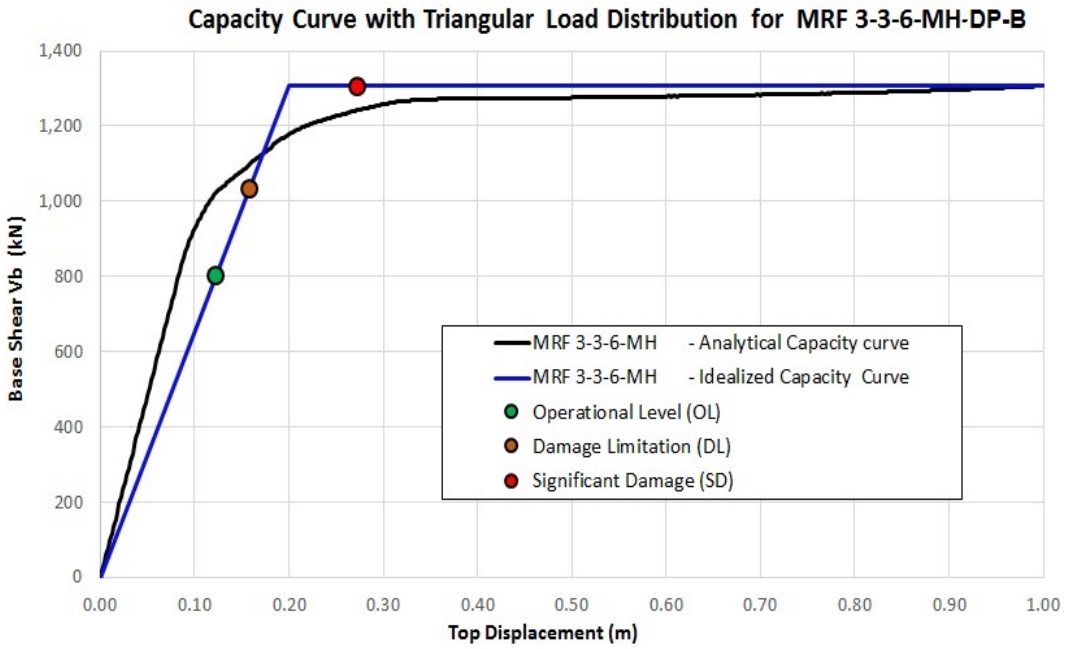

Figure A.33 Calculated and Idealized Capacity Curve for MRF-3-3-6-MH-DP-B for Triangular load pattern, T=0.87s.

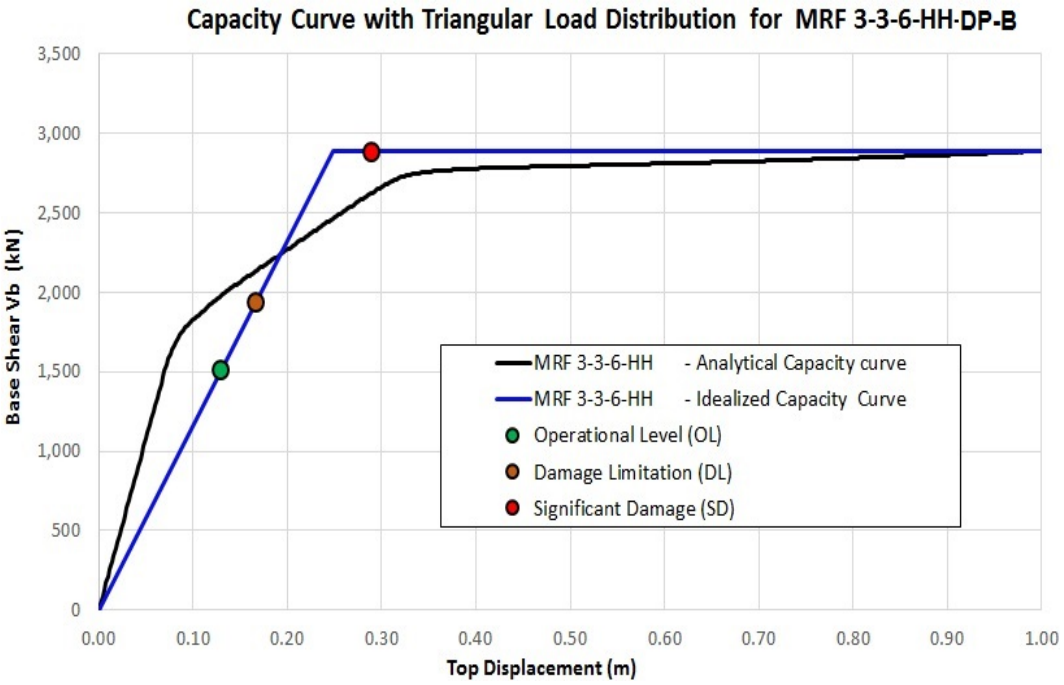

Figure A.34 Calculated and Idealized Capacity Curve for MRF-3-3-6-HH-DP-B for Triangular load pattern, T=0.59s.

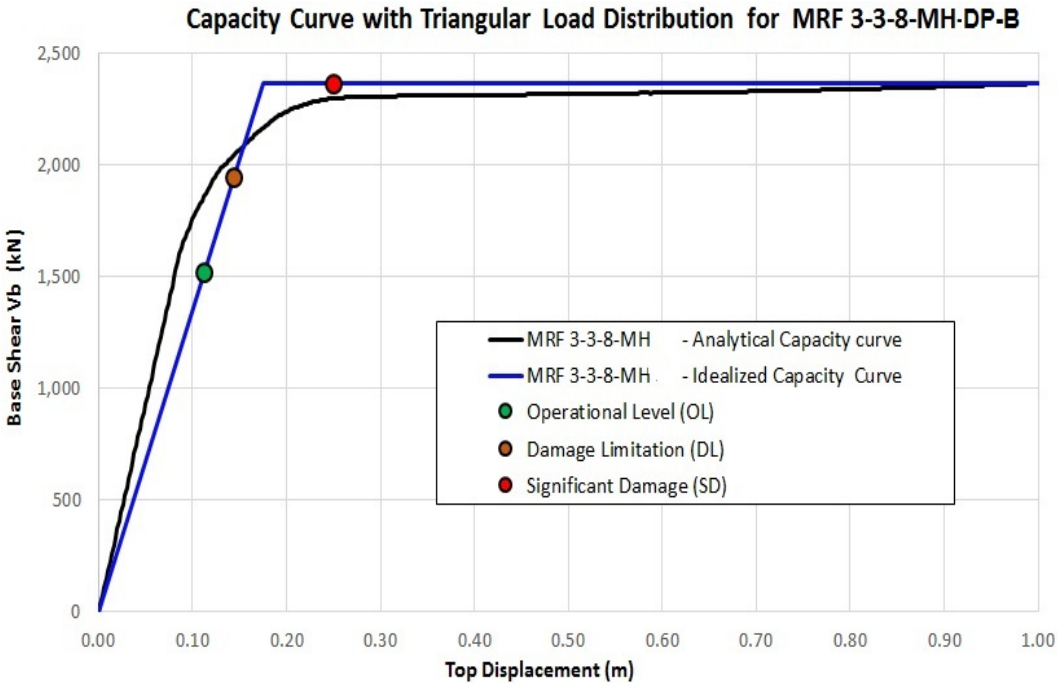

Figure A.35 Calculated and Idealized Capacity Curve for MRF-3-3-8-MH-DP-B for Triangular load pattern, T=0.83s.

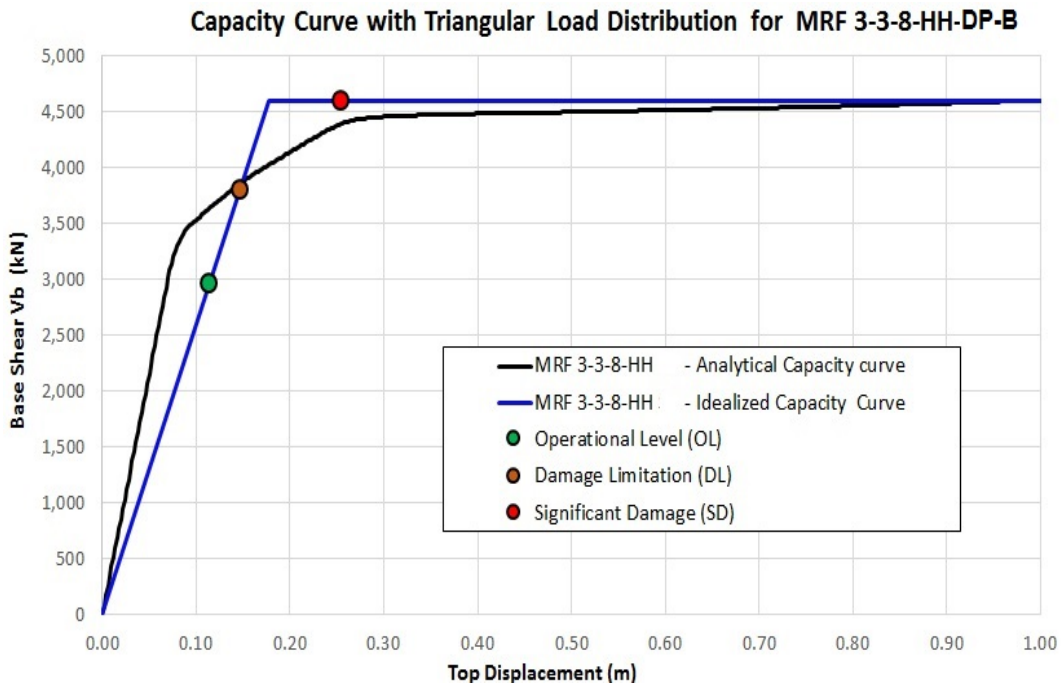

Figure A.36 Calculated and Idealized Capacity Curve for MRF-3-3-8-HH-DP-B for Triangular load pattern, T=0.59s.

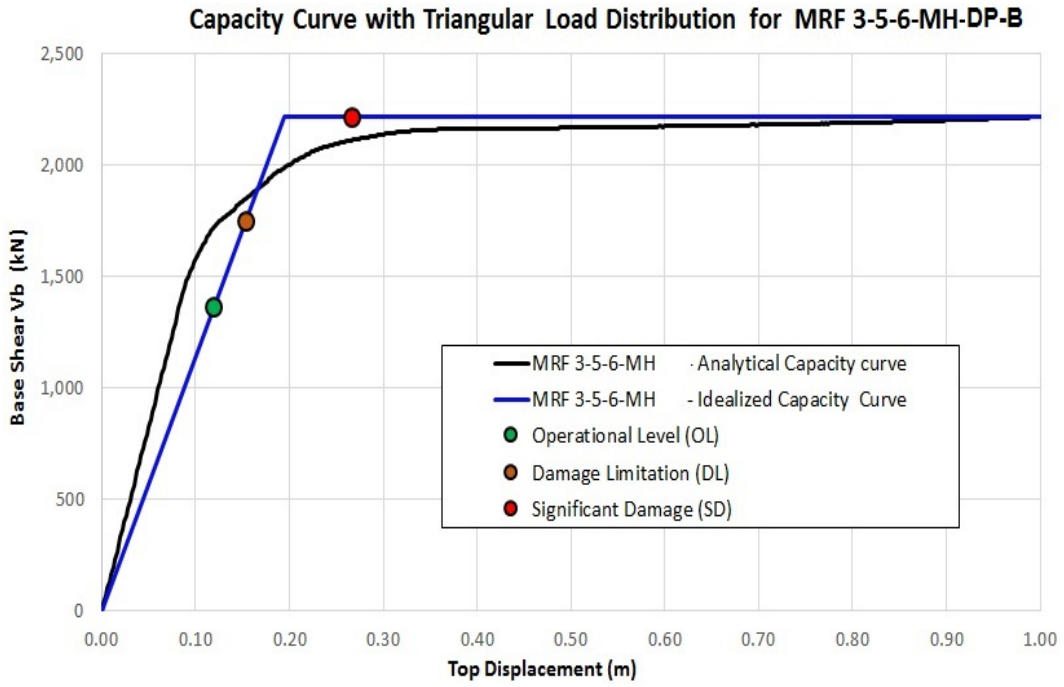

Figure A.37 Calculated and Idealized Capacity Curve for MRF-3-5-6-MH-DP-B for Triangular load pattern, T=0.86s.

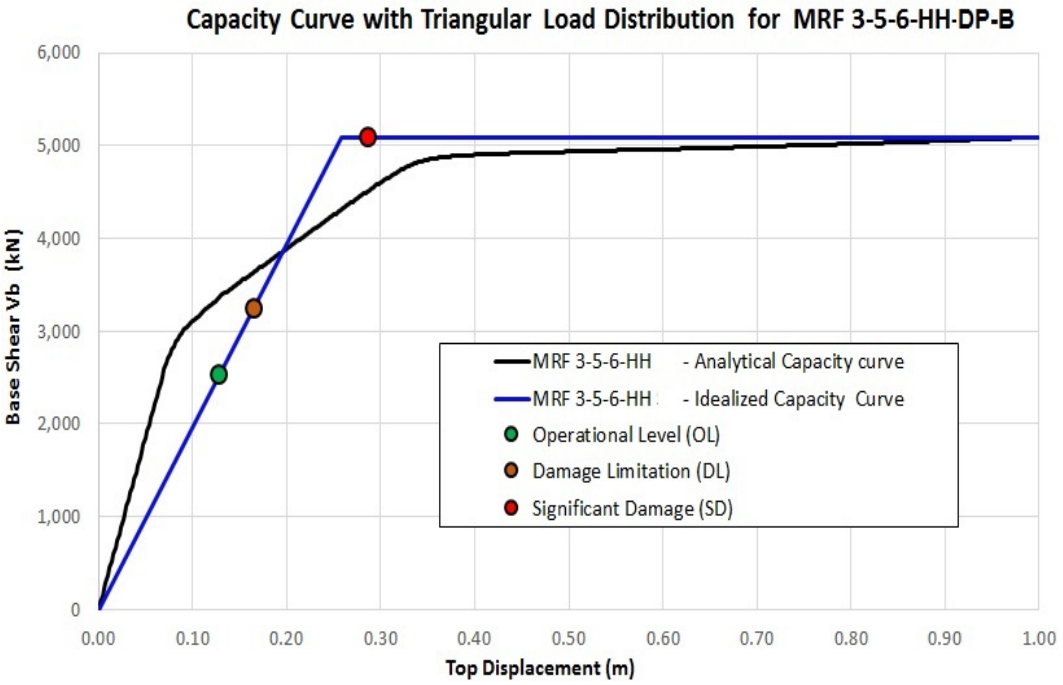

Figure A.38 Calculated and Idealized Capacity Curve for MRF-3-5-6-HH-DP-B for Triangular load pattern, T=0.58s.

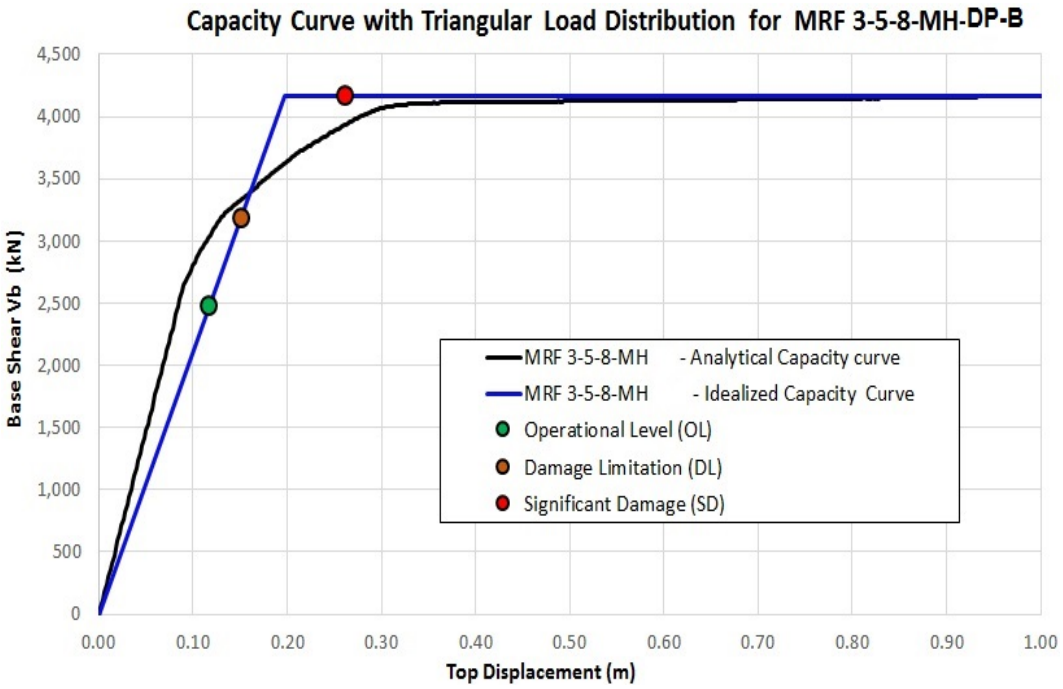

Figure A.39 Calculated and Idealized Capacity Curve for MRF-3-5-8-MH-DP-B for Triangular load pattern, T=0.85s.

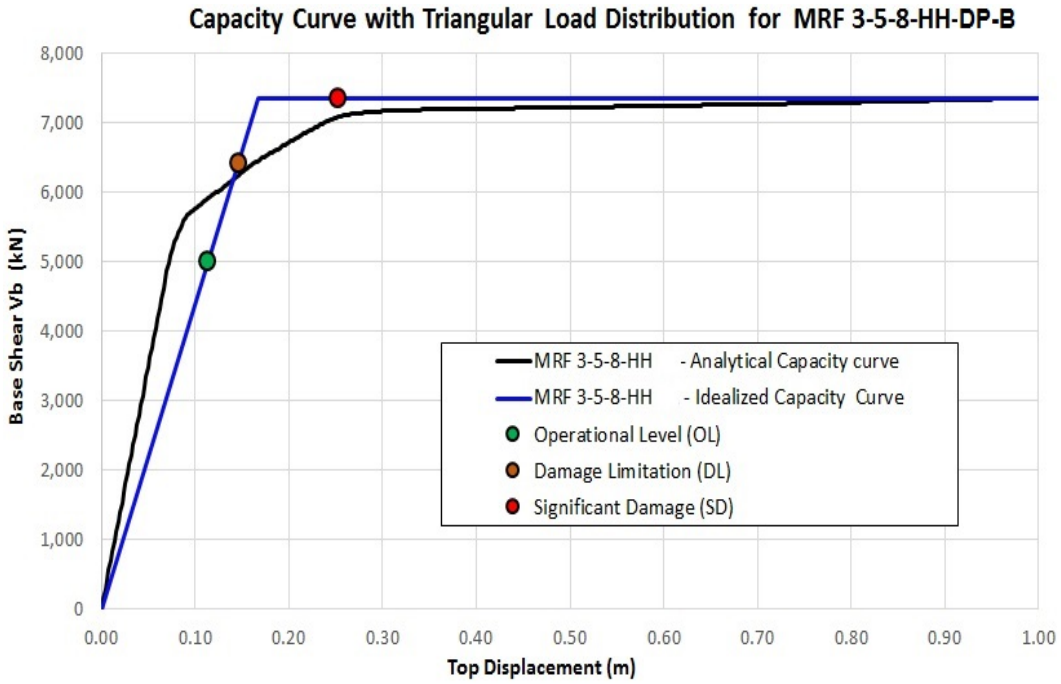

Figure A.40 Calculated and Idealized Capacity Curve for MRF-3-5-8-HH-DP-B for Triangular load pattern, T=0.59s.

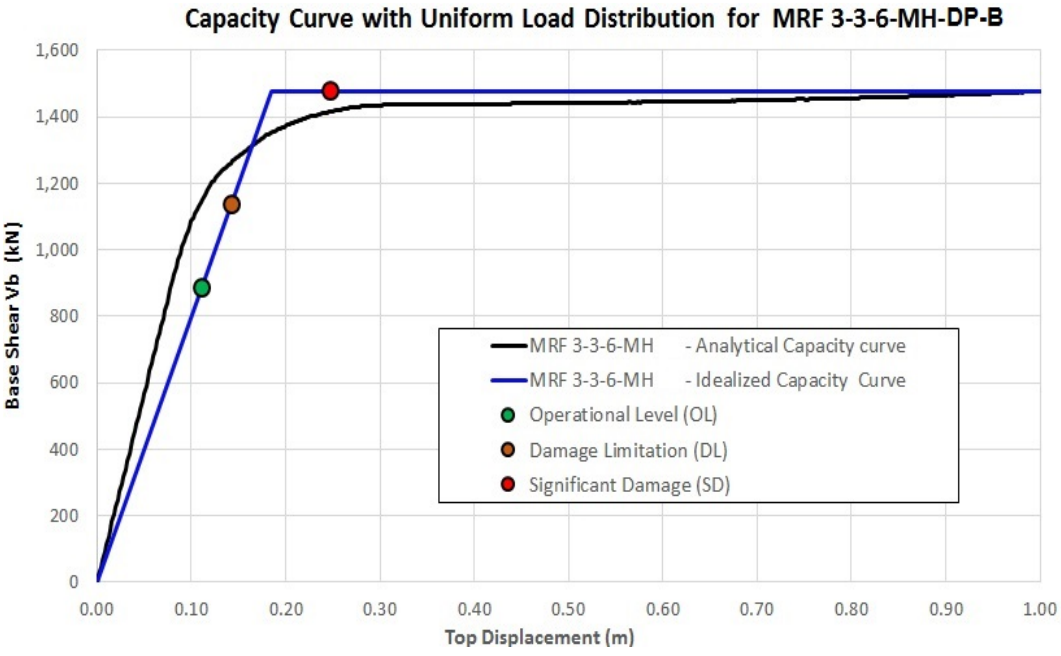

Figure A.41 Calculated and Idealized Capacity Curve for MRF-3-3-6-MH-DP-B for Uniform load pattern, T=0.87s.

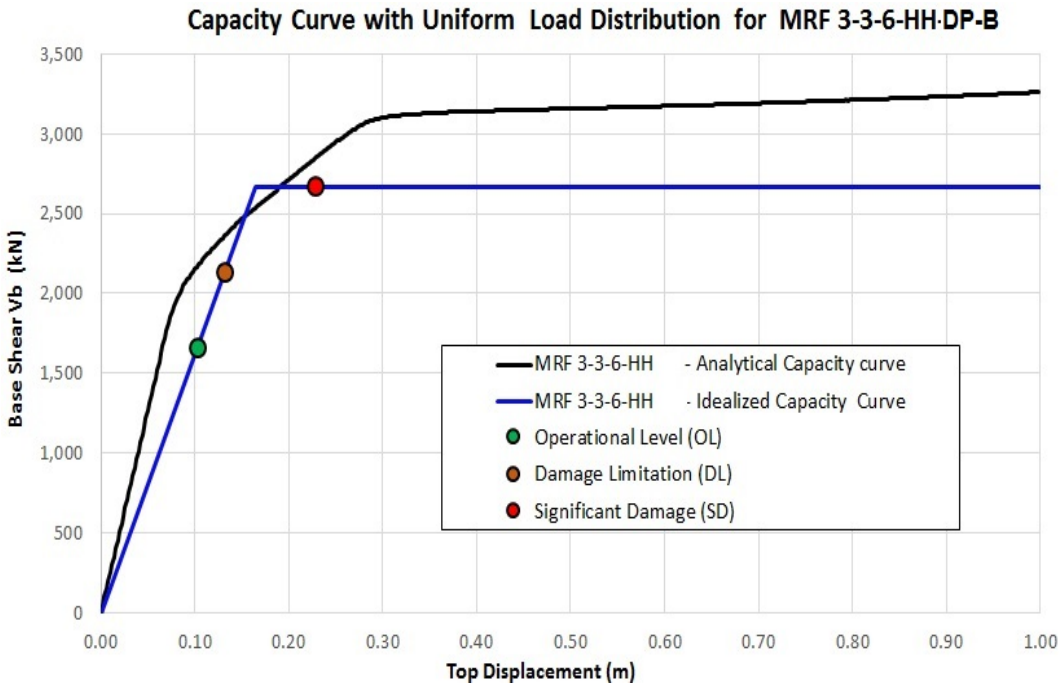

Figure A.42 Calculated and Idealized Capacity Curve for MRF-3-3-6-HH-DP-B for Uniform load pattern, T=0.59s.

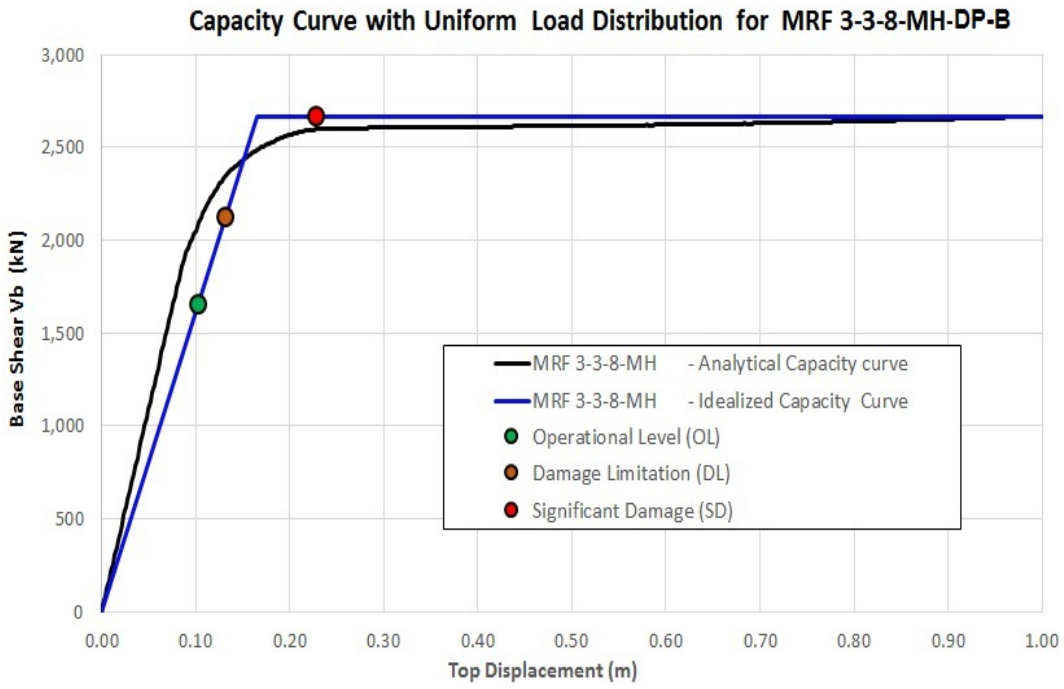

Figure A.43 Calculated and Idealized Capacity Curve for MRF-3-3-8-MH-DP-B for Uniform load pattern, T=0.83s.

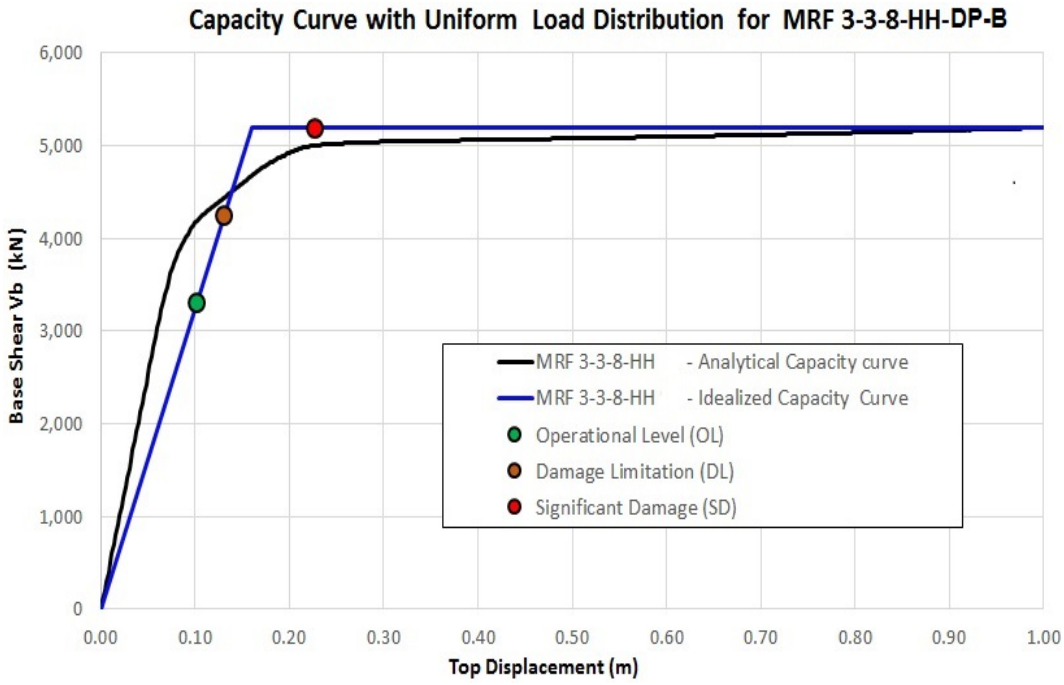

Figure A.44 Calculated and Idealized Capacity Curve for MRF-3-3-8-HH-DP-B for Uniform load pattern, T=0.59s.

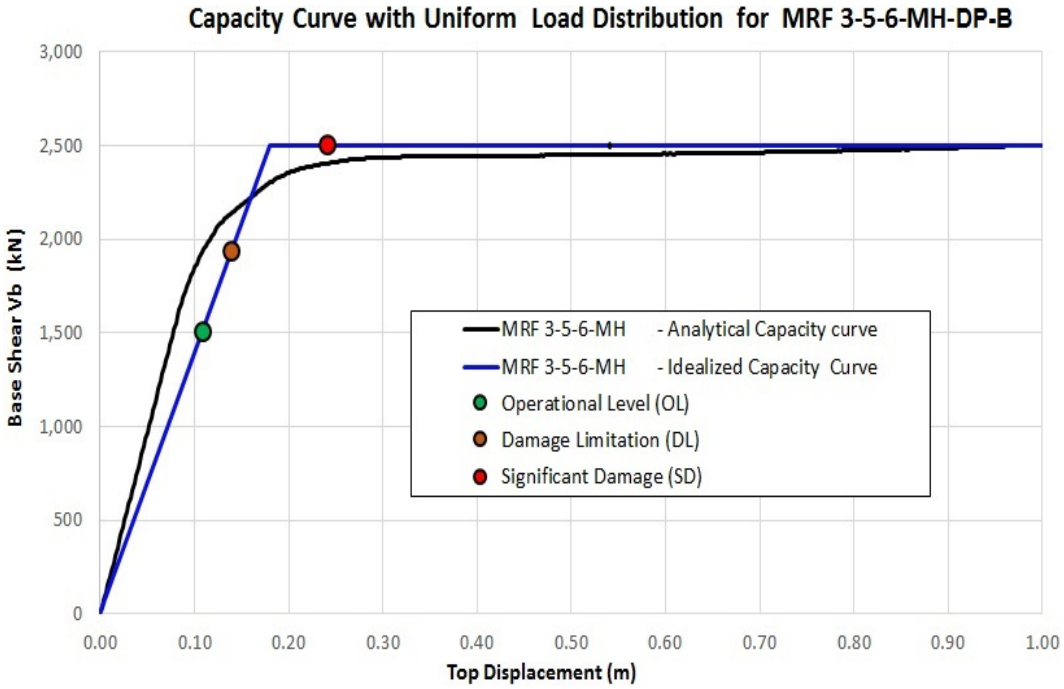

Figure A.45 Calculated and Idealized Capacity Curve for MRF-3-5-6-MH-DP-B for Uniform load pattern, T=0.86s.

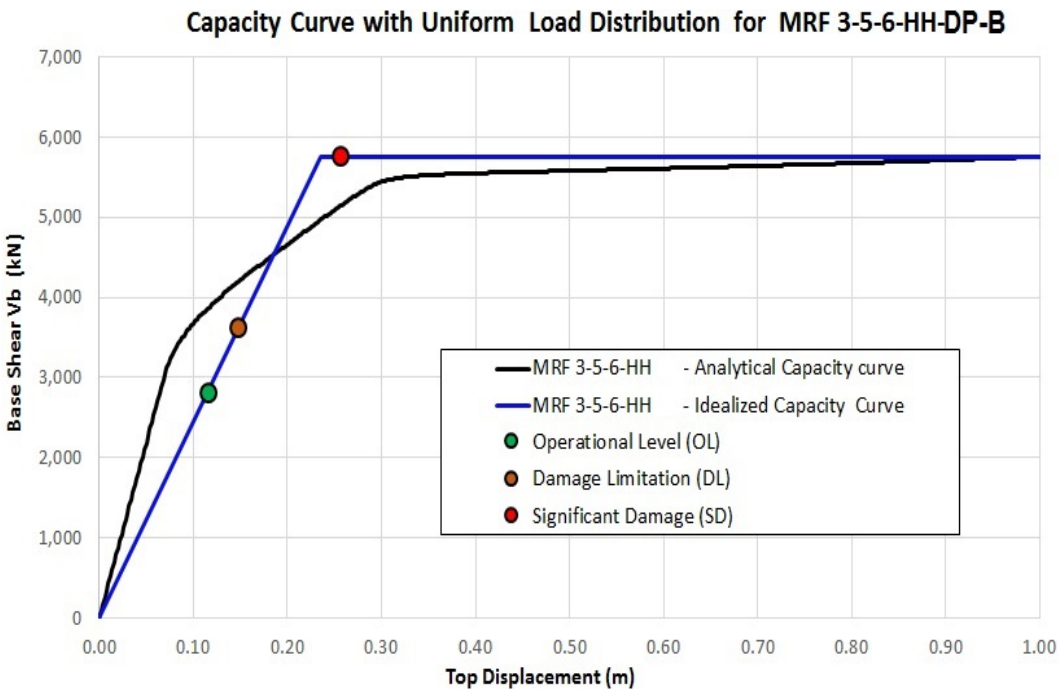

Figure A.46 Calculated and Idealized Capacity Curve for MRF-3-5-6-HH-DP-B for Uniform load pattern, T=0.58s.

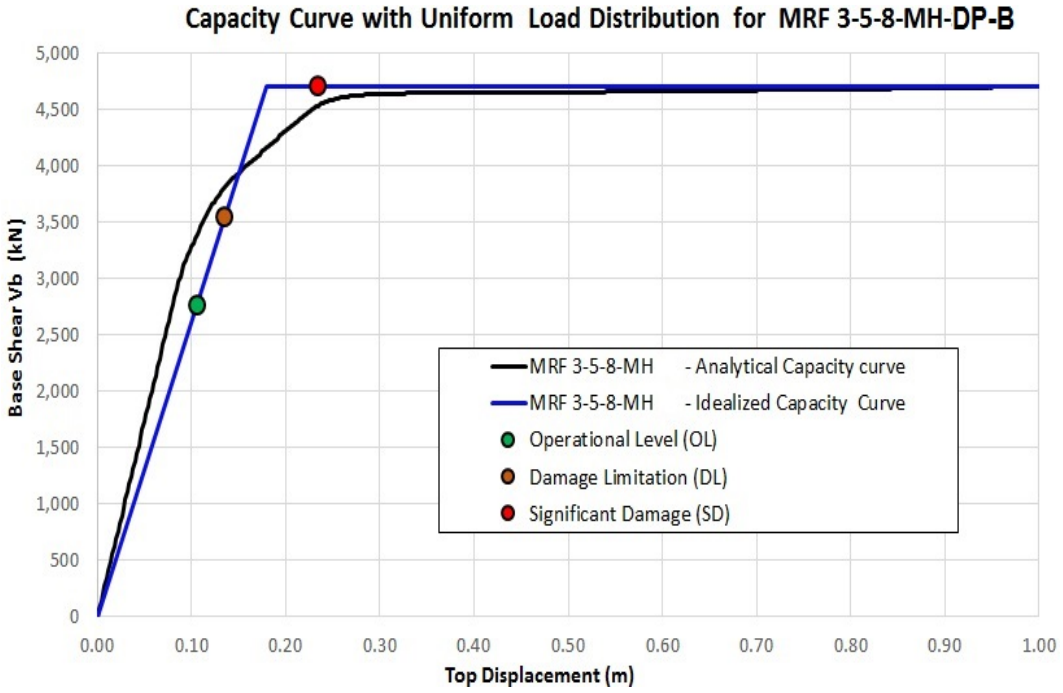

Figure A.47 Calculated and Idealized Capacity Curve for MRF-3-5-8-MH-DP-B for Uniform load pattern, T=0.85s.

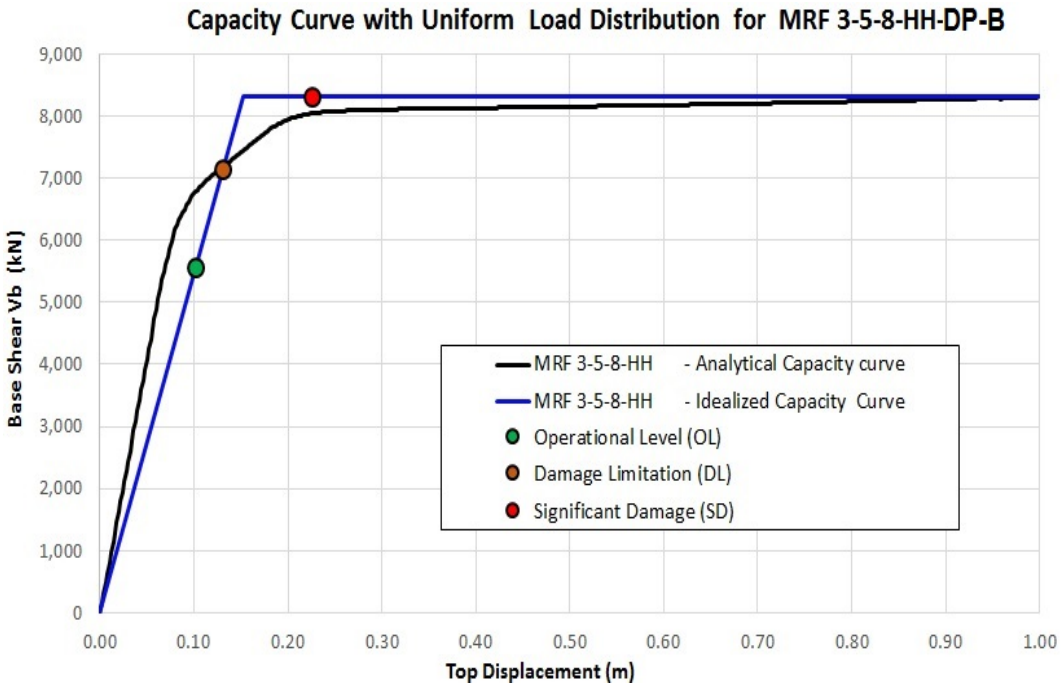

Figure A.48 Calculated and Idealized Capacity Curve for MRF-3-5-8-HH-DP-B for Uniform load pattern, T=0.59s.

Appendix B

Maximum strain performance for structural elements

In following figures are described the results for the maximum strain values measured for each element and each frame considering the 14 records analyzed, the information of each element contains:

- SF: Scale factor, corresponds to the scale factor that multiplies the record acceleration values according to the three levels of performance analyzed. Damage Limitation (DL) probability of exceedance 20% in 50 years (return period T=225 years) with SF=0.59, Significant Damage (SD) probability of exceedance 10% in 50 years (return period T=475 years) with SF=1 and Near Collapse or Collapse Prevention (CP) with a probability of exceedance 2% in 50 years (return period T=2475 years) with SF=1.73.

- Strain value, as the maximum value of the 14 records analyzed for each frame, a code of colors show the performance stage of the element when the maximum strain was measured: i) *Slight Damage* for strain values between 0.0021 and 0.016 with green color, ii) *Serious Damage* for strain values between 0.016 and 0.032 with yellow color, iii) V*Very Serious Damage* for strain values between higher than 0.032 as a limit for ultimate strain for the elements with a red color.

- Location were the maximum value of strain is measured, *bottom or top* for columns

and *right or left* end for beams. Also, the number or record that corresponds to the maximum strain value is described for each element.

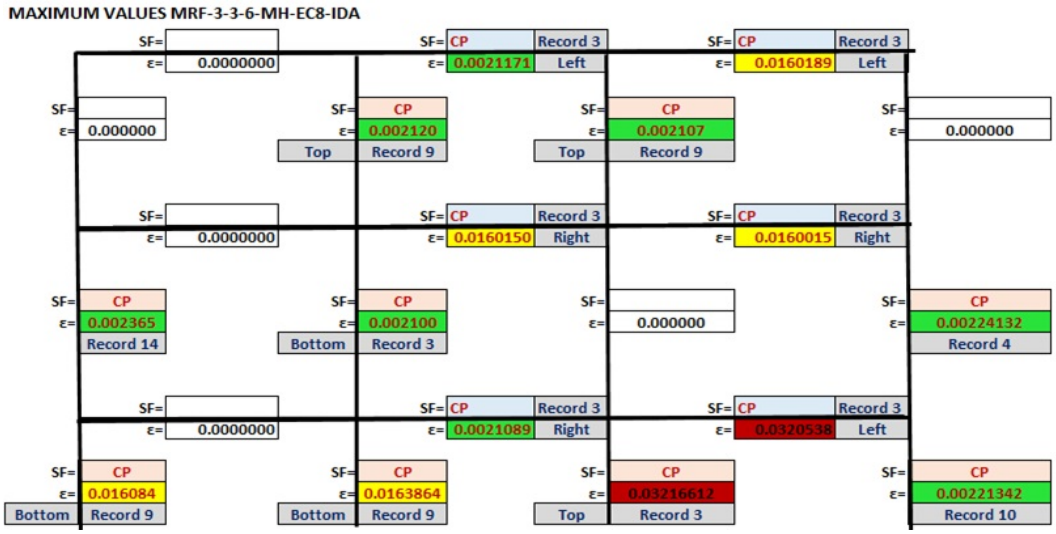

Figure B.1 Maximum strain values for each element for MRF-3-3-6-MH-EC8.

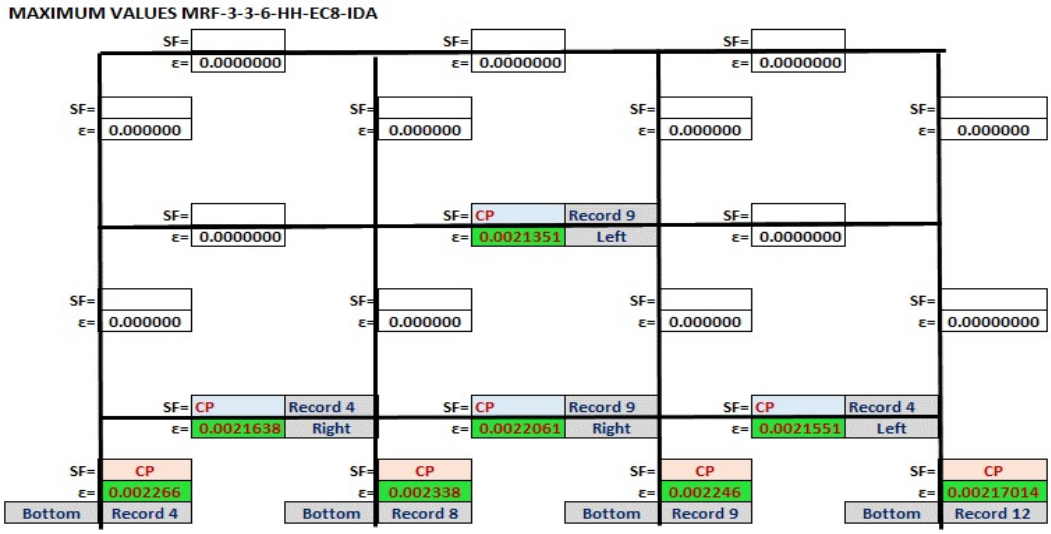

Figure B.2 Maximum strain values for each element for MRF-3-3-6-HH-EC8.

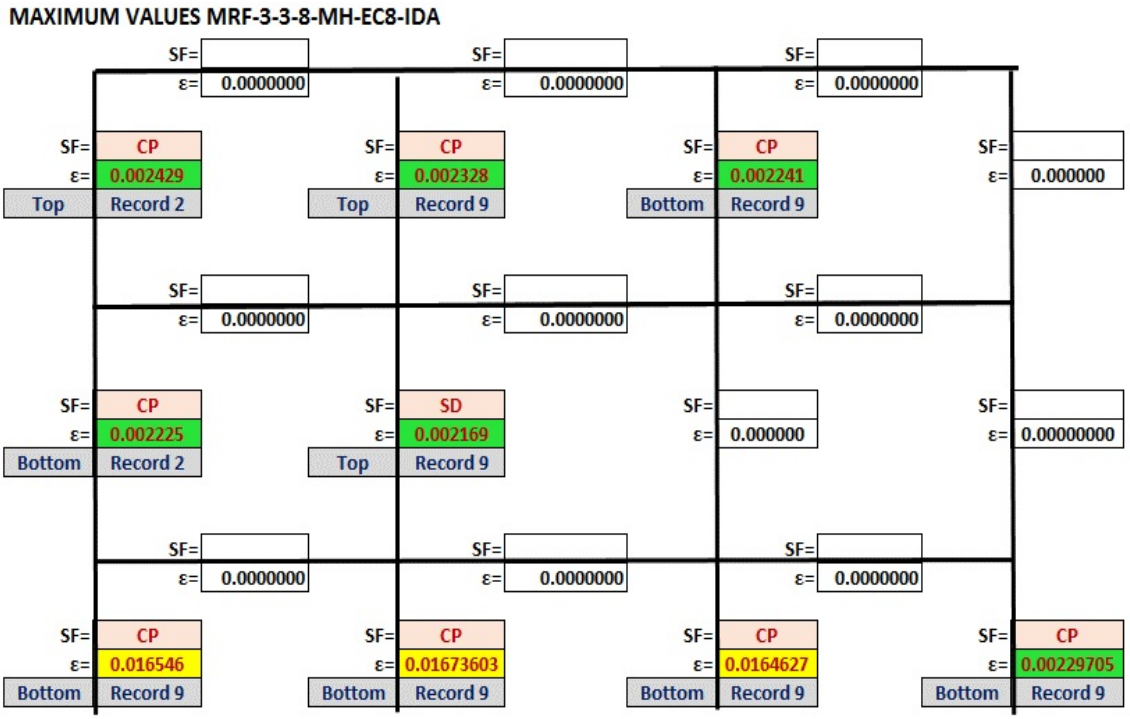

Figure B.3 Maximum strain values for each element for MRF-3-3-8-MH-EC8.

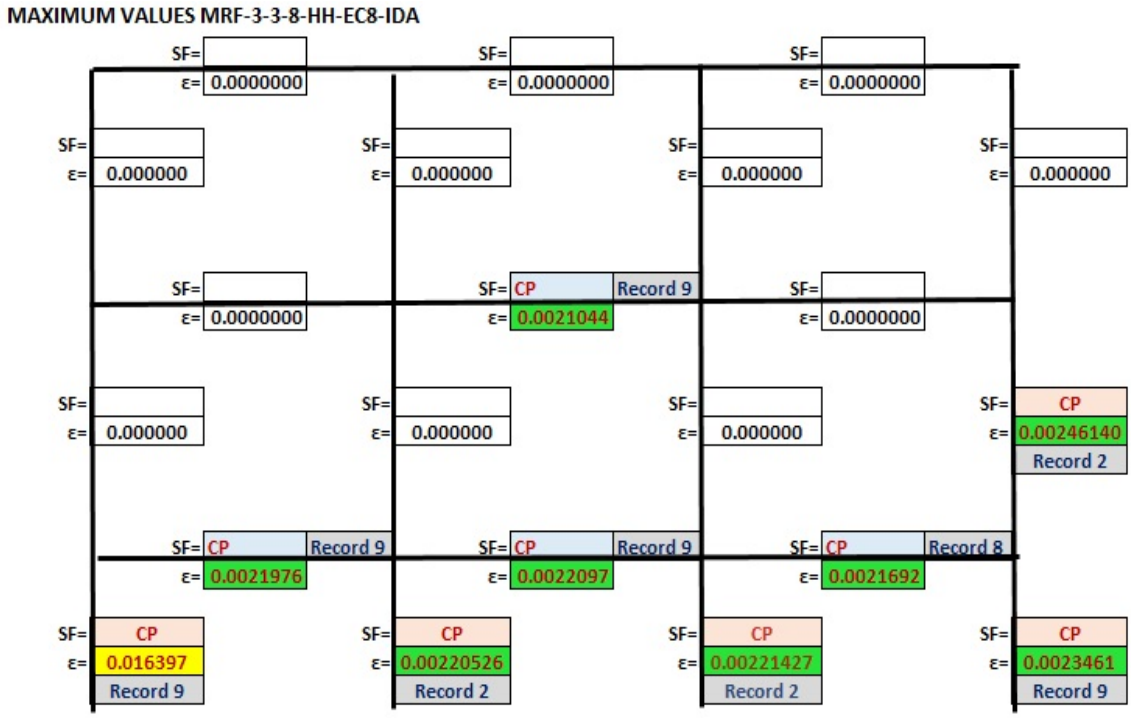

Figure B.4 Maximum strain values for each element for MRF-3-3-8-HH-EC8.

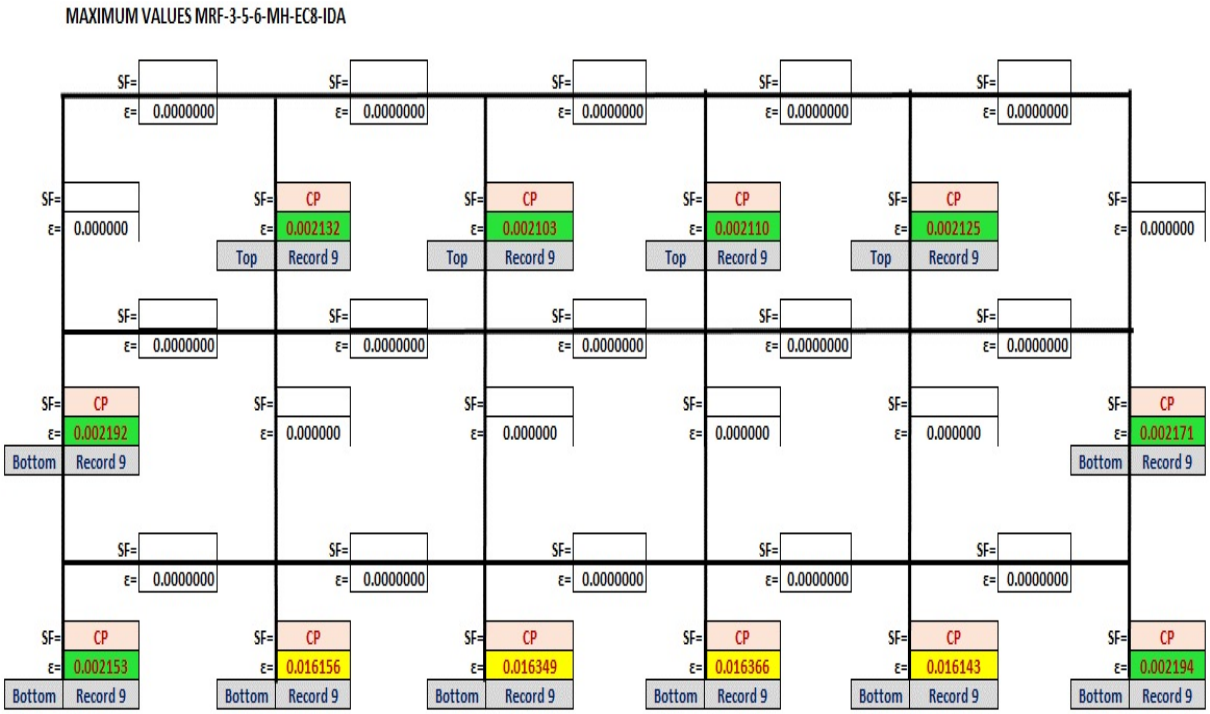

Figure B.5 Maximum strain values for each element for MRF-3-5-6-MH-EC8.

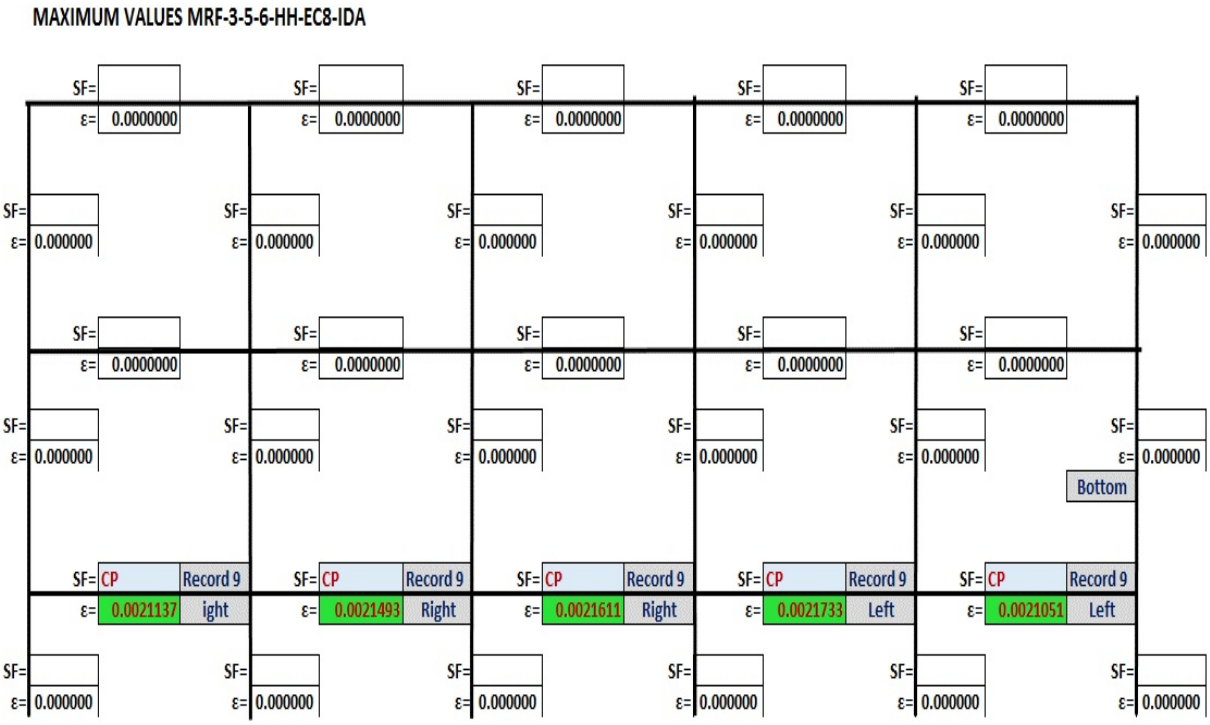

Figure B.6 Maximum strain values for each element for MRF-3-5-6-HH-EC8.

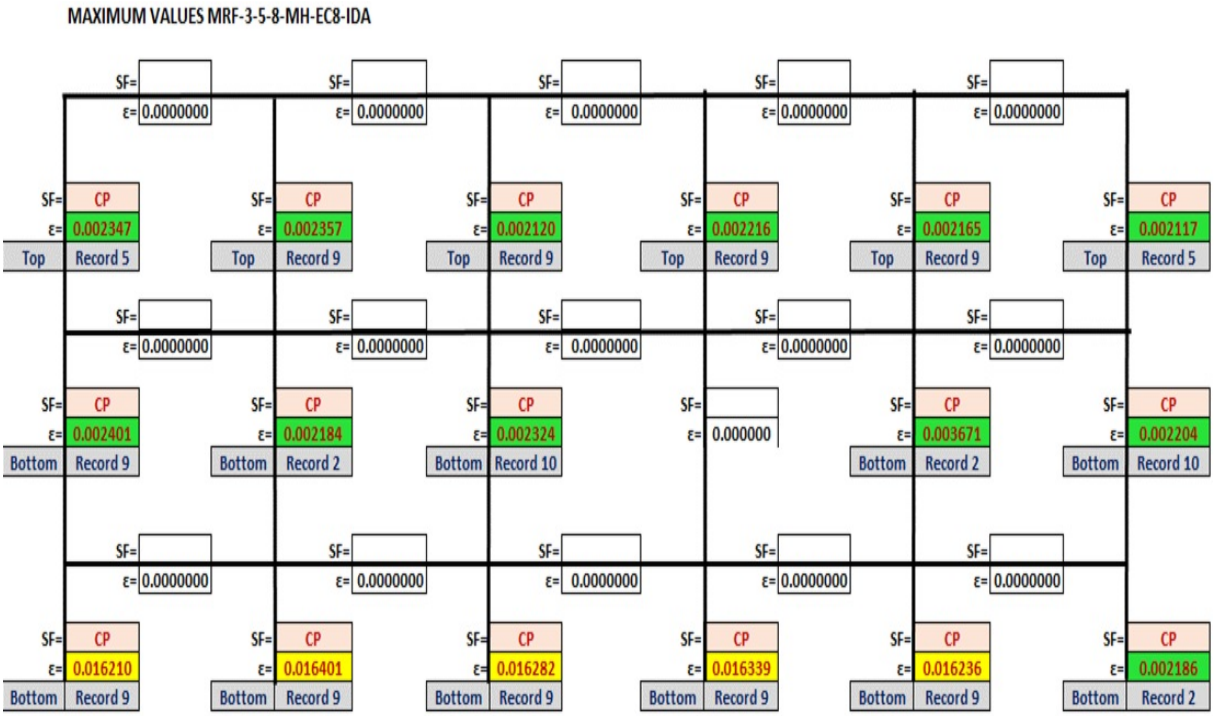

Figure B.7 Maximum strain values for each element for MRF-3-5-8-MH-EC8.

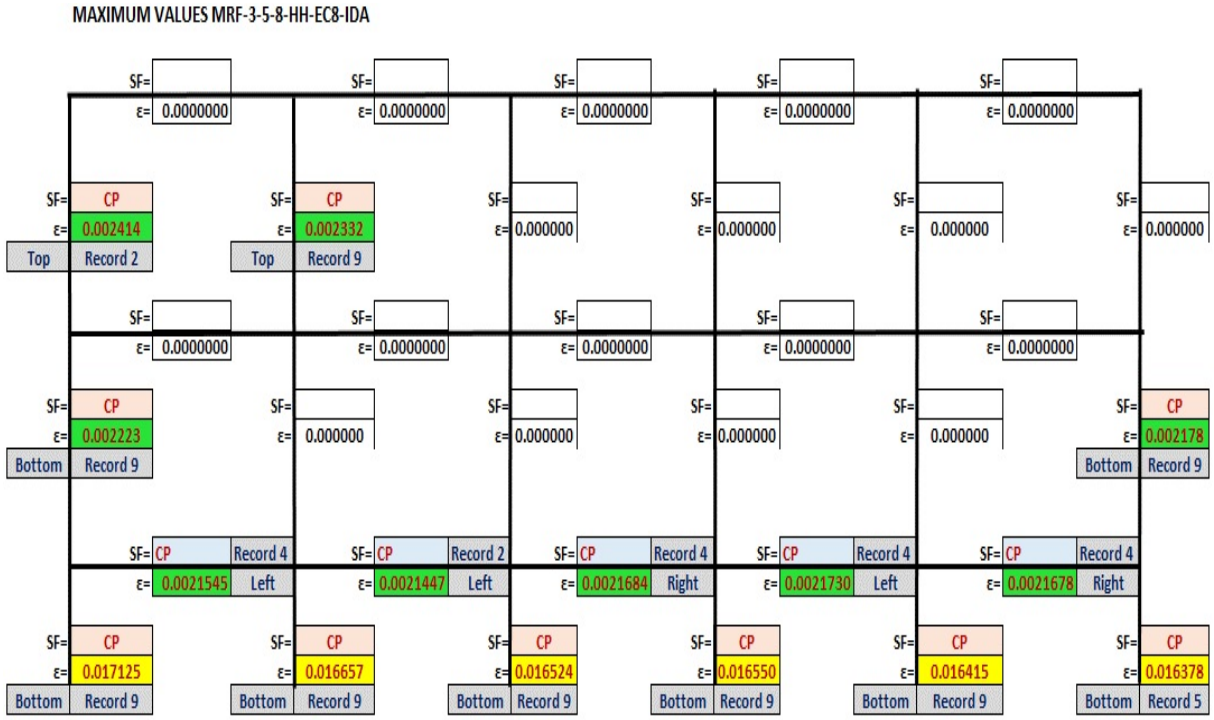

Figure B.8 Maximum strain values for each element for MRF-3-5-8-HH-EC8.

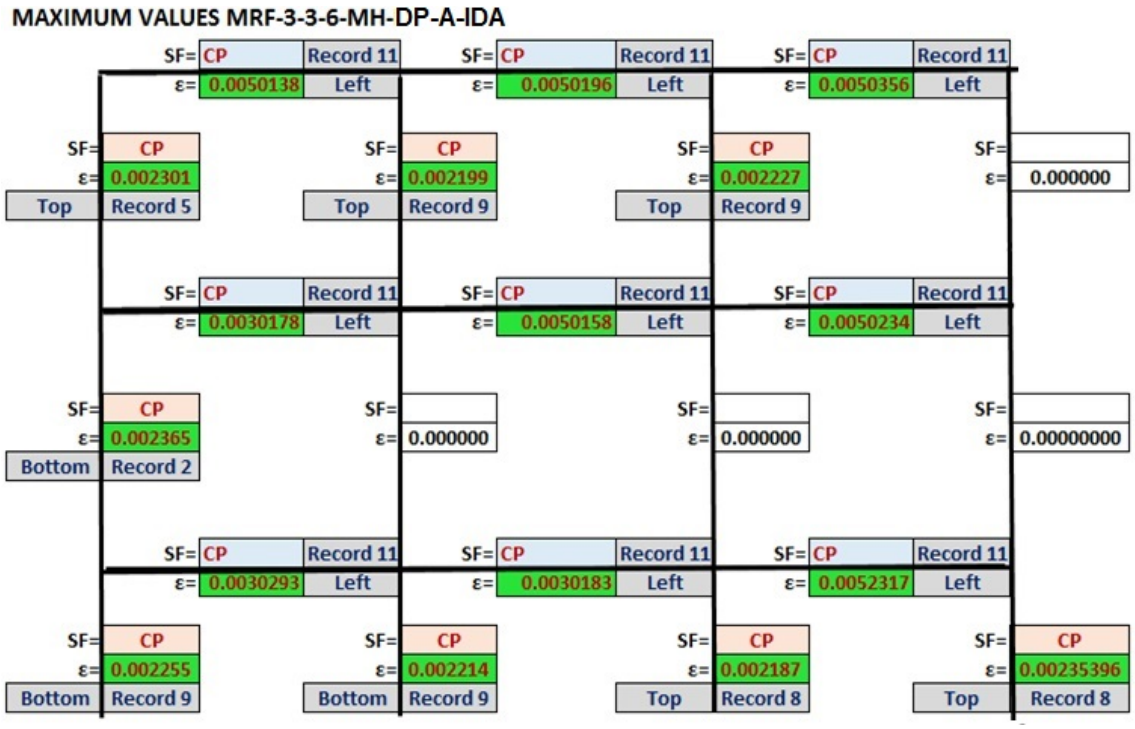

Figure B.9 Maximum strain values for each element for MRF-3-3-6-MH-DP-A.

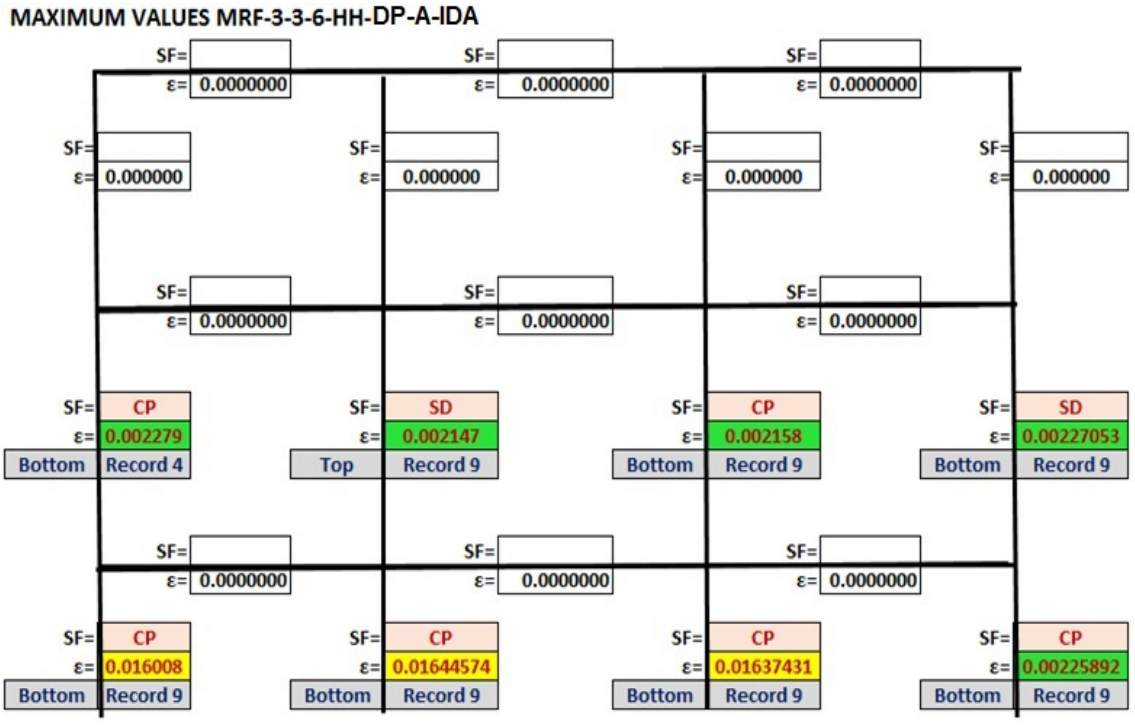

Figure B.10 Maximum strain values for each element for MRF-3-3-6-HH-DP-A.

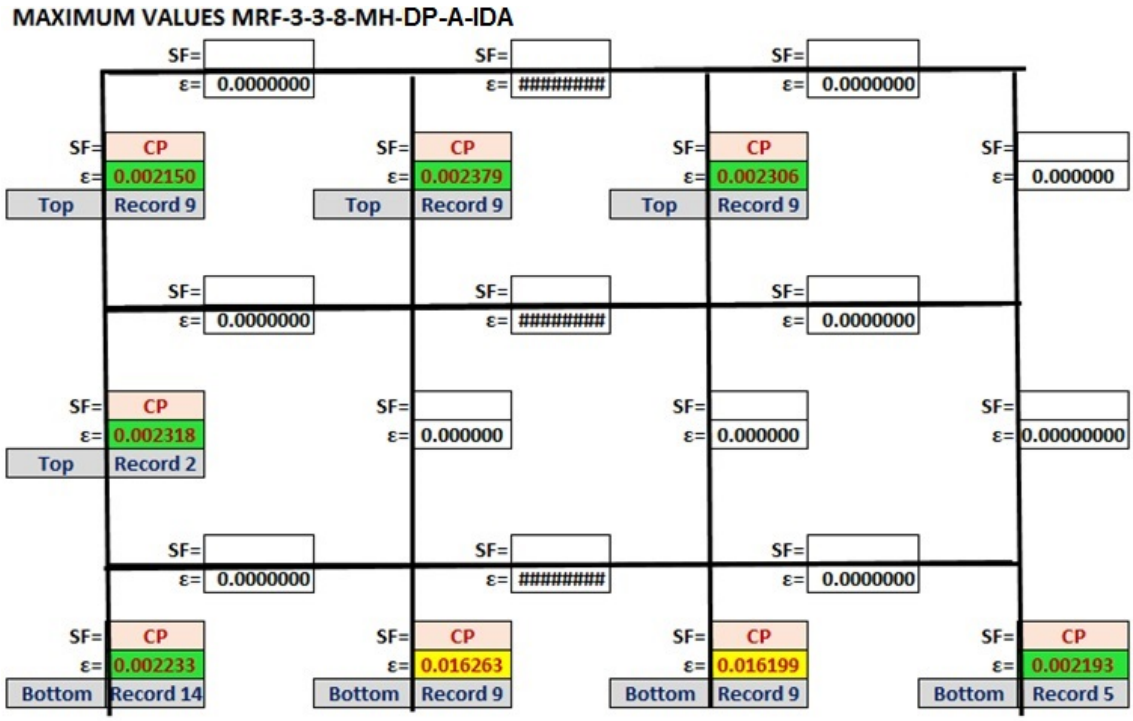

Figure B.11 Maximum strain values for each element for MRF-3-3-8-MH-DP-A.

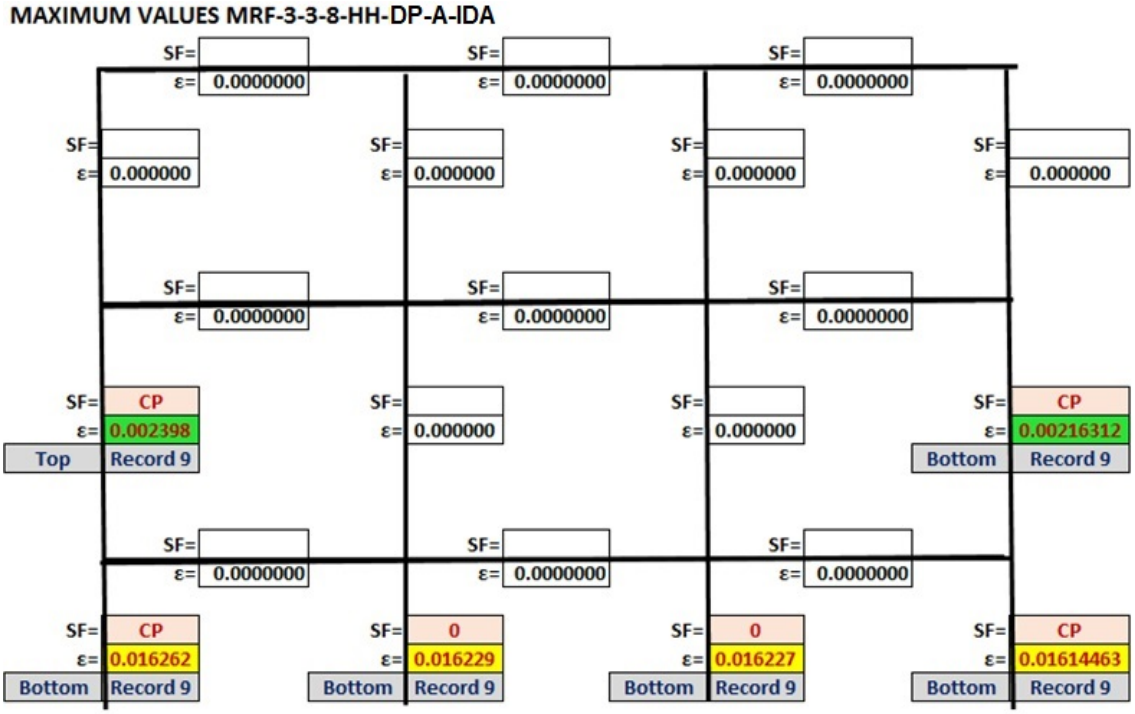

Figure B.12 Maximum strain values for each element for MRF-3-3-8-HH-DP-A.

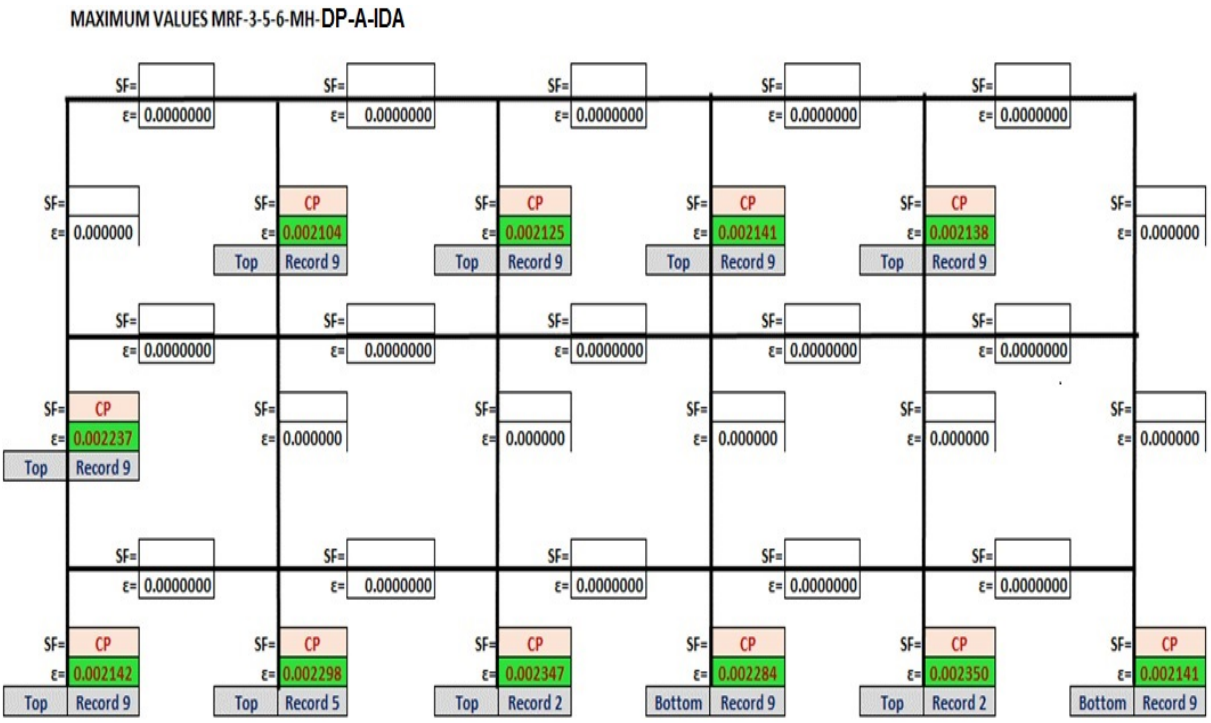

Figure B.13 Maximum strain values for each element for MRF-3-5-6-MH-DP-A.

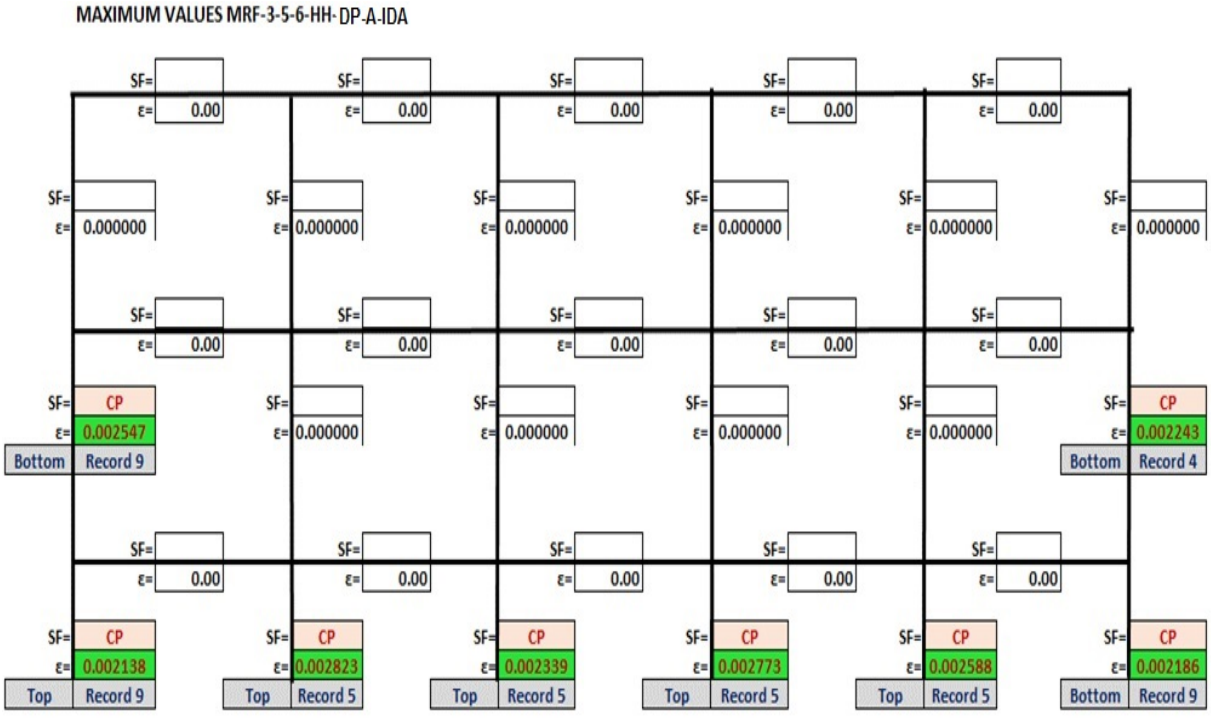

Figure B.14 Maximum strain values for each element for MRF-3-5-6-HH-DP-A.

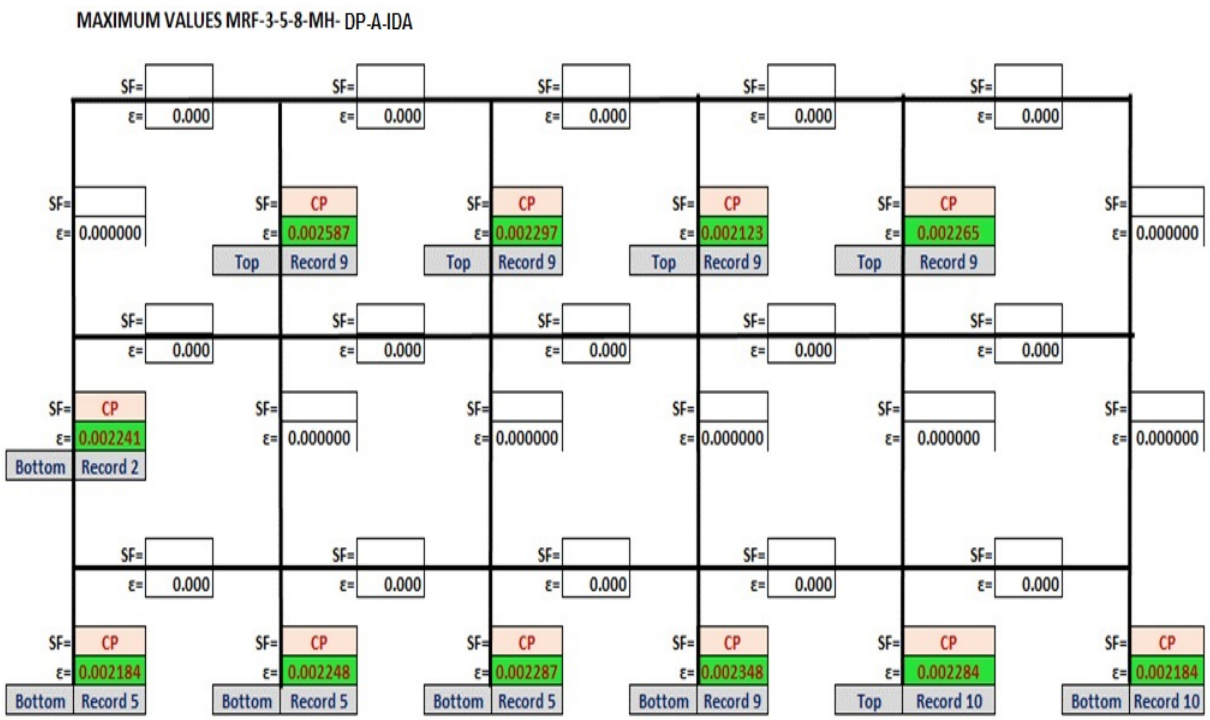

Figure B.15 Maximum strain values for each element for MRF-3-5-8-MH-DP-A.

Figure B.16 Maximum strain values for each element for MRF-3-5-8-HH-DP-A.

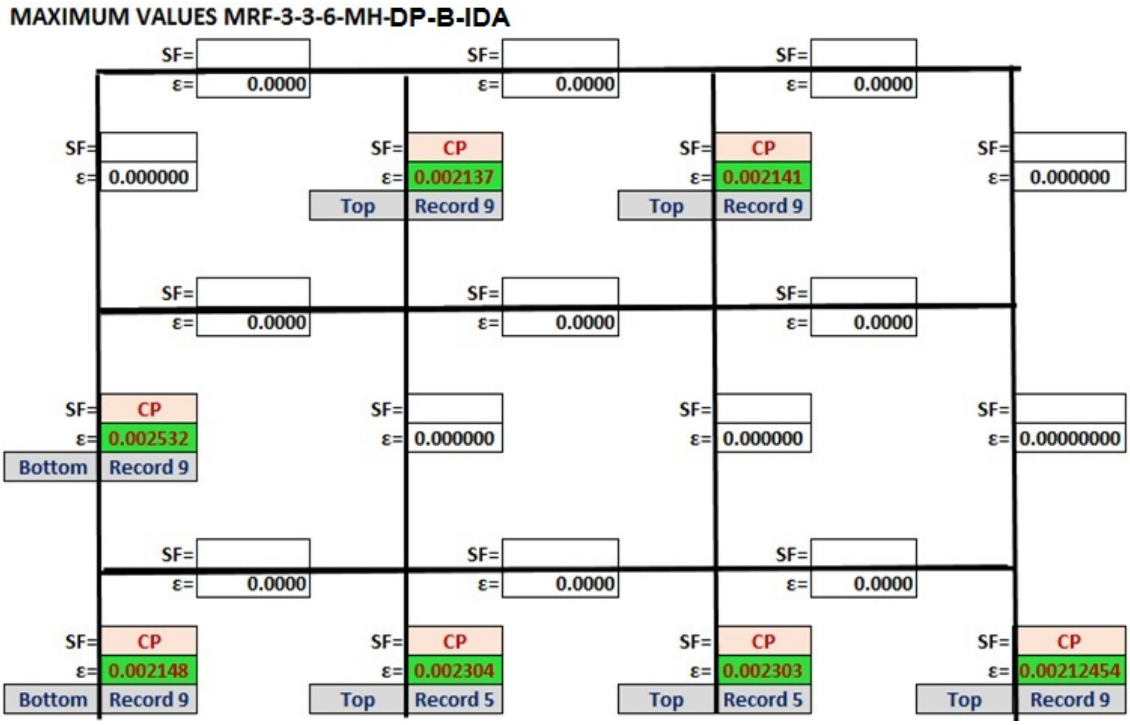

Figure B.17 Maximum strain values for each element for MRF-3-3-6-MH-DP-B.

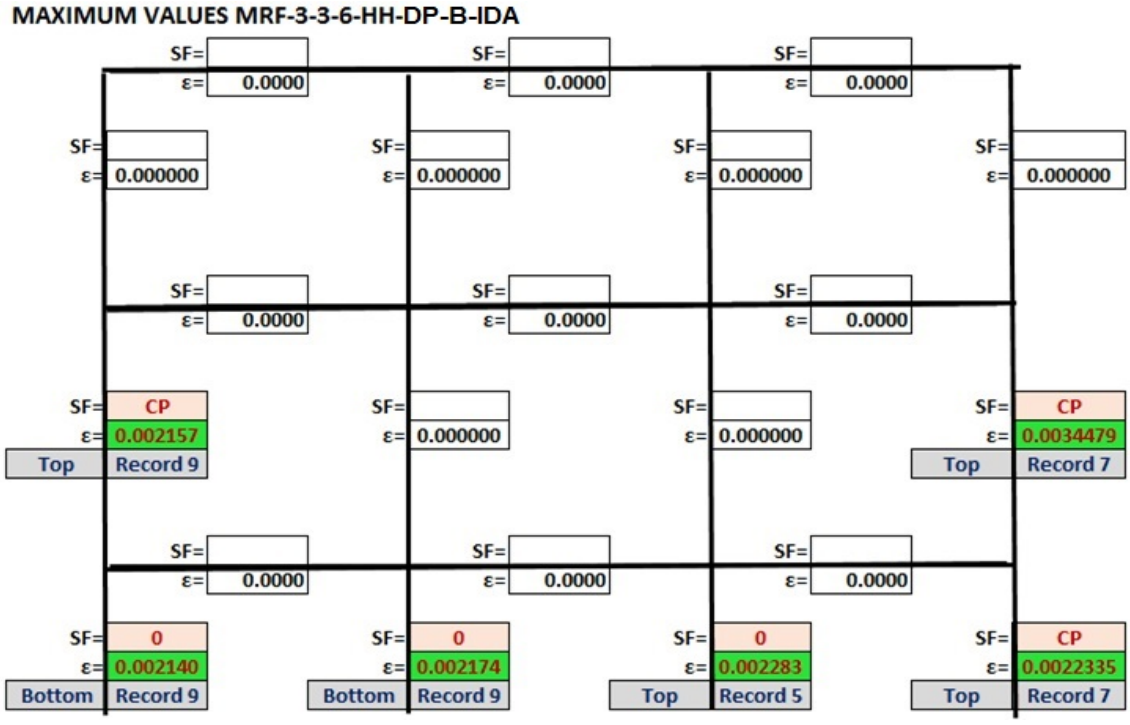

Figure B.18 Maximum strain values for each element for MRF-3-3-6-HH-DP-B.

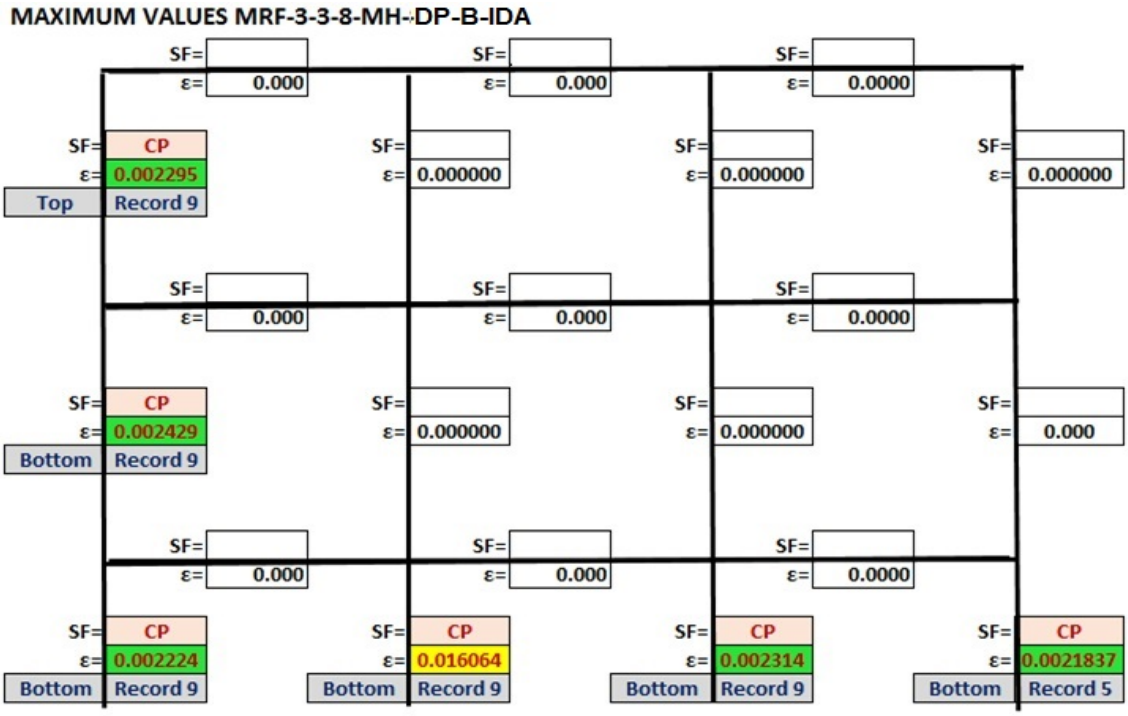

Figure B.19 Maximum strain values for each element for MRF-3-3-8-MH-DP-B.

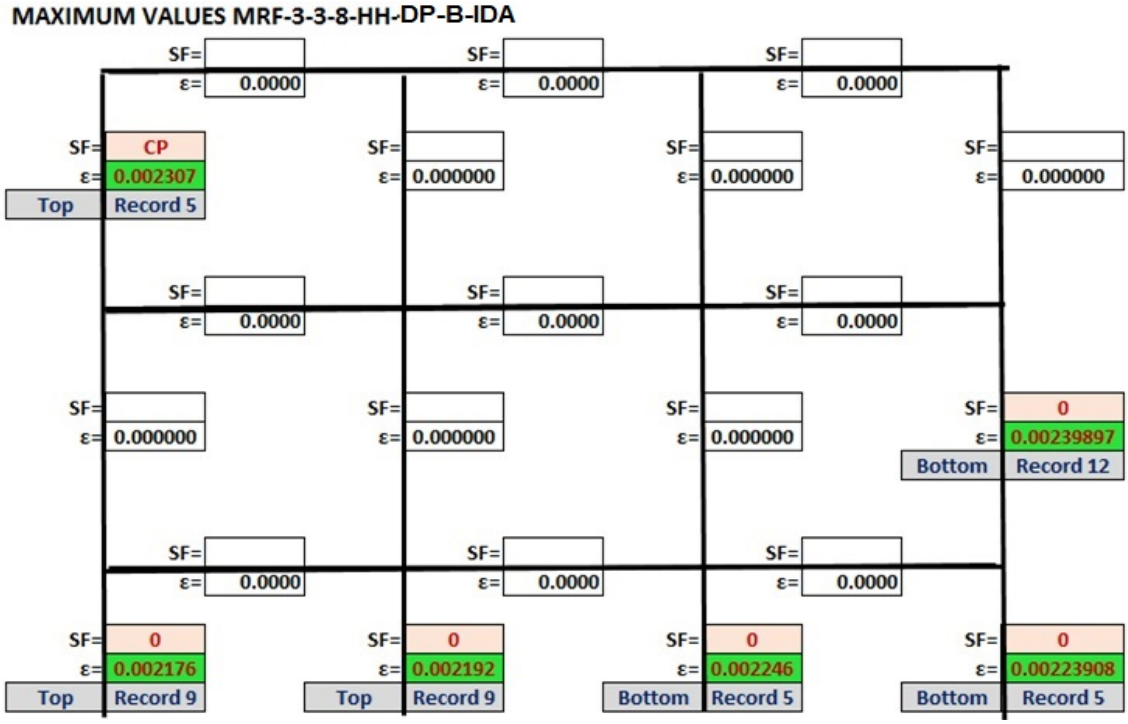

Figure B.20 Maximum strain values for each element for MRF-3-3-8-HH-DP-B.

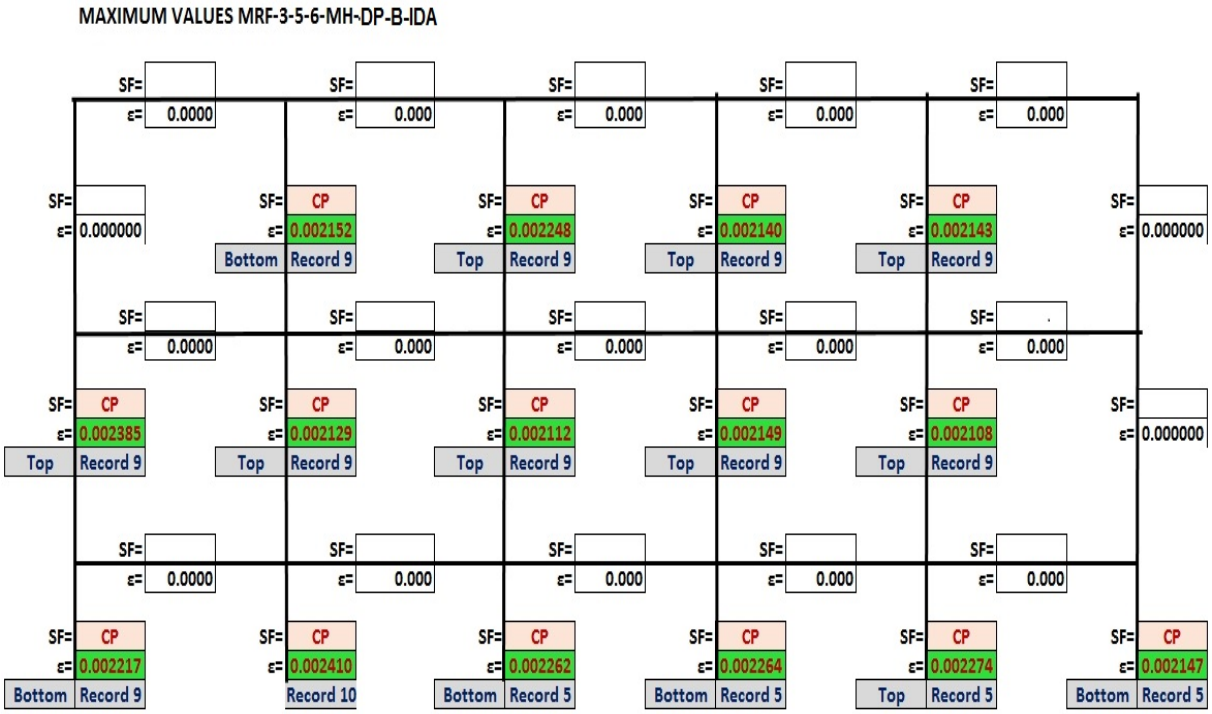

Figure B.21 Maximum strain values for each element for MRF-3-5-6-MH-DP-B.

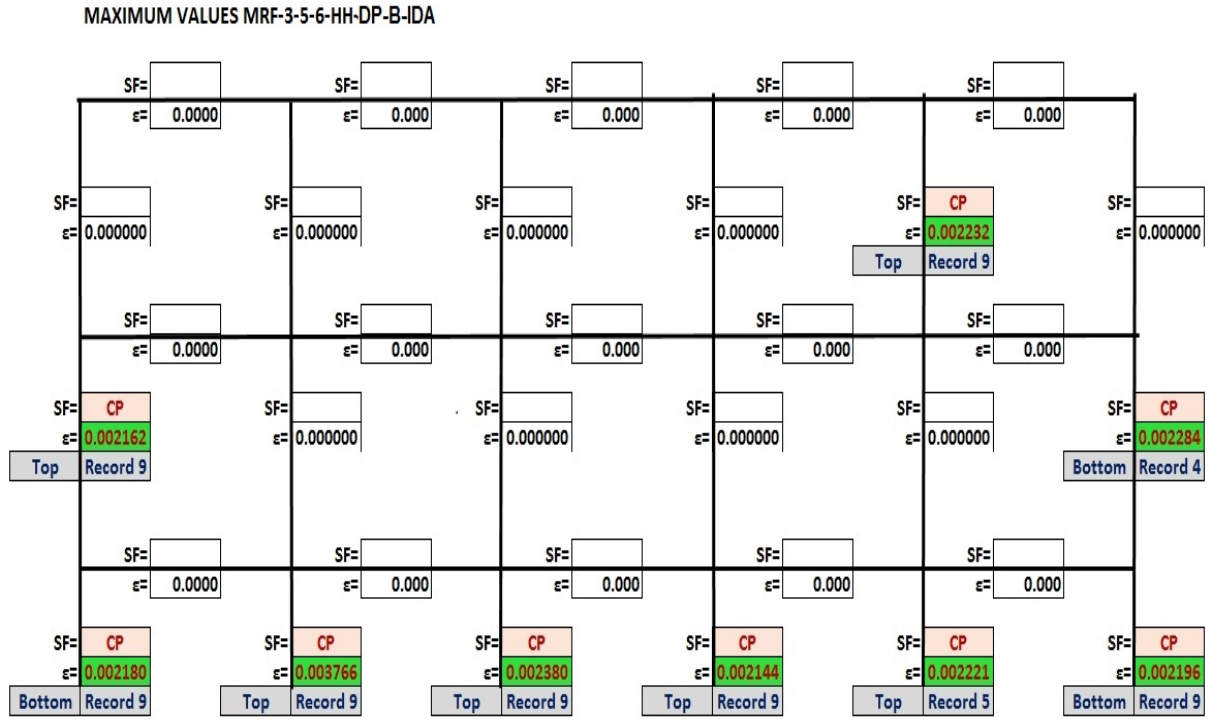

Figure B.22 Maximum strain values for each element for MRF-3-5-6-HH-DP-B.

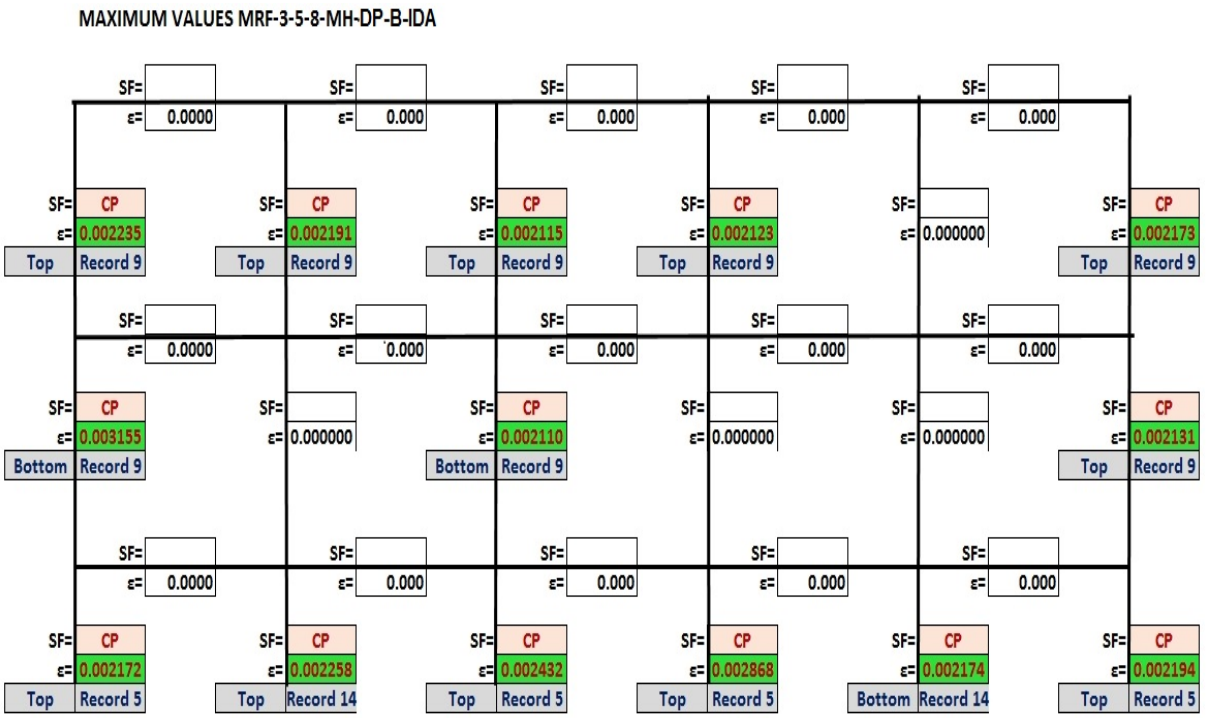

Figure B.23 Maximum strain values for each element for MRF-3-5-8-MH-DP-B.

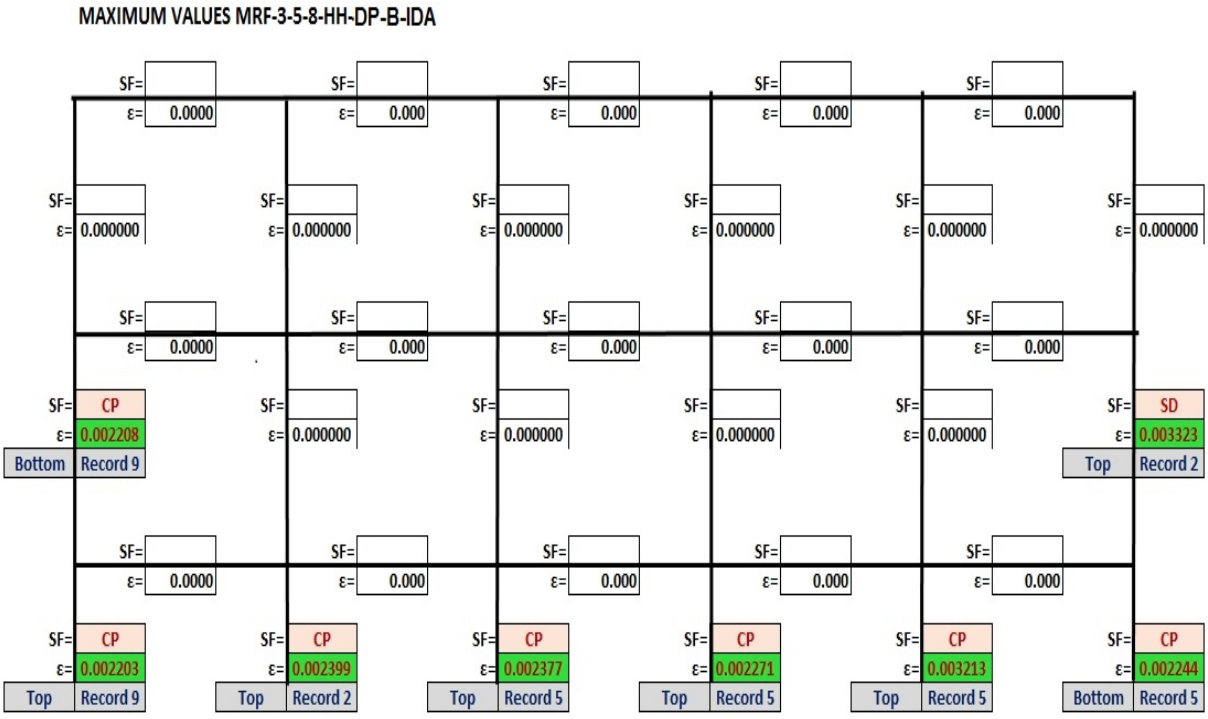

Figure B.24 Maximum strain values for each element for MRF-3-5-8-HH-DP-B.